

Universität
Rostock



Traditio et Innovatio

Pniktogenchemie Aktivierung kleiner Moleküle

Kumulative Dissertation

zur Erlangung des akademischen Grades

Doctor rerum naturalium (Dr. rer. nat.)

der Mathematisch-Naturwissenschaftlichen Fakultät

der Universität Rostock

vorgelegt von Henrik Beer, geboren am 17.11.1993 in Schwerin, 11.07.2022

https://doi.org/10.18453/rosdok_id00004146

Die vorliegende Arbeit wurde in der Zeit von Oktober 2018 bis Juli 2022 am Institut für Chemie der Universität Rostock am Lehrstuhl für Anorganische Chemie in der Arbeitsgruppe von Prof. Dr. Axel Schulz angefertigt.



Dieses Werk ist lizenziert unter einer
Creative Commons Namensnennung 4.0 International Lizenz.

1. Gutachter: Prof. Dr. Axel Schulz
2. Gutachter: Prof. Dr. Christian Müller

Datum der Verteidigung: 06.12.2022

Erklärung

Ich versichere hiermit an Eides statt, dass ich die vorliegende Arbeit selbstständig angefertigt und ohne fremde Hilfe verfasst habe. Dazu habe ich keine außer den von mir angegebenen Hilfsmitteln und Quellen verwendet und die den benutzten Werken inhaltlich und wörtlich entnommenen Stellen habe ich als solche kenntlich gemacht.

Rostock, 11.07.2022

Henrik Beer

Danksagungen

Ohne die Unterstützung zahlreicher Personen wäre diese Doktorarbeit nicht möglich gewesen.

Zuallererst möchte ich Herrn **Prof. Dr. Axel Schulz** für das in mich gesetzte Vertrauen, dieses interessante Forschungsthema zu bearbeiten, danken. Die vielen hilf- und lehrreichen Gespräche, das Interesse an meiner Arbeit und vor allem für die großartige Unterstützung in allen Situationen in den letzten Jahren haben großen Anteil an dieser Arbeit.

Nicht minderen Anteil an dieser Arbeit hat Herr **Dr. Jonas Bresien**, welcher mich seit der Bachelorarbeit in allen Dingen des Laboralltags unterstützt hat. Darüber hinaus möchte ich mich für die Einarbeitung in das Themengebiet der quantenchemischen Rechnungen als auch für die Durchführung von vielen weiterführenden Berechnungen bedanken.

Außerdem möchte ich mich bei Herrn **Dr. Alexander Villinger** und **Isabel Schicht** für das Vermessen von Einkristallen und die Verfeinerung der Strukturen bedanken. Insbesondere bei Alex möchte ich mich für die Einführung in die Röntgeneinkristallstrukturanalyse bedanken, wodurch ich auch außerhalb der normalen Servicezeiten Kristalle aufsetzen und vermessen konnte.

Eine synthetische Arbeit ist ohne die komplette Infrastruktur des Hauses nicht möglich. Daher möchte ich mich bei allen Service- und Werkstattmitarbeitern bedanken, die mir immer mit Rat und Tat zur Seite standen. Insbesondere möchte ich mich bei Herrn **Dr. Dirk Michalik** und **Heike Borgwaldt** für das Vermessen von unzähligen NMR-Proben und den damit verbundenen Sonderwünschen danken. Ebenfalls möchte ich mich bei den Mechanikern **Peter Kumm** und **Martin Riedel** bedanken, welche viele Sonderanfertigungen innerhalb kürzester Zeit hergestellt haben und bei jedem noch so speziellen Problem eine Lösung gefunden haben.

Bei **Daniel Gschwind** und **Alexander Linke** möchte ich mich für die geleistete Arbeit im Zuge ihrer Bachelor- bzw. Masterarbeit danken. Ein großes Dankeschön an **Dr. Julia Rothe**, **Dr. René Labbow**, **Dr. Kevin Bläsing**, **Moritz Scharnhölz** und **Dr. Tim Suhrbier** die immer ein offenes Ohr für die zahlreichen kleinen und großen Fragestellungen im Laboralltag hatten. Ohne euch wäre die Zeit nur halb so produktiv und lustig gewesen.

All meinen Freunden danke ich für die vielen schönen Momente im Laufe der letzten 10 Jahre des Chemiestudiums. Insbesondere **Maximilian Schlicht** und **Tim Völzer** möchte ich für die ganzen gemeinsamen Jahre danken. Seit der Schulzeit sind wir unseren Weg gemeinsam gegangen und haben das jeweilige Studium in Rostock gemeistert. Zusammen mit **Tim Völzer** und seiner Expertise in der Femtosekundspektroskopie konnten wir gemeinsam ein Paper veröffentlichen.

Abschließend möchte ich mich bei meiner Familie bedanken. Insbesondere meiner Schwester **Elisa** und meinen Schwiegereltern **Sibylle** und **Mario** möchte ich mich für die Unterstützung außerhalb des Laboralltages danken. Die gemeinsamen Auszeiten in Thüringen und Schweden haben mir immer viel Kraft gegeben und Platz für neue Ideen geschaffen. Meiner Frau **Louise** danke ich zusätzlich für die riesige Unterstützung in den letzten 7 Jahren, auch wenn es im Labor öfter mal spät geworden ist. Die gemeinsame Zeit und deine wundervollen Ideen lassen es nie langweilig werden. Danke für einfach Alles!

Zusammenfassung

In der vorliegenden Dissertation werden die Ergebnisse der Untersuchungen zur Reaktion von Biradikalen der Form $[P(\mu-NR)]_2$ mit kleinen Molekülen präsentiert. Unter anderem wurden Moleküle, wie *para*-Wasserstoff, BRØNSTED-Säuren und aromatische Thioketone, aktiviert und deren Additionsprodukte isoliert und vollständig charakterisiert. Des Weiteren wurde durch die Insertion von Isonitrilen (CN–R) in die 4-gliedrigen cyclischen Biradikale, 5-gliedrige Ringsysteme erhalten. Diese wiesen Eigenschaften eines molekularen Schalters auf, welche mittels NMR-Spektroskopie in Lösung und zum Teil auch durch Röntgeneinkristallstrukturanalyse im Festkörper untersucht werden konnten. Durch Reaktion von $[P(\mu-N\text{Ter})]_2$ mit Thiophosgen konnte ein formales „CS“-Fragment durch Insertion in das viergliedrige N_2P_2 -Ringsystem abgefangen werden. Aus der resultierenden Verbindung konnte ein hochlabiles, fünfgliedriges Biradikal generiert werden, welches durch Folgereaktion mit kleinen Molekülen abgefangen wurde.

Summary

In this thesis the results on the reaction of biradicals ($[P(\mu-NR)]_2$) with small molecules are presented. Among others, small molecules such as *para*-hydrogen, Brønsted acids or aromatic thioketones were activated and their addition products were isolated and characterised completely. Furthermore, 5-membered ring systems were obtained by inserting isonitriles (CN–R) into the 4-membered cyclic biradicals $[P(\mu-NR)]_2$. The insertion products showed properties of a molecular switch that could be observed by NMR spectroscopy in solution and partly also by single crystal X-ray structure analysis in the solid state. By reacting $[P(\mu-N\text{Ter})]_2$ with thiophosgene, a formal "CS" fragment could be captured by insertion into the four-membered N_2P_2 ring system. From the resulting compound, a highly labile, five-membered biradical could be generated, which was captured by subsequent reaction with small molecules.

Für Louise

Inhaltsverzeichnis

1	Zielsetzung und Motivation.....	1
2	Einleitung.....	3
2.1	Biradikale.....	3
2.2	Anwendung von Biradikalen.....	7
2.2.1	Aktivierung kleiner Moleküle.....	7
2.2.2	Molekulare Schalter.....	8
3	Ergebnisse und Diskussion.....	13
3.1	Untersuchungen zu Molekularen Schaltern.....	13
3.1.1	Untersuchung zu $[P(\mu\text{-N}Ter)]_2RNC$ (R = Dmp, <i>t</i> Bu).....	13
3.1.2	Variation des sterisch anspruchsvollen Substituenten am Ring.....	19
3.1.3	Variation des Pniktogens.....	21
3.1.4	Thiocarbonyl als Isonitril-Ersatz.....	23
3.2	Aktivierung kleiner Moleküle.....	25
3.2.1	Reaktion von $[P(\mu\text{-N}Ter)]_2CS$ (15) mit Abfangreagenzien.....	25
3.2.2	Reaktion von $[P(\mu\text{-N}Ter)]_2$ (1Ter) mit Thioketonen.....	28
3.2.3	Reaktion von $[P(\mu\text{-N}Ter)]_2$ (1) mit BRØNSTED-Säuren.....	30
3.2.4	<i>Para</i> -Wasserstoff-Aktivierung.....	33
4	Zusammenfassung und Ausblick.....	35
5	Referenzen.....	37
6	Ausgewählte Originalpublikationen.....	43
6.1	A chemical reaction controlled by light-activated molecular switches based on heterocyclopentanediyls.....	46
6.2	Photoisomerization of a phosphorus-based biradicaloid: ultrafast dynamics through a conical intersection.....	55

6.3	Reversible switching between housane and cyclopentenediyl isomers: an isonitrile-catalysed thermal reverse reaction.....	64
6.4	A Cyclic Thioketone as Biradical Heterocyclopentane-1,3-diyl: Synthesis, Structure and Activation Chemistry.....	72
6.5	Synthesis of Bicyclic P,S-Heterocycles via the Addition of Thioketones to a Phosphorus-Centered Open-Shell Singlet Biradical.....	82
6.6	Trapping of Brønsted acids with a phosphorus centered biradicaloid – synthesis of hydrogen pseudohalide addition products.....	91
7	Anhang.....	101
7.1	Weitere Publikationen.....	101
7.1.1	Heterocyclopentenediyls vs Heterocyclopenta-dienes: A Question of Silyl Group Migration	101
7.1.2	Hyperpolarization Effects in Parahydrogen Activation with Pnictogen Biradicaloids: Metal-free PHIP and SABRE.....	113
7.1.3	Insertion of Ruthenium into an inorganic, cyclic biradicaloid	119

Abkürzungsverzeichnis

AO	Atomorbital	Mes	Mesityl (2,4,6-Trimethylphenyl)
Äq.	Äquivalent(e)	MO	Molekülorbital
CInt	konische Durchschneidung (<i>conical intersection</i>)	Mtp	2,6-Dimethyl-4- <i>tert</i> -Butylphenyl
DFT	Dichtefunktionaltheorie	Naph	Naphthalen
Dmp	2,6-Dimethylphenyl	NBO	natürliches Bindungsorbital
ESR	Elektronenspinresonanz-Spektroskopie	NHC	<i>N</i> -heterozyklisches Carben
<i>et al.</i>	<i>et alii/aliae</i> (und andere)	NMR	<i>nuclear magnetic resonance</i> (Kernresonanz)
exp.	experimentell	PES	Potenzialenergiehyperfläche (<i>potential energy hypersurface</i>)
Fc	Ferrocenyl	Ref.	Referenz
GIAO	<i>gauge-independent AO</i>	RT	Raumtemperatur
HOMO	höchstes besetztes MO (<i>highest occupied molecular orbital</i>)	<i>t</i> Bu	<i>tert</i> -Butyl
IR	Infrarot	Ter	Terphenyl (2,6-Dimesitylphenyl)
IUPAC	International Union of Pure and Applied Chemistry	THF	Tetrahydrofuran
kov.	kovalent	TS	Übergangszustand (<i>transition state</i>)
LB	LEWIS-Base	WCC	<i>weakly coordinating cation</i> (schwach koordinierendes Kation)
LS	LEWIS-Säure		
LUMO	tiefstes unbesetztes MO (<i>lowest unoccupied molecular orbital</i>)		
μ -	verbrückend (in Formeln)		

Übersicht Quantenmechanische Rechnungen

Bezeichnung	Bedeutung
DLPNO	domain-based local pair natural orbital
CCSD(T)	coupled cluster singles doubles perturbative triples
CASSCF	Complete Active Space Self Consistent Field
NEVPT	n -electron valence state perturbation theory
TD-DFT	time-dependent density-functional theory
MRCI	multireference configuration interaction

Maßeinheiten

In dieser Arbeit werden die im Internationalen Einheitensystem (SI) gültigen Maßeinheiten verwendet. Alle davon abweichenden Einheiten und deren Umrechnung in SI-Einheiten sind im Folgenden aufgeführt:

Größe	Einheit	Bezeichnung	Umrechnung in SI-Einheiten
Frequenz	MHz	Megahertz	$1 \text{ MHz} = 1 \times 10^6 \text{ s}^{-1}$
	Hz	Hertz	$1 \text{ Hz} = 1 \text{ s}^{-1}$
Länge	Å	Ångström	$1 \text{ Å} = 1 \times 10^{-10} \text{ m}$
Leistung	mW	Milliwatt	$1 \text{ mW} = 1 \times 10^{-3} \text{ kg m}^2 \text{ s}^{-1}$
Temperatur	°C	Grad Celsius	$\vartheta/^\circ\text{C} = T/\text{K} - 273.15$
Volumen	mL	Milliliter	$1 \text{ mL} = 1 \text{ cm}^3 = 1 \times 10^{-6} \text{ m}^3$
Wärmemenge	kJ	Kilojoule	$1 \text{ kJ} = 1 \times 10^3 \text{ m}^2 \text{ kg s}^{-2}$
Wellenzahl	cm^{-1}	reziproke Zentimeter	$1 \text{ cm}^{-1} = 100 \text{ m}^{-1}$
Zeit	h	Stunde	$1 \text{ h} = 3.6 \times 10^3 \text{ s}$
	min	Minute	$1 \text{ min} = 60 \text{ s}$

Strukturformelverzeichnis

Abk.	Strukturformel
Ter	
Hyp	
tBuNC	
DmpNC	
MesNC	
MtpNC	
1Ter	
1Hyp	

Abk.	Strukturformel
2Dmp	
2Mtp	
4DmpfBu	
4fBufBu	
5DmpfBu	
6Ter	
7Ter	
8Dmp	

Abk.	Strukturformel
8Mes	
8tBu	
9	
10Dmp	
10Mes	
11Dmp	
11Mes	
12Mtp	
12tBu	
14	

Abk.	Strukturformel
15	
16	
17	
18	
19	
20	
21	

Abk.	Strukturformel
22	
23	
24	
25	

Abk.	Strukturformel
26	
27	
28	
29	
30	

2 Einleitung

2.1 Biradikale

Die IUPAC definiert Biradikale als Moleküle mit einer geraden Elektronenanzahl, welche an zwei, mitunter delokalisierten, Radikalzentren lokalisiert sind, die weitestgehend unabhängig voneinander sind.^[1] In der Literatur werden weitere Begriffe wie Disbiradikal, Diradikal und Bi- oder Diradikaloid verwendet, welche auf den ersten Blick sehr ähnlich erscheinen, aber bei genauerer Betrachtung feine Unterschiede ausdrücken. ABE (Abbildung 1) unterscheidet in seinem 2013 veröffentlichten Paper lediglich zwischen Biradikalen (keine Austauschwechselwirkung (J) zwischen den Radikalzentren; Bi zwei (lateinisch)) und Diradikalen (Wechselwirkung zwischen den Radikalzentren; Di = zwei (griechisch)).^[2]

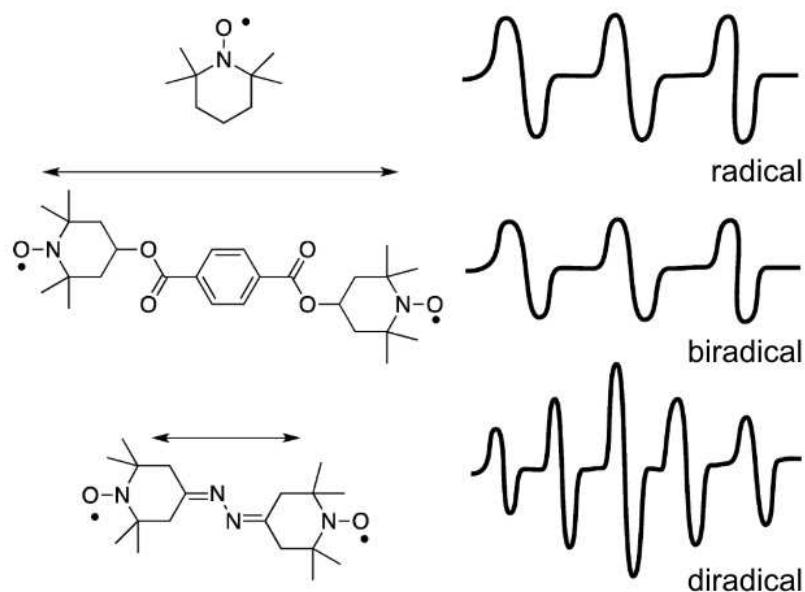
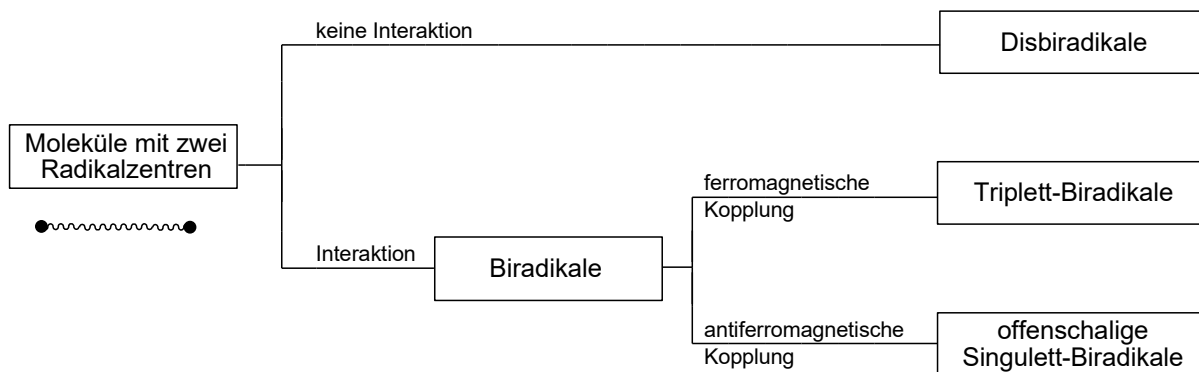


Abbildung 1. ESR-Spektren von verschiedenen Bis(nitroxiden) mit verschiedenen Austauschwechselwirkungen (J) – Abbildung entnommen aus „Diradicals“ von M. ABE.^[2]

SCHULZ hat 2018 mit einer Veröffentlichung eine systematische Bezeichnung vorgeschlagen, welche als Grundlage die Interaktion zwischen den Radikalzentren besitzt und mit lateinischen Vorsilben (Bi = zwei, Dis = auseinander) eine Differenzierung vorgenommen. Somit können Disbiradikale als „echte“ Biradikale mit (fast) keiner Interaktion zwischen den Radikalzentren

angesehen und alle restlichen Spezies als Biradikale bezeichnet werden (Schema 2).^[3] In der gesamten Arbeit wird die Bezeichnung nach SCHULZ verwendet.



Schema 2. Systematische Bezeichnung von Molekülen mit zwei Radikalzentren auf Grundlage der Interaktion zwischen den Radikalzentren (Bi = Zwei, Dis = auseinander).

Eine Unterscheidung von Biradikalen, also Molekülen mit einer signifikanten Interaktion zwischen den beiden Radikalzentren, kann außerdem hinsichtlich der Kopplung ihrer Radikalelektronen vorgenommen werden. Radikalelektronen von Singulett-Biradikalen koppeln antiferromagnetisch miteinander und Triplett-Biradikale ferromagnetisch. Mittels ESR-Spektroskopie lassen sich die drei verschiedenen Typen von Molekülen mit zwei Radikalzentren unterscheiden. Die radikalischen Elektronen von Triplett-Biradikalen koppeln miteinander, wohingegen die der Disbiradikale keine Kopplung im ESR-Spektrum aufzeigen. Singulett-Biradikale besitzen keinen Gesamtspin bzw. ist die Spindichte überall im Raum gleich null und daher sind diese ESR-inaktiv.

Bereits kleinste Moleküle, wie das hochsymmetrische ($D_{\infty h}$) O_2 -Molekül, können in verschiedenen energetischen Zuständen in der Natur vorkommen. Da die Unterscheidung zwischen Singulett- und Triplett-Zuständen relativ abstrakt ist, kann diese mit Hilfe von MO-Diagrammen (Abbildung 2) veranschaulicht werden. Ein Singulett-Zustand bezieht sich auf ein System, in dem alle Elektronen gepaart vorkommen (Gesamtspin $S=0$), wohin gegen der Triplett-Zustand zwei ungepaarte Elektronen besitzt (Gesamtspin $S=1$). Die beiden formal radikalischen Elektronen von Singulett-Sauerstoff 1O_2 kommen hingegen spingepaart vor. Dieser Zustand ist nach der Hundschen Regel allerdings energiereicher, reaktiver und deshalb kurzlebiger als der Triplett-Zustand 3O_2 . In der Natur kommt Sauerstoff fast ausschließlich im energieärmeren Triplett-Zustand vor, was ein Leben auf der Erde überhaupt erst möglich macht.

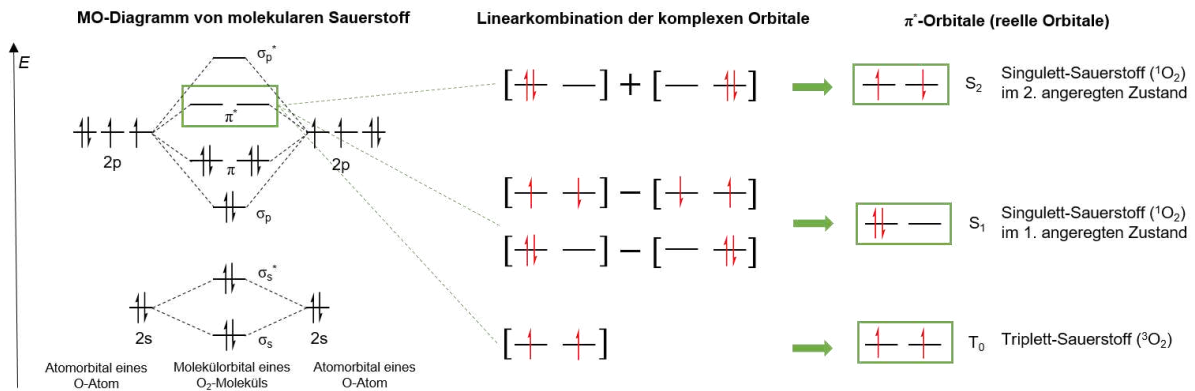
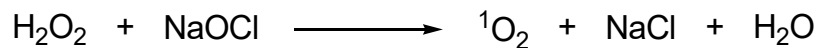


Abbildung 2. Molekülorbitaldiagramme von Sauerstoff im Triplett-Zustand (T_0), ersten angeregten Zustand (S_1) und zweiten angeregten Zustand (S_2).

Singulett-Sauerstoff wird im Labormaßstab aus der Reaktion von Wasserstoffperoxid mit Natriumhypochlorit gewonnen und als wirkungsvolles und selektives Oxidationsmittel eingesetzt (Schema 3).



Schema 3. Erzeugung von Singulett-Sauerstoff (¹O₂) im Labormaßstab.

Die hohe Reaktivität von Radikalen war bereits im 18. Jahrhundert bekannt und wurde von LAVOISIER in seiner Veröffentlichung „*Traité élémentaire de chimie*“ beschrieben. Die um 1830 entwickelte Radikaltheorie von LIEBIG, WÖHLER und LAURENT trug zusätzlich zum Verständnis von Radikalen bzw. Radikalreaktionen bei. Im Jahre 1915 beschrieben SCHLENK und BRAUN das erste paramagnetische Biradikal, welches durch die Behandlung von Bis-diphenyl-*m*-xylylendichlorid mit einer Kupferlegierung hergestellt wurde.^[4]

Aufgrund der sehr hohen Reaktivität von Radikalen bzw. Biradikalen war es lange Zeit nicht möglich, kontrollierte chemische Reaktionen durchzuführen. Mit Hilfe von großen sperrigen Substituenten, wie z.B. Terphenyl (Ter = 2,6-Bis(2,4,6-trimethylphenyl)-phenyl) und Supermesityl (Mes* = 2,4,6-tri-tert-butyl-phenyl), war es möglich, diese kinetisch zu stabilisieren und die Polymerisierung zu verhindern.^[5–8] Ein Durchbruch in der Biradikalchemie des Phosphors gelang 1995 NIECKE *et al.* mit der Synthese des ersten bei Raumtemperatur stabilen Singulett-Biradikals.^[9] Im Laufe der Jahre konnten von einigen Arbeitsgruppen weitere 4-gliedrig-zentrierte Biradikale synthetisiert werden, wobei diverse Hauptgruppenelemente und Substituenten verwendet wurden. Aufgrund der Menge an verschiedenen Biradikalen können diese hier nicht vollständig erfasst werden. Daher wird nur eine kleine Auswahl in Abbildung 3 präsentiert.^[10,11,20,12–19] Für eine umfassende

Zusammenfassung wird hier auf den 2021 erschienenen Buchartikel von SCHULZ und Mitarbeiter verwiesen.^[21]

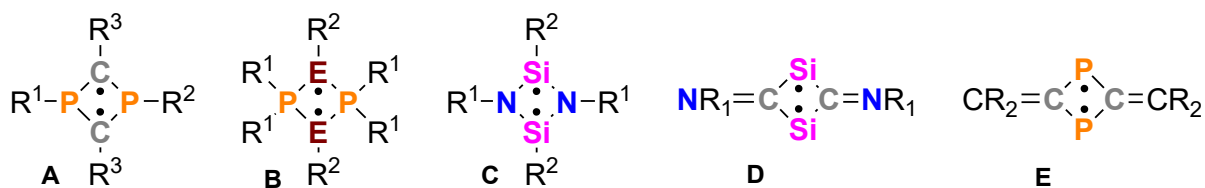
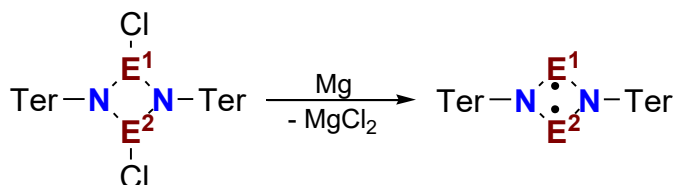


Abbildung 3. Verschiedene viergliedrig-zentrierte offenschalige Singulett-Biradikale. **A:** Niecke 1995, Yoshifuji 2003; **B:** Bertrand (E = B) 2002, Schnöckel (E = Al) 2009; **C:** Power (E = Ge) 2004, Lappert (E = Sn) 2004, Sekiguchi (E = Si) 2011; **D:** So 2012; **E:** Grützmacher 2017, Ghadwahl 2017.

Das erste stabile Singulett-Biradikal, bestehend aus Gruppe 15 Elementen, konnte 2011 von der Arbeitsgruppe-SCHULZ durch Reduktion von $[\text{ClP}(\mu\text{-NTer})]_2$ synthetisiert werden (Schema 4).



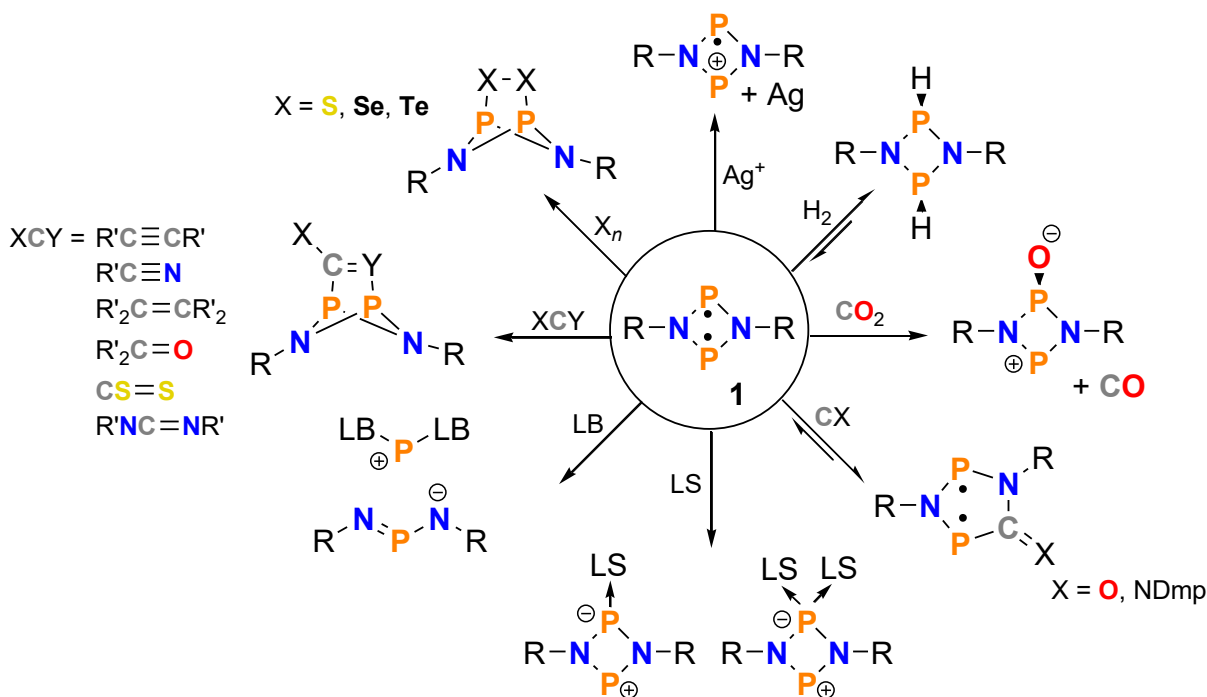
Schema 4. Synthese der Gruppe 15 Biradikale $[\text{E}(\mu\text{-NTer})]_2$ ($\text{E}^{1,2} = \text{P}$ (**1**); $\text{E}^{1,2} = \text{As}$ (**30**); $\text{E}^1 = \text{P}$, $\text{E}^2 = \text{As}$ (**9**)).^[7,22,23]

Da in dieser Arbeit hauptsächlich mit dem Biradikalsystem $[\text{E}^{1,2}(\mu\text{-NR})]_2$ ($\text{E} = \text{P}$, As ; $\text{R} = \text{Ter}$, Hyp) gearbeitet wurde, wird in den folgenden Abschnitten nur dieses Ringfragment (Schema 4) weiter thematisiert.

2.2 Anwendung von Biradikalen

2.2.1 Aktivierung kleiner Moleküle

Die stabilen Singulett-Biradikale $[P(\mu\text{-N}Ter)]_2$ (**1Ter**) und $[P(\mu\text{-NHyp})]_2$ (**1Hyp**) werden seit ca. 10 Jahren ausführlich von der Arbeitsgruppe SCHULZ untersucht. Dabei konnte vor allem **1Ter** mit zahlreichen Reaktionspartnern umgesetzt werden (Schema 5).^[24–33]



Schema 5. Übersicht über die Aktivierungsreaktionen von **1**. Die Reaktion mit Chalkogenen (S, Se, Te) und den Mehrfachbindungssystemen (XCY) wurden sowohl für **1Ter** als auch für **1Hyp** untersucht. Alle anderen Reaktionen nur für **1Ter**.

Die Aktivierung von Alkenen und Alkinen mit **1Ter** und **1Hyp** erfolgt über eine [2+2]-Cycloaddition und führt zu überbrückten Käfigverbindungen. Dabei fungieren die beiden Phosphoratome als Brückenkopf-atome. Bei Raumtemperatur kann **1Ter** Wasserstoff aktivieren und bei Temperaturen über 60 °C wieder reversibel abspalten. LS führen zu einer Mono- oder Doppelkoordination eines einzelnen Phosphoratoms, wohingegen starke LB zwei P–N-Bindungen spalten können und somit ein schwach wechselwirkendes Ionenpaar entsteht. Interessanterweise führen kleine Moleküle mit geringen sterischen Anspruch, wie Kohlenstoffmonoxid oder Isonitrile, zu einer Insertion in eine P–N-Bindung. Die daraus

resultierenden 5-gliedrigen Biradikalsysteme können mit Hilfe von Licht zu geschlossenschaligen Molekülen mit einer P–P-Einfachbindung umgewandelt werden. Sie weisen Eigenschaften eines molekularen Schalters auf.^[27,33]

2.2.2 Molekulare Schalter

Der Begriff des molekularen Schalters wurde erstmals in den 1980er Jahren verwendet und beschrieb dabei die Umwandlung von DNA-gebundenen Proteinen mittels UV-Licht.^[34] In den letzten 40 Jahren wurden viele Untersuchungen an solchen Molekülen durchgeführt, welche durch Änderung von äußeren Einflüssen wie Temperatur, pH-Wert, elektrische Spannung oder Bestrahlung, zwischen zwei oder mehreren (meta)stabilen Zuständen geschaltet bzw. umgewandelt werden können.^[35–37] Anwendungen von molekularen Schaltern liegen z.B. im Bereich von ultraschnellen molekularen Geräten^[38] oder Photokatalysatoren,^[39,40] da die verschiedenen stabilen Zustände häufig unterschiedliche Eigenschaften besitzen.

Entscheidend für die Anwendung ist das Verständnis des Mechanismus der Isomerisierung. Die Photoisomerisierung zwischen den stabilen Grundzuständen erfolgt meist über einen kurzlebigen elektronisch angeregten Zustand im Bereich von Femto- bis Pikosekunden.^[41,42] Zum einen können photochemische Reaktionen adiabatisch (die chemische Veränderung findet entlang einer einzelnen Potenzialenergiehyperfläche statt) oder zum anderen nichtadiabatisch (die Reaktion verläuft durch eine konische Durchschneidung (CInt)) ablaufen (Abbildung 4).^[43,44] Der Ablauf einer nichtadiabatischen Reaktion beruht auf einer starken vibronischen Kopplung zwischen Kern- und Elektronbewegung, wobei ein Übergang von einem zum anderen elektronischen Zustand ohne Abgabe von Strahlung möglich ist.^[41,42,45–47]

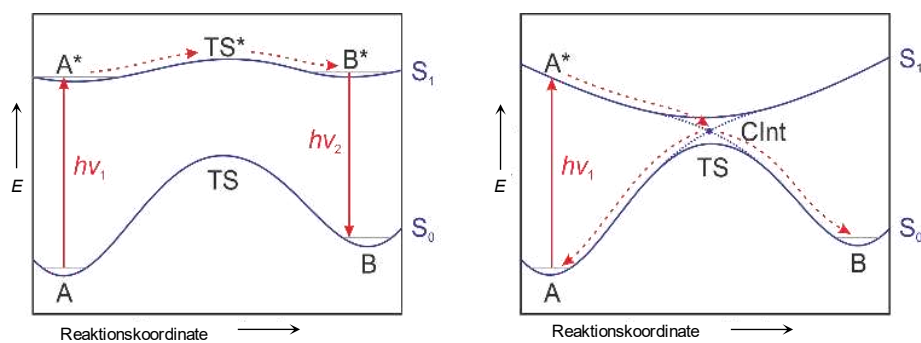
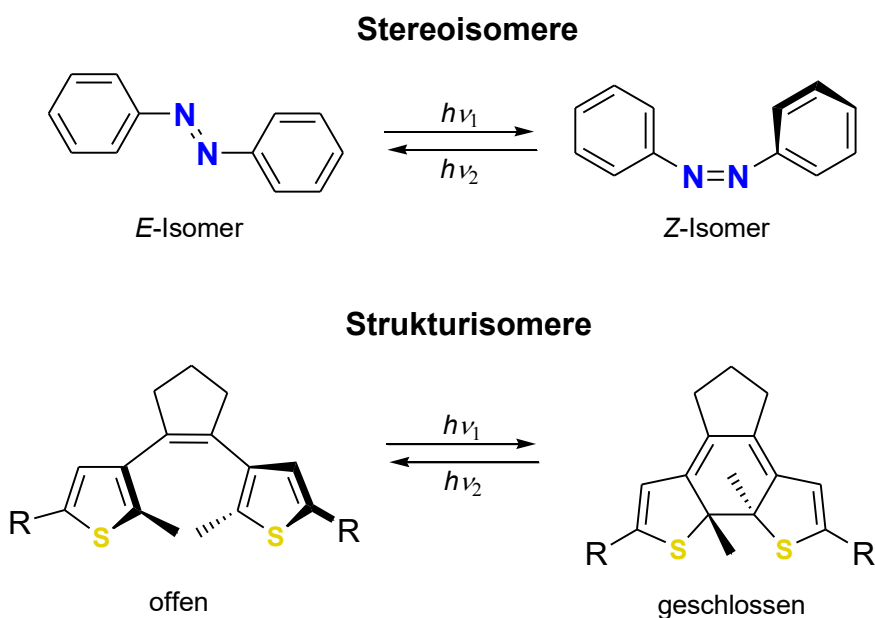


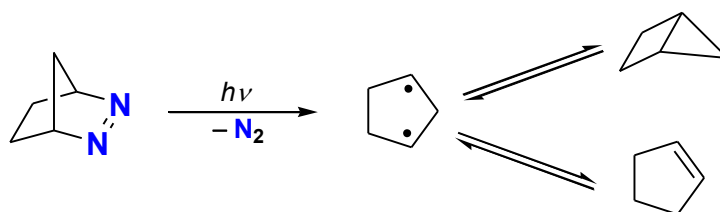
Abbildung 4. Vereinfachte zweidimensionale Darstellung einer adiabatischen (links) und nichtadiabatisch (rechts) Photoreaktion (A → B). Die Abbildungen wurden entnommen aus den Referenzen^[42,43].

Die meisten (lichtaktiven) molekularen Schalter lassen sich in zwei verschiedene Kategorien einteilen. Zum einen Stereoisomere, bei denen sich die Struktur verändert, ohne dass Atombindungen gebrochen oder neu geknüpft werden. Zum anderen Strukturisomere, wobei eine Umverteilung der Bindungen stattfindet.^[36] Meist sind photochrome Verbindungen, also intensiv gefärbte Verbindungen, besonders gut geeignete Untersuchungsobjekte, da unter Bestrahlung eine deutliche Farb- bzw. Strukturänderung zu beobachten ist. In der Literatur sehr bekannte farbige Verbindungen sind Azobenzene-Derivate, welche bereits im Jahre 1937 durch HARTLEY hinsichtlich der *E/Z*-Stereoisomerisierung untersucht wurden. Das intensiv rot gefärbte *E*-Isomer, konnte unter Bestrahlung mit UV-Licht, in das gelbe *Z*-Isomer überführt werden. Eine Strukturelle Aufklärung der beiden Isomere erfolgte durch ROBERTSON im Jahre 1939.^[48-50] Diarylethen-Derivate gehen unter Bestrahlung eine photoinduzierte-Cyclisierungsreaktion zwischen beiden zentralen Kohlenstoffatomen ein und sind damit Beispiele für Strukturisomere (Schema 6).^[51-53]



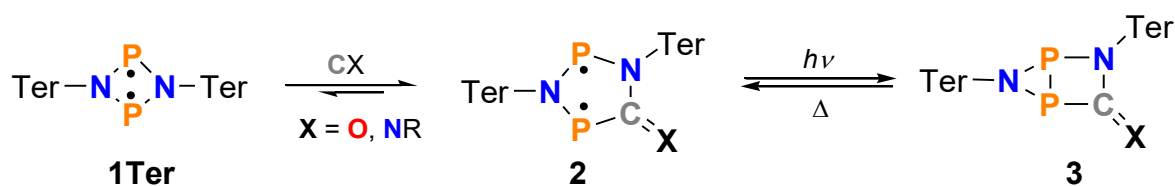
Schema 6. Unterteilung von Molekularen Schalter in Stereoisomere (z.B. Azobenzene, oben) und Strukturisomere (z.B. Diarylethen, unten).

Ein weiteres Molekül, welches durch Temperaturerhöhung eine Strukturänderung vollzieht, ist das erstmalig 1975 von BUCHWALTER und CLOSS synthetisierte Cyclopentan-1,3-diy, bei welchem es sich um ein Triplett-Biradikal handelt.^[54,55] Aus 2,3-Diazabicyclo-[2.2.1]hept-2-en konnte unter Bestrahlung mit UV-Licht bei 5,5 K das Triplett-Biradikal gewonnen werden, welches bei höheren Temperaturen entweder ein geschlossenschaliges Hausan- oder ein Cyclopenten-Derivat bildet (Schema 7).^[56]



Schema 7. Synthese des Closs-Biradikals durch Bestrahlung.

Bereits im Abschnitt 2.2.1 konnte gezeigt werden, dass die Arbeitsgruppe um SCHULZ 2015 das erste Cyclopentan-1,3-diyli Singulett-Biradikal aus der Reaktion von **1Ter** mit CO und Isonitrilen synthetisieren konnten (Schema 8). Diese 5-gliedrigen Heterocyclen (P_2N_2C) mit einer exocyclischen CO bzw. Isonitrileinheit wiesen ebenfalls Eigenschaften eines molekularen Schalters auf.



Schema 8. Synthese von Cyclopentan-1,3-diylen.

Im Zuge der Bachelorarbeit von E. Zander im Jahre 2017 wurde das 5-gliedrige Biradikal $[P(\mu\text{-N}Ter)]_2\text{DmpNC}$ (**2Dmp**) hinsichtlich der Eigenschaften eines molekularen Schalters untersucht. Dazu wurde zunächst das Biradikal mittels UV/Vis-Spektroskopie untersucht. Es konnten drei Maxima (410 nm, 510 nm, 643 nm) im Bereich des sichtbaren Lichts detektiert werden. Der für die photochemische Hinreaktion **2Dmp** \rightarrow **3Dmp** wichtigste Übergang vom HOMO ins LUMO befindet sich bei 643 nm und kann mit einer roten Laser-Diode induziert werden. Die Rückreaktion vom Hausan zum Biradikal erfolgte ausschließlich thermisch und konnte nicht durch Einstrahlen von Licht einer anderen Wellenlänge beeinflusst werden. Erste quantenmechanische Rechnungen an einem Modellsystem gaben Aufschluss über den Anregungsmechanismus durch eine konische Durchschneidung und die Relaxation in den Grundzustand des Biradikals **2H** bzw. des Hausans **3H**.

Außerdem konnte ein Konzept entwickelt werden, womit dieses System mittels NMR-Spektroskopie analysiert werden konnte.^[57] Hierzu wurde ein von der Gschwind-Gruppe 2013 publizierter Aufbau angepasst und genutzt.^[58] Als Lichtquelle wurde eine Laser Diode verwendet, welche mittels Glasfaserkabel mit dem Probenröhrchen (Abbildung 5) verbunden

wurde. Über temperaturabhängige NMR-Bestrahlungsexperimente konnte eine Halbwertszeit der thermischen Rückreaktion $3\mathbf{Dmp} \rightarrow 2\mathbf{Dmp}$ von 7 min ermittelt werden.

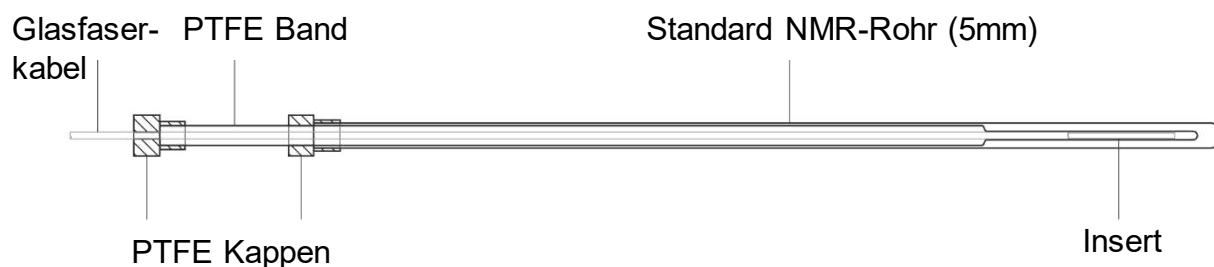


Abbildung 5. Systematischer Aufbau des Coaxial-Insert-NMR-Rohrs für Messungen unter Bestrahlung.

Die Strukturaufklärung von $2\mathbf{Dmp}$ erfolgte durch Röntgeneinkristallstrukturanalyse. Durch das Vermessen von tiefblauen Einkristallen bei Raumtemperatur im Dunkeln konnte eine vollständige Strukturaufklärung von $2\mathbf{Dmp}$ durchgeführt werden. Für das Hausanderivat war es nicht möglich, Kristalle zu erhalten. Eine Umwandlung des Biradikals war ebenfalls im Festkörper durch Bestrahlung mit einer roten Lampe möglich, aber die blauen Kristalle brachen dabei und waren somit ungeeignet für weitere Untersuchungen.^[57]

3 Ergebnisse und Diskussion

Zu Beginn der Promotionsarbeit lag der Fokus der Untersuchungen auf dem Biradikalsystem $[\text{P}(\mu\text{-N}^{\text{Ter}})]_2\text{DmpNC}$, welches erste interessante Ergebnisse im Zuge der Promotion von A. Hinz und der Bachelorarbeit von E. Zander lieferten.^[57,59] Dabei sollte der Anregungsprozess grundlegend untersucht und mechanistisch verstanden werden. Ebenfalls sollte der Einfluss von verschiedenen organischen Substituenten am Isonitril untersucht werden. Darüber hinaus sollten weitere Biradikalsysteme (Variation des sterisch anspruchsvollen Substituenten, Austausch von Pniktogenen, isovalenzelektronische Gruppen zum Isonitril) synthetisiert und untersucht werden.

Als zweites großes Themengebiet stand die Aktivierung weiterer kleiner Moleküle mit verschiedenen Biradikalsystemen im Vordergrund der Untersuchungen, die keine Eigenschaften eines molekularen Schalters besaßen und im Abschnitt 3.2 näher beschrieben werden.

3.1 Untersuchungen zu Molekularen Schaltern

3.1.1 Untersuchung zu $[\text{P}(\mu\text{-N}^{\text{Ter}})]_2\text{RNC}$ (R = Dmp, *t*Bu)

Die thermische Rückreaktion von $3\text{Dmp} \rightarrow 2\text{Dmp}$ wurde bereits während der Bachelorarbeit von E. Zander mittels temperaturabhängiger NMR- und UV/Vis-Spektren untersucht. Dabei konnte eine Halbwertszeit von 7 min bei Raumtemperatur ermittelt werden.^[57] Mit dem stabilen fünfgliedrigen Biradikal $[\text{P}(\mu\text{-N}^{\text{Ter}})]_2\text{DmpNC}$ (2Dmp) in der Hand sollte zunächst der Anregungsprozess genauer experimentell untersucht werden. Da Photoisomerisierungen von molekularen Schaltern häufig auf einer Zeitskala im Piko- bzw. Femtosekundenbereich (10^{-12} – 10^{-15} s) stattfinden und durch einen Zustandswechsel an einer CInt geprägt sind, war es nicht möglich, diese Prozesse mittels NMR-Spektroskopie zu untersuchen, da diese Methode eine zu niedrige Zeitauflösung besitzt.^[60,61] In Kooperation mit der Arbeitsgruppe LOCHBRUNNER konnten Anregungs-Abfrage-Experimente in Lösung mit ultrakurzen Laserpulsen durchgeführt

werden. Dazu musste zunächst der experimentelle Aufbau dahingegen verändert werden, dass Messungen unter Schutzgas möglich waren. Dazu wurden sämtliche luftdurchlässigen Steckverbindungen durch luftdichte Schraubanschlüsse ersetzt, das Durchflusszellensystem direkt in der Glovebox befüllt und anschließend in den Laserraum transportiert. Die von T. Völzer ausgewerteten transienten Spektren ergaben, dass 3 wesentliche Prozesse nach 210 fs, 1.5 ps und nach mehr als 1 ns stattfanden. Darüber hinaus konnte eine Quantenausbeute von 25 % ermittelt werden.^[62]

Mit diesen Informationen wurden weiterführende quantenchemische Rechnungen durchgeführt, wodurch die praktischen Ergebnisse interpretiert und validiert werden konnten. Mithilfe von IRC- (*Intrinsic Reaction Coordinate*) und PES- (*Relaxed Potential Energy Surface*) Scans wurden die Anregungsprozesse an einem Modellsystem (**2H** → **3H**) berechnet.

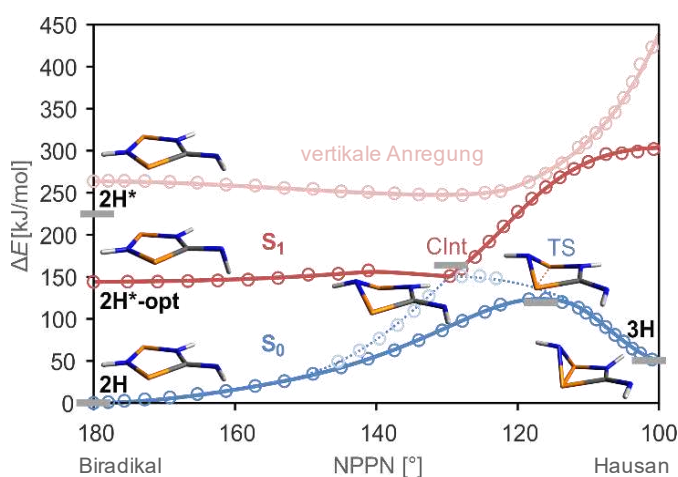


Abbildung 6. Grundzustand (S_0 , NEVPT2/CAS(2,2)/def2-TZVP) und erster angeregter Zustand (S_1 , TD-DFT/TDA PBE-D3/def2-TZVP) entlang des NPPN Diederwinkels. Die intensiven blauen und roten Linien gehören zum berechneten minimalen Energiepfad. Die hellrote Linie zeigt das vertikale Energieprofil des jeweils aus der Grundzustandsstruktur angeregten Moleküls. Die grauen Balken zeigen die Single-Point-Energien auf dem MRCI+Q/CAS(8,6)/def2-TZVP Niveau.

Die Berechnungen zeigten, dass der Energiepfad zwischen dem Biradikal **2H** und dem Hausan **3H** über einen einzigen Übergangszustand (TS, Abbildung 6, blaue Linie) verläuft. Die P–P-Bindungsbildung bzw. -brechung findet somit gleichzeitig mit der Faltung des gesamten Ringsystems entlang der P–P-Bindung (NPPN-Diederwinkel) in einem konzertierten Prozess statt. Der Energieunterschied zwischen dem lokalen Minimum **3H** und dem globalen Minimum **2H** auf der S_0 -PES des Grundzustandes beträgt $\Delta E_{\text{MRCI}} = 50.4 \text{ kJ/mol}$. Die vertikale Anregung des Biradikals **2H** (S_0 -PES) führt zu einem schwingungsangeregten Zustand **2H*** (S_1 -PES, Abbildung 6, hellrote Linie). Durch Drehung der NH-Gruppe um die C–N-Bindung ist die Minimumsstruktur des ersten angeregten Zustands (**2H*-opt**) nicht länger planar, auch wenn

die Struktur des 5-gliedrigen Ringes nahezu unverändert bleibt. Da die Energiefläche des optimierten ersten angeregten Zustandes sehr flach verläuft, kann der Übergang durch die konische Durchschneidung (**CInt**) bis hin zum Übergangszustand (**TS**) als nahezu barrierefreier Übergang angesehen werden. Ausgehend vom **TS** fallen ca. 75 % der Moleküle (exp. Quantenausbeute von 25 %) in die globale Minimumsstruktur des Biradikals **2H** zurück und 25 % werden unter Bildung einer P–P-Einfachbindung in das Hausan umgewandelt. Die Bildung der σ -Bindung zwischen den beiden Phosphoratomen erfolgt durch einen photochemischen, disrotatorischen Ringschlussmechanismus. Wiederrum erfolgt die Rückreaktion **3H** \rightarrow **2H** über symmetrieverbotene thermische disrotatorische Ringöffnungsreaktion, wodurch die relativ geringe Halbwertszeit von 7 min begründet werden kann. Da die Struktur der Moleküle an den stationären Punkten durch das Modellsystem bekannt waren, wurden ergänzende Rechnungen an dem realen System **2Dmp** \rightarrow **3Dmp** durchgeführt, deren Ergebnisse (Abbildung 6, graue Balken) sehr gut mit dem Modellsystem übereinstimmen. Die in Abbildung 6 gezeigten minimalen Reaktionspfade sind eine sehr vereinfachte Darstellung des Mechanismus, da lediglich der NPPN–Diederwinkel berücksichtigt wurde. Während der Anregungsprozesses spielen weitere strukturelle Veränderungen wie z.B. Verringerung des P–P-Abstands, Rotation um die C–N Bindung am Isonitril und Abwinklung des organischen Substituenten eine wichtige Rolle. Da für jede Veränderung in einem Diagramm eine neue Achse hinzukommen würde, ist eine grafische Darstellung nicht möglich, da es ein Problem n -ter Ordnung ist (siehe Supporting der Publikation Kapitel 6.2).

Nachdem der Anregungsprozess von **2Dmp** \rightarrow **3Dmp** verstanden wurde, sollten andere Systeme hinsichtlich der thermischen Rückreaktion und deren Beeinflussung untersucht werden. Bereits Alexander Hinz setzte **1Ter** mit CN–*t*Bu um und konnte dabei die Adduktspezies **4*t*Bu*t*Bu** aus einer Benzollösung isolieren.^[27] Im Zuge dieser Arbeit konnte ebenfalls von der grünen Lösung der aufgelösten farblosen Kristalle von **4*t*Bu*t*Bu** ein Gleichgewicht im $^{31}\text{P}\{^1\text{H}\}$ -NMR-Spektrum (Abbildung 7. $^{31}\text{P}\{^1\text{H}\}$ -NMR-Spektren von aufgelösten Kristallen von **4*t*Bu*t*Bu**.) zwischen **1Ter**, **3*t*Bu** und **4*t*Bu*t*Bu** beobachtet werden. Unter Bestrahlung konnte das Gleichgewicht vollständig auf die Seite des Hausan-Isomers verschoben werden (Abbildung 7, $t = 0$ min). Nachdem das Gleichgewicht sich wieder einstellte ($t = 240$ min), konnte das Ausgangsspektrum beobachtet werden. Der Anregungsprozess konnte durch wiederholtes Bestrahlen der gleichen Lösung im NMR-Rohr mehrmals wiederholt werden und somit konnte die Reversibilität des Gleichgewichtes bestätigt werden.

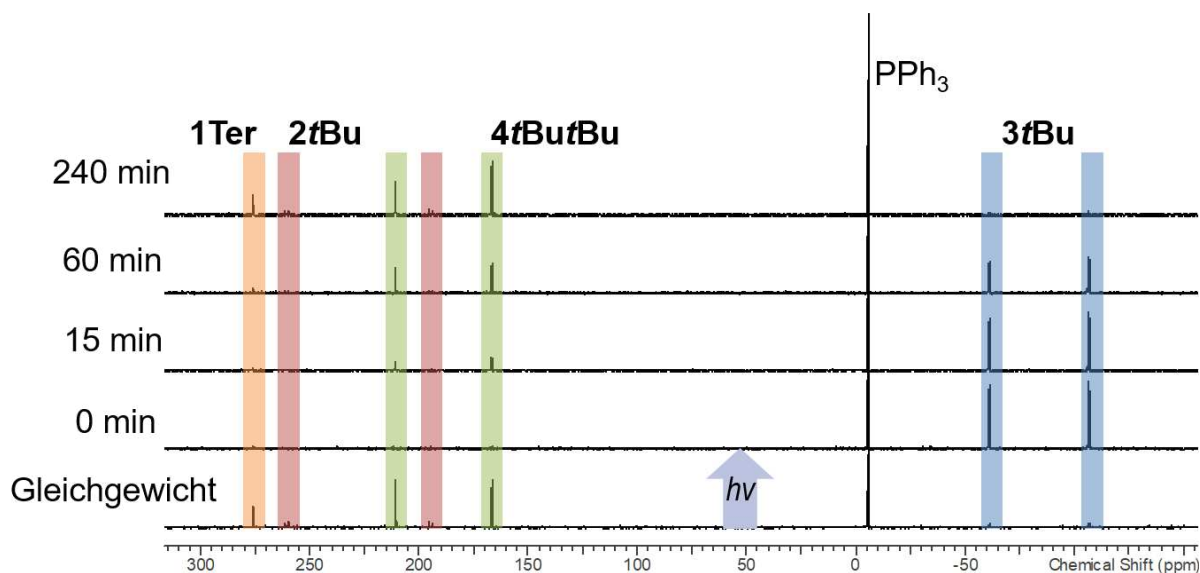
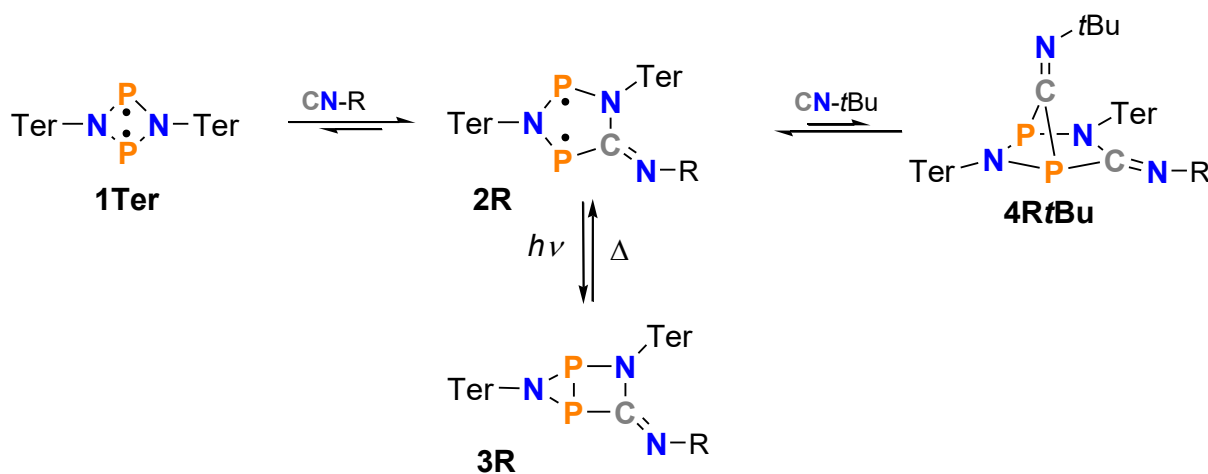


Abbildung 7. $^{31}\text{P}\{^1\text{H}\}$ -NMR-Spektren von aufgelösten Kristallen von **4tBuBu**.

Im Falle des gemischten Isomers **4DmpBu** konnte beobachtet werden, dass **2Dmp** im Verhältnis 1:1 mit $\text{CN-}t\text{Bu}$ nur zu sehr geringen Teil zum Addukt umgewandelt wurde (<10 %). Eine Kristallisation von **4DmpBu** aus aromatischen Lösungsmitteln war nicht möglich. Daher wurde **2Dmp** mit einem großen Überschuss an $\text{CN-}t\text{Bu}$ umgesetzt, sodass das Isonitril gleichzeitig als Reaktant und Lösungsmittel fungierte. Auf diesem Wege konnte **4DmpBu** aus einer gesättigten $\text{CN-}t\text{Bu}$ -Lösung bei $-20\text{ }^\circ\text{C}$ kristallisiert werden (Abbildung 8).^[63]



Schema 9. Gleichgewichtsreaktion von **1Ter** mit verschiedenen Isonitrilen ($\text{R} = \text{Dmp}, t\text{Bu}$).

Temperaturabhängige NMR-Untersuchungen von **3Dmp** \rightarrow **2Dmp** in Anwesenheit von $\text{CN-}t\text{Bu}$ ergaben, dass die Geschwindigkeit der Rückreaktion ($\tau_{1/2} = 7\text{ min}$ ohne $\text{CN-}t\text{Bu}$) um mehrere Größenordnungen deutlich beschleunigt wurde. Im Verhältnis 1:1 (**2Dmp**: $\text{CN-}t\text{Bu}$)

bei $-20\text{ }^{\circ}\text{C}$ verlief die Rückreaktion $3\text{Dmp} \rightarrow 2\text{Dmp}$ und die anschließende Adduktbildung bereits sehr schnell (Abbildung 9 B, links). Eine Temperaturerniedrigung auf $-30\text{ }^{\circ}\text{C}$ und der gleichzeitigen Erhöhung des $\text{CN-}t\text{Bu}$ Anteils auf 10 Äq. beschleunigte die thermische Rückreaktion sogar noch weiter (Abbildung 9 B, rechts). Das thermische Gleichgewicht von $2\text{Dmp} \rightarrow 4\text{Dmp}t\text{Bu}$ wurde somit deutlich von der Kinetik der photochemischen Hin- und der thermischen Rückreaktion von $3\text{Dmp} \rightarrow 2\text{Dmp}$ beeinflusst.

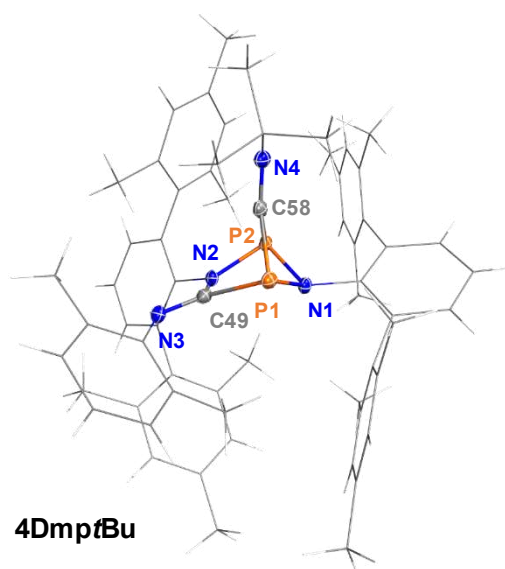


Abbildung 8. Molekülstruktur von $4\text{Dmp}t\text{Bu}$ im Einkristall. Thermische Ellipsoide entsprechen 50 % Wahrscheinlichkeit bei 123 K.

Quantenchemische Rechnungen zeigten, dass ein minimaler Energiepfad über eine offenkettige Spezies $5\text{Dmp}t\text{Bu}$ möglich ist und energetisch niedriger liegt als eine direkte P–P-Bindungsspaltung von 3Dmp . Dabei erfolgte ein nukleophiler Angriff des freien $\text{CN-}t\text{Bu}$ an das Stickstoffatom (PNP) von 3Dmp , sodass die P–N-Bindung gespalten wurde und das kurzlebige Intermediat $5\text{Dmp}t\text{Bu}$ entstand. Eine Rotation um die P–C-Bindung (CPCN) und eine erneute Bildung einer P–N-Bindung (CPNP) führte zum Biradikal 2Dmp und freiem Isonitril. Die anschließende Reaktion von 2Dmp mit $\text{CN-}t\text{Bu}$ führte zum energetischen Minimum $4\text{Dmp}t\text{Bu}$ ($\Delta G^{\circ} = 7.2\text{ kJ/mol}$ (DLPNO-CCSD(T)/def2-TZVP//UPBE-D3/def2-SVP, $c^{\circ} = 1\text{ mol L}^{-1}$), $3\text{Dmp} \rightarrow 4\text{Dmp}t\text{Bu}$; Abbildung 9 A).

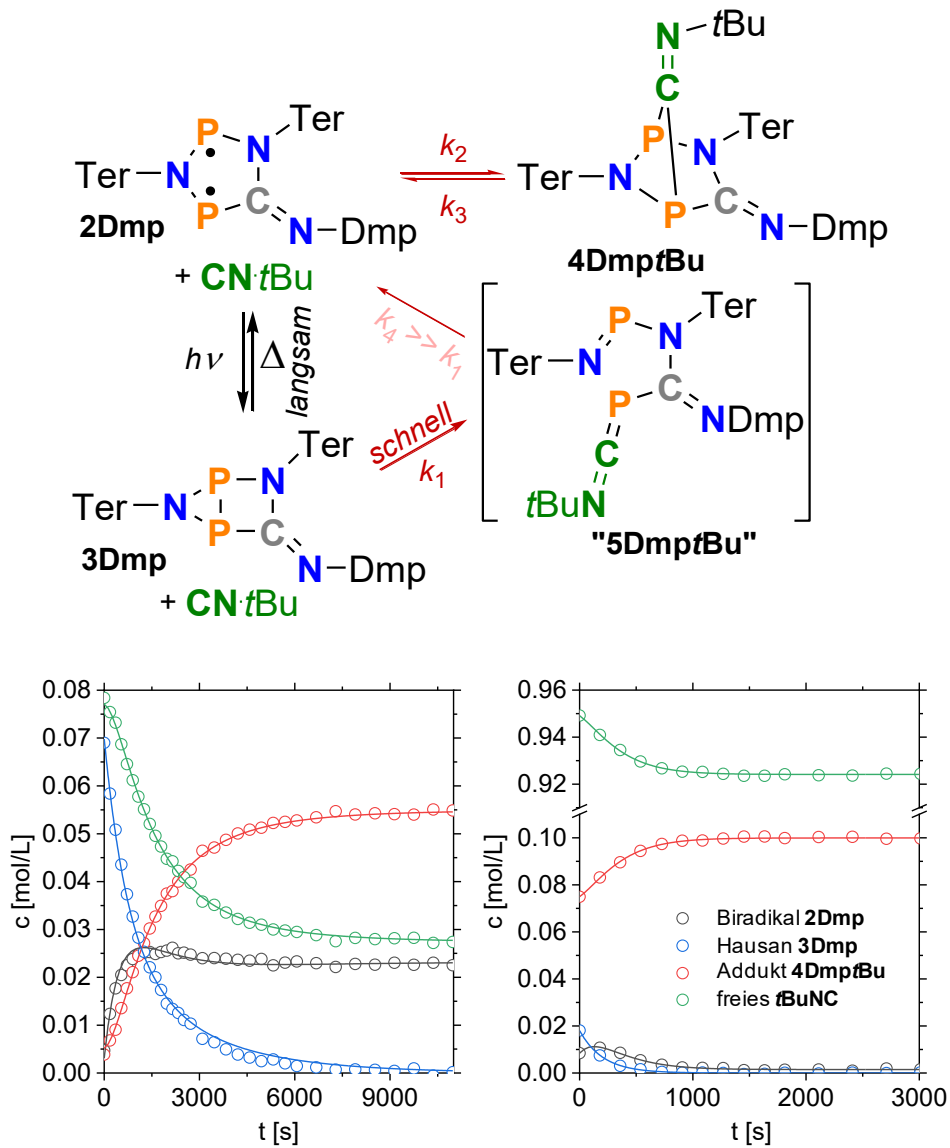
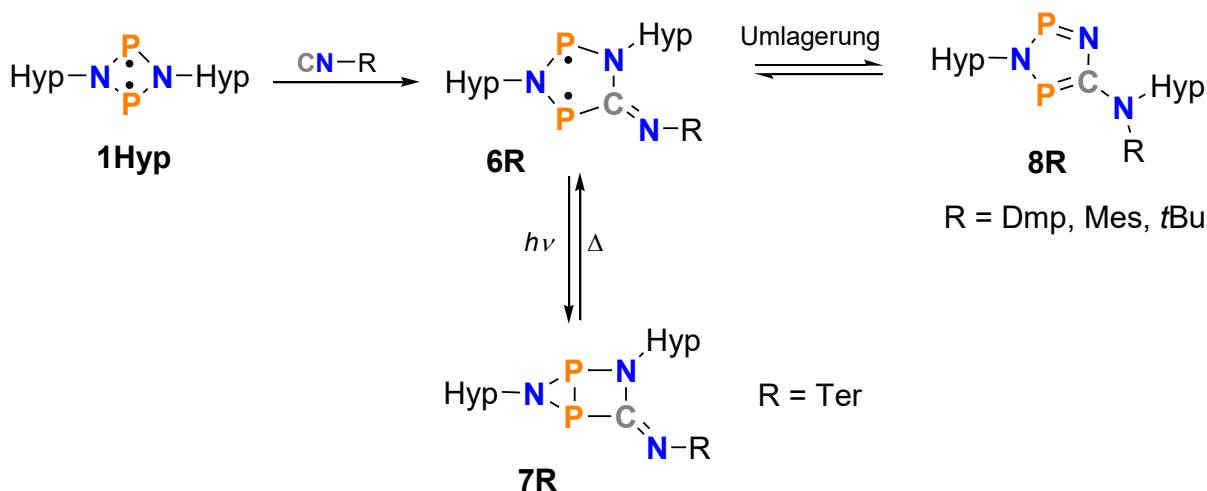


Abbildung 9. Oben: Schematische Darstellung der CN-tBu-katalysierten Rückreaktion von **3Dmp** \rightarrow **2Dmp** über einen offenkettigen Mechanismus **5DmptBu**. Unten: Zeitabhängiger Konzentrationsverlauf der Verbindungen **2Dmp**, **3Dmp** und **4DmptBu** aus den Integralen der $^{31}\text{P}\{^1\text{H}\}$ -NMR-Spektren. (links: -20°C , 1 Äq. CN-tBu; rechts: -30°C , 10 Äq. CN-tBu).

3.1.2 Variation des sterisch anspruchsvollen Substituenten am Ring

Bereits im Jahre 2016 führte Anne-Kristin Rölke im Rahmen ihrer Promotionsarbeit zahlreiche Versuche mit dem Biradikal **1Hyp** durch, welche im Zuge meiner Arbeit weitergeführt und vervollständigt wurden.^[64,65]



Schema 10. Reaktion von **1Hyp** mit verschiedenen Isonitrilen. Im Falle von $\text{R} = \text{Dmp, Mes, } t\text{Bu}$ konnte eine Umlagerungsreaktion eines Hypersilyl-Substituenten an das exozyklische Stickstoffatom beobachtet werden. Die gebildeten Heterocyclopentadiene sind gelb. Für CN-Ter konnte keine Umlagerungsreaktion beobachtet werden und das blaue Heterocyclopentandiyl (**6Ter**) wies Eigenschaften eines molekularen Schalters auf.

1Hyp wurde mit verschiedenen Isonitrilen CN-R ($\text{R} = \text{Dmp, Mes, } t\text{Bu, Ter}$) umgesetzt. Dabei konnte im Falle von CN-Ter (**6Ter**) eine blaue Lösung erhalten werden, welche ebenfalls wie die im Kapitel 3.1.1 beschriebenen Verbindungen Eigenschaften eines molekularen Schalters besaß und mittels zeit- und temperaturabhängiger $^{31}\text{P}\{^1\text{H}\}$ -NMR-Spektren untersucht werden konnte. Interessanterweise konnte im Falle der sterisch weniger anspruchsvollen Isonitrile ($\text{R} = \text{Dmp, Mes, } t\text{Bu}$, Abbildung 10) eine gelbe Lösung beobachtet werden. Mithilfe von Röntgeneinkristallstrukturanalyse konnten die Verbindungen untersucht werden. Dabei konnte eine Wanderung des Hypersilylsubstituenten vom Ringstickstoffatom an das exozyklische Stickstoffatom beobachtet werden (Schema 10). Quantenmechanische Rechnungen zeigten, dass im Fall der weniger sterisch anspruchsvollen Isonitrile ein deutlicher Energiegewinn aus der Migration resultierte ($\Delta G^\circ = -62.1 \text{ kJ/mol}$ (**6Dmp** \rightarrow **8Dmp**), -62.7 kJ/mol (**6Mes** \rightarrow **8Mes**), -29.5 kJ/mol (**6tBu** \rightarrow **8tBu**); DLPNO-CCSD(T)/def2-TZVP//UPBE-D3/def2-SVP). Die Umlagerungsreaktion **6Ter** \rightarrow **8Ter** ist hingegen mit $\Delta G^\circ = +25.8 \text{ kJ/mol}$ deutlich endergonisch und lief daher nicht ab.

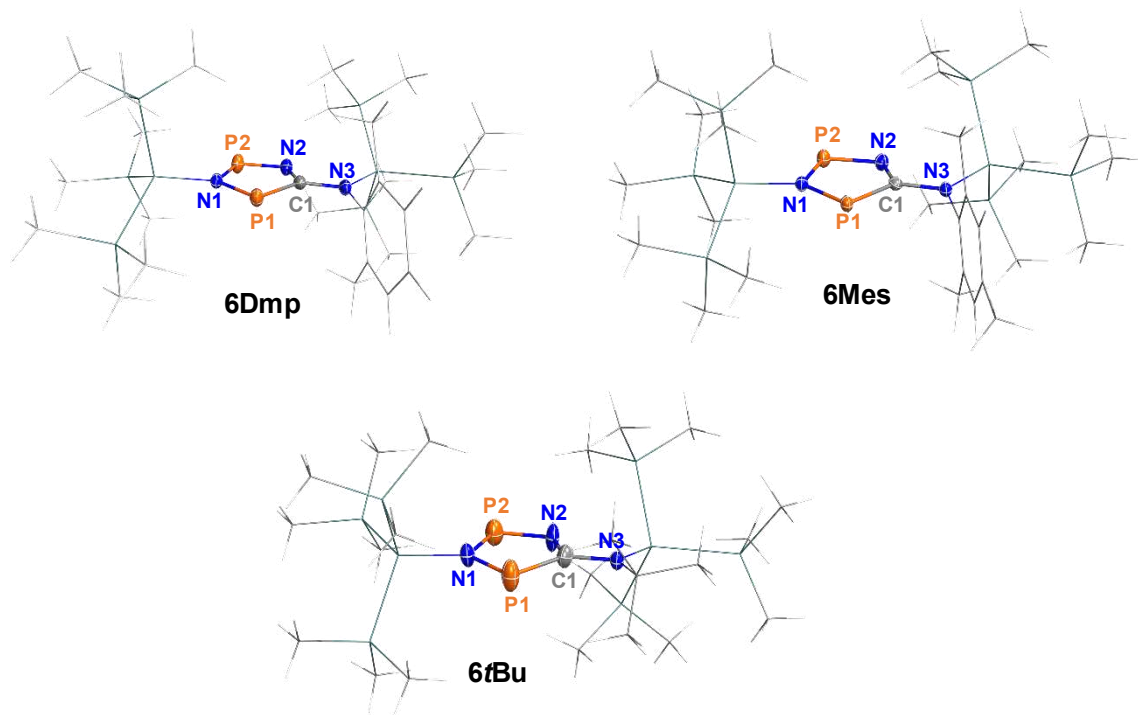
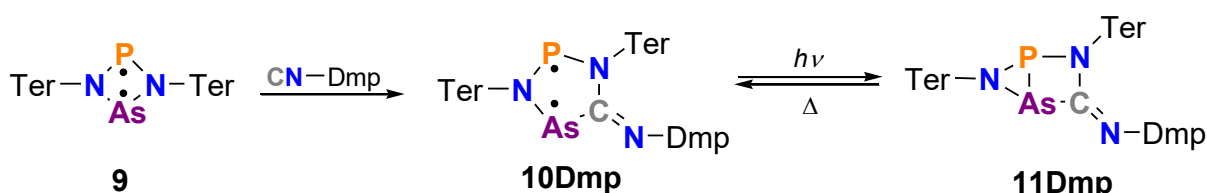


Abbildung 10. Molekülstrukturen der Heterocyclopentadiene **6Dmp**, **6Mes** und **6tBu** im Einkristall. Thermische Ellipsoide entsprechen 50 % Wahrscheinlichkeit bei 123 K. Die Verbindungen **6Dmp** und **6Mes** wurden bereits von Anne-Kristin Rölke synthetisiert und werden der Vollständigkeit nochmals mit aufgeführt.

3.1.3 Variation des Pniktogens

Nachdem im Kapitel 3.1.3 der organische Substituent am zentralen viergliedrigen Ring variiert wurde, sollte zunächst ein Phosphoratom gegen ein Arsenatom ausgetauscht werden und hinsichtlich der Eigenschaften eines molekularen Schalters überprüft werden. Bereits 2016 konnte Alexander Hinz erste Reaktionen mit dem gemischten Gruppe-15-Biradikal (**9**) durchführen und CN–Dmp aktivieren (Schema 11). Das 5-gliedrige Biradikal (**10Dmp**) konnte durch UV-Licht zum Hausanisomer (**11Dmp**) umgewandelt werden. Weiterführende Untersuchungen erfolgten nicht.



Schema 11. Reaktion des gemischten Biradikals **9** mit DmpNC.

Die praktischen Arbeiten zu diesem Themengebiet wurden zum Ende der Dissertation nahezu fertiggestellt, konnten aber aus Zeitgründen noch nicht publiziert werden. Der Vollständigkeit halber werden die Ergebnisse zum Teil hier mit aufgeführt.

Das Biradikal **9** wurde mit verschiedenen Isonitrilen CN–R (R = Dmp, Mes, Mtp, *t*Bu) umgesetzt. Im Falle des CN–*t*Bu konnte, wie für das PP-Biradikal **1Ter**, ausschließlich das überbrückte Addukt isoliert werden. Alle Produkte aus der Reaktion von **9** mit aromatisch substituierten Isonitrilen konnten, bis auf **10Mtp**, kristallisiert werden. Die grünen Biradikale (**10**) konnten in Lösung durch Bestrahlung bei Temperaturen unter -40 °C im $^{31}\text{P}\{^1\text{H}\}$ -NMR-Spektrum teilweise zum Hausan (**11**) umgewandelt werden. Interessanterweise konnten die Verbindungen **10Dmp** und **10Mes** auch im Kristall zum Hausanisomer geschaltet werden, ohne dass der Kristall zerbrach. Für die Biradikalstrukturen **10Dmp** und **10Mes** wurden die Einkristalle bei RT unter Ausschluss von Licht auf dem Röntgendiffraktometer gemountet, auf -150 °C abgekühlt und die Messung durchgeführt. Anschließend wurden die Einkristalle direkt auf dem Röntgendiffraktometer bei -150 °C mit einer Taschenlampe bestrahlt und erneut eine Messung durchgeführt, um die Molekülstruktur für das Hausanisomer **11** zu erhalten. So konnten aus einem Einkristall zwei Molekülstrukturen (Einkristall-zu-Einkristall-Isomerisierung) gewonnen werden und die Struktur des Hausans (P–As-Bindungsbildung unter Bestrahlung) bestätigt werden (Abbildung 11). Werden die aromatischen Isonitrile im Überschuss eingesetzt, (10- bis 15-facher Überschuss) so konnten die überbrückten

Verbindungen **12** (Abbildung 11) beobachtet werden. Im Falle von CN–Mtp war es möglich das Addukt **12Mtp** aus der Gleichgewichtsreaktion zu kristallisieren.

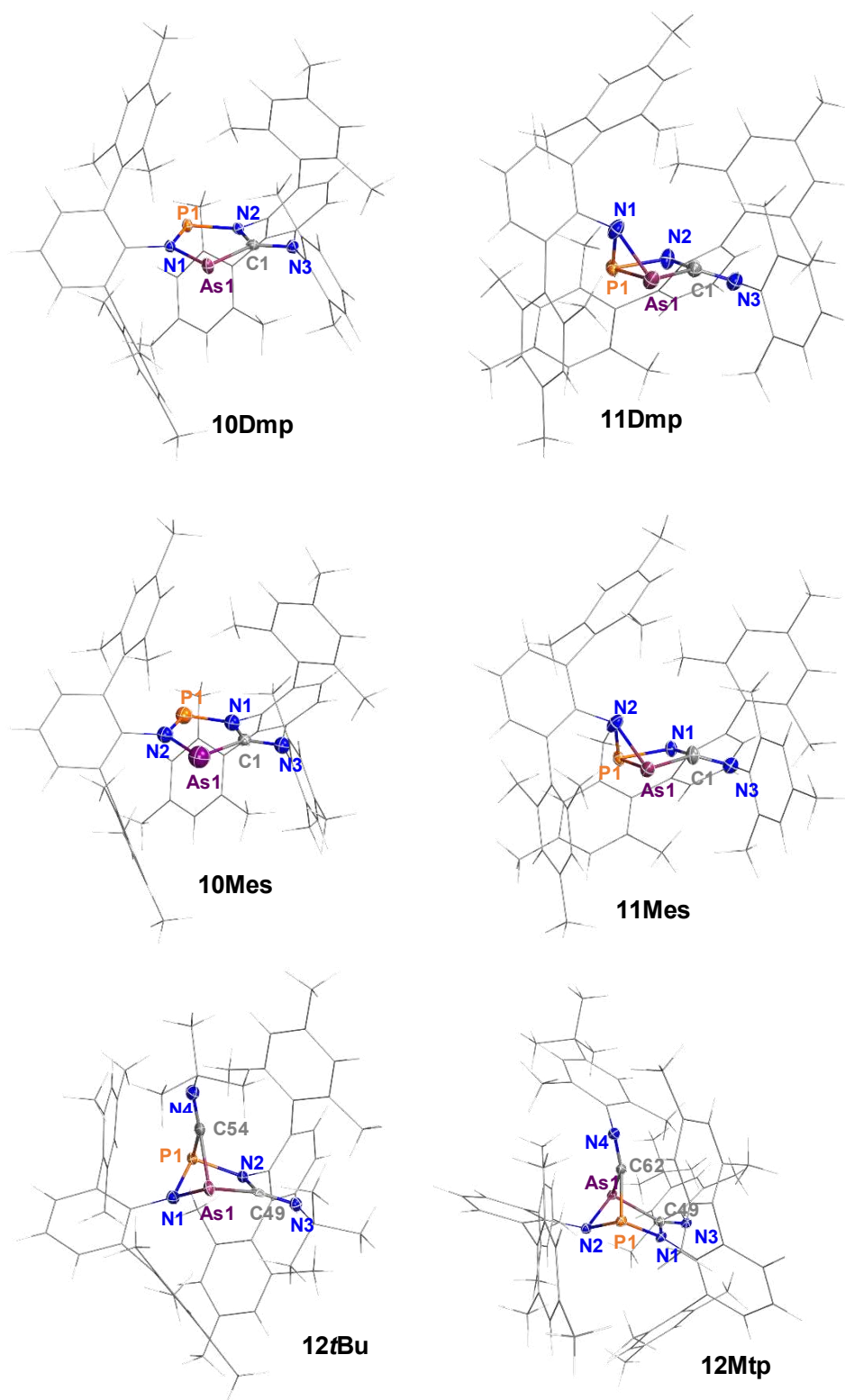
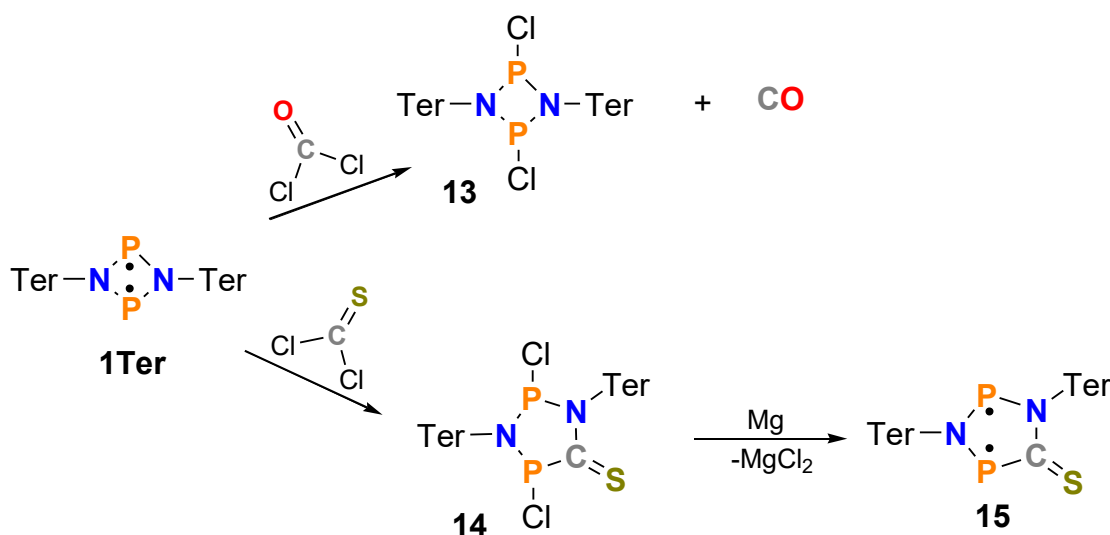


Abbildung 11. Molekülstrukturen der Verbindungen **10Dmp**, **11Dmp**, **10Mes**, **10Mes**, **12fBu** und **12Mtp** im Einkristall. Thermische Ellipsoide entsprechen 50 % Wahrscheinlichkeit bei 123 K. Die Isonitrile inserieren selektiv in die As–N-Bindung des Biradikals **9**.

3.1.4 Thiocarbonyl als Isonitril-Ersatz

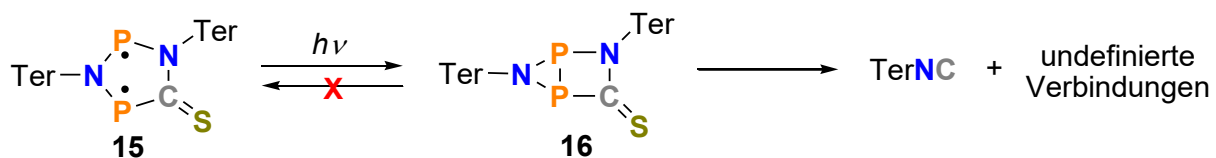
Nachdem in den vorherigen Kapiteln der sterisch anspruchsvolle Substituent (Ter zu Hyp) und ein Pniktogen (P→As) am zentralen viergliedrigen ausgetauscht wurde, sollte versucht werden die Isonitrilgruppe durch die isovalenzelektronische CS-Einheit zu substituieren. Aus der Literatur ist bekannt, dass reines CS sehr reaktiv ist und rasch zu undefinierten (CS)_n Produkten polymerisiert. CS kann im Labormaßstab durch großen präparativen Aufwand z.B. photochemisch, thermisch oder elektrochemisch aus CS₂ hergestellt werden.^[66–69]

NMR-Experimente zeigten, dass **1Ter** (orange) durch Phosgen chloriert und gasförmiges CO freigesetzt wurde, welches nicht weiter mit **13** (hellgelb) reagierte. Die gleiche Reaktion von **1Ter** wurde mit Thiophosgen wiederholt (Schema 12). Interessanterweise konnte in diesem Fall ein Farbumschlag von orange nach hellbraun festgestellt werden und die chlorierte fünfgliedrige Spezies (**14**) mit einer insertierten CS-Einheit kristallisiert werden.^[70] Reduktionsversuche von **14** mit elementarem Magnesium zeigten eine Blaufärbung der Lösung (**15**) ähnlich dem in Kapitel 3.1.1 diskutierten fünfgliedrigen Biradikal **2Dmp**.



Schema 12. Reaktion von **1Ter** mit Phosgen und Thiophosgen und Reduktion von **14** mit elementarem Magnesium zum neuen fünfgliedrigen Biradikal (**15**).

Eine Kristallisation von **15** war nicht möglich, da die Lösung bei RT sich sehr schnell entfärbte. In diversen Kristallisationsversuchen konnte CN–Ter als Zersetzungsprodukt isoliert werden. Bestrahlungsexperimente zeigten, dass eine Umwandlung zum Hausan möglich, aber keine Rückreaktion zu beobachten war. Weitere Untersuchungen deuteten darauf hin, dass Verbindung **16** instabil ist und sich unter Einwirkung von Licht zu CN–Ter und undefinierten Phosphorverbindungen zersetzte (Schema 13).



Schema 13. Hausanisomerisierung von Biradikal **15**. Anschließende Zersetzung vom Hausan **16** zu CN–Ter und undefinierten Phosphorverbindungen.

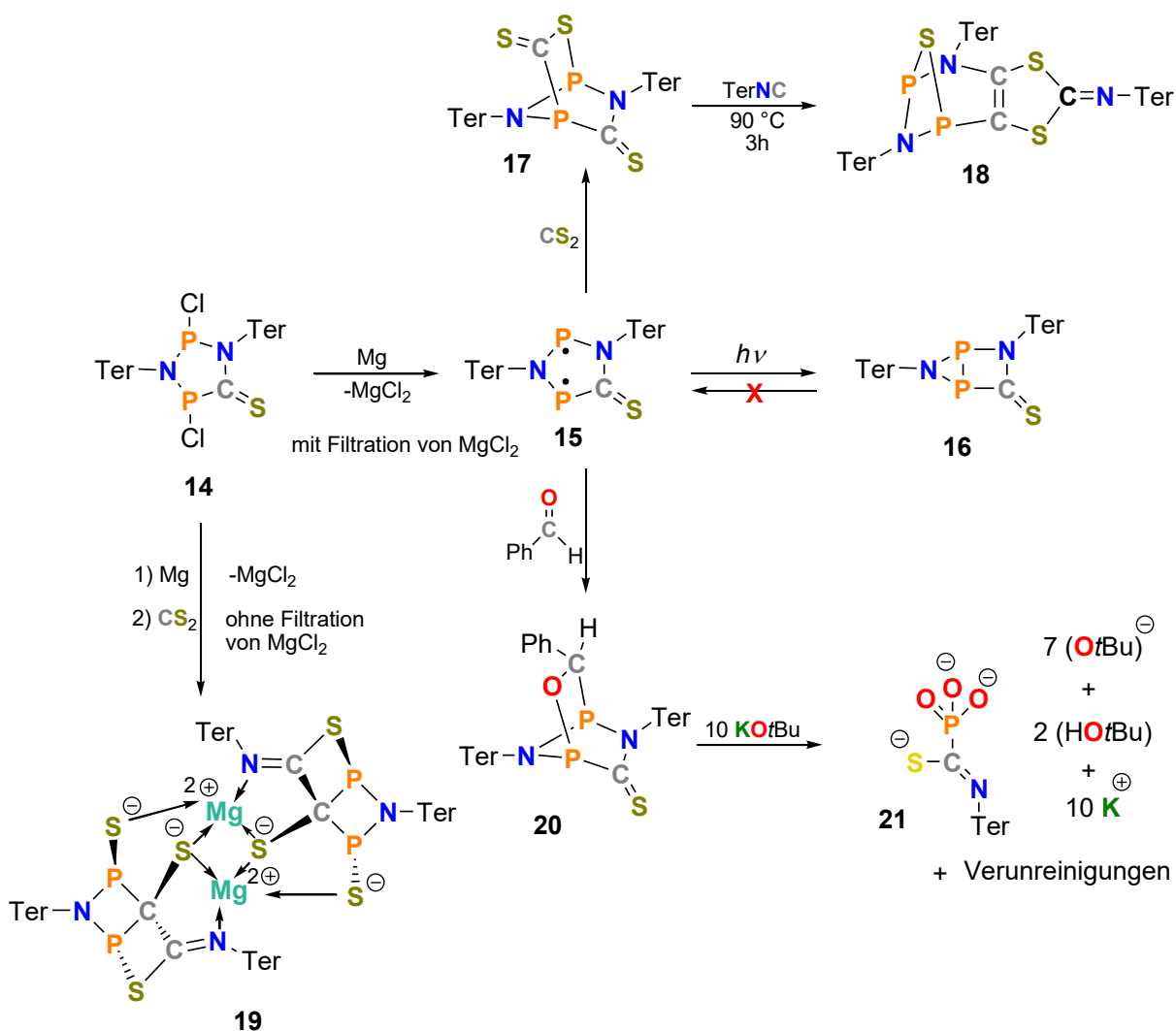
Quantenmechanische Rechnungen (CASSCF(8,6)/def2-TZVP) belegten, dass das fünfgliedrige Biradikal **15** lediglich einen Biradikalcharakter von 13 % besitzt, welcher deutlich niedriger ist als der von Verbindung **2Dmp** ($\beta = 28\%$)^[71,72]. Da eine Isolierung von **15** nicht möglich war, wurden als Strukturbeweis Abfangreaktionen durchgeführt, welche im Kapitel 3.2.1 diskutiert werden.

3.2 Aktivierung kleiner Moleküle

Dieses Kapitel befasst sich mit der Aktivierung kleiner Moleküle durch verschiedene Biradikale, deren Produkte keine Eigenschaften eines molekularen Schalters besitzen.

3.2.1 Reaktion von $[P(\mu\text{-N}Ter)]_2CS$ (**15**) mit Abfangreagenzien

Das photoinstabile Biradikal **15** konnte durch Reduktion unter Ausschluss von Licht in ca. 90 prozentiger Reinheit ($^{31}P\{^1H\}$ -NMR-Spektrum) hergestellt werden. Das Produkt ist als Feststoff bei Temperaturen von $-20\text{ }^\circ\text{C}$ kurzzeitig (ca. 5 Tage) lagerbar.



Schema 14. Übersicht der Reaktion von **15** mit verschiedenen Abfangreagenzien und deren Folgereaktionen.

Aufgrund des niedrigeren Biradikalcharakters reagierte **15** mit typischen Abfangreagenzien wie BTMSA, CN-R (R = Dmp, *t*Bu), Selen und Tolan nicht. Mit CS₂ und Benzaldehyd konnten die entsprechenden [2.2.1] bicyclischen Additionsprodukte (**17**, **20**) aus einer frisch von Mg und MgCl₂ filtrierten Lösung von **15** synthetisiert und kristallisiert werden (Abbildung 12). Wird CS₂ direkt zur Reaktionslösung der Reduktion zugegeben, entsteht ein dimerer Mg(II)-Komplex, wobei jedes Mg(II)-Ion von drei Schwefel- und einem iminischen Stickstoffatom umgeben ist. Bei höheren Temperaturen um 90 °C reagierte **17** mit einem, bei der Zersetzung von **16** freigewordenen, Äq. CN-Ter zu Verbindung **18**. Bei der versuchten Deprotonierung von **20** konnte ein komplexes Salz (**21**) hergestellt werden (Schema 14).

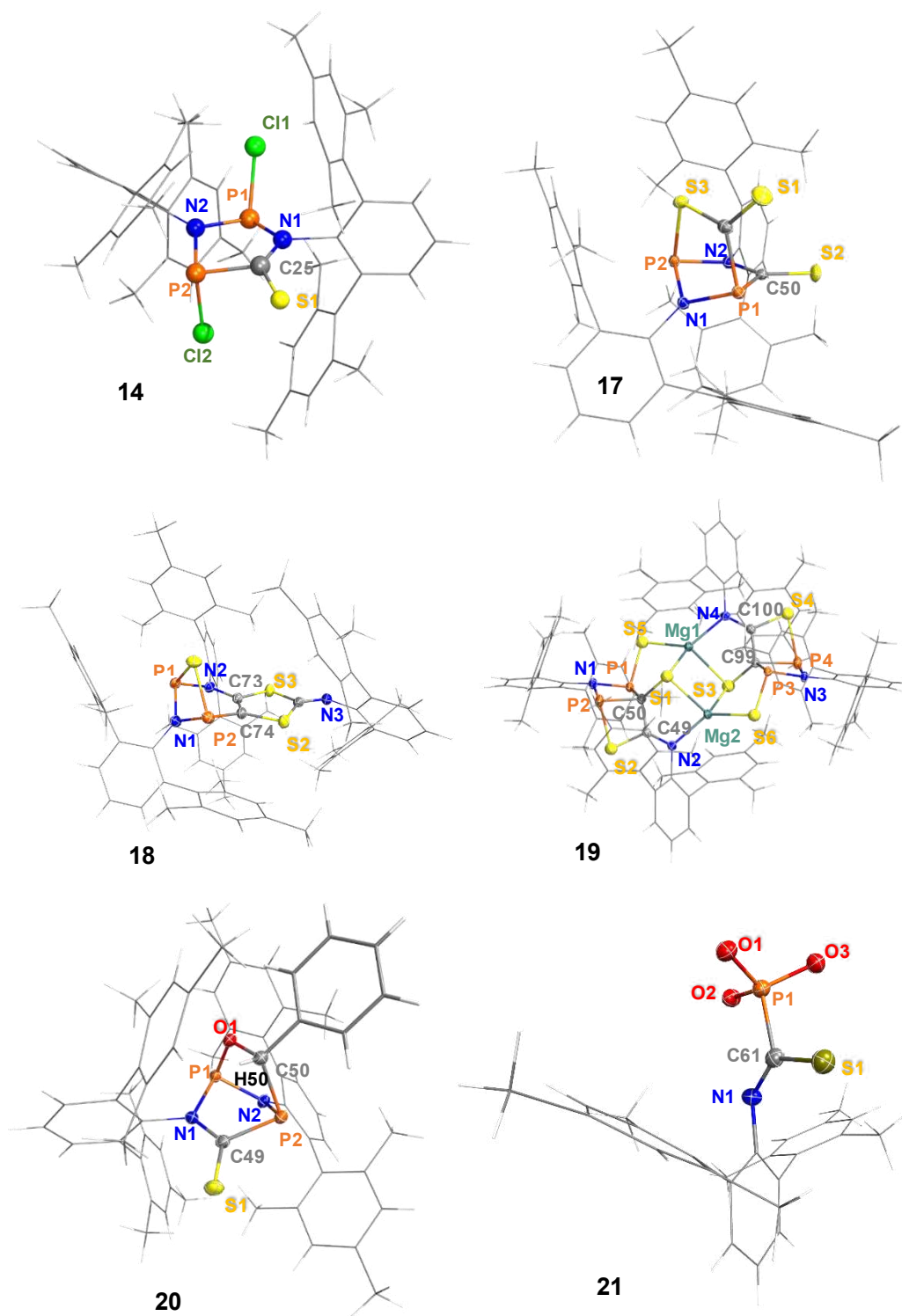
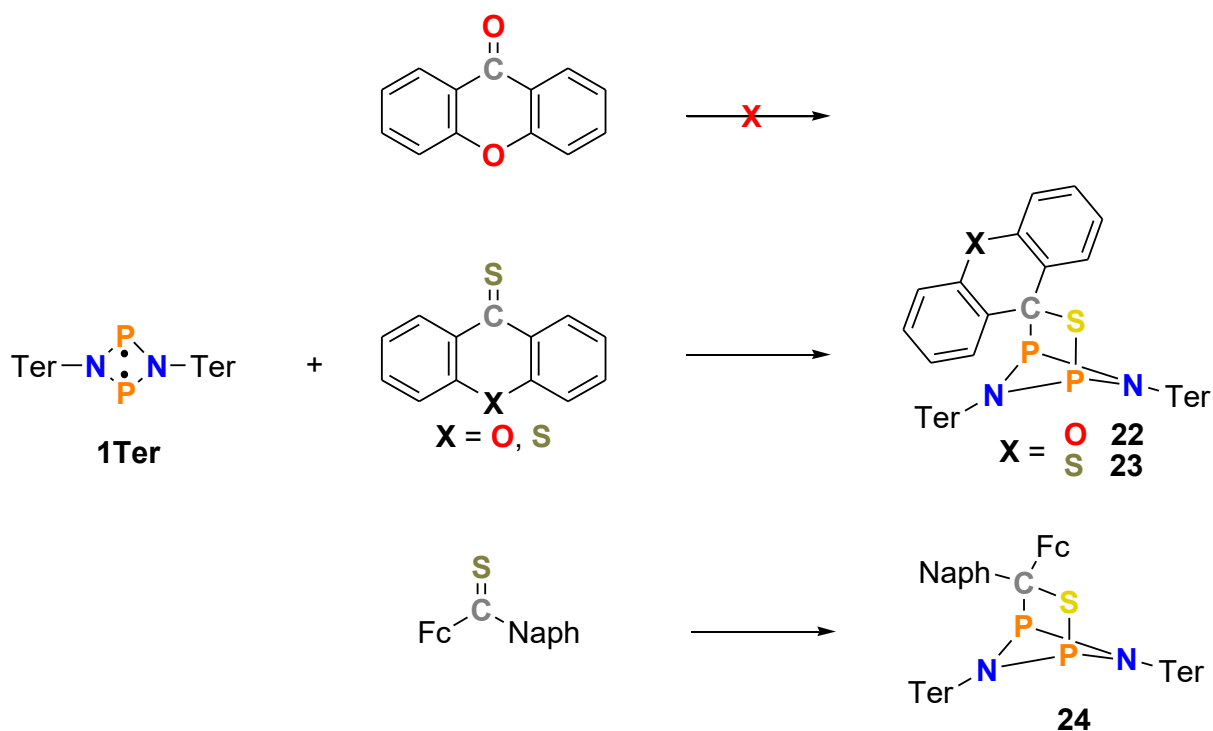


Abbildung 12. Molekülstrukturen von **14** (Konnektivitätsbeweis), der Additionsprodukte von **15** mit CS_2 (**17**) und PhCO(H) (**20**) und deren Folgeprodukte (**18**, **19**, **21**) im Einkristall. Der Übersichtlichkeit wurde für Verbindung **21** lediglich die zentrale Einheit abgebildet. Die Kaliumatome und ((H)OtBu)-Einheiten ordnen sich halbkugelförmig über den Sauerstoffatomen an, wobei jedes Kaliumatom mit 2 bis 4 ((H)OtBu)-Einheiten wechselwirkt. Thermische Ellipsoide entsprechen 50 % Wahrscheinlichkeit bei 123 K. Durch die Isolierung der Additionsprodukte (**17**, **20**) konnte die postulierte und berechnete Struktur des Biradikals (**15**) nachgewiesen werden.

3.2.2 Reaktion von $[P(\mu\text{-N}Ter)]_2$ (**1Ter**) mit Thioketonen

In den vergangenen Jahren wurden mit dem Biradikal (**1Ter**) bis auf ein CS_2 -Addukt keine C=S-Doppelbindungen aktiviert und deren Additionsprodukte untersucht.^[28] In Kooperation mit Prof. Mlostoń von der Universität Łódź wurden uns 3 Thioketone (9*H*-xanthene-9-thione, 9*H*-Thioxanthene-9-Thion, Fc-β-Naphtyl-Thioketon) zur Verfügung gestellt (Schema 15). Diese wurden mit **1Ter** umgesetzt und es konnten die entsprechenden [2.1.1] bicyclischen Verbindungen (**22**, **23**, **24**) isoliert und kristallisiert werden (Abbildung 13). Da bereits einige Produkte von C=O-Doppelbindungsaktivierungen (CO, CO₂, (CH₃)₂C=O, PhCO(H)) bekannt waren, wurde zusätzlich zu den Thioketonen Xanthon mit **1Ter** umgesetzt. Jedoch konnte in verschiedenen Lösungsmitteln, verschiedenen Temperaturen und mit bis zu 20-fachen Überschuss keine Reaktion beobachtet werden. Quantenchemische Rechnungen (DLPNO-CCSD(T)/def2-TZVP//PBE-D3/def2-TZVP) zeigten, dass die Reaktionen von **1Ter** mit Thioketonen exergonisch ($\Delta_R G_{Toluol}^\circ = -30.0$ (**22**); -41.0 (**23**); -51.3 (**24**) kJ/mol) verläuft. Im Gegensatz dazu ist die Reaktion mit Xanthon aufgrund der sterischen Hinderung des organischen Rückgrates und der kürzeren und stabileren C=O-Doppelbindung ($\Sigma r_{cov}(C=O) = 1.24 \text{ \AA}$; $\Sigma r_{cov}(C=S) = 1.61 \text{ \AA}$)^[73] endergonisch ($\Delta_R G_{Toluol}^\circ = +14.2$ kJ/mol).^[74]



Schema 15. Reaktion von **1Ter** mit Xanthon (keine Reaktion) und verschiedenen Thioketonen zu [2.1.1] bicyclischen Verbindungen.

Hochtemperatur-NMR-Experimente von Verbindung **22** und **23** zeigten, dass die Additionsprodukte thermisch instabil sind und eine reversible Abspaltung der Thioketone oberhalb von 60 °C stattfand.

Der Versuch, die aktivierte C–S-Bindung von **22** mit gasförmigen Wasserstoff umzusetzen, um den entsprechende Thioalkohol herzustellen, war nicht erfolgreich. Eine Umsetzung von **22** mit Wasserstoff lieferte das bekannte Wasserstoffaddukt von **1Ter** ($[\text{HP}(\mu\text{-NTer})_2]$) und das Thioketon.

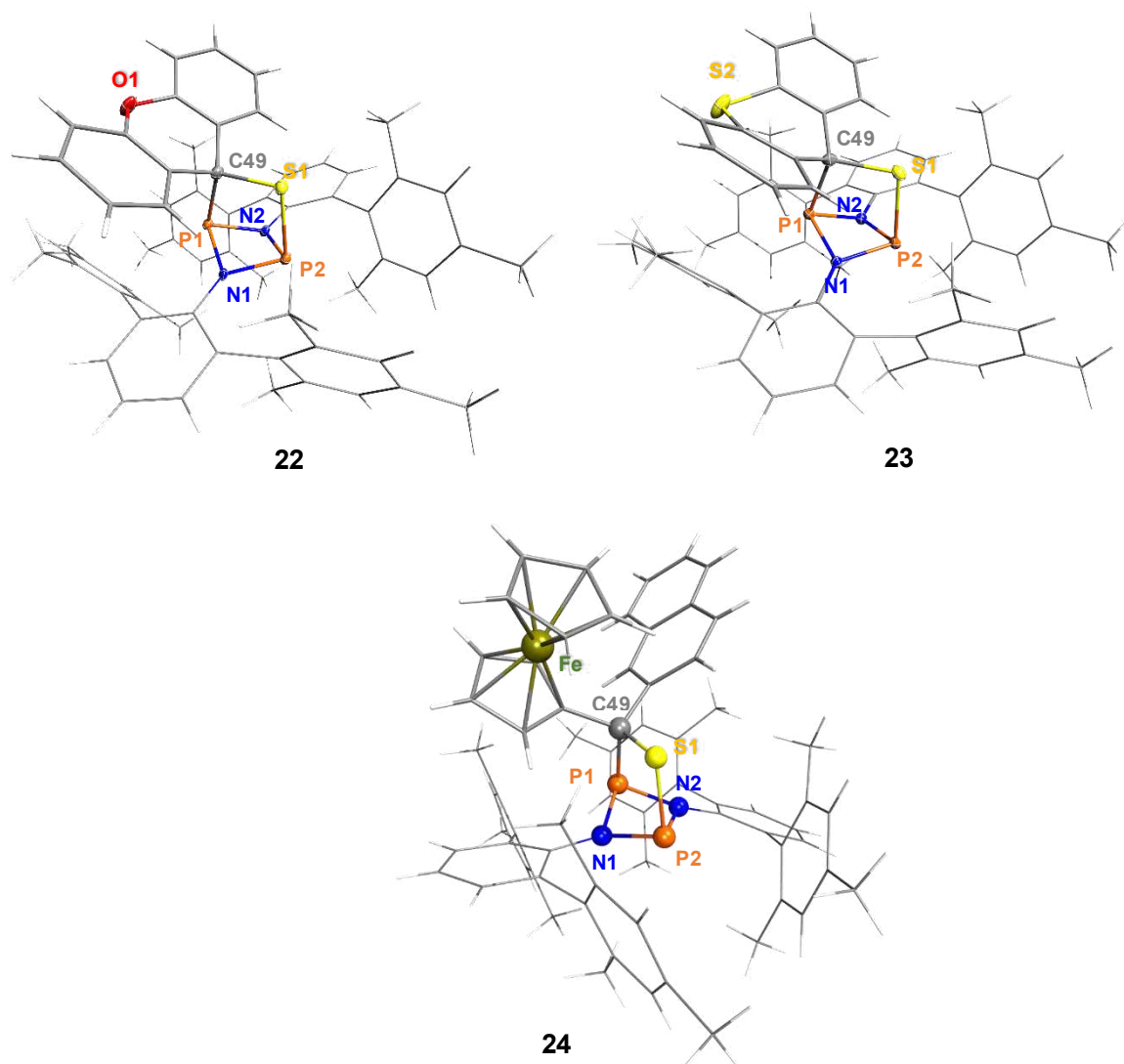
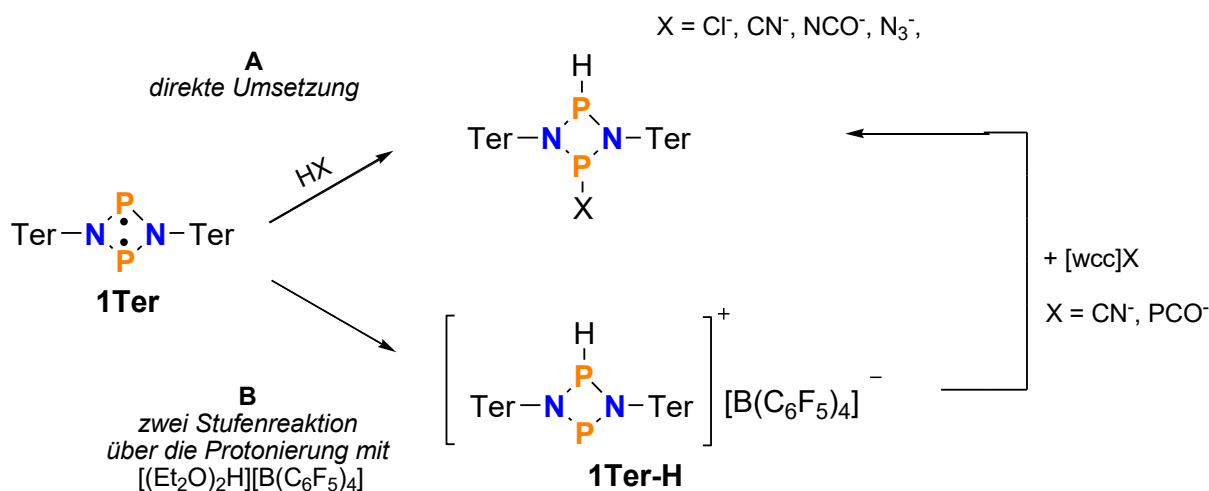


Abbildung 13. Molekülstrukturen von **22** und **23** im Einkristall. Thermische Ellipsoide entsprechen 50 % Wahrscheinlichkeit bei 123 K. Molekülstruktur von Verbindung **24** (Konnektivitätsbeweis) – Darstellung als „ball and stick“ aufgrund mangelnder Datenqualität.

3.2.3 Reaktion von $[P(\mu\text{-N}Ter)]_2$ (**1**) mit BRØNSTED-Säuren

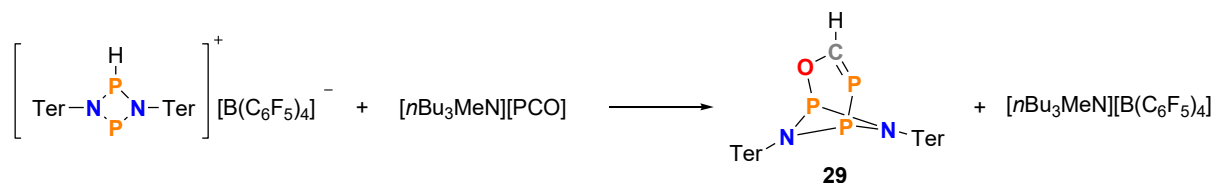
Halogenwasserstoffe wie HCl gelöst in Wasser sind klassische und bei RT stabile BRØNSTED-Säuren. Im Gegensatz dazu sind (Pseudo)Halogenwasserstoffe wie HCN, HN_3 , HNCO, HNCS oder HPCO auch BRØNSTED-Säuren, welche bereits bei sehr tiefen Temperaturen zur Polymerisation neigen.^[75-77] Labile (Pseudo)Halogenwasserstoffe lassen sich durch Adduktbildung mit starken LS wie $\text{B}(\text{C}_6\text{F}_5)_3$ stabilisieren und isolieren.^[78,79] Daher sollte versucht werden, mithilfe des Biradikals **1Ter** (Pseudo)Halogenwasserstoffe zu stabilisieren bzw. abzufangen. Dabei sollten zwei verschiedene Reaktionswege verfolgt werden. Zum einen die direkte Umsetzung (**A**) der aus den Natriumsalzen und Stearinsäure frisch hergestellten wasserfreien (Pseudo)Halogenwasserstoffe mit einer Lösung von **1Ter** und zum anderen ein zweistufiger Reaktionsweg (**B**) über das protonierte Kation des Biradikals $[\text{HP}(\mu\text{-N}Ter)_2\text{P}]^+$ (**1Ter-H**). **1Ter-H** wurde von Dr. Lukas Chojetzki im Rahmen seiner Promotionsarbeit untersucht und dieser führte ein Vergleichsexperiment mit $[\text{WCC}]\text{CN}$ durch (Schema 16). Sowohl die direkte Umsetzung (Reaktionsweg **A**) von **1Ter** mit HCN als auch der zweistufige Reaktionsweg **B** über **1Ter-H** zeigten als Produkt das HCN-Addukt **26**.



Schema 16. Synthese von (Pseudo)Halogenwasserstoffaddukten von **1Ter**.

Die entsprechenden BRØNSTED-Säureaddukte konnten über Reaktionsweg **A** in guten Ausbeuten zwischen 50-80 % (**25-28**) isoliert, kristallisiert und vollständig charakterisiert werden (Abbildung 15).^[80] In Lösung und Festkörper konnten nur die jeweiligen *cis*-Addukte beobachtet werden. Im Falle des HN_3 -Adduktes konnte auch bei höheren Temperaturen keine Stickstoffabspaltung im Sinne einer STAUDINGER-Reaktion beobachtet werden.

Die sehr instabilen (Pseudo)Halogenwasserstoffe wie HPCO bzw. HNCS konnten nicht über das entsprechende Natriumsalz und Stearinsäure erzeugt werden. Im Falle des PCO^- konnte das Anion durch ein schwach-koordinierendes Kation ($[\textit{n}\text{-Bu}_3\text{NMe}]^+$) stabilisiert und isoliert werden. Eine Umsetzung von $[\textit{n}\text{-Bu}_3\text{NMe}]\text{PCO}$ mit $[\text{HP}(\mu\text{-N}\text{Ter})_2\text{P}]^+$ (**1Ter-H**) und der anschließenden Strukturaufklärung mithilfe der Röntgeneinkristallstrukturanalyse lieferte ein [3.1.1]-hetero-propellan ähnliches Strukturmotiv **29** mit einer verbrückenden PCO-Einheit auf den Phosphorbrückenköpfen (Schema 17).



Schema 17. Synthese von **29** über Reaktionsweg **B**.

Durch quantenmechanische Rechnungen wurde die Umlagerungsreaktion von Verbindung **29** ausgehend vom **29HPCO_{exo}**-Isomer zur [3.1.1]-Hetero-propellanstruktur **29PC(H)O** untersucht. Der entscheidende Prozess ist die Wanderung des Wasserstoffatoms (P–H) zum Kohlenstoffatom der PCO-Einheit mit der gleichzeitigen Rotation um die P–C-Achse, was eine P–O Bindungsbildung begünstigt (Abbildung 14). Der exergonische Isomerisierungsprozess vom *exo*-Isomer zur Verbindung **29PC(H)O** ist mit einem Energiegewinn von ca. 25 kJ/mol verbunden.

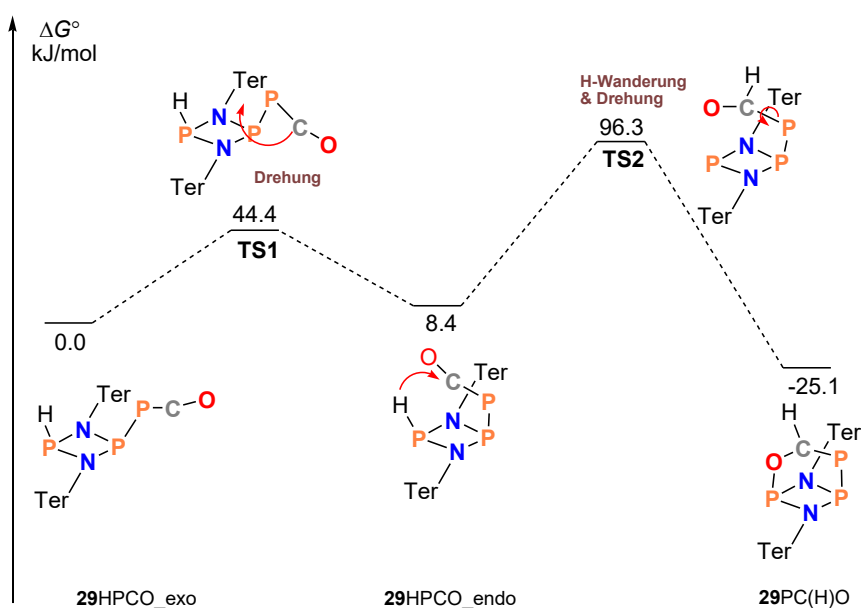
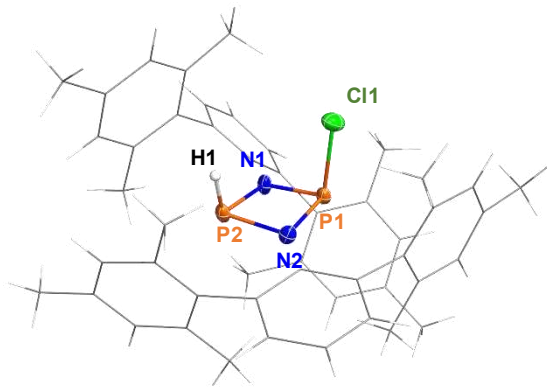
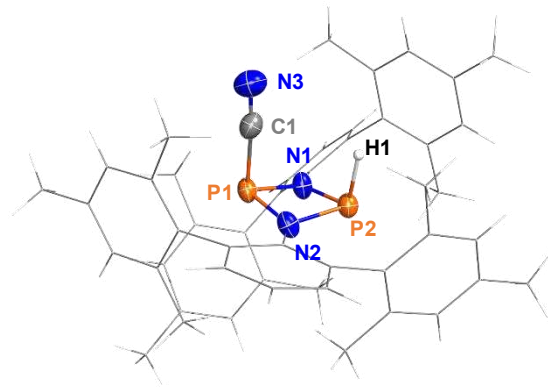


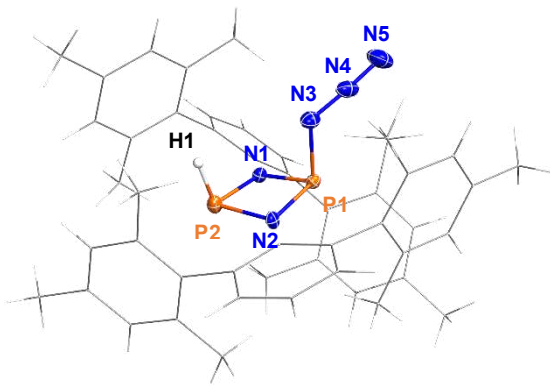
Abbildung 14. Berechneter Mechanismus (DLPNO-CCSD(T)/def2-TZVP//PBE-D3/def2-SVP) der Isomerisierung vom **29HPCO_{exo}** Isomer zu Verbindung **29PC(H)O**.



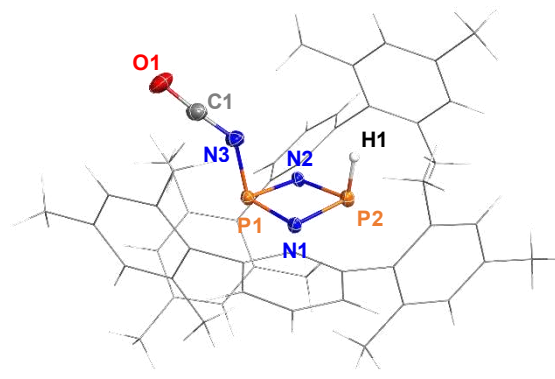
25



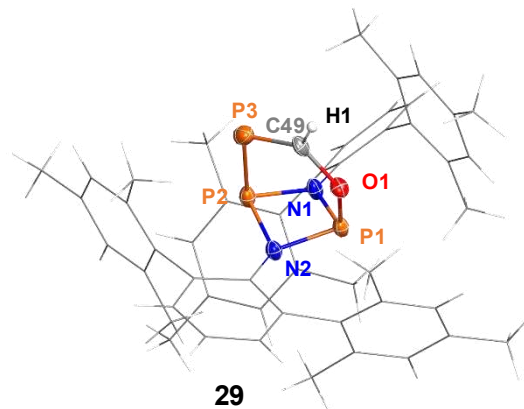
26



27



28



29

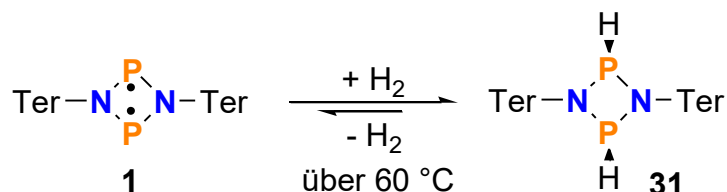
Abbildung 15. Molekülstrukturen der Verbindungen **25** bis **29** im Einkristall. Thermische Ellipsoide entsprechen 50 % Wahrscheinlichkeit bei 123 K.

3.2.4 *Para*-Wasserstoff-Aktivierung

Wasserstoff kommt in der Natur in 3 verschiedenen Isotopen als ^1_1H Protium, ^2_1D Deuterium und ^3_1H Tritium vor. In NMR-Routineexperimenten werden die ^1_1H -Wasserstoffkerne in deuterierten Lösungsmitteln untersucht. An bestimmten Positionen können Wasserstoffatome durch Deuteriumatome markiert werden. Die chemischen Eigenschaften bleiben erhalten, aber die physikalischen Eigenschaften werden durch den Isotopenaustausch verändert, wodurch die markierte Position gesondert untersucht werden kann.

Moderne Untersuchungsmethoden wie PHIP (*Para*-Hydrogen Induced Polarization)^[81] bzw. SABRE (Signal Amplification By Reversible Exchange)^[82] ermöglichen es mit Hilfe eines Hyperpolarisationstransfer von *para*-Wasserstoff (Singulett-Wasserstoff) auf das zu untersuchende Molekül, das Kernspinresonanzsignal um mehrere Größenordnungen zu verstärken.^[83] Mithilfe dieser Techniken lassen sich Hydrierungsreaktionen mechanistisch untersuchen oder NMR-Kontrastmittel herstellen. Das natürliche Vorkommen von *para*-Wasserstoff liegt bei Raumtemperatur bei ungefähr 25 %. Bei niedrigen Temperaturen vergrößert sich der Anteil des *para*-Wasserstoffs gegenüber dem *ortho*-Wasserstoff deutlich, sodass bei der Verflüssigungstemperatur von Wasserstoff bei ca. 20 K fast ausschließlich *para*-Wasserstoff vorliegt und so selektiv für NMR-Untersuchungen genutzt werden kann.

Wie bereits im Kapitel 2.2.1 gezeigt aktiviert **1Ter** molekularen Wasserstoff bei Raumtemperatur. Die konzertierte Gleichgewichtsreaktion von **1Ter** zu **31** liegt bei Raumtemperatur nahezu vollständig auf der Seite des Produktes (Schema 18). Wird die Temperatur erhöht so verschiebt sich die Lage des Gleichgewichtes deutlich auf die Seite der Edukte, bis bei Temperaturen von über 60 °C der Wasserstoff vollständig reversibel abgespalten wird.^[31]



Schema 18. Reaktion von **1Ter** mit molekularem Wasserstoff.

Bereits im Jahre 2019 führte die Arbeitsgruppe ZHIVONITKO in Kooperation mit der Arbeitsgruppe SCHULZ Untersuchungen mit *para*-Wasserstoff an **1Ter** durch.^[84] Im Rahmen dieser Arbeit wurden weitere Biradikalsysteme (Abbildung 16), welche aus den vorherigen

Kapiteln bekannt sind, durch die Arbeitsgruppe ZHIVONITKO untersucht.^[85] Für die 4-gliedrigen Biradikale **9** und **30** konnte ähnlich wie für Verbindung **1Ter** eine Aktivierung von *para*-Wasserstoff beobachtet werden. ¹H und ³¹P-NMR-Untersuchungen zeigten eine deutliche Signalverstärkung der addierten *para*-Wasserstoffatome (300-fach (**30**) und 1000-fach (**9**)) durch den Polarisationstransfer auf die Hetero-Atomkerne. Aufgrund der Gleichgewichtsreaktion der verschiedenen Biradikale mit Wasserstoff (Beispiel **1Ter**, Schema 18) erfolgte im Falle des Biradikals **9** eine konstante immer wieder verstärkende Polarisierung des ³¹P-NMR-Kerns. Durch eine spezielle Pulsabfolge konnte dadurch sogar eine 2000-fache Signalverstärkung bei 40 °C (Verschiebung des Gleichgewichtes, Schema 18) beobachtet werden.

Im Falle der 5-gliedrigen Biradikale konnte nur eine geringere Signalverstärkung experimentell beobachtet werden. Daher wurden die Experimente für die Verbindungen **2Dmp** und **10Dmp** bei deutlich höheren Temperaturen durchgeführt, wodurch vor allem für das gemischte 5-gliedrige Biradikal **10Dmp** überhaupt eine Signalverstärkung (¹H- und ³¹P-NMR-Spektrum) beobachtet werden konnte. Leider war es nicht möglich, das Derivat [As(μ -NTer)]₂DmpNC zu synthetisieren, da Verbindung **30** nicht mit DmpNC reagierte.

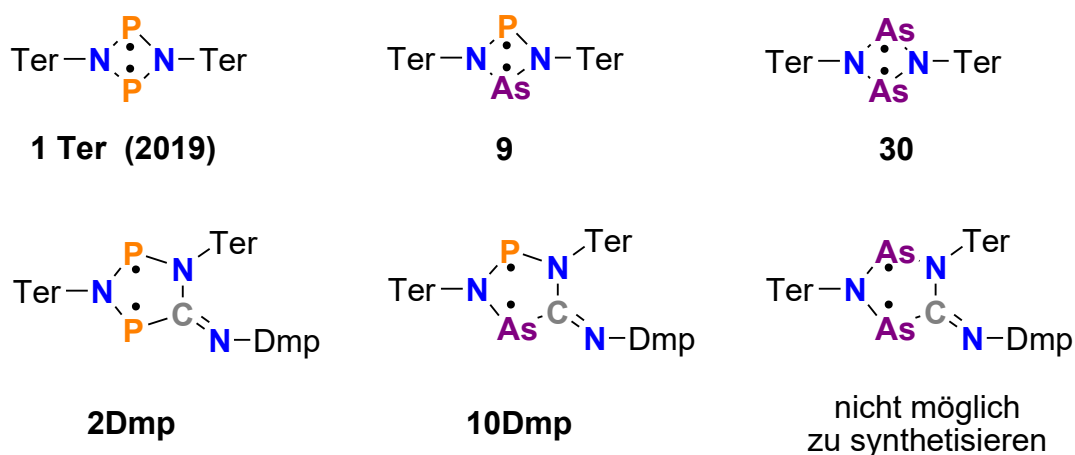


Abbildung 16. Durch PHIP untersuchte Biradikalsysteme.

4 Zusammenfassung und Ausblick

Im Rahmen dieser Arbeit konnte das photochemische Schaltverhalten der 5-gliedrigen Biradikale (**2**) und die thermischen Rückreaktionen der Hausane (**3**) tiefgründig untersucht werden. Die Photoisomerisierung folgte einem nichtadiabatischen Anregungsprozess, wobei die angeregten Moleküle durch eine konische Durchschneidung in den Grundzustand zurückfielen. Die thermischen Rückreaktionen konnte durch NMR-spektroskopische Untersuchungen in Lösung bei verschiedenen Temperaturen untersucht werden. Durch den Einfluss katalytischer Mengen CN-*t*Bu konnte die Rückreaktion deutlich beschleunigt werden und ein alternativer Reaktionsweg über einen nukleophilen Angriff des Isonitrils und dem daraus resultierenden offenkettigen Derivat (**5**) gefunden werden. Im Falle des weniger sterisch anspruchsvollen Hypersilylsubstituenten am Ringsystem konnten, anstelle der 5-gliedrigen Biradikale, die Dienverbindungen (**8**) isoliert werden. Wiederrum ist das sterisch sehr anspruchsvolle CN-Ter für eine Hypersilylmigration zu groß, sodass hier das Biradikal (**6**) beobachtet und mittels Bestrahlung in das Hausanisomer (**7**) überführt werden konnte. Das Schaltverhalten der gemischten Biradikale (**10**) konnte in Lösung als auch im Einkristall (Einkristall-zu-Einkristall-Isomerisierung) beobachtet und analysiert werden. Durch die Reaktion von **1Ter** mit Thiophosgen und der anschließenden Reduktion des chlorierten 5-gliedrigen Ringsystems konnte das instabile und sehr lichtempfindliche Biradikal **15** synthetisiert werden. Die irreversible Photoisomerisierung zum Hausan (**16**) konnte in Lösung gezeigt werden.

Durch die Aktivierung kleiner Moleküle des CS-insertierten Biradikals (**15**) und der Untersuchung der Folgereaktion an den überbrückten [2.2.1]-bicyclischen Additionsprodukten, konnte die Struktur des Biradikals bewiesen werden. Darüber hinaus konnten durch **1Ter** weitere kleine Moleküle wie Thioketone und BRØNSTED-Säuren aktiviert, isoliert und vollständig charakterisiert werden. *Para*-Wasserstoff-Experimente an verschiedenen 4- und 5-gliedrigen Biradikalen zeigten Hyperpolarisationseffekte in den entsprechenden ¹H- und ³¹P-NMR-Spektren. Somit konnten zum bereits 2019 untersuchten Derivat **1Ter** weitere metallfreie Verbindungen gefunden werden, welche Hyperpolarisationseffekte aufwiesen. Im Falle von Biradikal **9** konnte zusätzlich ein neuer Höchstwert der Signalverstärkung (Faktor 10³) für metallfreie Derivate detektiert werden.

5 Referenzen

- [1] P. Müller, *Pure Appl. Chem.* **1994**, *66*, 1077–1184.
- [2] M. Abe, *Chem. Rev.* **2013**, *113*, 7011–7088.
- [3] A. Schulz, *Dalton Trans.* **2018**, *47*, 12827–12837.
- [4] M. B. W. Schlenk, *Ber. Dtsch. Chem. Ges.* **1915**, *48*, 661–669.
- [5] P. P. Power, *Chem. Rev.* **1999**, *99*, 3463–3503.
- [6] P. P. Power, *Chem. Rev.* **2003**, *103*, 789–810.
- [7] T. Beweries, R. Kuzora, U. Rosenthal, A. Schulz, A. Villinger, *Angew. Chem. Int. Ed.* **2011**, 8974–8978.
- [8] A. Schulz, *Z. Anorg. Allg. Chem.* **2014**, *640*, 2183–2192.
- [9] E. Niecke, A. Fuchs, F. Baumeister, M. Nieger, W. W. Schoeller, *Angew. Chem. Int. Ed.* **1995**, *34*, 555–557.
- [10] H. Sugiyama, S. Ito, M. Yoshifuji, *Angew. Chem. Int. Ed.* **2003**, *42*, 3802–3804.
- [11] D. Scheschkewitz, H. Amii, H. Gornitzka, W. W. Schoeller, D. Bourissou, G. Bertrand, *Science* **2002**, *295*, 1880–1881.
- [12] K. Takeuchi, M. Ichinohe, A. Sekiguchi, *J. Am. Chem. Soc.* **2011**, *133*, 12478–12481.
- [13] D. Rottschäfer, B. Neumann, H.-G. Stammler, R. S. Ghadwal, *Chem. Eur. J.* **2017**, *23*, 9044–9047.
- [14] D. Rottschäfer, B. Neumann, H. Stammler, R. Kishi, M. Nakano, R. S. Ghadwal, *Chem. Eur. J.* **2019**, *25*, 3244–3247.
- [15] X. Wang, Y. Peng, M. M. Olmstead, J. C. Fettinger, P. P. Power, *J. Am. Chem. Soc.* **2009**, *131*, 14164–14165.
- [16] J. Hicks, C. Jones, *Organometallics* **2015**, *34*, 2118–2121.
- [17] H. Cox, P. B. Hitchcock, M. F. Lappert, L. J. M. Pierssens, *Angew. Chem. Int. Ed.* **2004**, *43*, 4500–4504.

- [18] P. Henke, T. Pankewitz, W. Klopper, F. Breher, H. Schnöckel, *Angew. Chem. Int. Ed.* **2009**, *48*, 8141–8145.
- [19] Z. Li, X. Chen, D. M. Andrada, G. Frenking, Z. Benkő, Y. Li, J. R. Harmer, C.-Y. Su, H. Grützmacher, *Angew. Chem. Int. Ed.* **2017**, *56*, 5744–5749.
- [20] S.-H. Zhang, H.-W. Xi, K. H. Lim, Q. Meng, M.-B. Huang, C.-W. So, *Chem. Eur. J.* **2012**, *18*, 4258–4263.
- [21] J. Bresien, L. Eickhoff, A. Schulz, E. Zander, in *Ref. Modul. Chem. Mol. Sci. Chem. Eng.*, Elsevier, **2021**, pp. 1–68.
- [22] S. Demeshko, C. Godemann, R. Kuzora, A. Schulz, A. Villinger, *Angew. Chem. Int. Ed.* **2013**, *52*, 2105–2108.
- [23] A. Hinz, A. Schulz, A. Villinger, *Angew. Chem. Int. Ed.* **2015**, *54*, 668–672.
- [24] A. Hinz, A. Schulz, A. Villinger, *Chem. Sci.* **2016**, *7*, 745–751.
- [25] A. Hinz, R. Kuzora, A. Rölke, A. Schulz, A. Villinger, R. Wustrack, *Eur. J. Inorg. Chem.* **2016**, *2016*, 3611–3619.
- [26] A. Hinz, A. Schulz, A. Villinger, *Chem. Eur. J.* **2014**, *20*, 3913–3916.
- [27] A. Hinz, A. Schulz, A. Villinger, *J. Am. Chem. Soc.* **2015**, 9953–9962.
- [28] A. Hinz, R. Kuzora, U. Rosenthal, A. Schulz, A. Villinger, *Chem. Eur. J.* **2014**, *20*, 14659–14673.
- [29] A. Hinz, A. Schulz, A. Villinger, *Chem. Commun.* **2016**, *52*, 6328–6331.
- [30] A. Hinz, A. Schulz, A. Villinger, *Chem. Commun.* **2015**, *51*, 1363–1366.
- [31] A. Hinz, A. Schulz, A. Villinger, *Angew. Chem. Int. Ed.* **2016**, *55*, 12214–12218.
- [32] A. Hinz, A. Schulz, W. W. Seidel, A. Villinger, *Inorg. Chem.* **2014**, *53*, 11682–11690.
- [33] A. Hinz, A. Schulz, A. Villinger, *Angew. Chem. Int. Ed.* **2015**, *54*, 2776–2779.
- [34] A. D. Johnson, A. R. Poteete, G. Lauer, R. T. Sauer, G. K. Ackers, M. Ptashne, *Nature* **1981**, *294*, 217–223.
- [35] A. Lather, V. K. Lamba, H. Malik, A. Ratner, *IRACST-Engineering Sci. Technol. An Int. J.* **2012**, *2*, 460–466.
- [36] J. L. Zhang, J. Q. Zhong, J. D. Lin, W. P. Hu, K. Wu, G. Q. Xu, A. T. S. Wee, W. Chen, *Chem. Soc. Rev.* **2015**, *44*, 2998–3022.

- [37] P. C. Knipe, S. Thompson, A. D. Hamilton, *Chem. Sci.* **2015**, *6*, 1630–1639.
- [38] B. L. Feringa, *Molecular Switches*, WILEY-VCH, Weinheim, Germany, **2001**.
- [39] R. Göstl, A. Senf, S. Hecht, *Chem. Soc. Rev.* **2014**, *43*, 1982–1996.
- [40] R. S. Stoll, S. Hecht, *Angew. Chem. Int. Ed.* **2010**, *49*, 5054–5075.
- [41] D. R. Yarkony, *J. Phys. Chem. A* **2001**, *105*, 6277–6293.
- [42] W. Domcke, D. R. Yarkony, *Annu. Rev. Phys. Chem.* **2012**, *63*, 325–352.
- [43] D. Wöhrle, M. W. Tausch, W.-D. Stohrer, Photochemie, *Photochemie*, Wiley-VCH, **1998**.
- [44] T. Förster, *Pure Appl. Chem.* **1970**, *24*, 443–450.
- [45] L. Salem, *J. Am. Chem. Soc.* **1974**, *96*, 3486–3501.
- [46] M. A. Robb, in *Adv. Ser. Phys. Chem. Vol. 17 Conical Intersect. Theory, Comput. Exp.* (Eds.: W. Domcke, D.R. Yarkony, H. Köppel), Singapore, **2011**, pp. 3–50.
- [47] F. Lépine, M. Y. Ivanov, M. J. J. Vrakking, *Nat. Photonics* **2014**, *8*, 195–204.
- [48] G. S. Hartley, *Nature* **1937**, *140*, 281.
- [49] R. Crystal, B. J. M. Robertson, *J. Am. Chem. Soc.* **1939**, *47*, 232–236.
- [50] G. C. Hampson, J. M. Robertson, *J. Am. Chem. Soc.* **1941**, *78*, 409–413.
- [51] Y. Yokoyama, *Chem. Rev.* **2000**, *100*, 1717–1739.
- [52] G. Berkovic, V. Krongauz, V. Weiss, *Chem. Rev.* **2000**, *100*, 1741–1754.
- [53] M. Irie, *Chem. Rev.* **2000**, *100*, 1685–1716.
- [54] S. L. Buchwalter, G. L. Closs, *J. Am. Chem. Soc.* **1975**, *97*, 3857–3858.
- [55] M. P. Conrad, R. M. Pitzer, H. F. Schaefer, *J. Am. Chem. Soc.* **1979**, *101*, 2245–2246.
- [56] M. Abe, C. Ishihara, S. Kawanami, A. Masuyama, *J. Am. Chem. Soc.* **2005**, *127*, 10–11.
- [57] E. Zander, Bachelorarbeit: *Untersuchungen Zu Fünfgliedrigen, Biradikaloiden Ringsystemen*, Universität Rostock, **2017**.
- [58] C. Feldmeier, H. Bartling, E. Riedle, R. M. Gschwind, *J. Magn. Reson.* **2013**, *232*, 39–44.
- [59] A. Hinz, Doktorarbeit: *Untersuchungen Zu Gruppe-15- Biradikaloiden*, Universität Rostock, **2015**.

- [60] M. Boggio-pasqua, *Computational Mechanistic Photochemistry: The Central Role of Conical Intersections. Theoretical and/or Physical Chemistry*, Université Toulouse III, **2015**.
- [61] K. F. Chang, M. Reduzzi, H. Wang, S. M. Poullain, Y. Kobayashi, L. Barreau, D. Prendergast, D. M. Neumark, S. R. Leone, *Nat. Commun.* **2020**, *11*, 1–7.
- [62] T. Völzer, H. Beer, A. Schulz, S. Lochbrunner, J. Bresien, *Phys. Chem. Chem. Phys.* **2021**, *23*, 7434–7441.
- [63] H. Beer, J. Bresien, D. Michalik, A. Schulz, A. Villinger, *Dalton Trans.* **2020**, *49*, 13986–13992.
- [64] A.-K. Rölke, Doktorarbeit: *Synthese Eines Hypersilyl-stabilisierten Phosphorbiradikaloids Sowie Untersuchungen Zur Reaktivität*, Universität Rostock, **2016**.
- [65] H. Beer, J. Bresien, D. Michalik, A.-K. Rölke, A. Schulz, A. Villinger, R. Wustrack, *J. Org. Chem.* **2020**, *85*, 14435–14445.
- [66] F. Cataldo, D. Heymann, *Eur. J. Solid State Inorg. Chem.* **1998**, *35*, 619–628.
- [67] E. K. Moltzen, M. P. Kramer, A. Senning, K. J. Klabunde, *J. Org. Chem.* **1987**, *52*, 1156–1161.
- [68] K. J. Klabunde, M. P. Kramer, A. Senning, E. K. Moltzen, *J. Am. Chem. Soc.* **1984**, *106*, 263–264.
- [69] R. Steudel, *Angew. Chem.* **1967**, *79*, 649–650.
- [70] H. Beer, A. Linke, J. Bresien, A. Villinger, A. Schulz, *Inorg. Chem. Front.* **2022**, *9*, 2659–2667.
- [71] E. Miliordos, K. Ruedenberg, S. S. Xantheas, *Angew. Chem. Int. Ed.* **2013**, *52*, 5736–5739.
- [72] J. Bresien, T. Kröger-Badge, S. Lochbrunner, D. Michalik, H. Müller, A. Schulz, E. Zander, *Chem. Sci.* **2019**, *10*, 3486–3493.
- [73] P. Pyykkö, M. Atsumi, *Chem. Eur. J.* **2009**, *15*, 12770–12779.
- [74] H. Beer, A. Linke, J. Bresien, G. Mlostoń, M. Celeda, A. Villinger, A. Schulz, *Inorg. Chem.* **2022**, *61*, 2031–2038.
- [75] L. Birckenbach, K. Kellermann, *Ber. Dtsch. Chem. Ges.* **1925**, *58*, 786–794.

- [76] L. Birckenbach, K. Kellermann, *Ber. Dtsch. Chem. Ges.* **1925**, *58*, 2377–2386.
- [77] H. Brand, A. Schulz, A. Villinger, *Z. Anorg. Allg. Chem.* **2007**, *633*, 22–35.
- [78] K. Bläsing, J. Bresien, R. Labbow, D. Michalik, A. Schulz, M. Thomas, A. Villinger, *Angew. Chem. Int. Ed.* **2019**, *58*, 6540–6544.
- [79] K. Bläsing, J. Harloff, A. Schulz, A. Stoffers, P. Stoer, A. Villinger, *Angew. Chem. Int. Ed.* **2020**, *132*, 10594–10599.
- [80] H. Beer, K. Bläsing, J. Bresien, L. Chojetzki, A. Schulz, P. Stoer, A. Villinger, *Dalton Trans.* **2020**, *49*, 13655–13662.
- [81] C. R. Bowers, D. P. Weitekamp, *J. Am. Chem. Soc.* **1987**, *109*, 5541–5542.
- [82] R. W. Adams, J. A. Aguilar, K. D. Atkinson, M. J. Cowley, P. I. P. Elliott, S. B. Duckett, G. G. R. Green, I. G. Khazal, J. López-Serrano, D. C. Williamson, *Science* **2009**, *323*, 1708–1711.
- [83] C. R. Bowers, D. P. Weitekamp, *Phys. Rev. Lett.* **1986**, *57*, 2645–2648.
- [84] V. V. Zhivonitko, J. Bresien, A. Schulz, I. V. Koptug, *Phys. Chem. Chem. Phys.* **2019**, *21*, 5890–5893.
- [85] V. V. Zhivonitko, H. Beer, D. O. Zakharov, J. Bresien, A. Schulz, *ChemPhysChem* **2021**, *22*, 813–817.

6 Ausgewählte Originalpublikationen

Dieses Kapitel beinhaltet die Originalpublikationen zu den im Kapitel 3 vorgestellten Arbeiten. Axel Schulz, mein Betreuer während der Forschungszeit, trug zu jeder Veröffentlichung bei, indem er die Forschungsprojekte koordinierte, jederzeit für wissenschaftliche Fragen und Diskussionen zur Verfügung stand und an den Manuskripten mitschrieb. Mein eigener Beitrag der jeweiligen Publikation ist jeweils gesondert hervorgehoben. Bei Fragen kontaktieren sie bitte: axel.schulz@uni-rostock.de

Das Themengebiet im **Kapitel 3.1** erfasst 5 zusammengefasste Publikationen:

1. „*A chemical reaction controlled by light-activated molecular switches based on heterocyclopentenediyls*“ (J. Bresien, T. Kröger-Badge, S. Lochbrunner, D. Michalik, H. Müller, A. Schulz, E. Zander, *Chem. Sci.* **2019**, *10*, 3486–3493)

Die Publikation und die Hintergrundinformation wurden zum Teil von mir verfasst. 50 % der Experimente wurden von mir durchgeführt und deren Ergebnisse zum Teil in meiner Masterarbeit diskutiert. Zu Beginn der Promotion wurden noch essentielle Daten gesammelt, welche zur Veröffentlichung der Ergebnisse nötig waren. Die restlichen Experimente wurden von Edgar Zander im Zuge seiner Bachelorarbeit durchgeführt, welche nicht von mir betreut wurde. Die quantenchemischen Rechnungen wurden von Dr. Jonas Bresien durchgeführt. Der eigene Gesamtbeitrag liegt bei ca. 30 %.

Notiz: Aufgrund einer Namensänderung 05/20 und der alphabetischen Auflistung aller Autoren bis 08/21 (DFG) ist hier mein Geburtsname (Müller) aufgelistet.

2. „*Photoisomerization of a phosphorus-based biradicaloid: ultrafast dynamics through a conical intersection*“ (T. Völzer, H. Beer, A. Schulz, S. Lochbrunner, J. Bresien, *Phys. Chem. Chem. Phys.* **2021**, *23*, 7434–7441)

Die Publikation und die Hintergrundinformationen wurden zum Teil von mir verfasst. 50 % der experimentellen Arbeiten wurden von mir durchgeführt. Die restlichen Experimente wurden zusammen mit Tim Völzer angefertigt. Die quantenchemischen Rechnungen wurden von Dr. Jonas Bresien durchgeführt. Der eigene Gesamtbeitrag liegt bei ca. 30 %.

3. „*Reversible switching between housane and cyclopentanediyli isomers: an isonitrile-catalysed thermal reverse reaction*“ (H. Beer, J. Bresien, D. Michalik, A. Schulz, A. Villinger, *Dalton Trans.* **2020**, *49*, 13986–13992)

Die Publikation und die Hintergrundinformationen wurden zum Teil von mir verfasst. Die experimentellen Arbeiten wurden vollständig von mir durchgeführt. Die quantenchemischen Rechnungen wurden zu großen Teilen von Dr. Jonas Bresien durchgeführt. Der eigene Gesamtbeitrag liegt bei ca. 45 %.

4. „*Heterocyclopentanediyli vs Heterocyclopentadienes: A Question of Silyl Group Migration*“ (H. Beer, J. Bresien, D. Michalik, A.-K. Rölke, A. Schulz, A. Villinger, R. Wustrack, *J. Org. Chem.* **2020**, *85*, 14435–14445)

Die Publikation wurde zum Teil und die Hintergrundinformationen vollständig von mir verfasst. Die experimentellen Arbeiten wurden zur Hälfte von mir und zur Hälfte von Anne-Kristin Rölke während ihrer Promotion durchgeführt. Ein Teil der Ergebnisse wurden bereits in der Dissertation von Anne-Kristin Rölke diskutiert. Die quantenchemischen Rechnungen wurden von mir angefertigt. Der eigene Gesamtbeitrag liegt bei ca. 50 %.

5. „*A Cyclic Thioketone as Biradical Heterocyclopentane-1,3-diyli: Synthesis, Structure and Activation Chemistry*“ (H. Beer, A. Linke, J. Bresien, A. Villinger, A. Schulz, *Inorg. Chem. Front.* **2022**, *9*, 2659–2667)

Die Publikation wurde zum Teil und die Hintergrundinformation vollständig von mir verfasst. Die experimentellen Arbeiten sowie die quantenchemischen Rechnungen wurden zu 50 % von mir und zu 50 % von Alexander Linke im Zuge seiner Masterarbeit durchgeführt, welche von mir betreut wurde. Der eigene Gesamtbeitrag liegt bei ca. 70 %.

Das Themengebiet im **Kapitel 3.2** erfasst vier thematisch zusammenhängende Publikationen wobei der eigene Beitrag zur Publikation 5 bereits in der Zusammenfassung des **Kapitels 3.1** beschrieben wird.

5. „*A Cyclic Thioketone as Biradical Heterocyclopentane-1,3-diyli: Synthesis, Structure and Activation Chemistry*“ Siehe Themengebiet Kapitel 3.1.
6. „*Synthesis of Bicyclic P,S-Heterocycles via the Addition of Thioketones to a Phosphorus-Centered Open-Shell Singlet Biradical*“ (H. Beer, A. Linke, J. Bresien, G. Mlostoń, M. Celeda, A. Villinger, A. Schulz, *Inorg. Chem.* **2022**, *61*, 2031–2038)

Die Publikation wurde zum Teil und die Hintergrundinformationen vollständig von mir verfasst. Die experimentellen Arbeiten sowie die quantenchemischen Rechnungen wurden zu 50 % von mir und zu 50 % von Alexander Linke im Zuge seiner Masterarbeit durchgeführt, welche von mir betreut wurde. Der eigene Gesamtbeitrag liegt bei ca. 65 %.

7. „*Trapping of Brønsted acids with a phosphorus centered biradicaloid – synthesis of hydrogen pseudohalide addition products*“ (H. Beer, K. Bläsing, J. Bresien, L. Chojetzki, A. Schulz, P. Stoer, A. Villinger, *Dalton Trans.* **2020**, *49*, 13655–13662)

Die Publikation und Hintergrundinformationen wurden zum Teil von mir verfasst. Die experimentellen Arbeiten wurden zu 90 % und die quantenchemischen Rechnungen zu 50 % von mir durchgeführt. Der eigene Gesamtbeitrag liegt bei ca. 65 %.

8. „*Hyperpolarization Effects in Parahydrogen Activation with Pnictogen Biradicaloids: Metal-free PHIP and SABRE*“ (V. V. Zhivonitko, H. Beer, D. O. Zakharov, J. Bresien, A. Schulz, *ChemPhysChem* **2021**, *22*, 813–817)

Die Hintergrundinformationen wurden zum Teil von mir verfasst. Die Synthese der Ausgangsverbindungen und die quantenchemischen Rechnungen wurden vollständig von mir durchgeführt. Die NMR-Untersuchungen wurden von der Arbeitsgruppe um Vladimir Zhivonitko angefertigt. Das Manuskript wurde zu großen Teilen von Vladimir Zhivonitko verfasst. Der eigene Gesamtbeitrag liegt bei ca. 20 %.

6.1 A chemical reaction controlled by light-activated molecular switches based on heterocyclopentenediyls

Jonas Bresien, Thomas Kröger-Badge, Stefan Lochbrunner, Dirk Michalik, Henrik Müller, Axel Schulz, Edgar Zander

Chem. Sci. **2019**, *10*, 3486–3493.

DOI: 10.1039/c8sc04893b

No permission needed for authors reprinting full articles in a thesis/dissertation according to the Royal Society of Chemistry. © Copyright 2020 Royal Society of Chemistry.

Onlinelink: <https://doi.org/10.1039/C8SC04893B>

Cite this: *Chem. Sci.*, 2019, 10, 3486

All publication charges for this article have been paid for by the Royal Society of Chemistry

Received 2nd November 2018
Accepted 17th February 2019

DOI: 10.1039/c8sc04893b

rsc.li/chemical-science

A chemical reaction controlled by light-activated molecular switches based on hetero-cyclopentenediyls[†]

Jonas Bresien,^{id}*^a Thomas Kröger-Badge,^a Stefan Lochbrunner,^{id}^{bc}
Dirk Michalik,^{ad} Henrik Müller,^{id}^a Axel Schulz,^{id}*^{acd} and Edgar Zander,^{id}^a

Molecular switches are molecules that can reversibly be shifted between at least two stable states with different physical and chemical properties, making them interesting for application as chemical sensors or molecular machines. We recently discovered that five-membered, cyclic biradicals based on group 15 elements are efficient and robust photochemical switches that can be activated by red light. The quantum yield of the photo-isomerization is as high as 24.6%, and the thermal equilibration of the photo-activation product proceeds rapidly at ambient temperature. The fully reversible process was studied by experimental and high-level *ab initio* techniques. We could further demonstrate that the biradical character could be completely turned on and off, so the system could be applied to control chemical equilibria that involve activation products of the cyclic biradicals.

Introduction

The term “molecular switch” originated in the early 1980s and was first used in conjunction with biological signal transmission.¹ Since then, it has found widespread use throughout chemistry, and generally refers to any kind of molecule that can exist in two or more (*meta*-)stable states. Interconversion can be induced by external stimuli such as temperature, chemical modifications, redox reactions, electric fields, or irradiation with photons.^{2–5} The most commonly known type of molecular switches are pH indicators, which are based on acid–base equilibria and therefore belong to the group of chemically activated compounds.^{6,7} Other chemically switchable systems may, for example, find application in the field of gas or ion sensing,^{5,8} or be used as redox indicators.⁷

Especially light-activated molecular switches promise diverse applications, *e.g.* as photoactuators^{9–11} or photo-regulated catalysts.^{12,13} Therefore, a growing research interest is aimed both at the synthesis of new systems as well as the

exploration of new fields of applications.^{14,15} Most light-activated molecular switches function by conformational changes.³ One of the most prominent examples is probably retinal, the chromophore of the receptor protein rhodopsin, which is found in the rods of the retina in mammals' eyes. Upon irradiation with visible light, retinal undergoes a conformational change resulting in a signalling cascade, which eventually leads to a visual stimulus.^{16–18} Therefore, it plays a crucial role in the functioning of the eye. Mechanistically, the isomerization of retinal can be traced back to an *E/Z* isomerization along a C–C double bond. Thus, it is not surprising that many synthetic, light activated molecular switches are based on a similar principle:¹⁹ For example, azobenzene may be isomerized from its *E* to its *Z* conformer by light in the UV region, while the *Z* → *E* isomerization is triggered by light in the blue region of the visible spectrum (Fig. 1a).^{20,21} The absorption maxima can be shifted by derivatization of azobenzene with electron donating or electron withdrawing groups.⁴ Another popular type of photo-switching is represented by photo-cyclization reactions,^{22,23} as observed, for example, in case of diarylethenes (Fig. 1a).²⁴ This class of molecular switches is based on the formation or breaking of chemical bonds. In fact, most (light-activated) molecular switches can be divided into these two categories, namely stereoisomerism (change of structure without modification of the chemical bonding pattern) and structural isomerism (including a redistribution of bonds).³ Other mechanisms are discussed in the literature, such as dipole, charge, or spin switching,³ but these processes often include some kind of structural change, too.

Understanding bond formation and breaking processes (or the nature of chemical bonds in general) has been a widely

^aInstitute of Chemistry, University of Rostock, Albert-Einstein-Str. 3a, D-18059 Rostock, Germany. E-mail: jonas.bresien@uni-rostock.de; axel.schulz@uni-rostock.de

^bInstitute of Physics, University of Rostock, Albert-Einstein-Str. 23-24, D-18059 Rostock, Germany

^cDepartment of Life, Light & Matter, University of Rostock, D-18051 Rostock, Germany

^dLeibniz Institute for Catalysis at the University of Rostock e.V., Albert-Einstein-Straße 29a, D-18059 Rostock, Germany

[†] Electronic supplementary information (ESI) available: Experimental information (incl. experimental setups), structure elucidation, syntheses, spectroscopic details and computational details. CCDC 1869014 and 1869015. For ESI and crystallographic data in CIF or other electronic format see DOI: 10.1039/c8sc04893b



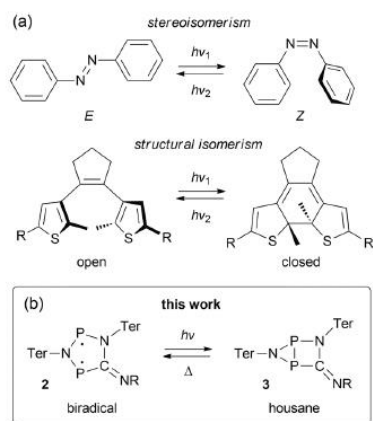


Fig. 1 Types of molecular switches. (a) Azobenzenes (top) and stilbenes can be categorized as stereoisomeric switches, while diarylethenes (bottom), spiropyranes, spiroxazines, and fulgimides are typical examples of structural isomeric switches. (b) We investigated the photo-switching behavior of hetero-cyclopentane-1,3-diyls (2), which display considerable singlet biradical character (R = ^tBu, Dmp (2,6-dimethylphenyl), Ter = 2,6-bis(2,4,6-trimethylphenyl)phenyl).

investigated topic throughout all areas of chemical science.^{25–28} Amongst others, singlet biradicals (or biradicaloids) are frequently cited as suitable model systems for bond formation and breaking processes due to their peculiar electronic structure, which is sometimes referred to as comprising a “partial bond” between the formal radical centres.²⁹ In this regard, singlet biradicals are promising candidates for molecular switches, as small structural changes should generally alter the bonding interaction between the radical centres significantly, thereby also affecting the biradical character. The latter being the source of many interesting properties, such as small-molecule activation^{30–33} or non-linear optical properties,^{29,34} it should be possible to switch these characteristics as well. Still, there are only few experimental examples in the literature taking advantage of such an approach.^{35–38}

We recently introduced stable hetero-cyclopentane-1,3-diyls based on group 15 elements (2, Fig. 1b).^{39–42} These five-

membered cyclic biradicals can be used to activate small molecules such as alkynes, carbon monoxide or isonitriles. Furthermore, preliminary investigations indicated that they can be isomerized by light to a closed-shell housane-type isomer (3) featuring a P–P single bond. Contrary to carbon based cyclopentane-1,3-diyls,^{43–46} the isomerization was shown to be reversible. Since we are not aware of molecular switches based on this class of compounds, we sought to study the photo-isomerization in more detail, so as to understand the mechanism of the photo-switching process and control the activation chemistry by switching the biradical character on and off.

Results and discussion

Photo-isomerization and thermal reverse reaction

We chose to begin our investigations on the system 2Dmp (Fig. 1b, R = Dmp = 2,6-dimethylphenyl), since it had proved to be the most stable derivative.⁴⁰ It was synthesized from the biradical [P(μ-NTer)]₂ (1, Ter = 2,6-dimesitylphenyl) by insertion of DmpNC according to published procedures (cf. ESI†). The UV-Vis spectrum exhibited a broad absorption band centred at 643 nm, *i.e.* in the red region of the visible spectrum (Fig. 2a). According to time-dependent density functional theory (TD-DFT), complete active space self-consistent field (CASSCF), and model multi-reference configuration interaction (MRCI) calculations, the absorption may be attributed to the formal HOMO → LUMO transition (*vide infra*; for detailed information on all calculations and proper electronic description of the singlet biradical please refer to the ESI, p. S40†). Since the “LUMO” is transannularly bonding in character between the two P atoms (Fig. S28 and S29;† cf. Fig. 7b), it seemed plausible that population of this orbital due to electronic excitation would lead to P–P bond formation and therefore to isomerization to the housane 3Dmp. Accordingly, irradiation of a blue, dilute solution of 2Dmp with red light (600–650 nm) resulted in quick discoloration (Fig. 3), and the absorption band at 643 nm vanished. When the irradiation was discontinued, the blue solution was fully recovered within 30 minutes (25 °C), as evidenced by UV-Vis measurements (Fig. S18†).

Since ³¹P NMR spectroscopy is exceptionally well suited to study molecules containing P atoms, we decided to irradiate our samples directly in the spectrometer, so we could trace the isomerization reactions as well as determine yields, reaction

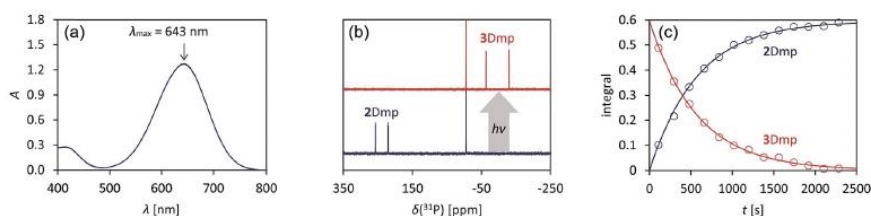


Fig. 2 Photo-isomerization of 2Dmp and thermal equilibration of 3Dmp at 25 °C. (a) UV-Vis spectrum of 2Dmp. (b) ³¹P NMR spectra of a solution of 2Dmp in the dark (bottom) and under irradiation (top). (c) Thermal reverse reaction (3Dmp → 2Dmp) monitored by ³¹P NMR spectroscopy (please see ESI† for data at different temperatures).



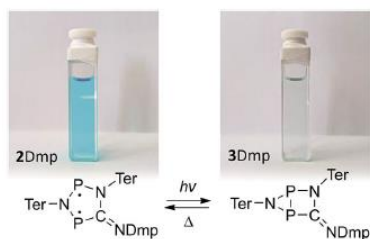


Fig. 3 Left: blue, dilute solution of 2Dmp in benzene. Right: colourless solution of the photo-product 3Dmp in benzene.

rates, the stability of the system and possible by-products. We adopted a setup previously published by the Gschwind group,⁴⁷ using a laser diode instead of an LED as light source. The diode was coupled with an optical fibre, which was inserted into an NMR tube equipped with a coaxial insert, allowing us to measure spectra under light (for technical details, see ESI†). Indeed, irradiation of 2Dmp with red light (638 nm) led to full conversion of the biradical 2Dmp to the housane 3Dmp (Fig. 2b). When the diode was switched off, the thermal equilibration could be monitored (Fig. 4). The thermal reverse reaction was found to be a first-order reaction with a half-life of about 7 min at ambient temperature ($k = 1.73(3) \times 10^{-3} \text{ s}^{-1}$), leading to quantitative recovery of 2Dmp (Fig. 2c). The activation barrier was determined according to the Eyring theory by re-determination of the rate constants at several temperatures, giving a Gibbs free energy of activation of $88(4) \text{ kJ mol}^{-1}$ at 25°C (cf. p. S25†), in good agreement with theoretical predictions

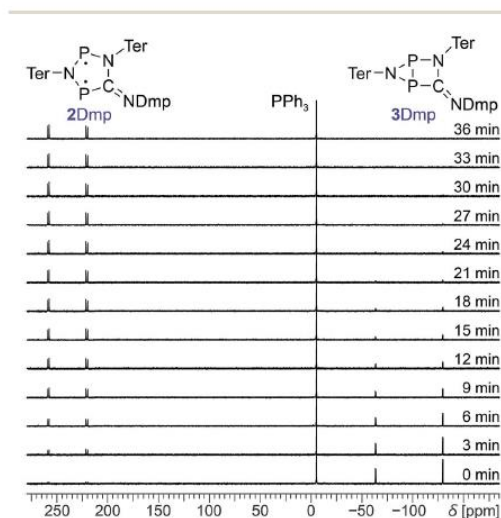


Fig. 4 Time-dependent ^{31}P NMR spectra of the thermal reverse reaction ($3\text{Dmp} \rightarrow 2\text{Dmp}$). PPh_3 was added as internal standard.

(ESI†). No signals of side products were observed in the ^{31}P NMR spectrum after several switching cycles. In a sealed tube, a solution of 2Dmp in benzene was stable for more than a year, and it did not lose its switching capacity.

Solid-state properties

Next, we investigated the solid-state properties of the molecular switch 2Dmp. Upon irradiation of a dark blue crystal with a red HeNe laser (633 nm, 0.1 mW), several cracks emanating from a circular, colourless spot could be observed (Fig. 5a–c). Increasing the light intensity (10 mW) led to complete discoloration, but also to fragmentation of the crystal (Fig. 5d and e). We attributed this observation to significant structural changes at the molecular level (*vide infra*) that caused stress within the crystal lattice and ultimately led to cracking of the crystal. When the light was switched off, a blue, polycrystalline material was recovered (Fig. 5f) that could be identified as 2Dmp by Raman spectroscopy (*vide infra*).

Notably, ambient light did not affect the integrity of single crystals at room temperature. However, at low temperatures such as -80°C , even low intensity (white) light eventually led to their disintegration. This can be understood in terms of the thermal reverse reaction: at ambient temperature, the rate of thermal equilibration is much higher than the rate of photo-conversion from ambient light, so the light is completely absorbed at the surface of the crystal. At low temperatures, though, the thermal reverse reaction is much slower than the rate of photo-conversion. Hence, given time, a critical number of molecules will have isomerized at some point, resulting in cracking of the crystal.

With this knowledge, we could now determine the crystal structure of 2Dmp. Notably, the crystal was mounted at *ambient* temperature, and then cooled to -150°C for measurement in complete darkness. (All previous attempts to obtain a complete data set failed since the crystals were mounted at low temperatures, leading to their disintegration due to irradiation by the mounting lamp.)⁴⁸ The molecular structure comprises a nearly planar, five-membered $\text{P}_2\text{N}_2\text{C}$ ring system (Fig. 6a). All P–N, P–C, and N–C bond lengths within the ring range between typical

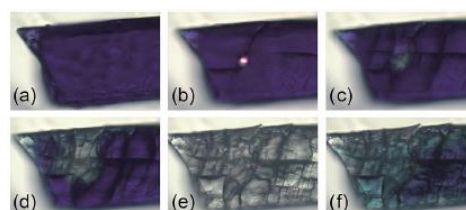


Fig. 5 Photos of a single crystal of 2Dmp at several stages of irradiation (25°C). The cracks in the crystal due to structural changes at the molecular level can be nicely seen. (a) Before irradiation. (b) During irradiation with red laser (633 nm, 0.1 mW). (c) Immediately after irradiation for 1 min (0.1 mW). (d) Immediately after irradiation for 5 min (0.1 mW). (e) Immediately after irradiation for 5 min (10 mW). (f) 10 min after irradiation (reverse reaction is not yet complete).



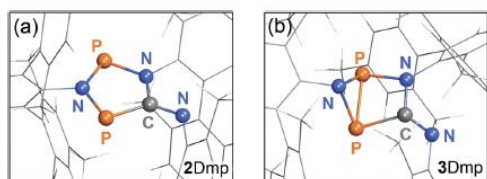


Fig. 6 (a) Structure of the planar P_2N_3C scaffold of 2Dmp as determined by single crystal X-ray diffraction. (b) Calculated structure of 3Dmp with a central hetero-bicyclo[2.1.0]pentane motif.

values⁴⁸ of a single and a double bond. The transannular $P\cdots P$ distance (2.9437(7) Å) is significantly longer than a P–P single bond ($\Sigma r_{cov} = 2.22$ Å),⁴⁸ in agreement with the biradical character of the compound (cf. p. S46†).

So far, all our efforts to obtain single crystals of the housane 3Dmp have failed. Crystallization under light led to a colourless solid; however, the crystals were too small for single-crystal X-ray analysis. Nonetheless, we performed dispersion corrected⁴⁹ density functional theory (DFT-D3) calculations to predict the structure (Fig. 6b). Contrary to 2Dmp, the five-membered P_2N_2C ring system of 3Dmp adopts an envelope conformation with a transannular P–P single bond (2.220 Å). Therefore, the structure changes significantly upon isomerization, explaining the

macroscopic changes observed in the material under irradiation.

The isomerization in the solid state could also be observed by Raman microscopy. Apart from visual changes of the material, the Raman spectrum changed significantly after irradiation. Especially, the C–N stretch of the exocyclic C=N double bond can be utilized as a probe to identify the isomers ($\bar{\nu}_{CN} = 1640$ cm^{-1} in 3Dmp, Fig. S25†).

Mechanism

Comprehensive computations were carried out to understand the mechanism of the photo-isomerization as well as the thermal reverse reaction. Since the correct quantum-mechanical treatment of biradicals requires multi-reference wave functions (which severely limits the size of systems that can be investigated), we opted to study the isomerization process using a model system bearing only hydrogen substituents (2H). Various calculations were performed to ascertain that this is indeed a suitable model (ESI†).

The CASSCF and MRCI results indicated that the electronic excitation of 2H leads to a non-stationary point on the S_1 potential energy surface (PES). Distortion of the molecule – mainly by folding of the five-membered ring along the $P\cdots P$ axis and concurrent shortening of the $P\cdots P$ interatomic distance – leads to a conical intersection (CIInt) between the S_1 and S_0 surface, therefore allowing radiationless deactivation of the excited state. The CIInt is in the vicinity of a transition state on the S_0 PES which connects the biradical 2H and the housane 3H, enabling thermal isomerization of 3H to 2H (Fig. 7a; for more details on the calculations, see p. S42†).

As indicated, a qualitatively correct wave function of a biradical requires multiple determinants. The same is true of excited states, at least if they are modelled as higher energy roots of the CI matrix. However, depending on the reference orbitals used for the CI, the resulting wave functions may be rather difficult to interpret. The more qualitative CASSCF approach (which neglects dynamic electron correlation) is probably best suited to understand the electronic structures of 2H in its ground and first excited singlet state. In particular, a state-specific CASSCF calculation yields a unique set of orbitals for each state. These orbitals are variationally optimized to best represent the electron distribution for a given state, *i.e.* fewer determinants are needed to describe the wave function, making it easier to interpret. The results for 2H nicely demonstrate that both the S_0 and S_1 state have considerable biradical character⁵⁰ (28 and 44%, respectively; cf. 27 and 36% for 2Dmp). The dominant contribution to the wave function of the ground state is transannularly anti-bonding between the two P atoms, whereas the dominant contribution to the S_1 state is bonding in nature, in agreement with earlier considerations (Fig. 7b). Note that the CASSCF results also correctly indicate that the electronic excitation involves redistribution of the whole electron density, rather than just one electron being excited into a vacant orbital. A rather detailed discussion of the electronic wave function and electronic excitation including MRCI results can be found in the ESI (p. S46†).

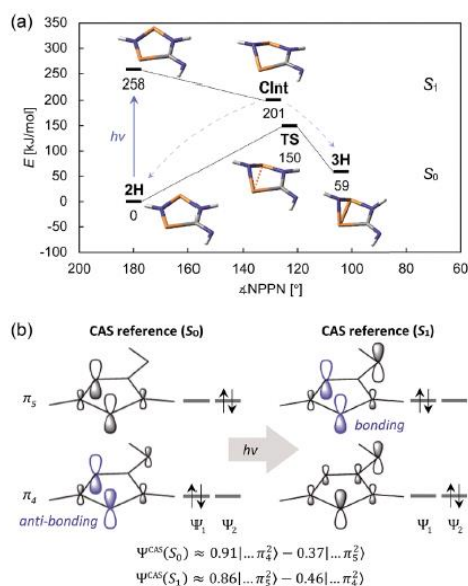
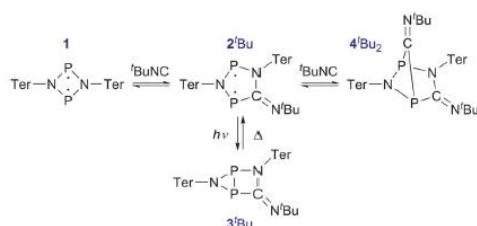


Fig. 7 (a) Schematic view of the ground state and first excited state PES of the model system 2H. (b) Simplified depiction of the relevant orbitals of a state-specific CAS (8, 6) calculation. Upon excitation, the electron density is redistributed, resulting in a mostly bonding interaction between the two P atoms. The approximate wave functions are given by $\Psi^{CAS} \approx c_1\Psi_1 + c_2\Psi_2$.





Scheme 1 The thermal equilibrium can be completely suppressed by irradiation.

Quantum yield

As demonstrated by the calculations, the excited state can deactivate through a conical intersection. However, this process can lead to the formation of both the starting material (2Dmp) or the photo-product (3Dmp). Thus, we were interested in the quantum yield of the photo-isomerization, *i.e.* the ratio of successful isomerizations to absorbed photons. Taking advantage of the different absorbances of 2Dmp and 3Dmp, we irradiated a dilute solution with a red HeNe laser (633 nm) and measured the transmitted laser intensity behind the sample. Due to photo-isomerization, the transmitted intensity increased over time, and the time-resolved data could be used to determine the quantum yield (p. S34†). With a value of 24.6(8)%, the photo-isomerization is rather efficient (*cf.* photosynthesis in plants: 5–12%;^{51–53} azobenzene: 11% (*trans* → *cis*), 42% (*cis* → *trans*);⁵⁴ diarylethenes: 13–59% (cyclization), 0.002–59% (cycloreversion) depending on the substituents;⁵⁵ retinal: 65%⁵⁶).

Manipulation of an equilibrium reaction

Having understood the photo-switching of the biradical 2Dmp, we were now interested whether it might be possible to manipulate a chemical reaction using this type of molecular switch. In particular, an equilibrium reaction involving activation chemistry of the biradical 2 seemed promising, as this would open the possibility to couple thermal and photochemical processes.

As previously shown, the reaction of 1 with ^tBuNC did not lead to quantitative formation of 2^fBu but rather to an equilibrium mixture of 1, 2^fBu, and 4^fBu₂, the addition product of the biradical 2^fBu and ^tBuNC (Scheme 1). The colourless adduct 4^fBu₂ could be isolated from the mixture by crystallization (ESI†).⁴⁰ When re-dissolving the colourless crystals, the blue-green equilibrium mixture of 1, 2^fBu, and 4^fBu₂ was recovered, as evidenced by ³¹P NMR experiments. The UV-Vis spectrum of the solution (Fig. 8a) showed a broad absorption band at 663 nm (2^fBu) and two absorption maxima at 463 and 491 nm (1). Accordingly, irradiation of the solution with a red laser diode (638 nm) led to photo-isomerization of the molecular switch 2^fBu. Thus, it was completely removed from the thermal equilibrium, resulting in quantitative formation of the housane 3^fBu and disappearance of the thermal products 1 and 4^fBu₂ (Fig. 8b); *i.e.* the thermal equilibrium involving the activation chemistry of the biradical was entirely suppressed by the photo-isomerization! This might be regarded as “quenching of the biradical character”, as previously proposed by Wang *et al.*³⁴

When the light source was switched off, the thermodynamic equilibrium mixture was slowly recovered. The housane 3^fBu decayed in a first order reaction with a half-life of about 57 min at 25 °C ($k = 2.03(4) \times 10^{-4} \text{ s}^{-1}$, Fig. 8c). The process was completely reversible, and even after several switching cycles, no side products could be observed in the ³¹P NMR spectrum.

Finally, the activation of ^tBuNC with the more stable biradical 2Dmp was investigated. Indeed, the expected adduct 4Dmp^fBu was formed in an equilibrium with 2Dmp (Scheme 2). To our surprise, irradiation of the blue solution with a red laser diode (638 nm) did not lead to discoloration as in the previous case. Even though formation of the photo-product 3Dmp was observed in the ³¹P NMR spectrum, quantitative conversion could not be achieved at ambient temperature, indicating that the rate of thermal equilibration was on the same order of magnitude as the rate of photo-conversion and therefore much faster than previously observed (*cf.* $t_{1/2} \approx 7$ min in the absence of ^tBuNC). In fact, as soon as the irradiation was discontinued, the thermal equilibrium was restored. Low-temperature investigations indicated that the ^tBuNC acted as a catalytic agent to accelerate the thermal reverse reaction of the housane 3Dmp (p. S31†). The mechanism of the catalyzed reverse reaction has yet

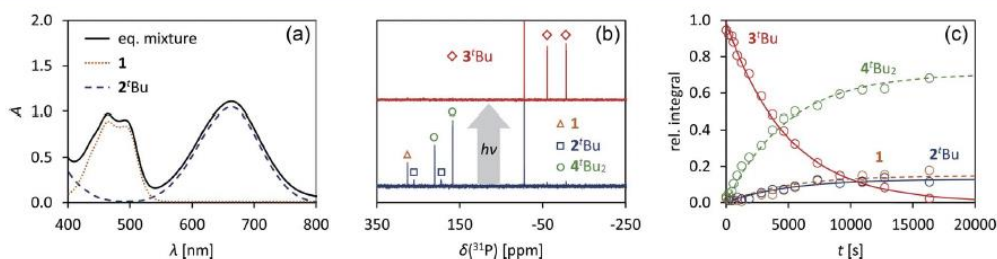
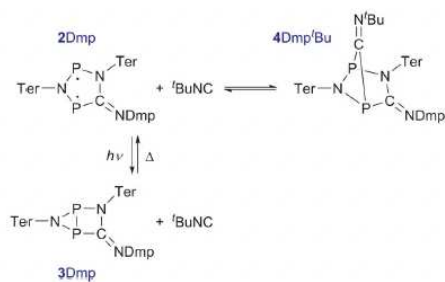


Fig. 8 (a) UV-Vis spectrum of an equilibrium mixture of 1, 2^fBu, 4^fBu₂, and ^tBuNC. (b) Upon irradiation with red light, the complete equilibrium is suppressed and the housane 3^fBu is formed exclusively, as evidenced by ³¹P NMR spectroscopy. (c) The thermal reverse reaction to recover the equilibrium species proceeds as first-order reaction.

Scheme 2 Reaction of 2Dmp with ^tBuNC.

to be investigated; this is outside the scope of this article and will therefore be explored in the future. For now, we just want to point out that it is possible to chemically manipulate the pathway of the thermal reverse reaction and thus influence the switching behaviour.

Conclusion

We could demonstrate that biradicals based on hetero-cyclopentane-1,3-diyls (2) are potent and chemically robust systems for application as molecular switches. They could be isomerized by red light to a closed-shell housane-type species (3) with a transannular bond, effectively quenching the biradical character. The biradical (2) was then fully recovered by a thermal reverse reaction in darkness. Substitution of the organic groups at the exocyclic C=N scaffold changed the properties of the systems, promising variability of key features such as stability, activation chemistry, and excitation wavelength.

The isomerization could be monitored by UV-Vis, NMR, and Raman spectroscopy. In the solid state, significant structural changes at the molecular level upon irradiation resulted in macroscopic changes such as fragmentation of crystals. Hence, even though the molecular process was fully reversible, the macroscopic crystallinity was lost upon isomerization. In solution, the switching process could be repeated many times without any indications of decomposition. While the rate of photo-isomerization depended on the light intensity, the rate of thermal reverse reaction could be influenced either by changes in temperature or chemically by addition of isonitriles.

In case of the ^tBu derivative 2^tBu, it was possible to completely suppress the thermal equilibrium related to the activation chemistry of the biradical upon irradiation. This serves as a proof-of-principle that chemical reactions can be controlled by molecular switches that take advantage of kinetically stabilized biradicals.

The mechanisms of both photo- and thermal isomerization were studied in detail using multi-reference calculations as well as experimental data. Formal one-electron excitation of 2 led to a transannularly bonding interaction and thus distortion of the molecule on the S₁ PES. Deactivation proceeded through a conical intersection and hence radiationlessly. The quantum

yield of the photochemical isomerization was determined to be 24.6(8)%. The thermal reverse reaction (3 → 2) proceeded through a single transition state on the ground state PES and was found to be a first-order reaction.

In future studies, we will further investigate the scope of hetero-cyclopentane-1,3-diyls as molecular switches, especially with respect to the control of chemical reactions, such as [2 + 2] additions of alkynes and alkenes.

Experimental

For detailed information on syntheses, equipment, analytical data, computational methods *etc.* please also consult the ESI.†

All manipulations were carried out under oxygen- and moisture-free conditions under an inert atmosphere of argon using standard Schlenk or dry box techniques.

NMR spectroscopy under irradiation

All irradiation experiments were performed on a Bruker AVANCE 250 MHz spectrometer. Light was directed into the sample using a multimode optical fibre with 1000 μm core diameter. To ensure inert conditions, the NMR tubes were filled in a glove box and equipped with a conical insert that could host the optical fibre. Thus, the sample volume could be kept isolated from the outside atmosphere. As light source we used a 700 mW laser diode (638 nm), which was mounted on the far end of the optical fibre. The outer cladding of the fibre was removed for about 5 cm on the sample side and the glass surface was roughened to ensure uniform irradiation of the sample, as previously reported.⁴⁷

UV-Vis spectroscopy

UV-Vis spectra were recorded on a Perkin-Elmer Lambda 19 UV-Vis spectrometer. For irradiation studies, the samples were irradiated outside the spectrometer using white or monochromated light (600–650 nm).

Determination of the quantum yield

We used a self-constructed setup mounted on a standard optical table (*cf.* ESI†). The samples were prepared in a glove box and filled in gas-tight cuvettes with an optical path length of 1 cm. The solutions were irradiated with a HeNe laser (633 nm) and the transmitted laser intensity was measured using a photo diode. The laser intensity was chosen so high that the rate of photo conversion was much larger than the rate of thermal equilibration; hence, the reverse reaction could be neglected. We derived the following time law for the signal sig(*t*) measured at the photo diode:

$$\frac{1}{\text{sig}(t)} = a + \left(\frac{1}{\text{sig}(0)} - a \right) 10^{-\frac{\phi \epsilon I_0}{N_A \times h\nu} t}$$

ϕ is the quantum yield, ϵ the molar extinction coefficient, I_0 the incident laser intensity, N_A Avogadro's number, $h\nu$ the energy of a photon, and a a fitting parameter related to the detection sensitivity. For a derivation of this formula and detailed description of the experimental setup, please refer to the ESI.†



Two different concentrations of 2Dmp in benzene were prepared. The samples were irradiated for 15 seconds, and each of those measurements was repeated multiple times. The data for each of the two concentrations were combined and evaluated by non-linear fitting procedures.

Computational methods

Electronic structure computations were performed using Gaussian09⁵⁷ (DFT, CASSCF) or ORCA 4.0.1⁵⁸ (CASSCF, MRCI). Structure optimizations were run using pure density functionals in conjunction with the D3BJ⁴⁹ dispersion correction. The investigation of the PES of the model system was done using CAS(8,6) computations, including all π -type orbitals of 2H (*i.e.* those belonging to the A'' irrep, point group C_3).

To obtain an idea of the reliability of DFT methods to predict experimental properties of the biradical systems 1 and 2, we performed a survey of different methods and compared their results to experimental as well as high-level *ab initio* data. Generally, DFT methods are suitable to predict molecular structures and first excitation energies with reasonable accuracy; however, the absolute KS energies are notoriously bad due to single-determinantal treatment of the KS wave function. Notably, the PBE functional⁵⁹ outperformed all other methods at predicting NMR data. Please refer to the ESI† for in-depth information.

Conflicts of interest

There are no conflicts to declare.

Acknowledgements

We are indebted to Henry Dube for sparking the idea that led to this study. We thank the University of Rostock for access to the cluster computer, and especially Malte Willert for his assistance with the queuing system and software installations. We thank Alexander Villinger for assistance with X-ray crystallography. Special thanks are due to Peter Kumm for his continuous commitment in the technical workshop. Financial support by the DFG (SCHU 1170/11-1) is gratefully acknowledged.

Notes and references

- 1 A. D. Johnson, A. R. Poteete, G. Lauer, R. T. Sauer, G. K. Ackers and M. Ptashne, *Nature*, 1981, 294, 217–223.
- 2 M.-M. Russew and S. Hecht, *Adv. Mater.*, 2010, 22, 3348–3360.
- 3 J. L. Zhang, J. Q. Zhong, J. D. Lin, W. P. Hu, K. Wu, G. Q. Xu, A. T. S. Wee and W. Chen, *Chem. Soc. Rev.*, 2015, 44, 2998–3022.
- 4 D. Bléger and S. Hecht, *Angew. Chem., Int. Ed.*, 2015, 54, 11338–11349.
- 5 P. C. Knipe, S. Thompson and A. D. Hamilton, *Chem. Sci.*, 2015, 6, 1630–1639.
- 6 A. F. Hollemann, E. Wiberg and N. Wiberg, *Lehrbuch der Anorganischen Chemie*, Walter de Gruyter, Berlin, Germany, 102nd edn, 2007.
- 7 R. W. Sabnis, E. Ross, J. Köthe, R. Naumann, W. Fischer, W.-D. Mayer, G. Wieland, E. J. Newman and C. M. Wilson, in *Ullmann's Encyclopedia of Industrial Chemistry*, Wiley-VCH, Weinheim, Germany, 2009.
- 8 N. A. Rakow and K. S. Suslick, *Nature*, 2000, 406, 710–713.
- 9 H. Finkelmann, E. Nishikawa, G. G. Pereira and M. Warner, *Phys. Rev. Lett.*, 2001, 87, 015501.
- 10 S. Kobatake, S. Takami, H. Muto, T. Ishikawa and M. Irie, *Nature*, 2007, 446, 778–781.
- 11 T. Ube and T. Ikeda, *Angew. Chem., Int. Ed.*, 2014, 53, 10290–10299.
- 12 R. S. Stoll and S. Hecht, *Angew. Chem., Int. Ed.*, 2010, 49, 5054–5075.
- 13 R. Göstl, A. Senf and S. Hecht, *Chem. Soc. Rev.*, 2014, 43, 1982–1996.
- 14 E. Orgiu, N. Crivillers, M. Herder, L. Grubert, M. Pätzelt, J. Frisch, E. Pavlica, D. T. Duong, G. Bratina, A. Salleo, N. Koch, S. Hecht and P. Samorì, *Nat. Chem.*, 2012, 4, 675–679.
- 15 M. El Gemayel, K. Börjesson, M. Herder, D. T. Duong, J. A. Hutchison, C. Ruzié, G. Schweicher, A. Salleo, Y. Geerts, S. Hecht, E. Orgiu and P. Samorì, *Nat. Commun.*, 2015, 6, 6330.
- 16 G. Wald, *J. Gen. Physiol.*, 1948, 31, 489–504.
- 17 G. Wald, *J. Gen. Physiol.*, 1949, 32, 367–389.
- 18 G. Wald, *Science*, 1968, 162, 230–239.
- 19 B. L. Feringa, R. A. van Delden, N. Koumura and E. M. Geertsema, *Chem. Rev.*, 2000, 100, 1789–1816.
- 20 G. S. Hartley, *Nature*, 1937, 140, 281.
- 21 J. M. Robertson, *J. Chem. Soc.*, 1939, 0, 232–236.
- 22 Y. Yokoyama, *Chem. Rev.*, 2000, 100, 1717–1740.
- 23 G. Berkovic, V. Krongauz and V. Weiss, *Chem. Rev.*, 2000, 100, 1741–1754.
- 24 M. Irie, *Chem. Rev.*, 2000, 100, 1685–1716.
- 25 L. Salem and C. Rowland, *Angew. Chem., Int. Ed. Engl.*, 1972, 11, 92–111.
- 26 *Diradicals*, ed. W. T. Borden, Wiley-Interscience, New York, 1982.
- 27 F. Breher, *Coord. Chem. Rev.*, 2007, 251, 1007–1043.
- 28 M. Abe, *Chem. Rev.*, 2013, 113, 7011–7088.
- 29 K. Okuno, Y. Shigeta, R. Kishi and M. Nakano, *J. Phys. Chem. Lett.*, 2013, 4, 2418–2422.
- 30 A. Hinz, R. Kuzora, U. Rosenthal, A. Schulz and A. Villinger, *Chem.–Eur. J.*, 2014, 20, 14659–14673.
- 31 A. Hinz, R. Kuzora, A.-K. Rölke, A. Schulz, A. Villinger and R. Wustrack, *Eur. J. Inorg. Chem.*, 2016, 2016, 3611–3619.
- 32 J. Bresien, A. Hinz, A. Schulz and A. Villinger, *Eur. J. Inorg. Chem.*, 2018, 2018, 1679–1682.
- 33 J. Bresien, A. Hinz, A. Schulz and A. Villinger, *Dalton Trans.*, 2018, 47, 4433–4436.
- 34 J.-J. Wang, Z.-J. Zhou, H.-M. He, D. Wu, Y. Li, Z.-R. Li and H.-X. Zhang, *J. Phys. Chem. C*, 2016, 120, 13656–13666.
- 35 H. Li, A. C. Fahrenbach, A. Coskun, Z. Zhu, G. Barin, Y.-L. Zhao, Y. Y. Botros, J.-P. Sauvage and J. F. Stoddart, *Angew. Chem., Int. Ed.*, 2011, 50, 6782–6788.



- 36 A. T. Buck, J. T. Paletta, S. A. Khindurangala, C. L. Beck and A. H. Winter, *J. Am. Chem. Soc.*, 2013, 135, 10594–10597.
- 37 J. Sun, Y. Wu, Y. Wang, Z. Liu, C. Cheng, K. J. Hartlieb, M. R. Wasielewski and J. F. Stoddart, *J. Am. Chem. Soc.*, 2015, 137, 13484–13487.
- 38 P. Ravat, T. Solomek, D. Häussinger, O. Blacque and M. Juricek, *J. Am. Chem. Soc.*, 2018, jacs.8b05465.
- 39 A. Hinz, A. Schulz and A. Villinger, *Angew. Chem., Int. Ed.*, 2015, 54, 2776–2779.
- 40 A. Hinz, A. Schulz and A. Villinger, *J. Am. Chem. Soc.*, 2015, 137, 9953–9962.
- 41 A. Hinz, A. Schulz and A. Villinger, *Chem. Sci.*, 2016, 7, 745–751.
- 42 A. Schulz, *Dalton Trans.*, 2018, 47, 12827–12837.
- 43 F. Kita, W. Adam, P. Jordan, W. M. Nau and J. Wirz, *J. Am. Chem. Soc.*, 1999, 121, 9265–9275.
- 44 W. Adam, W. T. Borden, C. Burda, H. Foster, T. Heidenfelder, M. Heubes, D. A. Hrovat, F. Kita, S. B. Lewis, D. Scheutzow and J. Wirz, *J. Am. Chem. Soc.*, 1998, 120, 593–594.
- 45 D. Y. Zhang, D. A. Hrovat, M. Abe and W. T. Borden, *J. Am. Chem. Soc.*, 2003, 125, 12823–12828.
- 46 M. Abe, W. Adam, W. T. Borden, M. Hattori, D. A. Hrovat, M. Nojima, K. Nozaki and J. Wirz, *J. Am. Chem. Soc.*, 2004, 126, 574–582.
- 47 C. Feldmeier, H. Bartling, E. Riedle and R. M. Gschwind, *J. Magn. Reson.*, 2013, 232, 39–44.
- 48 P. Pyykkö and M. Atsumi, *Chem.–Eur. J.*, 2009, 15, 12770–12779.
- 49 S. Grimme, S. Ehrlich and L. Goerigk, *J. Comput. Chem.*, 2011, 32, 1456–1465.
- 50 E. Miliordos, K. Ruedenberg and S. S. Xantheas, *Angew. Chem., Int. Ed.*, 2013, 52, 5736–5739.
- 51 J. B. Skillman, *J. Exp. Bot.*, 2007, 59, 1647–1661.
- 52 S. W. Hogewoning, E. Wientjes, P. Douwstra, G. Trouwborst, W. van Ieperen, R. Croce and J. Harbinson, *Plant Cell*, 2012, 24, 1921–1935.
- 53 K. Stranius and K. Börjesson, *Sci. Rep.*, 2017, 7, 41145.
- 54 G. Zimmerman, L. yung Chow and U. jin Paik, *J. Am. Chem. Soc.*, 1958, 80, 3528–3531.
- 55 K. Morimitsu, S. Kobatake and M. Irie, *Mol. Cryst. Liq. Cryst.*, 2005, 431, 451–454.
- 56 A. Kropf, in *Methods Enzymol.*, 1982, vol. 81, pp. 384–392.
- 57 M. J. Frisch, G. W. Trucks, H. B. Schlegel, G. E. Scuseria, M. A. Robb, J. R. Cheeseman, G. Scalmani, V. Barone, B. Mennucci, G. A. Peterson, H. Nakatsuji, M. Caricato, X. Li, H. P. Hratchian, A. F. Izmaylov, J. Bloino, G. Zheng, J. L. Sonnenberg, M. Hada, M. Ehara, K. Toyota, R. Fukuda, J. Hasegawa, M. Ishida, T. Nakajima, Y. Honda, O. Kitao, H. Nakai, T. Vreven, J. A. Montgomery Jr, J. E. Peralta, F. Ogliaro, M. Bearpark, J. J. Heyd, E. Brothers, K. N. Kudin, V. N. Staroverov, T. Keith, R. Kobayashi, J. Normand, K. Raghavachari, A. Rendell, J. C. Burant, S. S. Iyengar, J. Tomasi, M. Cossi, N. Rega, J. M. Millam, M. Klene, J. E. Know, J. B. Cross, V. Bakken, C. Adamo, J. Jaramillo, R. Gomperts, R. E. Stratmann, O. Yazyev, A. J. Austin, R. Cammi, C. Pomelli, J. W. Ochterski, R. L. Martin, K. Morokuma, V. G. Zakrzewski, G. A. Voth, P. Salvador, J. J. Dannenberg, S. Dapprich, A. D. Daniels, O. Farkas, J. B. Foresman, J. V. Ortiz, J. Cioslowski and D. J. Fox, *Gaussian09, Revision E.01*, Gaussian Inc, 2013.
- 58 F. Neese, *Wiley Interdiscip. Rev.: Comput. Mol. Sci.*, 2018, 8, e1327.
- 59 J. P. Perdew, K. Burke and M. Ernzerhof, *Phys. Rev. Lett.*, 1996, 77, 3865–3868.



6.2 Photoisomerization of a phosphorus-based biradicaloid: ultrafast dynamics through a conical intersection

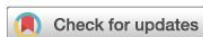
Tim Völzer, Henrik Beer, Axel Schulz, Stefan Lochbrunner, Jonas Bresien

Phys. Chem. Chem. Phys. **2021**, *23*, 7434–7441.

DOI: 10.1039/d1cp00428j

Reproduced from Ref. *Phys. Chem. Chem. Phys.*, 2021, 23, 7434 with permission from the PCCP Owner Societies.

Onlinelink: <https://doi.org/10.1039/D1CP00428J>


 Cite this: *Phys. Chem. Chem. Phys.*,
2021, 23, 7434

Photoisomerization of a phosphorus-based biradicaloid: ultrafast dynamics through a conical intersection†

 Tim Völzer,^{†a} Henrik Beer,^{†b} Axel Schulz,^{b,c} Stefan Lochbrunner^{a,c} and Jonas Bresien^{†*b}

 Received 29th January 2021,
Accepted 18th March 2021

DOI: 10.1039/d1cp00428j

rsc.li/pccp

As previously reported, photoisomerization of the open-shell singlet biradicaloid [TerNP]2CNDmp (**2**) yields its closed-shell housane-type isomer (**3**). In the present study, pump-probe spectroscopy was applied to investigate the excited-state dynamics of the photoisomerization, indicating ultrafast de-excitation of the S_1 state through a conical intersection, in agreement with computational predictions. The structural and electronic changes during the isomerization process are discussed to gain an understanding of the reaction pathway and the transformation of the biradicaloid to a closed-shell species.

Introduction

Photochromic compounds, *i.e.* light-activated molecular switches with two different (meta)stable states that exhibit different absorption spectra,¹ promise diverse applications, *e.g.* as ultrafast molecular electronic devices,² photoactuators,^{3–5} or photo-regulated catalysts.^{6,7} Key to their application is an understanding of the underlying isomerization mechanisms. As the photoisomerization between the two stable ground state isomers proceeds *via* an electronically excited state, the isomerization typically occurs on the femto- to picosecond timescale.^{2,8,9} Thus, investigation of the excited state dynamics of the photoisomerization process requires ultrafast spectroscopic techniques such as pump-probe spectroscopy with femtosecond laser pulses.^{9–11}

In general, photochemical reactions can proceed adiabatically (*i.e.* the chemical change occurs along a single potential energy surface, PES) or nonadiabatically,^{12,13} that is the reaction is controlled by a conical intersection (CInt) between two electronic states (Fig. 1).^{8,9,11,14–16} In the latter case, the reactivity is governed by strong coupling between nuclear and electronic motion (*i.e.* vibronic coupling), which allows a molecule to transfer from one electronic PES to another without emission of radiation. The photoisomerization of photochromic molecular switches is typically controlled by

state-switching at conical intersections,¹⁷ which usually results in dynamics on a sub-picosecond timescale.^{2,9,11,18}

Six years ago, we started to investigate photo-switchable singlet biradicaloids (**B**, Scheme 1),^{19–22} that can be isomerized to a closed-shell housane-type species (**C**) by irradiation with red light ($\lambda_{\text{max}} = 643$ nm for the most stable derivative **2**). Biradicaloids of type **B** are highly fascinating systems both from a chemical as well as physical standpoint, as they combine characteristics of singlet biradicaloids (such as unique electronic structure, high reactivity)^{23–31} with those of molecular switches, *i.e.* the biradical character^{32–36} can be switched “on” and “off” by an outside stimulus. Some first investigations demonstrated that this behaviour can be exploited to influence a chemical reaction that depends on the activation chemistry of the biradicaloid.^{20,21} Moreover, biradicaloids of type **B** can be viewed as stable, heteroatom-substituted analogues of cyclopentadienyl, a usually short-lived intermediate in organic chemistry.^{37–42} Recently, efforts have been made to synthesize a variety of such

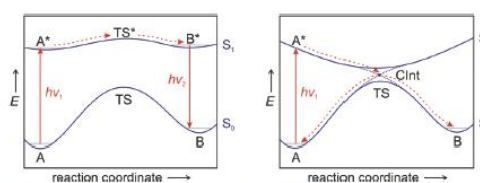


Fig. 1 Simplified representation of an adiabatic (left) and nonadiabatic (right) photochemical reaction $A \rightarrow B$. The conical intersection (CInt) should be pictured in a second dimension “behind” the reaction coordinate. Figure adapted from refs. 9 and 12.

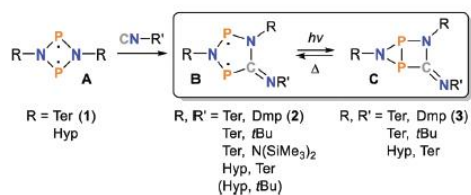
^a Institute of Physics, University of Rostock, Albert-Einstein-Str. 23-24, 18059 Rostock, Germany

^b Institute of Chemistry, University of Rostock, Albert-Einstein-Str. 3a, 18059 Rostock, Germany. E-mail: jonas.bresien@uni-rostock.de

^c Department Life, Light & Matter, University of Rostock, 18051 Rostock, Germany

† Electronic supplementary information (ESI) available: Transient absorption spectroscopy, computational details. See DOI: 10.1039/d1cp00428j

‡ T. V. and H. B. contributed equally to this work.



Scheme 1 The photo-switchable biradicaloid **B** is generated from $[\text{P}(\mu\text{-NR})_2]$ (**A**) by insertion of isonitriles into an N–P bond (Ter = 2,6-dimesitylphenyl, Hyp = $\text{Si}(\text{SiMe}_3)_3$, Dmp = 2,6-dimethylphenyl). Photoisomerization to housane **C** proceeds under irradiation with red light. Contrary to **B**, the closed-shell species **C** does not possess significant biradical character.

heteroatom-stabilized systems,^{19,37,43–48} demonstrating the interest in this class of compounds.

Being the most stable derivative of **B**, biradicaloid **2** (*i.e.* R = Ter, R' = Dmp; *cf.* Scheme 1) was used in various studies which investigated its structure–property relationships.^{19–21} Just recently, the ground-state reaction kinetics of the thermal reverse reaction (**3** → **2**) were studied in more detail.²¹ In contrast, the mechanism of photoisomerization had only been predicted using computational models,²⁰ indicating state-switching between the adiabatic S_1 and S_0 surfaces at a conical intersection. It was therefore of special interest to investigate the excited-state dynamics experimentally and to expand on the theoretical description of the excited-state PES.

Results and discussion

Electronic structure

To begin, we will shortly revisit the electronic structure of biradicaloid **2**, as this will help to understand the excited state dynamics and photoisomerization reaction. The electronic structure has partly been discussed in our previous publications,^{19,20} yet a few crucial points, especially regarding the biradical character, deserve further attention.

Singlet biradicals and biradicaloids (“diradical(oid)s”) may be used synonymously^{26,28,49–51} need to be described by multi-reference wavefunctions^{52–60} to account for the significant amount of non-dynamic^{61–63} electron correlation. This “strong” correlation between the radical electrons arises from the near degeneracy of the frontier molecular orbitals (FMOs). Thus, in the delocalized picture, two closed-shell determinants (with doubly occupied HOMO and LUMO, respectively) are mixed in the configuration interaction (CI) expansion of the wavefunction (Fig. 2, left). However, the biradical character of the system is better represented in the localized orbital picture (Fig. 2, right), which is a mathematically equivalent representation of the wavefunction.³⁰ The two “radical centres”, which are mainly localized at the P atoms, are antiferromagnetically^{27,35} coupled ($\Delta E_{S-T} = -76.9 \text{ kJ mol}^{-1}$ for model system **2H** at MRCISD+Q^{64,65}/CAS(8,6)^{52–60} level of theory, *cf.* Table S2, ESI†), resulting in a singlet ground state.

Various measures exist to quantify the “biradical character”, *i.e.* the amount of non-dynamic electron correlation.³⁰ For example,

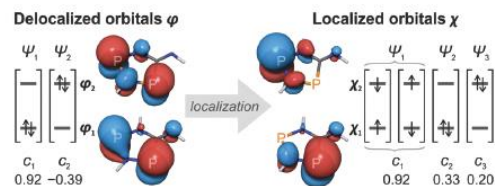


Fig. 2 Multireference wavefunction $\Psi = \sum c_i \Psi_i$ of biradicaloid **2** in the delocalized (left) and localized orbital basis (right). For clarity, the simplified CAS(2,2) results of model compound **2H** are depicted (the multireference character of **2** is essentially identical, *cf.* ESI†, p. S20f). The two closed-shell configuration state functions (CSFs, Ψ_i) in the delocalized basis transform to an open-shell (biradical, covalent) and two closed-shell (ionic) CSFs in the localized orbital basis. The two wavefunctions (delocalized/localized basis) are mathematically identical.

the β scale³⁶ defined as $\beta = 2c_2^2/(c_1^2 + c_2^2)$ with $0 < \beta < 1$ directly relates the biradical character to the CI expansion coefficients in the delocalized orbital basis (Fig. 2, left) and is applicable to arbitrary CAS-CI wavefunctions. In the case of biradicaloid **2**, β amounts to 25% (CAS(8,6)/def2-TZVP,^{66,67} *cf.* ESI†, p. S20f), implying an admixture of (zwitter)ionic character to the (covalent) biradical state, as demonstrated by the CI expansion in the localized orbital basis (Fig. 2, right). In this vein, all related P-based biradicaloids ($\beta = 15\text{--}28\%$)^{68,69} possess some zwitterionic character, which could also be demonstrated experimentally by their reactivity towards Lewis acids and bases.⁷⁰

In the context of the photochemistry of biradicaloid **2**, it is worthy to note that pairs of orbitals with bonding/antibonding character correlate most strongly. Here, the transannular interaction between the two P atoms is weakly antibonding in the formal HOMO φ_1 (out-of-phase combination of the p atomic orbitals), whereas the LUMO φ_2 is weakly bonding in character (Fig. 3). This is, of course, a prerequisite for the biradical character of compound **2**, but also implies that electronic excitation results in a change of the bonding pattern: formally, a single electron is transferred from the HOMO into the LUMO upon excitation, so that the antibonding transannular interaction in the S_0 state becomes predominantly bonding in the S_1 state (Fig. 3; note the

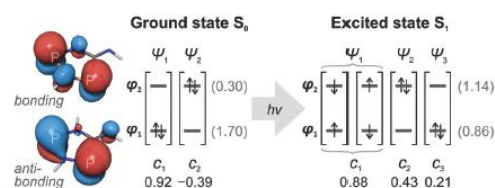


Fig. 3 State-averaged CASSCF wavefunctions $\Psi = \sum c_i \Psi_i$ of the S_0 (left) and S_1 state (right) of **2H**. The orbitals are averaged over the four biradical states (3 singlets, 1 triplet)³⁰ and are nearly identical to the delocalized, ground-state orbitals in Fig. 2. Note that the first CSF Ψ_1 of the S_1 state represents a zwitterionic configuration in the delocalized orbital basis. The occupation numbers of the orbitals are given in brackets, indicating a primarily antibonding transannular interaction in the S_0 state and a weakly bonding interaction in the S_1 state.

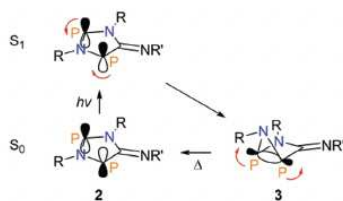
different occupation numbers of the orbitals in each state).²⁰ Deformation of the planar ring system on the S_1 potential energy surface (PES) ultimately results in a significant overlap of the p atomic orbitals, leading to σ -bond formation between the two P atoms in a disrotatory process. Hence, the biradical character of **2** is inextricably connected to the photochemistry of the system.

Ground-state and excited-state PES

As indicated in Scheme 1, the above-mentioned photoinduced σ -bond formation between the two P atoms of biradicaloid **2** leads to the formation of its housane-type isomer **3**, which is best described as a closed-shell species (*cf.* Fig. S10, ESI†). As expected, the HOMO of **3** describes the P–P σ -bond, whereas the LUMO is the corresponding (unoccupied) antibonding orbital (Fig. S10, ESI†), suggesting that the bonding/antibonding character of HOMO and LUMO is inverted with respect to biradicaloid **2**. Thus, the photochemical, disrotatory bond formation follows the usual Woodward–Hoffmann rules for electrocyclic ring-closure reactions.^{71,72} The thermal reverse reaction, however, must also proceed in a disrotatory manner (formally violating the Woodward–Hoffman rules) due to the bicyclic structure of housane **3**, resulting in a rather large activation barrier and long lifetime (Scheme 2). The stability of related bicyclo[2.1.0]pentene is attributed to the same phenomenon.⁷²

In agreement with above considerations, a conical intersection (CIInt) between ground and first excited singlet state can be localized approximately halfway along the reaction path between the isomers **2** and **3**,²⁰ allowing the formation of the housane **3** from excited molecules of **2** in a nonadiabatic reaction pathway.

To understand and interpret the excited state dynamics (*vide infra*), the topology of the excited state PES was investigated. We chose to begin our study using the model system 2H/3H ($R = R' = H$; Fig. 4), on the one hand to gain a qualitative picture, and on the other hand to employ high-level, multi-reference *ab initio* methods for which the actual molecules (2/3) would be too large. As discussed above, multi-reference methods are required for correct description of the biradical character of compound **2**. Yet, DFT can sometimes give good results nonetheless, either if the biradical character is not too large and the single-determinant Kohn–Sham approach still



Scheme 2 Simplified depiction of the relevant occupied orbitals of biradicaloid **2** and housane **3** that dictate the interconversion between both isomers. The σ -bond formation between both P atoms occurs via a photochemical, disrotatory ring-closure. The bicyclic housane **3** undergoes a thermal, disrotatory ring opening which leads back to the biradicaloid **2**. This reaction is formally symmetry-forbidden and explains the relative stability (half-life: 7 min at 25 °C)²⁰ of the highly strained housane **3**.

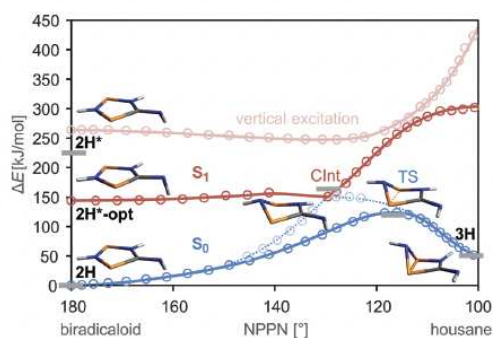


Fig. 4 Ground state (S_0) and excited state (S_1) potential energy surface of **2H/3H** projected along the NPPN dihedral angle (DFT and NEVPT2/CASSCF results). The solid blue and red lines correspond to the minimum energy paths (MEPs). The faded red line indicates the vertical excitation profile, *i.e.* the first excitation energy of the respective ground-state structure. The grey bars indicate the results of MRCI computations.²⁰ For computational details, please refer to the ESI† p. S12ff and Fig. S6.

approximately holds true,^{61,73} or if the multi-reference character can be approximately treated using the broken-symmetry (BS) formalism, which represents the wavefunction as a single determinant using localized spin-orbitals.^{34,35,74–77} (This is comparable to the localized orbital picture of the CASSCF wavefunction; however, as only a single determinant is used, the BS formalism introduces unphysical spin polarization.)

Consequently, the ground- and excited-state PES of 2H/3H were computed using both (U)DFT/TD-DFT^{78–84} (PBE-D3^{85–88}/def2-TZVP^{66,89}) as well as multi-reference *ab initio* calculations (MRCI^{64,65} and NEVPT2^{90–92}/CASSCF;^{52–60} for detailed descriptions of all computations please see the ESI†). The results of all three approaches agree reasonably well (*cf.* ESI† p. S12ff and Table S2), so it can be expected that DFT will also produce reasonable results for the actual system 2/3, which cannot be fully treated by multi-reference *ab initio* methods (*vide infra*).

As previously reported,^{20,21} the ground-state minimum energy path (MEP) between biradicaloid 2H and housane 3H (blue line in Fig. 4) proceeds *via* a single transition state (TS), *i.e.* P–P bond formation/breaking and folding of the ring system (described by the NPPN dihedral angle) occur concurrently in a concerted process. The housane represents a local minimum on the ground-state PES, while the biradicaloid 2H is the thermodynamically favoured isomer ($\Delta E_{\text{MRCI}} = 50.4 \text{ kJ mol}^{-1}$, *i.e.* the reverse reaction is essentially quantitative). The activation barrier for the reverse reaction is $\Delta E_{\text{MRCI}} = 69.0 \text{ kJ mol}^{-1}$. These data are in good agreement with experimental results for the thermal reverse reaction of the system 2/3,^{20,21} indicating that the model system describes the chemical changes within the five-membered heterocycle reasonably well.

Vertical excitation of the biradicaloid 2H leads to a vibrationally excited state within the S_1 electronic PES ($2H^*$, Fig. 4). Structural relaxation results in torsion of the exocyclic N–H group around the C–N bond ($2H^*\text{-opt}$). Thus, the minimum structure on the S_1 PES

is no longer planar (the C_s symmetric structure corresponds to a transition state, cf. ESI† p. S14), even though the structure of the five-membered ring system (disregarding the substituents) remains almost unchanged.

The S_1 MEP (red line in Fig. 4) indicates that the folding potential of the five-membered ring system starting from $2H^*$ -opt is very flat and leads to a conical intersection (CInt) with the ground state PES in an almost barrier-free process. In terms of the expected excited-state dynamics, this indicates that the S_1 state should decay rapidly, seeing that no substantial barrier needs to be overcome starting from the vertically excited structure $2H^*$. After passing the CInt, the molecules can either revert to the biradicaloid $2H$ or form the housane $3H$. In agreement with the experimentally observed quantum yield of 24.6(8)% for the photoisomerization $2 \rightarrow 3$,²⁰ the CInt is located on the biradicaloid side of the ground-state TS, and the ground-state PES near the CInt generally slopes towards the biradicaloid $2H$, so re-formation of a larger fraction of the biradicaloid would be expected.

Note that the extended conical intersection seam (a $3N - 8$ dimensional hyperline where S_0 and S_1 states are degenerate)¹⁵ is orthogonal to the folding coordinate depicted in Fig. 4 (cf. Fig. S9, ESI†). Decay of the excited state can occur everywhere along the seam,¹⁷ and given the overall flatness of the S_1 PES, it is likely that deactivation along the seam plays an important role in this system. At the CInt, which is the minimum energy point on the seam, degeneracy of both states is lifted by the gradient difference and derivative coupling vectors (the so-called branching space).^{15,93} Here, the gradient difference vector roughly corresponds to the reaction coordinate on the S_0 PES, i.e. the degeneracy is lifted in both directions along the reaction path. Therefore, the S_1 MEP between biradicaloid and housane crosses the seam in the region of the CInt.

Once again, note that essentially the same critical points (minima, TS, CInt) were identified by all computational methods used (DFT, NEVPT2/CASSCF, MRCI) and their relative energies are in good agreement (Table S2, ESI†). Therefore, the PES of the actual molecules $2/3$ (including the Ter and Dmp substituents) was investigated using DFT only (PBE-D3/def2-TZVP) owing to the size of the system. The stationary points that were found on the PES of $2/3$ are similar to the stationary points on the model surface, especially with regard to the structures of the five-membered heterocycle and their relative positions on the S_0 and S_1 surfaces (Fig. 5). Thus, the same general conclusions can be drawn from the PES of the “actual” system $2/3$ and the model system $2H/3H$. Moreover, it is worthy to note that the ground-state PES of $2/3$ computed here agrees well with previous calculations at the more accurate DLPNO-CCSD(T)/def2-TZVP//PBE-D3/def2-SVP level of theory.²¹

With respect to excitation energies, one might argue that more accurate results would be obtained using hybrid functionals due to the reduced self-interaction error.⁸⁴ While this is true, of course, we deliberately decided to use the pure functional PBE for structure optimizations due to its faster performance. The somewhat qualitative nature of the excited-state PES should be kept in mind, though. Nonetheless, the hybrid functional PBE0^{85,86,94} was applied to calculate UV-vis absorption

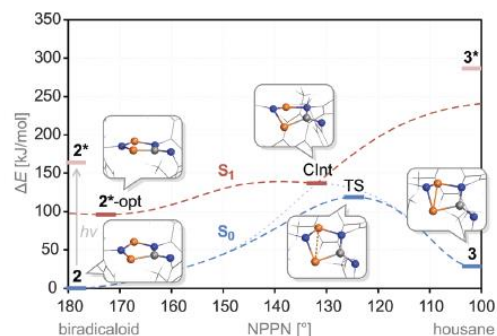


Fig. 5 Approximate ground state (S_0) and excited state (S_1) potential energy surface of $2/3$ projected along the NPPN dihedral angle. The stationary points (minima, TS, CInt) were computed at the (U)PBE-D3/def2-TZVP level of theory, using the TD-DFT/TDA method for excited states (cf. ESI† p. S19f). A full view of the optimized structures including the substituents can be found in Fig. S11 (ESI†).

spectra, which were found to be in good agreement with experimental results (Fig. 6).

Transient absorption spectroscopy

To corroborate our theoretical results, we investigated the underlying mechanisms of the photoisomerization $2 \rightarrow 3$ by means of transient absorption spectroscopy. To that end, the change in absorbance of a solution of 2 in THF ($c = 0.0079 \text{ mol L}^{-1}$) was monitored following photoexcitation at 650 nm. Unless stated otherwise, all measurements were performed applying pump fluences of 3 mJ cm^{-2} with the polarisations of pump and probe being oriented in the magic angle relatively to each other, to exclude any anisotropy effects. Polarisation- and fluence-dependent measurements are discussed in the ESI† p. S5ff, including the investigation of the polarisation anisotropy evolution.

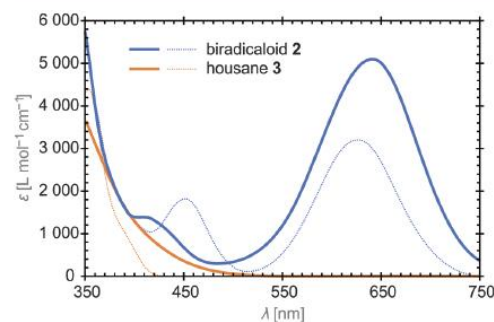


Fig. 6 Static UV-vis absorption spectra of biradicaloid 2 and housane 3 (solid lines). The approximate spectrum of 3 was extrapolated from deconvoluted time-dependent UV-vis spectra of the thermal reverse reaction $3 \rightarrow 2$ (cf. Fig. S1a, ESI†). The calculated spectra are depicted as dotted lines (TD-DFT, PBE0-D3/def2-TZVP).

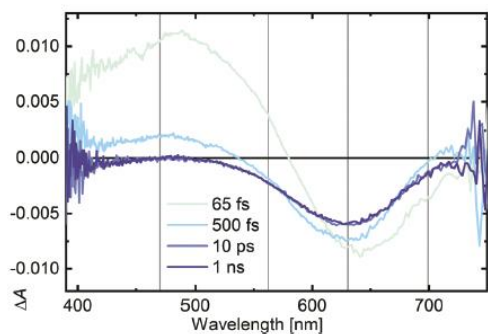


Fig. 7 Temporal evolution of transient spectra. Note that the curves for the two longest times are virtually identical. The vertical lines indicate characteristic wavelengths for which the time traces are depicted in Fig. 8.

The transient spectra, as depicted in Fig. 7, are characterized by a negative contribution, *i.e.* reduced absorption, dominating the spectral region above 600 nm. Given the congruence to the static absorption spectrum of biradicaloid 2 (Fig. 6), we attribute this signal to the ground state bleach (GSB) of the biradicaloid species. Below 550 nm, the signal turns to positive values, *i.e.* an increased absorption. As the housane 3 does not exhibit any significant absorption bands in the visible range (Fig. 6), this positive contribution is due to excited state absorption (ESA) of an electronically excited state (2^*) of biradicaloid 2.

Considering the temporal evolution of the transients, we identify three distinct phases. First, within several hundred femtoseconds, most of the ESA signal decays, while for the GSB peak, a shrinkage and an apparent blue shift of its central wavelength proceed simultaneously. In the following few picoseconds, the remains of the positive contribution vanish, while the negative one apparently broadens. Afterwards, both spectral

form and signal strength stay constant throughout the entire examined time span.

In accordance with these observations, we fitted the data over the entire spectral range from 390 to 740 nm in terms of a triexponential decay

$$\Delta A(\lambda, t) = A_1(\lambda) \cdot e^{-\frac{t}{\tau_1}} + A_2(\lambda) \cdot e^{-\frac{t}{\tau_2}} + A_3(\lambda) \cdot e^{-\frac{t}{\tau_3}}$$

with the decay-associated spectra (DAS) $A_i(\lambda)$ and the respective exponential lifetimes τ_i , which result as $\tau_1 = 210$ fs, $\tau_2 = 1.5$ ps, and $\tau_3 \gg 1$ ns. To judge the quality of the fit, Fig. 8a compares the time traces at the characteristic wavelengths indicated in Fig. 7 to the respective fitted curves. On the one hand, the excellent agreement of fit and data demonstrates the sufficiency of the three exponential components. On the other hand, the necessity of all three components becomes evident, as the traces exhibit two distinct ultrafast dynamics, even with opposite signs in some cases, plus the constant long-term tail described by the diverging third time constant.

Besides the obtained lifetimes, the fit also yields amplitude spectra associated with the respective decay component (Fig. 8b). The DAS of the fastest component around 200 fs contains a major contribution from the decaying ESA as well as a reduction of the negative signals beyond 650 nm.

Polarization-dependent measurements (*cf.* ESI,† p. S7f and Fig. S4a) show no systematic dependence of the ESA, whereas the negative contribution exhibits growing signal strength when tuning the probe polarisation from perpendicular to parallel, as expected for the GSB.⁹⁵ Furthermore, the spectrum for the perpendicular case with weak GSB signatures indicates that the ESA is present even in the red spectral region, implying a strong overlap of GSB and ESA. This was also corroborated by computed transient absorption spectra (Fig. S16 and S17, ESI†). As the ESA (unlike the GSB) decays almost completely during the fastest process, the negative signals increasingly dominate the spectral shape. Consequently, the maximum position of the negative signal

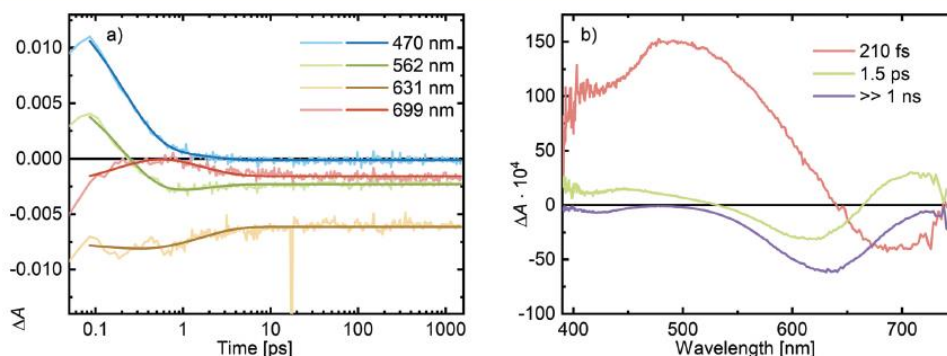


Fig. 8 (a) Time traces for the characteristic wavelengths marked in Fig. 7. Pale colours indicate the data while dark ones represent the fitted curves, demonstrating excellent agreement. All lines level after about 10 ps. (b) Decay associated spectra (DAS) for the three exponential components of the global fit. Due to the effective averaging over all spectra inherent to any fitting procedure, we are able to resolve a weak peak between 400 and 450 nm featured in the long-term contribution.

may apparently change without an actual shift of the underlying peak position taking place.

We attribute the 210 fs component to the relaxation of the electronically excited molecules into the electronic ground state through the conical intersection (CIInt). The time constant is within the typical order of magnitude for nonadiabatic processes.^{2,8,9} Given that the molecules of 2 are in a “hot” state after vertical excitation (*cf.* Fig. 5), it is reasonable to assume that they can explore a large fraction of the S_1 PES and the CIInt is therefore easily reached. (Thermal equilibration with the first solvent sphere typically occurs on a 10 ps timeframe^{96,97} and should have no significant impact on the excited-state dynamics.) Thus, the time constant reflects the duration of the motion along the PES towards the CIInt. When passing through the CIInt and returning to the electronic ground state, the molecules can either form the housane 3 or revert to the biradicaloid 2 in a ratio of around 1:3, according to the photochemical quantum yield of 24.6(8)%.²⁰ Consequently, the ESA vanishes and the GSB is drastically reduced, although their overlapping seems to conceal most of the dynamics at wavelengths above 550 nm.

The second exponential component, decaying with a time constant of 1.5 ps, is characterized by a weak and broad positive contribution in the blue spectral region as well as a negative peak around 600 nm and a similar positive one at longer wavelengths (Fig. 8b). Considering their polarisation dependence (Fig. S4b, ESI†), the latter two follow the same dependence as the GSB, with maximum amplitudes for parallel polarisation. The short-wavelength contribution, however, lacks any systematic dependence, similar to the 210 fs amplitude spectra. To interpret these signatures, we must look closely at the state of the molecules at the beginning of these picosecond dynamics: After passing the conical intersection, all dynamics occur on the ground-state PES, excluding any ESA signals in the transient spectra. Nevertheless, the molecules have not yet adopted an equilibrium structure corresponding either to the biradicaloid 2 or housane 3. Due to the distorted geometry that is associated with the intersection point, the absorption spectra of molecules within this region of the ground-state PES differ from the static UV-vis absorptions of 2 and 3 (*cf.* Fig. S18 and S19, ESI†). Thus, we attribute the picosecond dynamics to the return of the distorted molecules to their equilibrium structures. In this context, the peak pair in the red region of the spectrum depicts a transient shift of the major absorption band of 2 back to its original ground state absorption, while the weak positive feature in the blue region of the corresponding DAS is interpreted as an additional absorption of the distorted biradicaloid and housane structures on the S_0 PES. This notion is corroborated by calculated UV-vis spectra of distorted structures on the S_0 PES, which exhibit the discussed spectral contributions (Fig. S18 and S19, ESI†). Furthermore, the positive contribution to the DAS may also be caused by a weak nonexponential contribution to the 210 fs dynamics in that wavelength region.

Following the geometrical rearrangement, the ultrafast dynamics are completed. The remaining exponential lifetime takes values well beyond the examined time range of about 1.5 ns, effectively

resulting in a constant contribution to the transient signal. The corresponding amplitude spectrum perfectly matches the static absorption of 2, with a weak negative peak just above 400 nm and a strong, broad one between 600 and 700 nm (Fig. 8b). Accordingly, this signature describes the GSB resulting from the fraction of molecules that isomerized to the housane 3, which lacks the respective absorption bands. Applying an excitation fluence of 3 mJ cm^{-2} to the 7.8 mM sample solution with a pump absorbance of at 100 μM thickness results in about 9% of the molecules becoming electronically excited, corresponding to a GSB amplitude of $\Delta A = -0.024$. As discussed before, this value is never reached due to the strong overlap with the ESA contribution. Yet, after the ultrafast processes are finished, one quarter of the bleach should remain present, as the housane 3 transforms back to its biradicaloid isomer 2 on a timescale of minutes ($t_{1/2} = 7 \text{ min}$).²⁰ Accordingly, the GSB is expected to equilibrate at $\Delta A = -0.006$, which is in perfect agreement with the experimental data.

Conclusions

We present theoretical and experimental evidence for the mechanism of photoisomerization of the biradicaloid 2 to its housane isomer 3. The photoisomerization follows a nonadiabatic reaction pathway, *i.e.* the excited-state molecules transfer to the ground-state PES at a conical intersection. The S_1 PES is rather flat, resulting in an ultrafast deactivation on a timescale of 200 fs. Due to the position of the conical intersection relative to the ground-state reaction coordinate, the quantum yield of photoisomerization is approx. 25%.

Moreover, careful evaluation of the electronic structure of biradicaloid 2 indicates that its biradical character is inextricably connected to the photochemistry of the system. The knowledge and understanding gained in this study will help us to further develop this relatively new class of biradicaloid molecular switches.

Author contributions

The project was conceived and planned by all authors. T. V. performed the transient absorption spectroscopy and evaluated the data. H. B. synthesized and characterized the samples. A. S., S. L. and J. B. deliberated the theoretical aspects of this work. J. B. performed the calculations. A. S., S. L., and J. B. supervised the project. All authors contributed to writing the manuscript.

Conflicts of interest

There are no conflicts to declare.

Acknowledgements

We gratefully acknowledge financial support by the Deutsche Forschungsgemeinschaft (DFG; SCHU 1170/12-2) and the DFG priority program SPP 2102 (LO 714/11-1). T. V. gratefully

acknowledges funding by the University of Rostock via the PhD Scholarship Programme. Moreover, we wish to thank the ITMZ at the University of Rostock for access to the cluster computer, and especially Malte Willert for his assistance with the queuing system and software installations.

Notes and references

- B. L. Feringa, R. A. van Delden, N. Koumura and E. M. Geertsema, *Chem. Rev.*, 2000, **100**, 1789–1816.
- Molecular Switches*, ed. B. L. Feringa, Wiley-VCH, Weinheim, Germany, 2001.
- H. Finkelmann, E. Nishikawa, G. G. Pereira and M. Warner, *Phys. Rev. Lett.*, 2001, **87**, 015501.
- S. Kobatake, S. Takami, H. Muto, T. Ishikawa and M. Irie, *Nature*, 2007, **446**, 778–781.
- T. Ube and T. Ikeda, *Angew. Chem., Int. Ed.*, 2014, **53**, 10290–10299.
- R. S. Stoll and S. Hecht, *Angew. Chem., Int. Ed.*, 2010, **49**, 5054–5075.
- R. Göstl, A. Senf and S. Hecht, *Chem. Soc. Rev.*, 2014, **43**, 1982–1996.
- D. R. Yarkony, *J. Phys. Chem. A*, 2001, **105**, 6277–6293.
- W. Domcke and D. R. Yarkony, *Annu. Rev. Phys. Chem.*, 2012, **63**, 325–352.
- U. Megerle, I. Pugliesi, C. Schrieffer, C. F. Sailer and E. Riedle, *Appl. Phys. B: Lasers Opt.*, 2009, **96**, 215–231.
- M. S. Schuurman and A. Stolow, *Annu. Rev. Phys. Chem.*, 2018, **69**, 427–450.
- D. Wöhrle, M. W. Tausch and W. Stohrer, *Photochemie*, Wiley-VCH, Weinheim, Germany, 1998.
- T. Förster, *Pure Appl. Chem.*, 1970, **24**, 443–450.
- L. Salem, *J. Am. Chem. Soc.*, 1974, **96**, 3486–3501.
- M. A. Robb, in *Advanced Series in Physical Chemistry*, Vol. 17: *Conical Intersections: Theory, Computation and Experiment*, ed. W. Domcke, D. R. Yarkony and H. Köppel, World Scientific Publishing, Singapore, 2011, pp. 3–50.
- F. Lépine, M. Y. Ivanov and M. J. J. Vrakking, *Nat. Photonics*, 2014, **8**, 195–204.
- M. Boggio-Pasqua, M. J. Bearpark and M. A. Robb, *AIP Conf. Proc.*, 2015, **1642**, 453–456.
- K. F. Chang, M. Reduzzi, H. Wang, S. M. Poullain, Y. Kobayashi, L. Barreau, D. Prendergast, D. M. Neumark and S. R. Leone, *Nat. Commun.*, 2020, **11**, 4042.
- A. Hinz, A. Schulz and A. Villinger, *J. Am. Chem. Soc.*, 2015, **137**, 9953–9962.
- J. Bresien, T. Kröger-Badge, S. Lochbrunner, D. Michalik, H. Müller, A. Schulz and E. Zander, *Chem. Sci.*, 2019, **10**, 3486–3493.
- H. Beer, J. Bresien, D. Michalik, A. Schulz and A. Villinger, *Dalton Trans.*, 2020, **49**, 13986–13992.
- H. Beer, J. Bresien, D. Michalik, A.-K. Rölke, A. Schulz, A. Villinger and R. Wustrack, *J. Org. Chem.*, 2020, **85**, 14435–14445.
- L. Salem and C. Rowland, *Angew. Chem., Int. Ed. Engl.*, 1972, **11**, 92–111.
- H. Grützmacher and F. Breher, *Angew. Chem., Int. Ed.*, 2002, **41**, 4006–4011.
- F. Breher, *Coord. Chem. Rev.*, 2007, **251**, 1007–1043.
- M. Abe, J. Ye and M. Mishima, *Chem. Soc. Rev.*, 2012, **41**, 3808–3820.
- M. Abe, *Chem. Rev.*, 2013, **113**, 7011–7088.
- S. González-Gallardo and F. Breher, *Comprehensive Inorganic Chemistry II*, Elsevier, 2013, vol. 1, pp. 413–455.
- S. Ito, *Tetrahedron Lett.*, 2018, **59**, 1–13.
- T. Stuyver, B. Chen, T. Zeng, P. Geerlings, F. De Proft and R. Hoffmann, *Chem. Rev.*, 2019, **119**, 11291–11351.
- W. W. Schoeller, *Eur. J. Inorg. Chem.*, 2019, 1495–1506.
- K. Yamaguchi, *Chem. Phys. Lett.*, 1975, **33**, 330–335.
- D. Doehnert and J. Koutecky, *J. Am. Chem. Soc.*, 1980, **102**, 1789–1796.
- V. Bachler, G. Olbrich, F. Neese and K. Wieghardt, *Inorg. Chem.*, 2002, **41**, 4179–4193.
- D. Herebian, K. E. Wieghardt and F. Neese, *J. Am. Chem. Soc.*, 2003, **125**, 10997–11005.
- E. Miliordos, K. Ruedenberg and S. S. Xantheas, *Angew. Chem., Int. Ed.*, 2013, **52**, 5736–5739.
- M. Abe, E. Kubo, K. Nozaki, T. Matsuo and T. Hayashi, *Angew. Chem., Int. Ed.*, 2006, **45**, 7828–7831.
- S. Yoshidomi and M. Abe, *J. Am. Chem. Soc.*, 2019, **141**, 3920–3933.
- W. Adam, W. T. Borden, C. Burda, H. Foster, T. Heidenfelder, M. Heubes, D. A. Hrovat, F. Kita, S. B. Lewis, D. Scheutzw and J. Wirz, *J. Am. Chem. Soc.*, 1998, **120**, 593–594.
- F. Kita, W. Adam, P. Jordan, W. M. Nau and J. Wirz, *J. Am. Chem. Soc.*, 1999, **121**, 9265–9275.
- D. Y. Zhang, D. A. Hrovat, M. Abe and W. T. Borden, *J. Am. Chem. Soc.*, 2003, **125**, 12823–12828.
- M. Abe, W. Adam, W. T. Borden, M. Hattori, D. A. Hrovat, M. Nojima, K. Nozaki and J. Wirz, *J. Am. Chem. Soc.*, 2004, **126**, 574–582.
- T. Nakamura, A. Takegami and M. Abe, *J. Org. Chem.*, 2010, **75**, 1956–1960.
- T. Nakamura, L. Gagliardi and M. Abe, *J. Phys. Org. Chem.*, 2010, **23**, 300–307.
- J. Fabian and R. Peichert, *J. Phys. Org. Chem.*, 2010, **23**, 1137–1145.
- S. Yoshidomi, M. Mishima, S. Seyama, M. Abe, Y. Fujiwara and T. Ishibashi, *Angew. Chem., Int. Ed.*, 2017, **56**, 2984–2988.
- B. J. Guddorf, C. Mück-Lichtenfeld, A. Hepp and F. Lips, *Chem. Commun.*, 2019, **55**, 12896–12899.
- J. Bresien, D. Michalik, A. Schulz, A. Villinger and E. Zander, *Angew. Chem., Int. Ed.*, 2021, **60**, 1507–1512.
- IUPAC Compendium of Chemical Terminology*, 2nd ed. (*The Gold Book*), ed. A. D. McNaught and A. Wilkinson, Blackwell Scientific Publications, Oxford, 1997.
- A. Schulz, *Dalton Trans.*, 2018, **47**, 12827–12837.
- S. E. Braslavsky, *Pure Appl. Chem.*, 2007, **79**, 293–465.
- D. Hegarty and M. A. Robb, *Mol. Phys.*, 1979, **38**, 1795–1812.
- R. H. A. Eade and M. A. Robb, *Chem. Phys. Lett.*, 1981, **83**, 362–368.

Paper

Published on 18 March 2021. Downloaded by University of Rostock on 4/22/2022 10:28:18 AM.

- 54 H. B. Schlegel and M. A. Robb, *Chem. Phys. Lett.*, 1982, **93**, 43–46.
- 55 P. E. M. Siegbahn, *Chem. Phys. Lett.*, 1984, **109**, 417–423.
- 56 F. Bernardi, A. Bottoni, J. J. W. McDouall, M. A. Robb and H. B. Schlegel, *Faraday Symp. Chem. Soc.*, 1984, **19**, 137.
- 57 M. A. Robb and U. Niaz, in *Reports in Molecular Theory*, ed. H. Weinstein and G. N aray-Szab o, CRC Press, Boca Raton, FL, 1990, Vol. 1, pp. 23–55.
- 58 M. J. Frisch, I. N. Ragazos, M. A. Robb and H. B. Schlegel, *Chem. Phys. Lett.*, 1992, **189**, 524–528.
- 59 N. Yamamoto, T. Vreven, M. A. Robb, M. J. Frisch and H. B. Schlegel, *Chem. Phys. Lett.*, 1996, **250**, 373–378.
- 60 M. Klene, M. A. Robb, M. J. Frisch and P. Celani, *J. Chem. Phys.*, 2000, **113**, 5653–5665.
- 61 C. J. Cramer and B. A. Smith, *J. Phys. Chem.*, 1996, **100**, 9664–9670.
- 62 J. W. Hollett and P. M. W. Gill, *J. Chem. Phys.*, 2011, **134**, 114111.
- 63 S. Grimme and A. Hansen, *Angew. Chem., Int. Ed.*, 2015, **54**, 12308–12313.
- 64 S. R. Langhoff and E. R. Davidson, *Int. J. Quantum Chem.*, 1974, **8**, 61–72.
- 65 L. Meissner, *Chem. Phys. Lett.*, 1988, **146**, 204–210.
- 66 F. Weigend and R. Ahlrichs, *Phys. Chem. Chem. Phys.*, 2005, **7**, 3297–3305.
- 67 A. Hellweg, C. H attig, S. H ofener and W. Klopper, *Theor. Chem. Acc.*, 2007, **117**, 587–597.
- 68 A. Hinz, A. Schulz, A. Villinger and J.-M. Wolter, *J. Am. Chem. Soc.*, 2015, **137**, 3975–3980.
- 69 A. Hinz, A. Schulz and A. Villinger, *Angew. Chem., Int. Ed.*, 2015, **54**, 668–672.
- 70 A. Hinz, A. Schulz and A. Villinger, *Chem. Commun.*, 2016, **52**, 6328–6331.
- 71 R. B. Woodward and R. Hoffmann, *J. Am. Chem. Soc.*, 1965, **87**, 395–397.
- 72 R. B. Woodward and R. Hoffmann, *Angew. Chem., Int. Ed. Engl.*, 1969, **8**, 781–853.
- 73 C. J. Cramer, *Essentials of Computational Chemistry: Theories and Models*, John Wiley & Sons, Ltd, Chichester, UK, 2004.
- 74 D. Cremer, *Mol. Phys.*, 2001, **99**, 1899–1940.
- 75 T. Soda, Y. Kitagawa, T. Onishi, Y. Takano, Y. Shigeta, H. Nagao, Y. Yoshioka and K. Yamaguchi, *Chem. Phys. Lett.*, 2000, **319**, 223–230.
- 76 J.-P. Malrieu and G. Trinquier, *J. Phys. Chem. A*, 2012, **116**, 8226–8237.
- 77 L. Noodleman, *J. Chem. Phys.*, 1981, **74**, 5737–5743.
- 78 R. Bauernschmitt and R. Ahlrichs, *Chem. Phys. Lett.*, 1996, **256**, 454–464.
- 79 M. E. Casida, C. Jamorski, K. C. Casida and D. R. Salahub, *J. Chem. Phys.*, 1998, **108**, 4439–4449.
- 80 R. E. Stratmann, G. E. Scuseria and M. J. Frisch, *J. Chem. Phys.*, 1998, **109**, 8218–8224.
- 81 C. Van Caillie and R. D. Amos, *Chem. Phys. Lett.*, 1999, **308**, 249–255.
- 82 C. Van Caillie and R. D. Amos, *Chem. Phys. Lett.*, 2000, **317**, 159–164.
- 83 F. Furche and R. Ahlrichs, *J. Chem. Phys.*, 2002, **117**, 7433–7447.
- 84 G. Scalmani, M. J. Frisch, B. Mennucci, J. Tomasi, R. Cammi and V. Barone, *J. Chem. Phys.*, 2006, **124**, 094107.
- 85 J. P. Perdew, K. Burke and M. Ernzerhof, *Phys. Rev. Lett.*, 1996, **77**, 3865–3868.
- 86 J. P. Perdew, K. Burke and M. Ernzerhof, *Phys. Rev. Lett.*, 1997, **78**, 1396.
- 87 S. Grimme, J. Antony, S. Ehrlich and H. Krieg, *J. Chem. Phys.*, 2010, **132**, 154104.
- 88 S. Grimme, S. Ehrlich and L. Goerigk, *J. Comput. Chem.*, 2011, **32**, 1456–1465.
- 89 F. Weigend, *Phys. Chem. Chem. Phys.*, 2006, **8**, 1057.
- 90 C. Angeli, R. Cimiraglia, S. Evangelisti, T. Leininger and J.-P. Malrieu, *J. Chem. Phys.*, 2001, **114**, 10252–10264.
- 91 C. Angeli, R. Cimiraglia and J.-P. Malrieu, *Chem. Phys. Lett.*, 2001, **350**, 297–305.
- 92 C. Angeli, R. Cimiraglia and J.-P. Malrieu, *J. Chem. Phys.*, 2002, **117**, 9138–9153.
- 93 M. Boggio-Pasqua, M. J. Bearpark, P. A. Hunt and M. A. Robb, *J. Am. Chem. Soc.*, 2002, **124**, 1456–1470.
- 94 C. Adamo and V. Barone, *J. Chem. Phys.*, 1999, **110**, 6158–6170.
- 95 H. E. Lessing and A. Von Jena, *Chem. Phys. Lett.*, 1976, **42**, 213–217.
- 96 T. Elsaesser and W. Kaiser, *Annu. Rev. Phys. Chem.*, 1991, **42**, 83–107.
- 97 S. A. Kovalenko, R. Schanz, H. Hennig and N. P. Ernsting, *J. Chem. Phys.*, 2001, **115**, 3256–3273.

6.3 Reversible switching between housane and cyclopentanediy1 isomers: an isonitrile-catalysed thermal reverse reaction

Henrik Beer, Jonas Bresien, Dirk Michalik, Axel Schulz, Alexander Villinger

Dalton Trans. **2020**, *49*, 13986–13992.

DOI: 10.1039/ d0dt02688c

No permission needed for authors reprinting full articles in a thesis/dissertation according to the Royal Society of Chemistry. © Copyright 2020 Royal Society of Chemistry.

Onlinelink: <https://doi.org/10.1039/D0DT02688C>

Cite this: *Dalton Trans.*, 2020, **49**,
13986Received 31st July 2020,
Accepted 24th August 2020
DOI: 10.1039/d0dt02688c
rsc.li/daltonReversible switching between housane and
cyclopentanediy l isomers: an isonitrile-catalysed
thermal reverse reaction†Henrik Beer,^a Jonas Bresien,^{a,*} Dirk Michalik,^{a,b} Axel Schulz^{a,b,c} and
Alexander Villinger^a

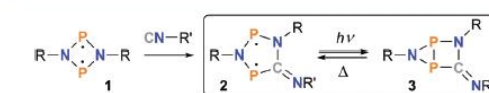
The photo-isomerization of an isolable five-membered singlet biradical based on C, N, and P ([TerNP]₂CNDmp, **2a**) selectively afforded a closed-shell housane-type isomer (**3a**) by forming a transannular P–P bond. In the dark, the housane-type species re-isomerized to the biradical, resulting in a fully reversible overall process. In the present study, the influence of tBuNC on the thermal reverse reaction was investigated: the isonitrile acted as a catalyst, thus allowing control over the thermal reaction rate. Moreover, tBuNC also reacted with the biradical to form an adduct species ([TerNP]₂CNDmp-CNtBu, **4a**), which can be regarded as the resting state of the system. The reactive species **2a** and **3a** could be re-generated *in situ* by irradiation with red light. The results of this study extend our understanding of this new class of molecular switches.

Introduction

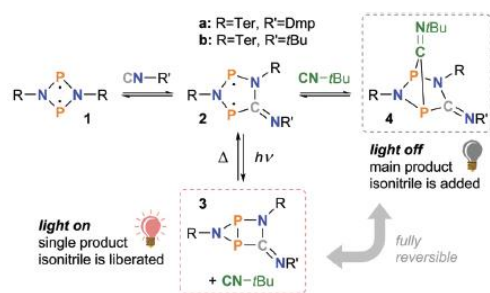
Singlet biradicals (also known as biradicaloids) are worthwhile target molecules in synthetic chemistry.^{1–5} Due to their unique electronic structure,^{6–10} they combine high reactivity with interesting properties such as small molecule activation,^{11–14} non-linear optical properties,^{15,16} or (potential) applicability as molecular switches.^{16–23} Especially for the latter use, it is desirable to devise systems whose two (meta-)stable states possess different degrees of biradical character, so the biradical character^{6,8,24–26} can be influenced by an outside stimulus.^{27–30}

As stable photo-switchable biradicals are barely known,^{22,31–33} we recently started to investigate the photochemistry of five-membered heterocycles, namely hetero-cyclopentanediy ls (**2**) generated from the four-membered biradical [P(μ-NR)]₂ (**1**, Scheme 1).^{20,21} In two recent publications^{23,34} we could show that these five-membered biradicals can be reversibly switched to the corresponding housane-type isomer (**3**) using red light, while the reverse reaction takes place under thermal regime.

^aInstitute of Chemistry, University of Rostock, Albert-Einstein-Straße 3a, 18059 Rostock, Germany. E-mail: jonas.bresien@uni-rostock.de, axel.schulz@uni-rostock.de
^bLeibniz Institute for Catalysis, Albert-Einstein-Straße 29a, 18059 Rostock, Germany
^cDepartment Life, Light & Matter, University of Rostock, 18051 Rostock, Germany
† Electronic supplementary information (ESI) available: Syntheses, equipment, analytical data, reaction kinetics, computations. CCDC 2013704. For ESI and crystallographic data in CIF or other electronic format see DOI: 10.1039/d0dt02688c



Scheme 1 Synthesis and photochemistry of hetero-cyclopentanediy ls (**2**). R = Ter (2,6-dimesitylphenyl), Hyp (tris(trimethylsilyl)silyl); R' = Mes (mesityl), Dmp (2,6-dimethylphenyl), tBu. Similar compounds can be obtained by reaction of **1** with CO (not shown).



Scheme 2 The molecular switch 2 could be utilized to control a chemical equilibrium reaction involving the activation of *t*BuNC by 2. The equilibrium with 1 is only observed for 2b.

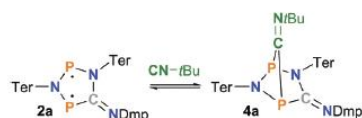
housane 3 towards *t*BuNC in comparison with the activation chemistry of biradical 2. Being the most stable derivative,^{21,23,34} the Ter and Dmp substituted variant of 2 (*i.e.* 2a, R = Ter, R' = Dmp) was chosen for these investigations.

Results and discussion

Molecular structure

As previously observed in NMR experiments,²³ the reaction of 2a with *t*BuNC led to formation of adduct 4a (Scheme 3). As it had only been characterized spectroscopically, it was of interest to isolate and fully characterize adduct 4a. This could be accomplished by using the isonitrile as solvent (*i.e.* in a large excess) and slowly evaporating the isonitrile until colourless crystals of the desired product 4a were obtained.

Compound 4a crystallized in the monoclinic space group *C2/c* with 8 formula units per cell. As expected, the five-membered N_2P_2C ring system of the former biradical moiety adopts an envelope conformation, contrary to the planar structure of the free biradical 2a (Fig. 1).²³ The two P atoms are bridged by the C atom of the former isonitrile moiety, resulting in a [2.1.1]-bicyclic structure; that is, the adduct can be regarded as a [2 + 1] cycloaddition product of the biradical 2a and *t*BuNC. It is worthy to note that the P1/P2–C58 bond lengths (1.888(1), 1.937(1) Å) are somewhat longer than typical P–C single bonds ($\Sigma r_{cov} = 1.86$ Å),⁴⁰ indicating a rather weak interaction. This is in agreement with the fact that the adduct formation is a reversible equilibrium reaction (*vide infra*). The overall struc-



Scheme 3 *t*BuNC could be activated using biradical 2a, leading to formation of adduct 4a.

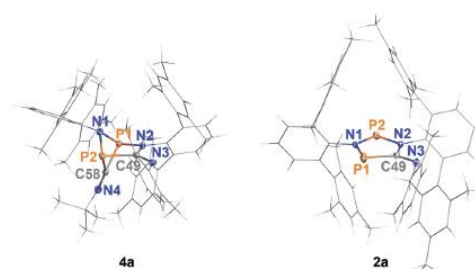


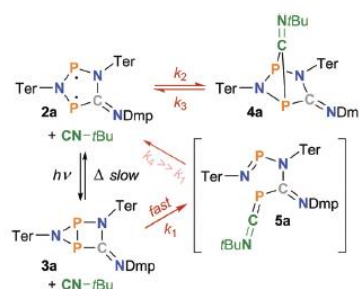
Fig. 1 Left: molecular structure of the adduct 4a in the crystal. Right: the molecular structure of the biradical 2a is depicted for comparison.²³ Thermal ellipsoids set at 50% probability (123 K). Selected bond lengths (Å) and angles (°): 4a: P1–N1 1.779(1), P1–N2 1.734(1), P1–C58 1.888(1), P2–N1 1.776(1), P2–C49 1.880(1), P2–C58 1.937(1), N2–C49 1.403(2), N3–C49 1.270(2), N4–C58 1.250(2), N1–P2–P1–N2 116.57(7); 2a: P1–N1 1.729(1), P1–C49 1.792(2), P2–N1 1.649(1), P2–N2 1.680(1), N2–C49 1.430(2), N3–C49 1.287(2), N1–P1–P2–N2 178.5(1).

ture is similar to other derivatives of 4a with different substituents.²¹

Photoisomerization and thermal reverse reaction

When dissolving colourless crystals of adduct 4a in THF or benzene, a blue solution was obtained. This could be attributed to partial dissociation of the adduct, which led to partial formation of the blue biradical 2a and *t*BuNC in an equilibrium mixture with adduct 4a (*cf.* Scheme 3). The mixture was then irradiated with red light (638 nm) in the NMR spectrometer, resulting in partial formation of the photoproduct 3a (70%, Scheme 4). All these reactions could easily be traced by ³¹P NMR spectroscopy, owing to the distinct AX spin systems of 2a (221.7, 258.3 ppm; 136 Hz), 3a (–129.1, –63.4 ppm; 65 Hz), and 4a (188.2, 222.7 ppm; 33 Hz). The experimental data correspond well to calculated values (Table S4†).

In contrast to irradiation of the pure biradical 2a or the equilibrium mixture associated with 2b (*cf.* Scheme 2),²³ it was



Scheme 4 The thermal reverse reaction 3a → 2a was found to be catalysed by *t*BuNC. The reactions considered for the kinetic model are highlighted in red.

however not possible to achieve full photoconversion; species 2a and 4a were detectable in the ^{31}P NMR spectrum even under irradiation (20% and 10%, respectively). Moreover, the thermal equilibrium mixture was restored almost instantly when the light source was switched off, indicating a rather fast thermal reverse reaction. (Note that for the pure system $2a \rightleftharpoons 3a$, the half-life of 3a was about 7 minutes at ambient temperature.)²³

These findings implied that the presence of *t*BuNC had an influence on the rate of the thermal reverse reaction $3a \rightarrow 2a$. This could be confirmed by low-temperature NMR experiments using different concentrations of *t*BuNC, which showed a direct proportionality between the rate of the thermal reverse reaction and the *t*BuNC concentration (Scheme 4 and ESI, p. S20ff†). It follows that besides the intramolecular P–P bond cleavage of 3a (as observed for the pure system $2a \rightleftharpoons 3a$), there must be an alternative pathway for the isomerization of the housane 3a to the biradical 2a, involving a reaction between *t*BuNC and 3a.

Reaction mechanism

To further shed light on the reaction mechanism, the reverse reaction was traced by ^{31}P NMR spectroscopy at different temperatures and at different concentrations of *t*BuNC. The NMR spectra were used to estimate the concentrations of all species in solution, and the time-dependent concentration data were then used to fit a kinetic model involving a second order reaction step between *t*BuNC and 3a (rate constant k_1 , Scheme 4). As the putative intermediate 5a (or any other intermediates) could not be observed spectroscopically, it was assumed that the reaction step *t*BuNC + 3a was the rate determining step, *i.e.* all reaction steps between 5a and 2a were much faster ($k_4 \gg k_1$) and therefore negligible. Also, taking into consideration that the thermal reverse reaction was orders of magnitude faster in the presence of *t*BuNC, the thermal equilibration of 3a *via* intramolecular P–P bond cleavage was neglected (Scheme 4).

The above considerations led to the following rate equations

$$\frac{d[2a]}{dt} = +k_1[3a][t\text{BuNC}] - k_2[2a][t\text{BuNC}] + k_3[4a]$$

$$\frac{d[3a]}{dt} = -k_1[3a][t\text{BuNC}]$$

$$\frac{d[4a]}{dt} = +k_2[2a][t\text{BuNC}] - k_3[4a]$$

$$\frac{d[t\text{BuNC}]}{dt} = -k_2[2a][t\text{BuNC}] + k_3[4a]$$

where [2a], [3a], [4a], and [tBuNC] are the concentrations of 2a, 3a, 4a, and *t*BuNC, respectively, and *t* is the reaction time. The differential equations were used in a non-linear fitting procedure (ESI, p. S21ff†) to obtain the parameters k_1 , k_2 , and k_3 as well as the initial concentrations of all species ($[2a]_0$, $[3a]_0$, $[4a]_0$, $[t\text{BuNC}]_0$) for all different temperatures and concentrations of *t*BuNC (Fig. 2 and ESI, p. S26ff†).

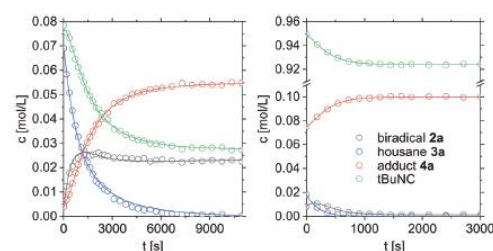


Fig. 2 Thermal reverse reaction $3a \rightarrow 2a$ in the presence of *t*BuNC. Left: $-20\text{ }^\circ\text{C}$, 1 equiv. *t*BuNC. Right: $-30\text{ }^\circ\text{C}$, 10 equiv. *t*BuNC. Experimental data plotted as circles; fit functions plotted as solid lines. For more temperatures and concentrations of *t*BuNC, please refer to the ESI, p. S26ff.†

Most importantly, the same rate constants were obtained when the concentration of *t*BuNC was varied and the temperature left unchanged (ESI†), in agreement with the consideration that k_1 is associated with a second order reaction. The temperature dependence of the rate constants was then exploited to estimate the activation barriers of the three reactions associated with k_1 , k_2 , and k_3 using transition state theory (Table 1, Fig. S11†). This gave $\Delta G^\ddagger = 75.9(6)\text{ kJ mol}^{-1}$ for the reaction of *t*BuNC and 3a at 298.15 K, which is lower than the activation barrier of intramolecular P–P bond cleavage ($\Delta G^\ddagger = 88(4)\text{ kJ mol}^{-1}$)²³ in accordance with experimental observation.

Moreover, it became evident from the concentration plots in Fig. 2 that the adduct 4a was the main product of the thermal reverse reaction, *i.e.* it can be regarded as the resting state of the system. Upon irradiation, the equilibrium was perturbed and the thermal reaction was formally shifted back to $t=0$, yielding the housane 3a and free *t*BuNC as main products. In the dark, the system relaxed to $t \rightarrow \infty$. As indicated, this process is fully reversible and can be repeated many times (>20) without detectable degradation of the system.

Computational study

The experimental data clearly demonstrated that the housane 3a reacted with *t*BuNC in a catalytic manner. However, up to this point, it remained unclear what the nature of the intermediate 5a was, as it could not be observed in any of the NMR spectra. We therefore decided to perform DFT and *ab initio* cal-

Table 1 Experimental enthalpies and entropies of activation

Step	ΔH^\ddagger [kJ mol ⁻¹]	ΔS^\ddagger [J (mol K) ⁻¹]	$\Delta G^\ddagger_{298\text{K}}$ ^a [kJ mol ⁻¹]
1 (k_1)	42.2 ± 0.3	-113 ± 1	75.9 ± 0.6
2 (k_2)	43 ± 3	-106 ± 11	74 ± 6
3 (k_3)	67 ± 6	-50 ± 23	82 ± 13

^a Extrapolated values. The rate constants could only be determined at lower temperatures due to the high reaction rates at ambient temperature.

calculations to investigate the reactivity of housane 3a towards *t*BuNC.

In a first step, a model system was chosen to obtain an initial impression of what the reaction between the housane and isonitrile might look like. To this end, all substituents (Ter, Dmp, *t*Bu) were replaced by methyl groups. Using this truncated model (2c, 3c), loose van der Waals complexes of 3c and MeNC as well as 2c and MeNC were optimized. These were then used as fixed end points for the calculation of a Nudged Elastic Band (NEB)^{41–46} trajectory, which resulted in an approximate Minimum Energy Path (MEP) connecting the two end points on the Potential Energy Surface (PES). Optimization of all stationary points as well as additional Intrinsic Reaction Coordinate (IRC)^{47,48} scans resulted in two possible reaction pathways that encompass a nucleophilic attack of the isonitrile at one of the P atoms of the housane as rate determining step (*via* TS1), leading to open-chain intermediate 5c (Fig. 3). Further reaction steps leading to the biradical 2c and free isonitrile involved either a nucleophilic attack by the N1 atom (*via* TS2) or an addition of the N4 atom to the second P atom (TS4), followed by [2 + 2] cycloreversion (TS5). All these steps exhibited very low activation barriers; thus, it would be expected that the concentration of all possible intermediates would be close to zero throughout the reaction (Fig. 3).

Additionally, the intramolecular P–P bond cleavage was calculated (*via* TS0), similarly to what was reported before for the reaction of the pure system 2a \rightleftharpoons 3a.²³ In comparison with the isonitrile-catalysed reaction, the activation energy (ΔG^\ddagger) of the intramolecular pathway is some 17 kJ mol⁻¹ higher, in agreement with our experimental observations.

Next, it was of interest to determine if the same reaction pathway could also be found in case of the “real” system 3a + *t*BuNC \rightarrow 2a + *t*BuNC. To keep matters simple and reduce the computational effort, we decided only to investigate the shorter pathway *via* TS2 (highlighted in red in Fig. 3) and the intramolecular P–P bond cleavage *via* TS0 (grey). Indeed, the results implied that the same nucleophilic attack of *t*BuNC is possible in case of 3a despite the presence of the bulky substituents, and that it has a lower activation barrier than the intramolecular P–P bond cleavage (Fig. 4). The calculated energies of TS0 and TS1 are somewhat larger than the experimental activation energies, but this is likely attributed to some multireference character of the species involved, which is expected to decrease the accuracy of these calculations (*cf.* ESI p. S29ff). Moreover, we did not include any solvent effects in our calculations. Nonetheless, the experimental trends are well reflected in the computational model. In particular, the computed mechanism also predicts the addition of *t*BuNC to housane 3a to be the rate determining step, in agreement with the kinetic model derived from NMR data.

Taking into consideration that a side-on adduct of the isonitrile and biradical was found in the model system (*cf.* A3 in Fig. 3), we were also interested in different adduct types of the actual biradical 2a. Given that the end-on adduct 4a was identified as the “resting state” of the system, it seemed particularly interesting to see if a side-on adduct might play a role in the reactivity of the biradical 2a or the housane 3a.

Contrary to the model system, though, our computations revealed that the side-on adducts (stationary points A2 and A3 in Fig. 4) of *t*BuNC and the biradical 2a are much higher in energy than the end-on adduct 4a. This agrees with the absence of other adduct species in the NMR spectra, and

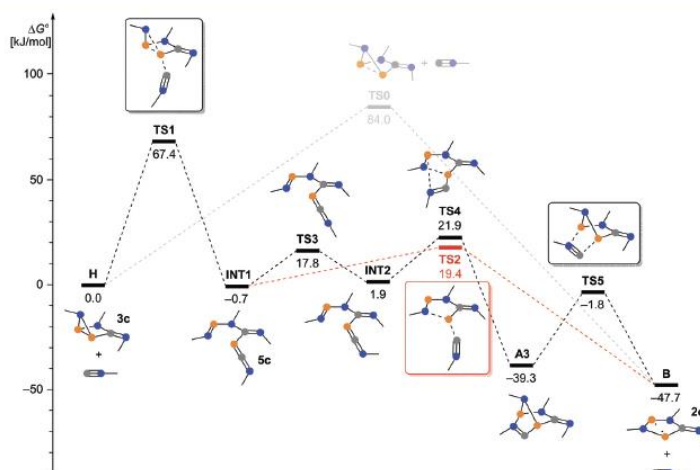


Fig. 3 Thermal reverse reaction of the model housane 3c (UPBE-D3/def2-TZVP, $p^\circ = 1$ atm). The addition of MeNC is the rate determining step, leading to formation of metastable adduct 5c (stationary point INT1). The adduct can react to biradical 2c *via* two pathways, both of which have very low activation barriers. The shortest path is highlighted in red.

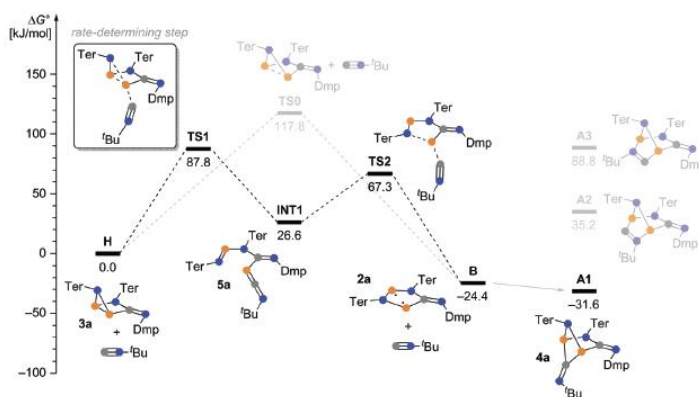


Fig. 4 Computed mechanism for the thermal reverse reaction of the housane **3a** in the presence of *t*BuNC (DLPNO-CCSD(T)/def2-TZVP//UPBE-D3/def2-SVP, $c^\circ = 1 \text{ mol L}^{-3}$). The reaction with *t*BuNC is energetically favoured in comparison with intramolecular P–P bond cleavage, in agreement with experimental results.

moreover, it indicates that the second reaction pathway found for the model system is most likely not favoured in case of the actual system, due to the large substituents. Furthermore, it is worthy to note that adduct **4a** is predicted to be the global minimum of the reaction coordinate, in accord with experimental observation.

Conclusions

In summary, our investigations of the thermal reverse reaction of the housane **3a** indicate that two distinct isonitrile adducts play an important role for the reactivity of the molecular switch $2a \rightleftharpoons 3a$: firstly, the biradical **2a** can activate the isonitrile in a $[2 + 1]$ cycloaddition reaction, resulting in a $[2.1.1]$ bicyclic structure, which also represents the global minimum of the reaction coordinate. Secondly, the housane **3a** can be activated by the isonitrile in a nucleophilic attack, leading to an unstable open-chain adduct (**5a**) that quickly fragments into the biradical **2a** and the isonitrile. This opens up a different pathway for the thermal reverse reaction of the housane **3a**, and allows chemical control over the rate of the thermal reverse reaction.

Moreover, knowledge of the adduct formation between housane **3a** and isonitrile will help us devise new reactions that take advantage of the nucleophilic activation of the housane. *Inter alia*, this could lead to stable adducts that facilitate trapping of the thermally labile housane species, or even open new avenues in photoswitchable reactions.

Experimental

General information

For detailed information on syntheses, equipment, analytical data, computational methods *etc.* please also consult the ESI.†

All manipulations were carried out under oxygen- and moisture-free conditions under an inert atmosphere of argon using standard Schlenk or Glovebox techniques. NMR spectra under irradiation were recorded using our previously published setup,^{2,3} which was adopted from a setup published by the Gschwind group.⁴⁹

Syntheses

Biradical **2a** was synthesized according to a modified literature procedure.²³ To a solution of $[\text{P}(\mu\text{-NTer})_2]$ (459 mg, 0.640 mmol) in benzene (10 mL), DmpNC (82 mg, 0.64 mmol) was added. An immediate colour change from red to deep blue was observed. After two hours the solvent was removed, and the blue residue was dried *in vacuo* (1×10^{-3} mbar). The product was crystallized from a minimal amount of fresh benzene at ambient temperature. The supernatant was removed by syringe and the crystals were dried *in vacuo* (1×10^{-3} mbar). Yield: 480 mg (0.560 mmol, 88%). Mp. 207 °C. CHN calcd (found) in %: C 80.73 (80.36), H 7.01 (6.54), N 4.95 (4.81). $^{31}\text{P}\{^1\text{H}\}$ NMR (C_6D_6 , 202.5 MHz): $\delta = 221.7$ (d, $^2J(^{31}\text{P}, ^{31}\text{P}) = 136$ Hz, 1P, NPC), 258.3 (d, $^2J(^{31}\text{P}, ^{31}\text{P}) = 136$ Hz, 1P, NPN). A full set of analytical data can be found in the ESI.†

Adduct **4a**: biradical **2a** (60 mg, 0.07 mmol) was dissolved in *t*BuNC (1.849 mg, 2.5 mL, 22.1 mmol). The light blue solution was stored at -20 °C. Only a few colorless crystals could be collected. Yield <20%. Mp. 148 °C. CHN calcd (found) in %: C 79.97 (79.05), H 7.36 (7.18), N 6.02 (5.87). Deviations due to adhering impurities, *cf.* ESI.† $^{31}\text{P}\{^1\text{H}\}$ NMR (243 K, THF- d_6 , 101.5 MHz): $\delta = 188.2$ (d, $^2J(^{31}\text{P}, ^{31}\text{P}) = 33$ Hz, 1P, NPC), 222.7 (d, $^2J(^{31}\text{P}, ^{31}\text{P}) = 33$ Hz, 1P, NPN). Additional analytical data can be found in the ESI.†

Kinetic studies

To investigate the thermal reverse reaction $3a \rightarrow 2a$ in the presence of *t*BuNC, solutions of the biradical **2a** with different con-

concentrations of *t*BuNC were irradiated in the NMR spectrometer (optical power output approx. 200 mW). When a dynamic steady-state between photoconversion (2a → 3a) and thermal reverse reaction (3a → 2a) was reached, the laser diode was turned off and the thermal equilibration (Fig. S5†) was traced by *in situ* ³¹P NMR spectroscopy. The concentrations of all species were inferred from the time-resolved NMR spectra. Using a non-linear fitting procedure, the differential rate equations were fitted to the experimental data, yielding the rate constants as fitting parameters. For more details, please refer to the ESI, p. S20ff.†

Computational methods

Computations were carried out using ORCA 4.2.1⁴⁶ and Gaussian 09.⁵⁰ Structure optimizations were performed using the PBE exchange–correlation functional^{51,52} in conjunction with Grimme's dispersion correction D3(BJ)^{53,54} and Ahlrichs's def2 basis set family.⁵⁵ Accurate electronic energies for optimized structures were computed by single-point DLPNO-CCSD (T)^{56–59} calculations employing the def2-TZVP basis set⁵⁵ and def2-TZVP/C correlation fitting basis.⁶⁰

Transition states were located on the PES using the Nudged Elastic Band (NEB) algorithm^{41–45} implemented in ORCA at the PBE-D3/def2-TZVP level of theory. All transition state (TS) structures were verified to be connected to the corresponding minima using Intrinsic Reaction Coordinate (IRC)^{47,48} scans.

For further details (including optimized structures, electronic and thermal energies, NMR data) please refer to the ESI, p. S29ff.†

Conflicts of interest

There are no conflicts to declare.

Acknowledgements

We thank the University of Rostock for access to the high-performance computing facilities, and especially Malte Willert for his assistance with the queuing system and software installations. Special thanks are due to Peter Kumm and Thomas Kröger-Badge for their continuous commitment in our institute's technical and electrical workshops. Furthermore, we wish to thank the DFG (SCHU/1170/12-2) for financial support.

Notes and references

- H. Grützmacher and F. Breher, *Angew. Chem., Int. Ed.*, 2002, **41**, 4006–4011.
- F. Breher, *Coord. Chem. Rev.*, 2007, **251**, 1007–1043.
- M. Abe, J. Ye and M. Mishima, *Chem. Soc. Rev.*, 2012, **41**, 3808–3820.
- M. Abe, *Chem. Rev.*, 2013, **113**, 7011–7088.
- S. González-Gallardo and F. Breher, in *Comprehensive Inorganic Chemistry II*, Elsevier, 2013, vol. 1, pp. 413–455.
- L. Salem and C. Rowland, *Angew. Chem., Int. Ed. Engl.*, 1972, **11**, 92–111.
- Diradicals*, ed. W. T. Borden, Wiley-Interscience, New York, 1982.
- E. Miliordos, K. Ruedenberg and S. S. Xantheas, *Angew. Chem., Int. Ed.*, 2013, **52**, 5736–5739.
- G. Gryn'ova, M. L. Coote and C. Corminboeuf, *Wiley Interdiscip. Rev.: Comput. Mol. Sci.*, 2015, **5**, 440–459.
- T. Stuyver, B. Chen, T. Zeng, P. Geerlings, F. De Proft and R. Hoffmann, *Chem. Rev.*, 2019, **119**, 11291–11351.
- A. Hinz, R. Kuzora, U. Rosenthal, A. Schulz and A. Villinger, *Chem. – Eur. J.*, 2014, **20**, 14659–14673.
- A. Hinz, R. Kuzora, A.-K. Rölke, A. Schulz, A. Villinger and R. Wustrack, *Eur. J. Inorg. Chem.*, 2016, **2016**, 3611–3619.
- J. Bresien, A. Hinz, A. Schulz and A. Villinger, *Dalton Trans.*, 2018, **47**, 4433–4436.
- J. Bresien, A. Hinz, A. Schulz and A. Villinger, *Eur. J. Inorg. Chem.*, 2018, **2018**, 1679–1682.
- J.-J. Wang, Z.-J. Zhou, H.-M. He, D. Wu, Y. Li, Z.-R. Li and H.-X. Zhang, *J. Phys. Chem. C*, 2016, **120**, 13656–13666.
- K. Okuno, Y. Shigeta, R. Kishi and M. Nakano, *J. Phys. Chem. Lett.*, 2013, **4**, 2418–2422.
- H. Li, A. C. Fahrenbach, A. Coskun, Z. Zhu, G. Barin, Y.-L. Zhao, Y. Y. Botros, J.-P. Sauvage and J. F. Stoddart, *Angew. Chem., Int. Ed.*, 2011, **50**, 6782–6788.
- A. T. Buck, J. T. Paletta, S. A. Khindurangala, C. L. Beck and A. H. Winter, *J. Am. Chem. Soc.*, 2013, **135**, 10594–10597.
- J. Sun, Y. Wu, Y. Wang, Z. Liu, C. Cheng, K. J. Hartlieb, M. R. Wasielewski and J. F. Stoddart, *J. Am. Chem. Soc.*, 2015, **137**, 13484–13487.
- A. Hinz, A. Schulz and A. Villinger, *Angew. Chem., Int. Ed.*, 2015, **54**, 2776–2779.
- A. Hinz, A. Schulz and A. Villinger, *J. Am. Chem. Soc.*, 2015, **137**, 9953–9962.
- P. Ravat, T. Šolomek, D. Häussinger, O. Blacque and M. Juriček, *J. Am. Chem. Soc.*, 2018, **140**, 10839–10847.
- J. Bresien, T. Kröger-Badge, S. Lochbrunner, D. Michalik, H. Müller, A. Schulz and E. Zander, *Chem. Sci.*, 2019, **10**, 3486–3493.
- K. Yamaguchi, *Chem. Phys. Lett.*, 1975, **33**, 330–335.
- V. Bachler, G. Olbrich, F. Neese and K. Wieghardt, *Inorg. Chem.*, 2002, **41**, 4179–4193.
- D. Herebian, K. E. Wieghardt and F. Neese, *J. Am. Chem. Soc.*, 2003, **125**, 10997–11005.
- M.-M. Russew and S. Hecht, *Adv. Mater.*, 2010, **22**, 3348–3360.
- J. L. Zhang, J. Q. Zhong, J. D. Lin, W. P. Hu, K. Wu, G. Q. Xu, A. T. S. Wee and W. Chen, *Chem. Soc. Rev.*, 2015, **44**, 2998–3022.
- D. Bléger and S. Hecht, *Angew. Chem., Int. Ed.*, 2015, **54**, 11338–11349.
- P. C. Knipe, S. Thompson and A. D. Hamilton, *Chem. Sci.*, 2015, **6**, 1630–1639.
- E. Niecke, A. Fuchs and M. Nieger, *Angew. Chem., Int. Ed.*, 1999, **38**, 3028–3031.

- 32 M. Abe, E. Kubo, K. Nozaki, T. Matsuo and T. Hayashi, *Angew. Chem., Int. Ed.*, 2006, 45, 7828–7831.
- 33 S. Yoshidomi and M. Abe, *J. Am. Chem. Soc.*, 2019, 141, 3920–3933.
- 34 H. Beer, J. Bresien, D. Michalik, A.-K. Rölke, A. Schulz, A. Villinger and R. Wustrack, *J. Org. Chem.*, 2020, acs.joc.0c00460.
- 35 W. Adam, W. T. Borden, C. Burda, H. Foster, T. Heidenfelder, M. Heubes, D. A. Hrovat, F. Kita, S. B. Lewis, D. Scheutzow and J. Wirz, *J. Am. Chem. Soc.*, 1998, 120, 593–594.
- 36 F. Kita, W. Adam, P. Jordan, W. M. Nau and J. Wirz, *J. Am. Chem. Soc.*, 1999, 121, 9265–9275.
- 37 D. Y. Zhang, D. A. Hrovat, M. Abe and W. T. Borden, *J. Am. Chem. Soc.*, 2003, 125, 12823–12828.
- 38 M. Abe, W. Adam, W. T. Borden, M. Hattori, D. A. Hrovat, M. Nojima, K. Nozaki and J. Wirz, *J. Am. Chem. Soc.*, 2004, 126, 574–582.
- 39 B. J. Guddorf, C. Mück-Lichtenfeld, A. Hepp and F. Lips, *Chem. Commun.*, 2019, 55, 12896–12899.
- 40 P. Pyykkö and M. Atsumi, *Chem. – Eur. J.*, 2009, 15, 12770–12779.
- 41 G. Mills, H. Jónsson and G. K. Schenter, *Surf. Sci.*, 1995, 324, 305–337.
- 42 H. Jónsson, G. Mills and K. W. Jacobsen, in *Classical and Quantum Dynamics in Condensed Phase Simulations*, World Scientific, 1998, pp. 385–404.
- 43 G. Henkelman and H. Jónsson, *J. Chem. Phys.*, 2000, 113, 9978–9985.
- 44 G. Henkelman, B. P. Uberuaga and H. Jónsson, *J. Chem. Phys.*, 2000, 113, 9901–9904.
- 45 E. Maras, O. Trushin, A. Stukowski, T. Ala-Nissila and H. Jónsson, *Comput. Phys. Commun.*, 2016, 205, 13–21.
- 46 F. Neese, *Wiley Interdiscip. Rev.: Comput. Mol. Sci.*, 2018, 8, e1327.
- 47 K. Ishida, K. Morokuma and A. Komornicki, *J. Chem. Phys.*, 1977, 66, 2153–2156.
- 48 K. Fukui, *Acc. Chem. Res.*, 1981, 14, 363–368.
- 49 C. Feldmeier, H. Bartling, E. Riedle and R. M. Gschwind, *J. Magn. Reson.*, 2013, 232, 39–44.
- 50 M. J. Frisch, G. W. Trucks, H. B. Schlegel, G. E. Scuseria, M. A. Robb, J. R. Cheeseman, G. Scalmani, V. Barone, B. Mennucci, G. A. Peterson, H. Nakatsuji, M. Caricato, X. Li, H. P. Hratchian, A. F. Izmaylov, J. Bloino, G. Zheng, J. L. Sonnenberg, M. Hada, M. Ehara, K. Toyota, R. Fukuda, J. Hasegawa, M. Ishida, T. Nakajima, Y. Honda, O. Kitao, H. Nakai, T. Vreven, J. A. Montgomery Jr., J. E. Peralta, F. Ogliaro, M. Bearpark, J. J. Heyd, E. Brothers, K. N. Kudin, V. N. Staroverov, T. Keith, R. Kobayashi, J. Normand, K. Raghavachari, A. Rendell, J. C. Burant, S. S. Iyengar, J. Tomasi, M. Cossi, N. Rega, J. M. Millam, M. Klene, J. E. Know, J. B. Cross, V. Bakken, C. Adamo, J. Jaramillo, R. Gomperts, R. E. Stratmann, O. Yazyev, A. J. Austin, R. Cammi, C. Pomelli, J. W. Ochterski, R. L. Martin, K. Morokuma, V. G. Zakrzewski, G. A. Voth, P. Salvador, J. J. Dannenberg, S. Dapprich, A. D. Daniels, O. Farkas, J. B. Foresman, J. V. Ortiz, J. Cioslowski and D. J. Fox, *Gaussian 09, Revision E.01*, Gaussian, Inc., Wallingford CT, 2013.
- 51 J. P. Perdew, K. Burke and M. Ernzerhof, *Phys. Rev. Lett.*, 1996, 77, 3865–3868.
- 52 J. P. Perdew, K. Burke and M. Ernzerhof, *Phys. Rev. Lett.*, 1997, 78, 1396–1396.
- 53 S. Grimme, J. Antony, S. Ehrlich and H. Krieg, *J. Chem. Phys.*, 2010, 132, 154104.
- 54 S. Grimme, S. Ehrlich and L. Goerigk, *J. Comput. Chem.*, 2011, 32, 1456–1465.
- 55 F. Weigend and R. Ahlrichs, *Phys. Chem. Chem. Phys.*, 2005, 7, 3297–3305.
- 56 C. Riplinger and F. Neese, *J. Chem. Phys.*, 2013, 138, 034106.
- 57 D. G. Liakos, M. Sparta, M. K. Kesharwani, J. M. L. Martin and F. Neese, *J. Chem. Theory Comput.*, 2015, 11, 1525–1539.
- 58 C. Riplinger, P. Pinski, U. Becker, E. F. Valeev and F. Neese, *J. Chem. Phys.*, 2016, 144, 024109.
- 59 D. G. Liakos, Y. Guo and F. Neese, *J. Phys. Chem. A*, 2020, 124, 90–100.
- 60 A. Hellweg, C. Hättig, S. Höfener and W. Klopper, *Theor. Chem. Acc.*, 2007, 117, 587–597.

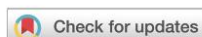
6.4 A Cyclic Thioketone as Biradical Heterocyclopentane-1,3-diyl: Synthesis, Structure and Activation Chemistry

Henrik Beer, Alexander Linke, Jonas Bresien, Alexander Villinger, and Axel Schulz
Inorg. Chem. Front. **2022**, *9*, 2659–2667.

DOI: 10.1039/D2QI00482H

Reproduced from Ref. *Inorg. Chem. Front.*, 2022, DOI: 10.1039/D2QI00482H with permission from the Chinese Chemical Society (CCS), Peking University (PKU), and the Royal Society of Chemistry.

Onlinelink: <https://doi.org/10.1039/D2QI00482H>

Cite this: *Inorg. Chem. Front.*, 2022, 9, 2659

Received 3rd March 2022,

Accepted 13th April 2022

DOI: 10.1039/d2qi00482h

rsc.li/frontiers-inorganic

A cyclic thioketone as biradical heterocyclopentane-1,3-diyl: synthesis, structure and activation chemistry†‡

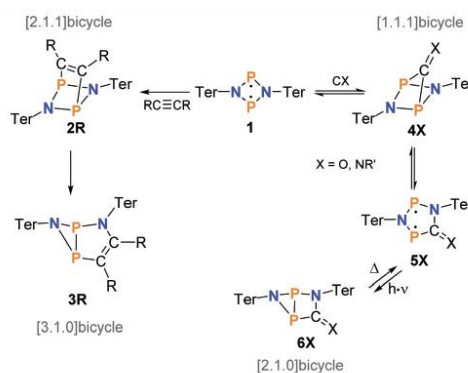
Henrik Beer,^{id} ^a Alexander Linke,^{id} ^{a,b} Jonas Bresien,^{id} ^a Alexander Villinger^{id} ^a and Axel Schulz^{id} ^{*a,b}

The reaction of the biradical $[(\mu\text{-N}(\text{Ter})\text{P})_2]$ with thiophosgene, SCCl_2 , leads to a cyclic phosphazathiourea derivative in very good yields. This synthetic approach represents a new possibility to prepare cyclic thioketones starting from four-membered cyclo-diphosphadiazanediyli by formal CS insertion with simultaneous oxidation of the two phosphorus atoms by the two chlorine atoms. When the phosphazathiourea derivative is reduced with magnesium chips, a deep blue, highly labile cyclic thioketone is formed, which can be regarded as a biradical heterocyclopentane-1,3-diyl. This new biradical can be converted to a housane species by light, which triggers transannular P–P bond formation. A thermal back-reaction was not observed, but scavenging reactions with CS_2 or PhCHO clearly indicate the intermediate formation of the labile, biradical cyclic thioketone. Various intercepted products, such as [2.2.1]bicyclic cage compounds could be isolated and structurally characterized. Freshly *in situ* generated biradical thioketone can be utilized to activate small molecules.

Introduction

Over the past 30 years, biradicals have evolved from laboratory curiosities to important building blocks for activation chemistry in many areas of organic and inorganic chemistry. Likewise, the physical properties, such as molecular switching, magnetic properties to supramolecular biradical structures, are the subject of modern research.^{1–4} The diphosphadiazanediyli, $[(\mu\text{-NR})\text{P}]_2$ ($\text{R} = \text{Ter} = 2,6\text{-dimesitylphenyl}$, **1**),⁵ is a four-membered heterocycle with a significant biradical character (25%) and is known to readily activate small molecules with single and multiple bonds (Scheme 1).^{6–10} Here, the activation of molecules with a triple bond, e.g. CO or isonitrile $\text{R}'\text{-NC}$ ($\text{R}' = t\text{butyl}$, diisopropylphenyl), proved to be particularly interesting,^{11,12} since in the first step the activation leads to a 1,1- or 1,2-bridged species (**2R** vs. **4X**; $\text{X} = \text{O}, \text{NR}'$; $\text{R}, \text{R}' = \text{aryl}$, alkyl), which further reacts under insertion into the four-membered

bered P_2N_2 ring of **1** (Scheme 1). For example, activation of CO with diphosphadiazanediyli **1** already occurs at room temperature (1 bar). However, unlike alkynes, which insert with both carbon atoms into the P_2N_2 ring of the [2.1.1]bicycle (species **2R**) to form a [3.1.0]bicycle (**3R**) with a transannular P–P bond,^{13,14} CO exhibits carbene-analogous reactivity, so that only the C atom of species **4O** is inserted into a P–N bond, resulting in the formation of a formal cyclic ketone (**5O**), in



Scheme 1 Activation of small molecules by biradical **1** resulting in the formation of different types of bicyclic compounds.

^aInstitut für Chemie, Universität Rostock, Albert-Einstein-Straße 3a, D-18059 Rostock, Germany. E-mail: axel.schulz@uni-rostock.de

^bLeibniz-Institut für Katalyse e.V. an der Universität Rostock, Albert-Einstein-Straße 29a, D-18059 Rostock, Germany

† On the occasion of the 90th birthday of Prof. Dr Wolfgang Beck.

‡ Electronic supplementary information (ESI) available: Experimental section, preparation of starting materials and compounds, structure elucidation, additional spectroscopic details and computational details. CCDC 2153623–2153626. For ESI and crystallographic data in CIF or other electronic format see DOI: <https://doi.org/10.1039/d2qi00482h>

which the biradical character is retained.¹¹ This biradical cyclic ketone (as well as the analogous isonitrile reaction products 5NR') can be regarded as a stable cyclopentane-1,3-diyl analogue (ca. 25% biradical character for all species 5X), which, in addition, exhibits photochromic molecular switching properties under the influence of light. That is, under irradiation, a transannular P-P bond is formed, resulting in a housane type closed-shell molecule (species 6X).^{9,12,15-18} When the irradiation is switched off, the system thermally reacts back, the P-P bond is cleaved and biradical 5X is recovered.

Phosphorus-heterocyclic species such as 1 and 5X belong to the class of open-shell singlet biradicals,^{11,15,16,18-30} which means that the spin density is exact zero at each point in space but yet they can be utilized as trapping reagents of highly reactive molecular fragments³¹ and molecular switches¹⁶⁻¹⁸ besides the activation of small molecules as discussed above.⁹ Therefore, based on the known properties of 5O, we wanted to investigate how the molecular switching properties as well as the molecular activation chemistry change when the oxygen is formally exchanged for a sulphur atom, *i.e.*, an analogous cyclic biradical thioketone of type 5S (Scheme 1) should be synthesized and its reactivity investigated. To the best of our knowledge, biradical thioketones have not been reported so far, although cyclic and alkyl thioketones are well-established (Chart 1).³²⁻³⁶ The isolation of stable thioketones (with respect to oligomerization)³⁷ as well as thioaldehydes can be achieved *via* kinetic stabilization by introducing spatially demanding substituents.^{14,38}

Substitution of the oxygen atom by a sulphur atom in a ketone leads to the formal formation of a thioketone and therefore to significant changes in the chemical reactivity as well as stability of the C=X carbon-chalcogen double bond (X = O, S). Firstly, the polarity of the bond changes (*cf.* EN(O) = 3.44 vs. EN(S) = 2.58, EN = Pauling electronegativity), *i.e.* the C-S bond is only very weakly polar (EN(C) = 2.55) compared to the strongly polar C=O bond. Secondly, there is the thermodynamic instability of C=S double bonds compared to the C=O double bonds in ketones, which often leads to oligomerization in the absence of steric protection. For example, in contrast to CO, the isovalence electronic carbon monosulfide, CS, is characterized by a pronounced instability, which is characterized by rapid polymerization in the absence of a suitable reaction partner.³⁹ The exact composition of polymeric (CS)_n has not yet been elucidated.^{40,41} Nevertheless, it is in principle possible to work with monomeric CS, but it has to be generated *in situ* in an elaborate way.⁴² One of the most common methods for CS generation represents the dissociation of

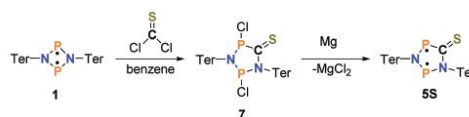
carbon disulphide, CS₂, which can be achieved photolytically, thermally, or *via* discharge processes.^{39,42-44} With respect to the electronic properties, a detailed study of vibrational stretching frequencies in a series of CO and CS metal complexes showed that CS has better σ -donor as well as π -acceptor properties than the isovalence-electronic CO.⁴⁵

Finally, while carbon monoxide, CO, is a stable gas and can be handled and purchased in gas cylinders, CS is only known to be a very short-lived species (*vide supra*). This in turn means that we had to come up with a completely new synthetic route, since the analogous reaction of 1 + CO \rightarrow 5O was not possible in case of 5S (Scheme 1). Here we would like to report the synthesis of a biradical cyclic thioketone 5S, its photoisomerization to a housane-type species, and its use in small-molecule activation.

Results and discussion

Synthesis

Reaction of thiophosgene with biradical 1. Since the direct reaction of biradical 1 with CS was impossible (see above), we switched to thiophosgene, S=CCl₂, as CS source. The reaction of 1 dissolved in benzene with S=CCl₂ proceeded with rapid color change of the solution of biradical 1 from orange to light brown after addition of the thiophosgene (Scheme 2). After working up the reaction solution, yellow-brown crystals could be isolated in good yields (>70%). Using single crystal X-ray structure analysis, the structure of product 7 was clearly demonstrated, although the data set was relatively poor (Fig. 1). As expected, the thiophosgene reacted with the inser-



Scheme 2 Synthesis of biradical 5S starting from 1 and thiophosgene.

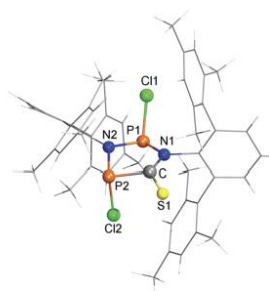


Fig. 1 Ball-and-stick representation of the molecular structure of 7 in the crystal. Only a ball-and-stick representation is shown due to a poor data set.

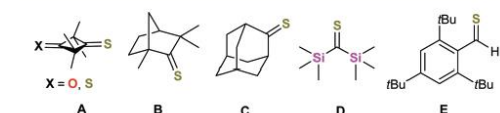


Chart 1 Selected examples of isolated stable thioketones (A–D) or thioaldehydes (E).³²⁻³⁶

tion of the C=S moiety into the four-membered heterocyclic ring of biradical **1** with simultaneous oxidation of the two phosphorus ring atoms, each of which is now attached to a chlorine atom in compound **7**.

The formation of **7** can also be followed very well in the ^{31}P NMR spectroscopy experiment, since relatively quickly (within a few minutes) the signal of the starting material **1** disappears and a series of new signals emerges in the spectrum instead, which we were able to assign to an isomeric mixture of two different *trans*- and one *cis*-isomer on the basis of computed NMR spectroscopic data (Chart 2). In solution, the ratio of these three different isomers could be estimated by solution ^{31}P NMR spectroscopy (*trans1* : *trans2* : *cis*, 10 : 60 : 1), where the formation of the *trans2*-isomer of **7** seems to be preferred. Computations at the DLPNO-CCSD(T)/def2-TZVP//PBE-D3/def2-TZVP level of theory clearly favour both *trans*-isomers of **7** over the *cis*-isomer (28.4 kJ mol $^{-1}$), with *trans1*-**7** slightly energetically favoured over *trans2*-**7** by 2.8 kJ mol $^{-1}$ at least in the gas phase. This isomeric mixture can be isolated (m.p. 180–189 °C) and used for follow-up chemistry.

Based on the isomeric mixture, yellow crystals could be isolated. A single crystal X-ray structure analysis clearly showed the presence of a *trans1*-isomer of **7** in the crystal (Fig. 1). However, the data set was too poor to allow a detailed discussion of the structural parameters. The presence of a mixture of diastereomers could possibly also be a cause for the difficulties related to the isolation of suitable single crystals (small diffraction angles of the crystal and multiple disordering). It can be assumed that there is a second isomer in the crystal which, due to the weak scattering of the crystal, is not considered as a disorder in the structure refinement. In agreement with quantum chemical calculations (see above), the slightly puckered central five-membered ring is formed by single bonds between the ring atoms. The C–S bond corresponds to a classical double bond ($d_{\text{exp}}(\text{C}=\text{S}) = 1.67(2)$ Å, cf. sum $\Sigma r_{\text{cov}}(\text{C}=\text{S}) = 1.61$ Å, $d_{\text{theo}}(\text{C}=\text{S}) = 1.67$ Å).

Synthesis of biradical 5S. With **7** in hand, we performed a series of reduction reactions aimed at the formation of **5S**, as shown in Scheme 2. Indeed, the reduction of **7** with Mg chips works, if a few essential boundary conditions are fulfilled, since the formed biradical **5S** is extremely sensitive and starts to decompose slowly as soon as formed. (i) It is essential to make sure that no grease gets into the reaction vessel. (ii) It must be run completely in the absence of light (see below).

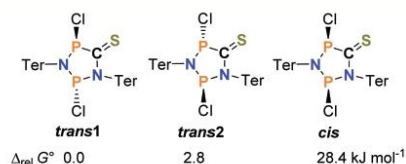


Chart 2 Isomers of **7** along with relative Gibbs energies (DLPNO-CCSD(T)/def2-TZVP//PBE-D3/def2-TZVP).

(iii) Mg turnings should be activated by stirring under argon atmosphere for 6 weeks using a glass covered magnetic stir bar. If these boundary conditions are met, then upon addition of Mg chips to **7** (dissolved in THF), it can be observed how the initial yellow color of the solution at room temperature gradually changes to green and then to deep blue (Fig. 2). The progress of the reaction must be monitored by $^{31}\text{P}\{^1\text{H}\}$ NMR spectroscopy, as over-reduction and decomposition occur rapidly. The ^{31}P NMR spectroscopic signals of the isomeric mixture of **7** at 96.6–195.4 ppm (*trans1*-, *trans2*- and *cis*-isomer, see ESI ‡) disappear while at the same time two new signals, two doublets at 243.0 ppm ($d, {}^2J(^1\text{H}, {}^{31}\text{P}) = 87$ Hz), 289.5 ppm ($d, {}^2J(^1\text{H}, {}^{31}\text{P}) = 87$ Hz) appear at lower field, which we could assign to the blue open-shell singlet biradical **5S**, in accord with the ^{31}P NMR spectroscopic data of **5O** and **5NDmp** (Table S4, \ddagger Dmp = 2,6-dimethylphenyl). When the reaction is almost complete, the solution should be separated from the magnesium, the solvent removed *in vacuo*, and the solid residue dried at 40 °C (water bath) for 30 minutes. Unfortunately, the product could not be recrystallized due to its extreme sensitivity to light, moisture and oxygen. Therefore, only the filtered, dried intensely blue raw product (yield 90% for the raw product, see ESI ‡) was used in follow-up chemistry. Note: It is best to use always a freshly prepared solution of **5S** for subsequent chemistry (see ESI ‡).

Dark blue **5S** is stable as a solid at –20 °C in the dark for a short time. However, despite great care, small amounts of by-products (e.g., [TerNPNTer]MgCl·THF, **7** and TerNC) always occur and clean isolation/crystallization at ambient temperatures was impossible. This blue raw-product (purity ca. 90%) quickly decomposes at temperatures above 125 °C. Nevertheless, the presence of **5S** was further proven by mass spectrometry, UV-Vis ($\lambda_{\text{max}} = 638$ nm) and trapping experiments (*vide infra*, see ESI ‡).

Light-induced isomerization of **5S**

Since photochemical transformation into the corresponding closed-shell singlet compound **6S**, so-called housanes (Scheme 1 and Fig. 3), has been observed for **5O** and **5NDmp**,^{1,9,11,12,17} the photochemical behaviour of this biradical **5S** was investigated. Quantum chemical calculations (DLPNO-CCSD(T)/def2-TZVP//PBE-D3/def2-TZVP, see ESI ‡) were first carried out to evaluate whether a minimum exists on the potential energy surface (PES) for the housane type species



Fig. 2 Reduction of **7** (left) with Mg chips at 25 °C in THF to give heterocyclopentane-1,3-diyI **5S** (right). Color changes during reaction (left): compound **7**. Middle: Green immediately after the start of the reaction and deep blue after about 10 min (right).

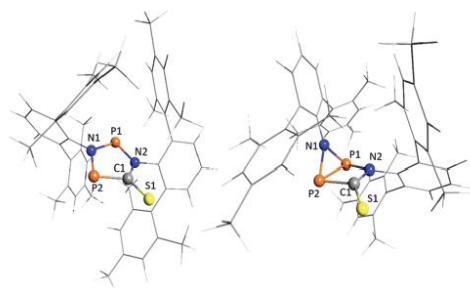
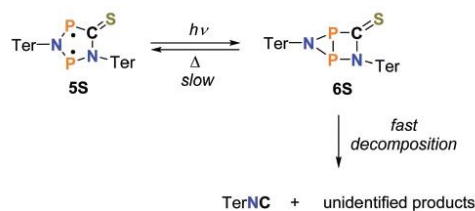


Fig. 3 Computed molecular structures of biradical 5S (left) and housane 6S (right).

6S. Indeed, such a local minimum could be found on the PES (Fig. 3). Housane formation is induced by a transannular P–P bond formation that also results in bending of the five-membered heterocycle. The bond formation between the two radical centers is accompanied by a significant shortening of the P–P distance from 2.95 Å (5S) to 2.21 Å (6S), which is consistent with the sum of the covalent radii for a P–P single bond of 2.22 Å.⁴⁶ Furthermore, folding of the nearly planar five-membered ring is observed: the N–P–P–C dihedral angle becomes smaller, which is evident from a decrease from 177.4° (5S) to 111.9° (6S).

The computed thermodynamic data of the 5S → 6S isomerization show that the biradical 5S is the energetically preferred constitutional isomer ($\Delta_r G^\circ = 47.5 \text{ kJ mol}^{-1}$). Although the free enthalpy of this isomerization is positive, light-induced excitation followed by relaxation should allow housane formation. Thus, if housane formation is observed experimentally, then this represents further direct experimental evidence for the presence of the biradical 5S in solution.

To experimentally investigate the light-induced isomerization in solution, a series of different ^{31}P NMR spectroscopic irradiation experiments was performed. An UV-Vis spectrum of the biradical 5S was recorded in advance in order to find out the proper wavelength for the irradiation experiment. The corresponding absorption maximum was observed at 638 nm (Fig. S8†), which also explains the deep blue color of a solution of 5S in THF. Subsequently, a series of different time and temperature variable ^{31}P NMR spectroscopic experiments was performed under irradiation. For this purpose, the freshly prepared blue reaction solution (*vide supra*, Scheme 2) separated from the MgCl_2 precipitate was first concentrated *in vacuo* and then a small amount of THF-d_3 was added in order to obtain the most intensive signals possible in the $^{31}\text{P}\{^1\text{H}\}$ NMR spectrum. The blue reaction solution was first irradiated at -20°C in the NMR spectrometer with red light (638 nm, Scheme 3) *via* an optical fiber connected to a laser diode (Fig. S14–S18†).¹⁵ Upon irradiation, the disappearance of the biradical signals at 240.5 ppm and 288.6 ppm is clearly visible and the appearance of two new doublets in the highfield region at



Scheme 3 Housane formation under irradiation ($\lambda = 638 \text{ nm}$).

-101.1 ppm and -81.5 ppm ($^1J_{\text{exp.}}(^{31}\text{P}, ^{31}\text{P}) = 22 \text{ Hz}$; cf. $-105.7/-99.4 \text{ ppm}$ and $^1J_{\text{exp.}}(^{31}\text{P}, ^{31}\text{P}) = 52 \text{ Hz}$ in 6O)¹¹ was observed (Fig. S19–S21†), indicating the presence of a housane type species.¹ In accordance with the housane formation $5\text{O} \rightarrow 6\text{O}$, irradiation of deep blue 5S also led to the pale yellow housane 6S.

In the further course of the NMR spectroscopic experiments, the isomerization reaction $6\text{S} \rightarrow 5\text{S}$ should be examined for its thermoreversibility, which is known for the lighter derivative 6O and in the isonitrile analogue 6NDmp. However, it was reported that the thermal reverse reaction is fully reversible only for 6NDmp while for 6O decomposition products are formed rapidly.^{11,12} For this purpose, further $^{31}\text{P}\{^1\text{H}\}$ NMR spectra were measured for a period of 1 h with an interval of 3 min and at -20 , 0 and 25°C with the light source switched off (Fig. S19–S21†). In all experiments, no reverse reaction could be observed. Although the intensity of housane 6S continuously decreased, no reappearance of the signals of the biradical 5S was observed, which only suggests a rapid decay of the housane. *I.e.* the regeneration of the biradical 5S is too slow to be observed. Since no thermal reverse reaction could be observed, an attempt was made to initiate the reverse reaction photochemically by irradiating with light of a wavelength of 455 and then 520 nm. However, again in both cases no photochemical reverse reaction could be detected at -20 , 0 and 25°C . Nonetheless, a significant decrease in the signal intensities of the housane 6S was observed over the entire time of the experiment. However, the only product we were able to crystallize was the decomposition product Ter-NC (Scheme 3). It should also be noted that no further ^{31}P NMR signals were observed upon thermal decomposition, while decomposition under irradiation resulted in a large number of signals in the ^{31}P NMR spectrum.

Trapping experiments

Although already both NMR and UV-Vis spectra as well as photochemical switching to a housane indicated the presence of the highly labile biradical 5S, trapping reactions were performed to study its activation chemistry. For this purpose, the biradical 5S was reacted with CS_2 , alkynes, Se, isonitriles, and PhCHO. While the addition of alkynes (tolane, $\text{Me}_3\text{Si-C}\equiv\text{C-SiMe}_3$), Se and isonitriles (*t*Bu–NC, Dmp–NC) did not lead to any reaction, immediate reactions were observed with CS_2 and PhCHO as trapping reagents.

Reaction with CS₂. The reaction of biradical 5S with CS₂ was attempted in two different ways (Scheme 4). Firstly, with *in situ* generated biradical 5S, and secondly, with isolated 5S after filtration from MgCl₂, which is formed during the reduction of 7 with Mg. Interestingly, both reactions yield different reaction products.

When CS₂ was added directly to a blue solution containing the transient biradical 5S (Scheme 4, top), an immediate color change from blue to reddish brown was observed. The measured ³¹P NMR spectrum revealed the disappearance of the phosphorus signals of the transient species 5S and the appearance of new signals, which could not be assigned to any known or expected species. Nevertheless, the reaction solution was left overnight at 5 °C to crystallize, and two different types of crystals were isolated: brown cuboidal crystals and yellow needles. While the yellow needles were identified as Ter-NC, which we had often observed as a decomposition product of 5S (*vide supra*), the reddish-brown cuboids were an unexpected product (8). The product is a dimeric (but not centrosymmetric) magnesium salt in which both magnesium(II) ions are coordinated by three sulfur atoms and one imino-nitrogen atom in a distorted tetrahedral coordination environment. Both heterocyclic bi-negatively charged anions are formed by a C-C coupling reaction, although the route of formation is not known, nor can it be easily deduced. In any case, the five-membered ring in 5S must have opened, both phosphorus atoms were sulfurized, and in addition to the C-C coupling, a P-C bond was also formed, leading to the formation of two four-membered rings fused to each other, the backbone of the heterocyclic dianion (Fig. 4).

Since the desired product was apparently not formed in the presence of unreacted magnesium or MgCl₂, the reaction of 5S

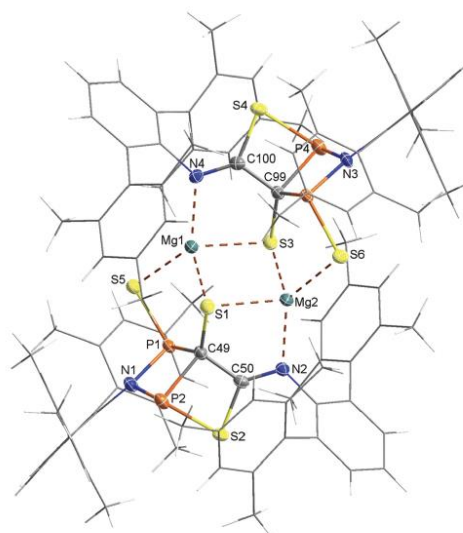
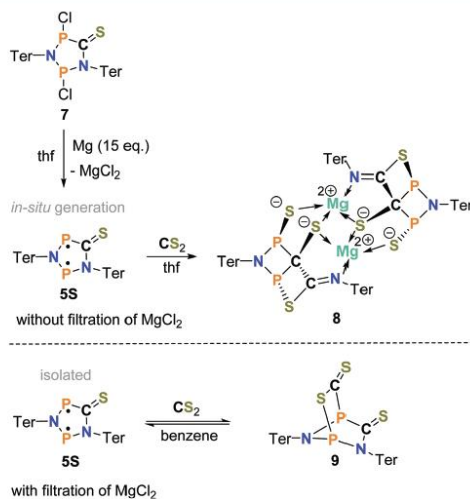


Fig. 4 ORTEP of 8 in the crystal. Ellipsoids set at 50% probability (123 K). Selected bond lengths (Å) and angles (°): P1–S5 2.048(1), P3–S6 2.055(1), C49–C50 1.487(4), C50–S2 1.735(3), C50–N2 1.295(3), C49–S1 1.805(3), Mg1–S1 2.471(1), Mg2–N2 2.09(2), Mg1–N4 2.089(2), Mg1–S1 2.471(1), Mg1–S3 2.5205(1), Mg1–S5 2.377(1), Mg2–S3 2.468(1), Mg2–S1 2.503(1), Mg1–Mg2 3.342(1); S1–Mg1–Mg2–S3 176.55(6).



Scheme 4 Reaction of biradical 5S with CS₂.

with CS₂ was repeated after removal of the solid magnesium and MgCl₂ by filtration (Scheme 4, bottom). This change in procedure was immediately noticeable in a different color change: from dark blue to dark green. Another difference from the previous experiment is the cleaner ³¹P{¹H} NMR spectrum recorded after the addition of CS₂. Essentially, two new signals are observed, namely two doublets at 89.1 and 177.3 ppm, respectively ($^2J(^{31}\text{P}, ^{31}\text{P}) = 16$ Hz). After recrystallization from *n*-hexane, green crystals suitable for single-crystal X-ray structural analysis were obtained overnight at 5 °C. The single crystal structure analysis revealed unequivocally the presence of cage compound 9 (Fig. 5), in which a C-S unit bridges both phosphorus atoms in the five-membered ring and an exocyclic C-S double bond remains in this formal [2.2.1]bicycle. It should be noted that single crystals of 9 co-crystallized with small amounts of [SP(μ-Nter)₂P](CS) (10, 3.5%, see Scheme 5 bottom, B layer Fig. S3†). The experimental detection of 10 is not really surprising, since a similar reaction has already been observed for the CO₂ adduct of 1 (species 11, Scheme 5 top).⁷ That is, the bridging CS₂ can also be decomposed by the release of carbon sulfide, CS, producing 10 and *in situ* generated highly reactive CS molecule.

X-ray structure determination of 9 revealed a [2.2.1]bicycle with a puckered P₂N₂C five-membered ring (Fig. 5, deviation from planarity ∠(N2–P2A–N2A–P1A) = 43°) and one exocyclic sulphur atom in each of both five-membered rings. Both exo-

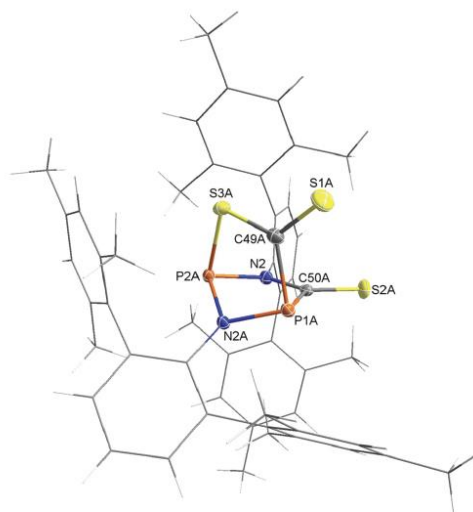
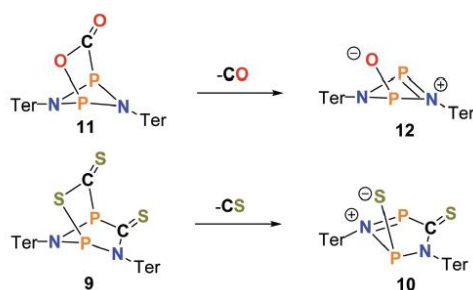


Fig. 5 ORTEP of **9** in the crystal. Ellipsoids set at 50% probability (123 K). Selected bond lengths (Å) and angles (°): P1A–C50A 1.855(2), P1A–C49A 1.871(2), P1A–N1A 1.749(2), C50A–N2 1.375(2), C50A–S2A 1.635(1), C49A–S1A 1.631(2), C49A–S3A 1.719(2); N1A–P2A–N2 92.97(8), P2A–N1A–P1A 108.7(1), N1A–P1A–C50A 92.01(8), N2–C50A–P1A 111.2(1), C50A–N2–P2A 115.5(1), S3A–C49A–P1A 116.24(9), C49A–S3A–P2A 95.45(6), S1A–C49A–S3A 125.7(1).



Scheme 5 Decomposition of bicycles **9** and **11**.

cyclic C–S lengths are significantly shorter than the C–S bridge ($d(\text{C50A–S2A}) = 1.635(1)$, $d(\text{C49A–S1A}) = 1.631(2)$ versus $d(\text{C49A–S3A}) = 1.719(2)$ Å) and indicate the presence of C–S double bonds (cf. $\Sigma r_{\text{cov}}(\text{C–S}) = 1.73$, $\Sigma r_{\text{cov}}(\text{C=S}) = 1.61$ Å).⁴⁶ All bonds within the two five-membered rings are in the range of (polarized) single bonds.⁴⁶

All reactions with CS_2 were carried out several times, and we found that the yields or product compositions changed depending on time, light and temperature. For this reason, we also took a closer look at the temperature stability of freshly prepared CS_2 addition product **9**. Since already **5S** and also **9**

always decompose slowly to Ter-NC and other mostly poorly soluble products we treated the raw product **9** (ca. 72% **9**, 25% **7**, 3% other species according to ^{31}P NMR spectrum) for three hours in benzene at 90 °C. An *in situ* ^{31}P NMR spectrum, recorded after 3 h of reaction time, shows a variety of decomposition products of which we could assign the following: at $\delta = 100.4$ (s, **7**), 173.6 (s, new species **13**), 195.2 (s, **7**), 230.6 (s, new species **13**), 263.4 (s, $[\text{ClP}(\mu\text{-Nter})_2]_2$), 276.6 (s, **1**) ppm. Nevertheless, we tried to isolate the new species. For this reason, after cooling the reaction mixture to ambient temperature all volatile components were removed *in vacuo* and the yellow residue was re-crystallized from *n*-hexane affording yellow crystals over night at 5 °C. Only a few crystals could be isolated from the viscous solution. Single-crystal X-ray structural analysis revealed without doubt the presence of a C–C coupling product (Fig. 6), which we assume was formed by the reaction of CS_2 -adduct **9** with the decomposition product Ter-NC (Scheme 6). Starting from **9**, which can release highly reactive CS (see Scheme 5), this inserts into the P–C bond with C–C bond formation, and then the resulting S–C–S fragment reacts with the isonitrile Ter-NC to give the final product **13**.

The molecular structure of **13** consists of a [3.1.1]bicyclic ring to which a further five-membered ring is fused as illustrated in Fig. 6. The central structural motif of the five-, six- and four-membered rings is wrapped in a pocket formed by three terphenyl substituents. While the five-membered ring with a C–C double bond ($d(\text{C74–C74}) = 1.355(2)$, cf. $\Sigma r_{\text{cov}}(\text{C=C}) = 1.34$ Å)⁴⁶ and an exocyclic C–N double bond is nearly planar (maximum deviation from planarity $\angle \text{C73–S3–C75–S2} = 6.9^\circ$), both the six-membered ring and the four-membered ring are highly puckered. The four-membered ring is nearly perpen-

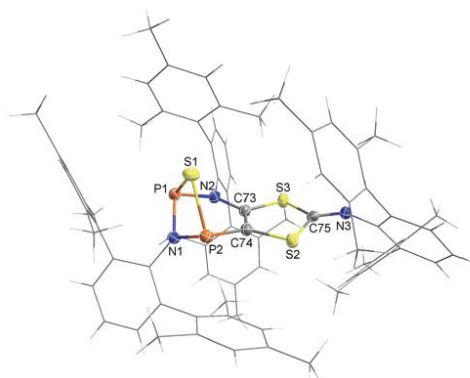
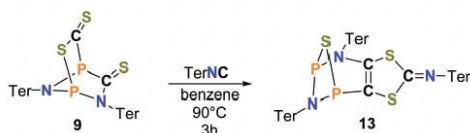


Fig. 6 ORTEP of **13** in the crystal. Ellipsoids set at 50% probability (173 K). Selected bond lengths (Å) and angles (°): C74–C75 1.355(2), C74–S2 1.749(2), C75–S2 1.759(2), C75–S3 1.762(2), C73–S3 1.749(2), P2–S1 2.1702(6), P1–S1 2.1571(6), P2–N1 1.729(1), P1–N1 1.734(1), P2–C74 1.812(2), C73–N2 1.397(2), C75–N3 1.274(2); C73–S3–C75 96.23(7), C74–S2–C75 96.48(7), S2–C75–S3 113.06(8), C73–C74–P2 123.8(1), N1–P2–C74 98.07(7), P2–N1–P1 102.91(7), N1–P1–S1 85.00(5), P1–S1–P2 77.49(2), N1–P2–S1 84.72(5), C74–C73–N2 123.95(1).



Scheme 6 Formation of C–C coupling product **13** upon thermal treatment of **9**.

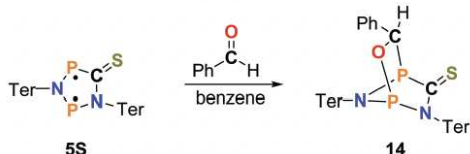
dicular to the six-membered ring ($\angle(S1-N1-C74-C73) = 89.3^\circ$). All C–S bonds (1.749–1.762 Å) are in the range of normal C–S single bonds ($\Sigma r_{cov}(C-S) = 1.78$ Å), as are all P–N (1.729–1.734 Å, *cf.* $\Sigma r_{cov}(P-N) = 1.82$ Å) and P–S (2.157–2.170 Å, *cf.* $\Sigma r_{cov}(P-S) = 2.14$ Å) bonds.⁴⁶ The C–N bond ($d(C73-N2) = 1.397(2)$ Å) in the six-membered ring corresponds to a single bond, while the exocyclic C–N bond with $d(C75-N3) = 1.274(2)$ Å is in the range of a double bond (*cf.* $\Sigma r_{cov}(C-N) = 1.46$ Å, *cf.* $\Sigma r_{cov}(C=N) = 1.27$ Å).⁴⁶

Reaction with benzaldehyde, PhCHO. Furthermore, we used benzaldehyde as a trapping reagent (Scheme 7). The reaction of biradical **5S**, prepared *in situ*, with benzaldehyde in benzene was completed after only 10 min at ambient temperature. Again, an immediate color change from blue to yellow could be observed after addition of the trapping reagent. The ³¹P NMR spectrum from the reaction solution shows two new main signals, two doublets at 124.8 and 31.9 ppm ($^2J(^{31}P, ^{31}P) = 16$ Hz). Such a signal pattern would be expected for a cage compound such as **14**. Yellow single crystals of **14** were obtained after concentration of the reaction solution and leaving it at 25 °C overnight.

The single crystal structure analysis showed the expected result, namely the presence of the [2.2.1]bicycle **14**, a cage compound with a CO bridge (Fig. 7). Bicycle **14** can be isolated in high purity. It decomposes above 140 °C. The most prominent structural motive of cage compound **14** is the puckered five-membered heterocycle with the C–O bridge ($d(C50-O1) = 1.448(2)$ Å) across the five-membered ring. Except from the exocyclic C–S bond ($d(C49-S1) = 1.644(2)$ Å), all bonds within the cage of **14** are in the range of typical single bonds.⁴⁶

Biradical character of **5S**

The biradical character of **5S** was computed utilizing CASSCF (8,6) calculations (CASSCF = complete active space self-consistent field; *cf.* p. S50†). From these CASSCF(8,6) calculations, the



Scheme 7 Reaction of biradical **5S** with benzaldehyde yielding addition product **14**.

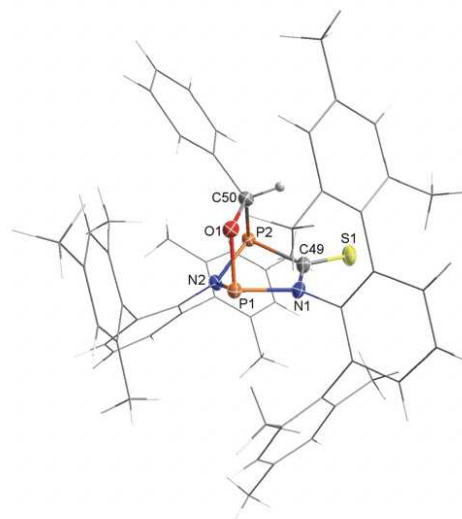


Fig. 7 ORTEP of **14** in the crystal. Ellipsoids set at 50% probability (123 K). The hydrogen atom H50 was included in the refinement at a calculated position using a riding model (with C–H = 0.95 Å and with $U_{iso} = 1.2$ times $U_{eq}(C)$). Selected bond lengths (Å) and angles ($^\circ$): N1–P1 1.795(2), N2–P1 1.717(2), N2–P2 1.737(2), C49–P2 1.862(2), C50–P2 1.921(2), C49–S1 1.644(2), C49–N1 1.362(2), C50–O1 1.448(2), P1–O1 1.626(1), O1–C50–P1 106.8(1), P1–N2–P2 105.08(8), N2–P1–N1 93.35(8), C49–N1–P1 114.0(1), N1–C49–S1 128.9(1), N1–C49–P2 110.2(1).

biradical character of only $\beta = 13\%$ was determined. This means that cyclopentane-1,3-diyl **5S** has a significantly smaller biradical character than comparable species, such as **5NDmp** ($\beta = 28\%$)¹⁵ and the lighter homolog **5O** ($\beta = 22\%$).¹¹ The frontier orbitals of cyclopentane-1,3-diyl **5S** (Fig. 8) indicate some diene character within the five-membered heterocycle of the molecule as manifested by some degree of delocalization along the CN bond. For example, the HOMO displays some π -bonding character along the CN bond. However, usually the

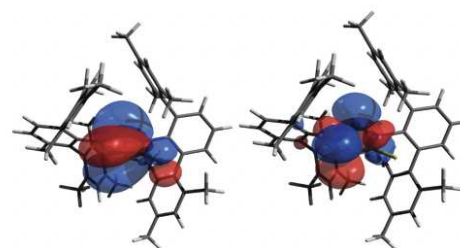


Fig. 8 Frontier molecular orbitals of **5S**: HOMO (left), LUMO (right). Both π -type MOs are the main contributors to the CASSCF wave function.

HOMO of related biradicals is mainly localized at both phosphorus atoms as in 5O and 5NDmp. The orbital character at the P atoms is dominantly p-character.

The smaller biradical character of biradical 5S is assumed to be the reason for the lower reactivity towards typical trapping reagents such as alkynes or isonitriles. The latter, for example, react easily with 5O and 5NDmp but not 5S (*vide supra*).

Conclusion

Starting from four-membered heterocyclic biradicals of the type, $[(\mu\text{-N-Ter})\text{P}]_2$, the synthesis of the novel five-membered cyclic thioketones 7 in reaction with thiophosgene, SCCl_2 , was achieved by a new synthetic route. The thiophosgene reacts with insertion of the CS group into a P–N bond of $[(\mu\text{-N-Ter})\text{P}]_2$ with simultaneous oxidation of both P atoms by the two chlorine atoms. With the cyclic ketone 7 in hand, the very labile, reactive biradical cyclo-thioketone 5S could be synthesized in reductions, but it is extremely sensitive to light. Red light can be used to convert the biradical thioketone 5S to a housane species with a transannular P–P bond, but this reaction is not reversible because decomposition begins immediately when exposed to light. Freshly *in situ* generated biradical thioketone 5S can be used to activate small molecules such as CS_2 or benzaldehyde, producing unprecedented caged compounds that can be isolated and characterized. In future work, we would like to further investigate biradical 5S with respect to *in situ* generation of CS and as a trapping reagent for labile molecular fragments.

Experimental section

All manipulations were carried out under oxygen- and moisture free conditions under argon using standard Schlenk or glovebox techniques at room temperature [298(3) K] unless noted otherwise. Removal of volatile substances *in vacuo* was carried out at 1×10^{-3} mbar. Further information on experimental procedures, preparation of starting materials, data acquisition and processing, purification procedures and a full set of analytical data for each compound as well as details on the computations can be found in the ESI.†

Conflicts of interest

There are no conflicts to declare.

Acknowledgements

We gratefully acknowledge financial support by the Deutsche Forschungsgemeinschaft (DFG; SCHU 1170/12-2). Moreover, we wish to thank the ITMZ at the University of Rostock for access to the cluster computer, and especially Malte Willert for

his assistance with the queuing system and software installations.

References

- J. Bresien, L. Eickhoff, A. Schulz and E. Zander, *Reference Module in Chemistry, Molecular Sciences and Chemical Engineering*, Elsevier, 2022.
- J. J. Dressler and M. M. Haley, Learning How to Fine-Tune Diradical Properties by Structure Refinement, *J. Phys. Org. Chem.*, 2020, 33, 1–13.
- J. Guo, Y. Yang, C. Dou and Y. Wang, Boron-Containing Organic Diradicaloids: Dynamically Modulating Singlet Diradical Character by Lewis Acid-Base Coordination, *J. Am. Chem. Soc.*, 2021, 143, 18272–18279.
- W. Zeng and J. Wu, Open-Shell Graphene Fragments, *Chem*, 2021, 7, 358–386.
- T. Beweries, R. Kuzora, U. Rosenthal, A. Schulz and A. Villinger, $[\text{P}(\mu\text{-N-Ter})]_2$: A Biradicaloid That Is Stable at High Temperature, *Angew. Chem., Int. Ed.*, 2011, 50, 8974–8978.
- A. Hinz, R. Kuzora, U. Rosenthal, A. Schulz and A. Villinger, Activation of Small Molecules by Phosphorus Biradicaloids, *Chem. – Eur. J.*, 2014, 20, 14659–14673.
- A. Hinz, A. Schulz and A. Villinger, Metal-Free Activation of Hydrogen, Carbon Dioxide, and Ammonia by the Open-Shell Singlet Biradicaloid $[\text{P}(\mu\text{-N-Ter})]_2$, *Angew. Chem., Int. Ed.*, 2016, 55, 12214–12218.
- L. Chojetzki, A. Schulz, A. Villinger and R. Wustrack, Cycloaddition of Alkenes and Alkynes to the P-centered Singlet Biradical $[\text{P}(\mu\text{-N-Ter})]_2$, *Z. Anorg. Allg. Chem.*, 2020, 646, 614–624.
- A. Schulz, Group 15 Biradicals: Synthesis and Reactivity of Cyclobutane-1,3-Diyl and Cyclopentane-1,3-Diyl Analogues, *Dalton Trans.*, 2018, 47, 12827–12837.
- L. Eickhoff, L. Ohms, J. Bresien, A. Villinger, D. Michalik and A. Schulz, A Phosphorus-Based Pacman Dication Generated by Cooperative Self-Activation of a Pacman Phosphane, *Chem. – Eur. J.*, 2022, 28, e202103983.
- A. Hinz, A. Schulz and A. Villinger, Heterocyclopentane-1,3-Diyls, *Angew. Chem., Int. Ed.*, 2015, 54, 2776–2779.
- A. Hinz, A. Schulz and A. Villinger, Tunable Cyclopentane-1,3-Diyls Generated by Insertion of Isonitriles into Diphosphadiazanediyls, *J. Am. Chem. Soc.*, 2015, 137, 9953–9962.
- A. Hinz, A. Schulz, W. W. Seidel and A. Villinger, A New Class of Azadipniciridines Generated by an Unusual Rearrangement Reaction, *Inorg. Chem.*, 2014, 53, 11682–11690.
- L. S. Szych, Y. Pilopp, J. Bresien, A. Villinger, J. Rabeah and A. Schulz, *Angew. Chem., Int. Ed.*, 2022, 61, e202114792.
- J. Bresien, T. Kröger-Badge, S. Lochbrunner, D. Michalik, H. Müller, A. Schulz and E. Zander, A Chemical Reaction Controlled by Light-Activated Molecular Switches Based on Hetero-Cyclopentanediylys, *Chem. Sci.*, 2019, 10, 3486–3493.

- 16 H. Beer, J. Bresien, D. Michalik, A. Schulz and A. Villinger, Reversible Switching between Housane and Cyclopentenediyl Isomers: An Isonitrile-Catalysed Thermal Reverse Reaction, *Dalton Trans.*, 2020, 49, 13986–13992.
- 17 T. Völzer, H. Beer, A. Schulz, S. Lochbrunner and J. Bresien, Photoisomerization of a Phosphorus-Based Biradicaloid: Ultrafast Dynamics through a Conical Intersection, *Phys. Chem. Chem. Phys.*, 2021, 23, 7434–7441.
- 18 J. Bresien, D. Michalik, H. Müller, A.-K. Rölke, A. Schulz, A. Villinger, R. Wustrack, H. Beer, J. Bresien, D. Michalik, A.-K. Rölke, A. Schulz, A. Villinger and R. Wustrack, Heterocyclopentenediyls vs Heterocyclopentadienes: A Question of Silyl Group Migration, *J. Org. Chem.*, 2020, 85, 14435–14445.
- 19 M. K. Sharma, D. Rottschäfer, T. Glodde, B. Neumann, H. Stammler and R. S. Ghadwal, Ein Offenschaliges Singulett-Sn I-Diradikal Und H₂-Spaltung, *Angew. Chem.*, 2021, 133, 6485–6489.
- 20 S. N. Intorp, M. Hodecker, M. Müller, O. Tverskoy, M. Rosenkranz, E. Dmitrieva, A. A. Popov, F. Rominger, J. Freudenberger, A. Dreuw and U. H. F. Bunz, Quinoidal Azaacenes: 99% Diradical Character, *Angew. Chem., Int. Ed.*, 2020, 59, 12396–12401.
- 21 D. Gerbig, B. Bernhardt, R. C. Wende and P. R. Schreiner, Capture and Reactivity of an Elusive Carbon-Sulfur Centered Biradical, *J. Phys. Chem. A*, 2020, 124, 2014–2018.
- 22 C. Saalfrank, F. Fantuzzi, T. Kupfer, B. Ritschel, K. Hammond, I. Krummenacher, R. Bertermann, R. Wirthensohn, M. Finze, P. Schmid, V. Engel, B. Engels and H. Braunschweig, CAAC-Stabilized 9,10-diboraanthracenes – Acenes with Open-Shell Singlet Biradical Ground States, *Angew. Chem., Int. Ed.*, 2020, 59, 19338–19343.
- 23 T. Stuyver, B. Chen, T. Zeng, P. Geerlings, F. De Proft and R. Hoffmann, Do Diradicals Behave Like Radicals?, *Chem. Rev.*, 2019, 119, 11291–11351.
- 24 W. W. Schoeller, The Niecke Biradicals and Their Congeners – The Journey from Stable Biradicaloids to Their Utilization for the Design of Nonlinear Optical Properties, *Eur. J. Inorg. Chem.*, 2019, 1495–1506.
- 25 F. E. Penotti, D. L. Cooper and P. B. Karadakov, Is the S₂N₂ Ring a Singlet Diradical? Critical Analysis of Alternative Valence Bond Descriptions, *Int. J. Quantum Chem.*, 2018, e25845.
- 26 A. Bauzá, D. Escudero, A. Frontera and R. Streubel, Electronic Structure of N₂P₂ Four-Membered Rings and the Effect of Their Ligand Coordination to M(CO)₅ (Cr, Mo, and W), *Organometallics*, 2015, 34, 355–360.
- 27 S. González-Gallardo and F. Breher, Main Group Biradicaloids, in *Compr. Inorg. Chem. II*, 2013, pp. 413–455.
- 28 M. Abe, W. T. Borden and M. Abe, Diradicals, *Chem. Rev.*, 2013, 113, 7011–7088.
- 29 E. Miliordos, K. Ruedenberg and S. S. Xantheas, Unusual Inorganic Biradicals: A Theoretical Analysis, *Angew. Chem.*, 2013, 125, 5848–5851.
- 30 Y. Hirano, G. Schnakenburg, R. Streubel, E. Niecke and S. Ito, New Aspects of 1,3-Diphosphacyclobutane-2,4-Diyls, *Helv. Chim. Acta*, 2012, 95, 1723–1729.
- 31 J. Bresien, A. Hinz, A. Schulz and A. Villinger, Trapping of Transient, Heavy Pnictogen-Centred Biradicals, *Dalton Trans.*, 2018, 47, 4433–4436.
- 32 E. U. Elam and H. E. Davis, Chemistry of Dimethylketene Dimer. VII. Dimers of Dimethylthioacetone, *J. Org. Chem.*, 1967, 32, 1562–1565.
- 33 N. Tokitoh, K. Kishikawa and R. Okazaki, Synthesis and Structure of the First Germaketenedithioacetal, *J. Chem. Soc., Chem. Commun.*, 1995, 1425.
- 34 R. Okazaki, A. Ishii, N. Fukuda, H. Oyama and N. Inamoto, Synthesis of 2,4,6-Tri-*t*-Butylthiobenzaldehyde, the First Stable Thiobenzaldehyde, *J. Chem. Soc., Chem. Commun.*, 1982, 1187.
- 35 A. Ricci, A. Degl'Innocenti, M. Fiorenza, P. Dembech, N. Ramadan, G. Seconi and D. R. M. Walton, Bis (Trimethylsilyl) Thioketone, *Tetrahedron Lett.*, 1985, 26, 1091–1092.
- 36 J. W. Greidanus, Chemistry of 2-Substituted Adamantanes. I Adamantane-1-thione, Its Dimer and Trimer, *Can. J. Chem.*, 1970, 48, 3530–3536.
- 37 T. Murai, The Construction and Application of C=S Bonds, *Top. Curr. Chem.*, 2018, 376, 31.
- 38 W. M. McGregor and D. C. Sherrington, Some Recent Synthetic Routes to Thioketones and Thioaldehydes, *Chem. Soc. Rev.*, 1993, 22, 199–204.
- 39 A. Senning and A. Sulfur, an Important Element in My Life, *Sulfur Rep.*, 2003, 24, 191–253.
- 40 F. Cataldo and D. Heymann, Carbon Disulfide Sonopolymer: A Comparison with Other Carbon Disulfide Polymers, *Eur. J. Solid State Inorg. Chem.*, 1998, 35, 619–628.
- 41 R. Steudel, Reaktion von Kohlenstoffmonosulfid Und -Monoselenid Mit Chalkogenen Und Halogenen, *Angew. Chem.*, 1967, 79, 649–650.
- 42 E. K. Moltzen, K. J. Klabunde and A. Senning, Carbon Monosulfide: A Review, *Chem. Rev.*, 1988, 88, 391–406.
- 43 E. K. Moltzen, M. P. Kramer, A. Senning and K. J. Klabunde, Carbon Monosulfide Chemistry in Solution. 4. Studies on the Reactivity of Carbon Monosulfide toward Amines and Thiols, *J. Org. Chem.*, 1987, 52, 1156–1161.
- 44 K. J. Klabunde, M. P. Kramer, A. Senning and E. K. Moltzen, Carbon Monosulfide Chemistry in Solution. Insertion into Sulfur-Chlorine Bonds, *J. Am. Chem. Soc.*, 1984, 106, 263–264.
- 45 M. A. Andrews, Correlations of the Vibrational Stretching Frequencies of Transition Metal Thiocarbonyls with Those of Their Carbonyl Analogs. Comparison of the Bonding Characteristics of Carbon Monosulfide and Carbon Monoxide Ligands, *Inorg. Chem.*, 1977, 16, 496–499.
- 46 P. Pykkö and M. Atsumi, Molecular Double-Bond Covalent Radii for Elements Li-E112, *Chem. – Eur. J.*, 2009, 15, 12770–12779.

6.5 Synthesis of Bicyclic P,S-Heterocycles via the Addition of Thioketones to a Phosphorus-Centered Open-Shell Singlet Biradical

Henrik Beer, Alexander Linke, Jonas Bresien, Grzegorz Mlostoń, Małgorzata Celeda, Alexander Villinger, Axel Schulz

Inorg. Chem. **2022**, *61*, 2031–2038.

DOI: 10.1021/acs.inorgchem.1c03207

Reprinted with permission from *Inorg. Chem.* 2022, 61, 4, 2031–2038. Copyright 2022 American Chemical Society.

Onlinelink: <https://doi.org/10.1021/acs.inorgchem.1c03207>

Synthesis of Bicyclic P,S-Heterocycles via the Addition of Thioketones to a Phosphorus-Centered Open-Shell Singlet Biradical

Henrik Beer, Alexander Linke, Jonas Bresien, Grzegorz Młostóć,* Małgorzata Celeda, Alexander Villingner, and Axel Schulz*

Cite This: *Inorg. Chem.* 2022, 61, 2031–2038

Read Online

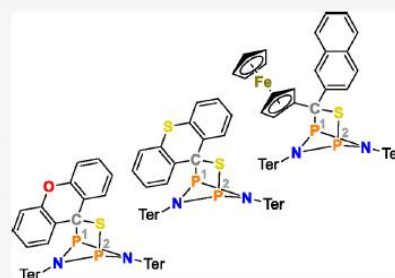
ACCESS |

Metrics & More

Article Recommendations

Supporting Information

ABSTRACT: Formal addition reactions between the open-shell singlet biradical $[P(\mu\text{-N}Ter)]_2$ (1Ter) and xanthione, thioxanthione, as well as ferrocenyl naphthyl thioketone were studied in detail. Reactions were performed at room temperature and led to the formation of strained [2.1.1]-cage P,S-heterocycles (3). All addition products were isolated and fully characterized by spectroscopic methods. Furthermore, reversible cleavage of the xanthione-biradical addition product into the parent compounds (biradical and thioketone) could be demonstrated by $^{31}\text{P}\{^1\text{H}\}$ NMR spectroscopy. The thermodynamic stability of all cyclization products with respect to the elimination of thioketone was studied by quantum-chemical computations including solvent effects. Regarding the dissociation of addition products 3 into the fragment molecules 1Ter and ketone/thioketone, calculations prove that a significantly larger distortion energy in ketones compared with thioketones causes lower thermodynamic stability of the ketone adducts.



INTRODUCTION

Pnictogen-centered open-shell singlet biradicals^{1–16} of the type $[E(\mu\text{-NR})_2]$ ($E = \text{P, As, Sb, Bi}$; $R = \text{Ter}$; $\text{Ter} = \text{terphenyl} = 2,6\text{-dimesitylphenyl}$; $[P(\mu\text{-NR})_2] = 1\text{Ter}$) have been used for some time to activate small molecules containing single and multiple bonds (Scheme 1).^{14,17–20} Among others, heterocumulenes such as CO_2 and CS_2 , bearing a carbon–chalcogen double bond, can be activated by 1Ter and converted to their corresponding addition products. Analogous conversion was also successfully performed using acetone as a biradical interceptor. So far, however, no aromatic ketones or thioketones have been studied in the reaction with 1Ter. The focus of the present work was the effect of the exchange of oxygen by sulfur; i.e., instead of ketones, we wanted to use the analogue thioketones. Furthermore, the thermodynamic stability of the bridged adducts should be investigated.

While, for example, CO_2 forms a labile cyclization product in the reaction with 1Ter, which immediately decomposes into CO, sulfur analogues, i.e., CS_2 , form a stable cyclization product, identified as a [2.1.1] bicyclic compound (Scheme 1),^{21–24} with a C–S bridge and an exocyclic C=S bond. Notably, the substitution of oxygen in a carbonyl group (C=O) by sulfur results in substantial changes in the chemical behavior of the resulting thiocarbonyl group (C=S). A significant difference was found with respect to drastically different values of the electronegativity between carbon (2.55) and oxygen (3.44) as well as carbon and sulfur (2.58). Therefore, this exchange results in a remarkable reduction of

the bond polarity of the C=S moiety compared to the carbonyl group. Reduction of the electronegativity difference has a substantial influence on the position of the valence orbitals: the 3p valence orbital of sulfur is energetically closer to the 2p valence orbital of carbon. This effect leads to a better interaction of both orbitals. However, the larger atomic diameter of the sulfur atom is opposed to this trend, which means that the magnitude of the overlap integral is smaller²⁵ than that in the analogous carbonyl group. Another important consequence is the smaller highest occupied molecular orbital–lowest unoccupied molecular orbital gap in the C=S group compared to the C=O group.²⁶ Furthermore, a decrease in the difference of the π charge densities at the carbon and sulfur can be observed, and one finds lowered ionization potentials as well as a red shift of the $n \rightarrow \pi^*$ and $\pi \rightarrow \pi^*$ transitions in the UV–vis spectrum.²⁷

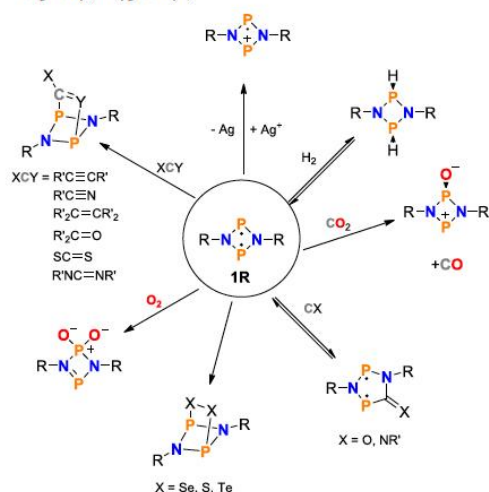
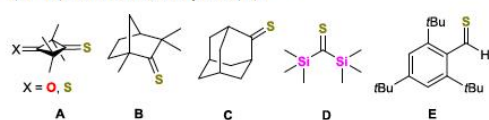
Both alkyl- and aryl-substituted thioketones are known. Some of the first examples of isolated stable thioketones are shown in Scheme 2. So, we raised the question of whether it is possible to activate thioketones of the types 2SS and 2OS (thioxanthenes) and ferrocenyl thioketone 2Fc as well as for a

Received: October 15, 2021

Published: January 18, 2022

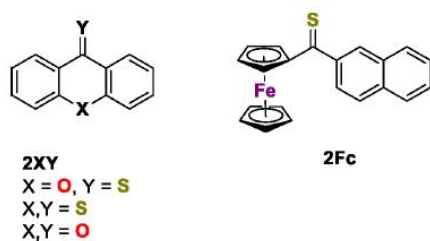


Scheme 1. Activation Chemistry of Biradical 1R (R = Terphenyl, Hypersilyl)

Scheme 2. Selected Examples of Isolated Stable Thioketones (A–D) and Thioaldehydes (E)^{28–40}

comparison of xanthone 200 (Scheme 3) by utilizing the biradical 1Ter. Because the phosphorus-based biradical

Scheme 3. Thioketones 2XY and 2Fc and Xanthone 200 Used in Reactions with 1Ter



embedded in two terphenyl substituents is particularly stable and easily accessible in good yields, we performed all addition reactions with 1Ter as a biradical.¹⁹

RESULTS AND DISCUSSION

Synthesis. Both the biradical $[P(\mu\text{-N}Ter)]_2$ (1Ter)^{19,41} and all thioketones (2OS, 2SS, and 2Fc)^{42,43} were prepared according to literature procedures and purified by standard methods. The reactions of thioketones 2OS, 2SS, and 2Fc with 1Ter were carried out in benzene at 25 °C. The course of the reaction was traced most easily by ³¹P{¹H} NMR spectroscopy.

For all thioketones, the reaction was completed after only a few minutes. The disappearance of the characteristic singlet of the starting material, biradical 1Ter, at 276 ppm was accompanied by the appearance of only two new signals for the addition product, the [2.1.1]-cage compound, at about 215 and 250 ppm (Table 1). After recrystallization from a saturated

Table 1. Selected Experimental Data: Yield, Decomposition Temperatures, and ³¹P{¹H} and ¹⁵N NMR Shifts of the Synthesized Thioketone Adducts in Solution^a

	3SS	3OS	3Fc
yield/%	54	63	^b
<i>T</i> _{dec} /°C	107	107	206
$\delta^{[31P]}$	215, 252	213, 249	214, 249
² $J(^{31}P, ^{31}P)$ /Hz	31	33	25
$\delta^{[15N]}$	173	213	-11

^aNMR experiments were carried out in C₆D₆. ^bOnly a few crystals embedded in a violet oil were obtained.

benzene or toluene solution at slightly elevated temperature, crystals suitable for single-crystal X-ray diffraction analysis were obtained at ambient temperature (Figure 1). The addition products 3SS and 3OS (Scheme 4) were isolated in satisfactory yields (50–60%). In the case of the ferrocenyl thioketone adduct 3Fc, isolation of a pure sample was more difficult and the final yield of the obtained product significantly lower.

A reaction of the xanthone 200 with 1Ter, on the other hand, was not observed either at room temperature or at a temperature of 80 °C. Quantum-chemical calculations prove that this is a thermodynamically nonfeasible reaction for this system (see below). A possible explanation for the non-observed addition reaction of compound 200 is possibly the shorter and thermodynamically more stable C=O double bond [cf. $\Sigma r_{cov}(C=O) = 1.24$ Å and $\Sigma r_{cov}(C=S) = 1.61$ Å] along with a larger distortion energy for the heterocyclic ring in 200.⁴⁴ Although the reaction between acetone and 1Ter has already been observed,⁴⁵ the organic frame of the xanthone 200 is significantly larger than the two methyl groups of the ketone (see the sections on distortion energies and thermodynamics). Because of a shorter C–O single bond in the biradical xanthone adduct 300, the benz-annellated unit of the xanthone 200 is drawn closer into the pocket formed by the terphenyl residues, which makes attachment to the biradical 1Ter via the C=O double bond energetically unfavorable. Furthermore, both the structure and electronic situation of 200 would change very much upon addition to 1Ter, resulting in a large distortion energy (see the Computations section).

Reactivity of P,S-[2.1.1]-Thioketone-Cage Compounds (3). The newly synthesized [2.1.1]-thioketone-cage compounds (3SS, 3OS, and 3Fc) are oxygen- and moisture-sensitive but thermally stable in the solid state to above 170 °C. All synthesized compounds 3 are very poorly soluble in all common solvents. In solution, however, the reversibility of the addition reaction for 3OS and 3OO is evident because at elevated temperature the thioketone is reversibly eliminated and the biradical is recovered. If the heated solution is then cooled back to room temperature, the signals of 3OS are almost exclusively observed again. In the case of 3OS, cleavage of the thioketone is completed at about 60 °C, whereas in the case of compound 3SS, cleavage is completed only at an

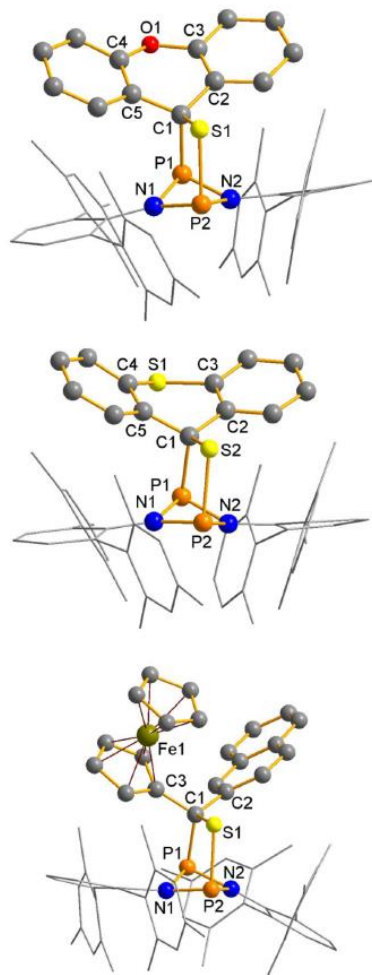
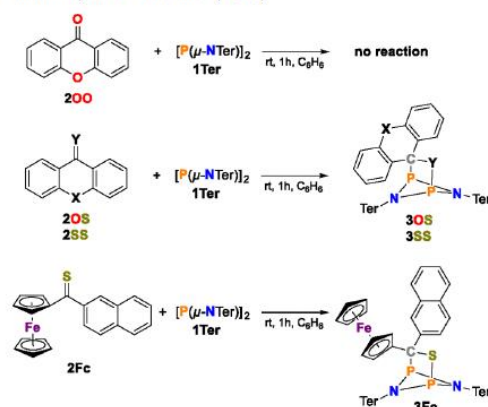


Figure 1. Ball-and-stick representations of the molecular structures of 3OS (top), 3SS (middle), and 3Fc (bottom) in the crystal (Ter substituent as a wireframe). Hydrogen atoms are omitted for clarity. Selected structural data are summarized in Table 1. ORTEP representations can be found in the Supporting Information, section 2.

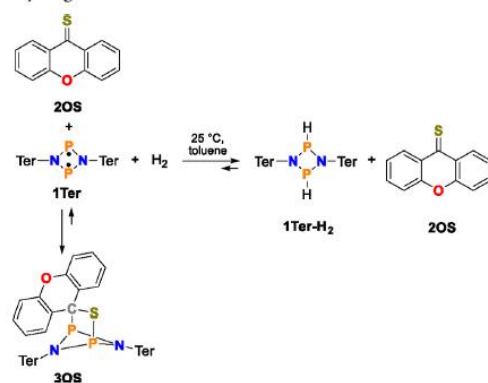
elevated temperature of 80 °C. These data are consistent with the calculated reaction energies $\Delta_r G^\circ$ (3OS, -30 kJ mol^{-1} ; 3SS, -41 kJ mol^{-1} ; see the Supporting Information, section 4; temperature-variable NMR experiments). The equilibria between $1\text{Ter} + 2\text{XY} \rightarrow 3\text{XY}$ (Scheme 4) at room temperature are almost completely on the side of the product 3XY ($X = \text{S}$, O ; $Y = \text{S}$); i.e., no signal for the starting material 1Ter is observed in the ^{31}P NMR experiment anymore. However, we wanted to see to what extent it is possible to shift this equilibrium when molecular hydrogen is added because it is known that 1Ter reacts reversibly with molecular hydrogen to

Scheme 4. Reaction of 1Ter with Thioketones (2OS, 2SS, and 2Fc) and Xanthone (2OO)



form 1Ter-H_2 already at low temperatures.^{46,47} It is also known that the 1Ter-H_2 adduct releases molecular hydrogen above 60 °C and 1Ter is recovered. Because it is known that most reactions of 1Ter with a substrate are equilibrium reactions, which are often very far on the side of the products, we treat 3OS also with molecular hydrogen. If molecular hydrogen is now added to a solution of 3OS (Scheme 5), the

Scheme 5. Reaction of Thioketone 3OS with Molecular Hydrogen



free four-membered biradical reacts rapidly to form the hydrogen adduct because 1Ter-H_2 is thermodynamically more stable than 3OS. Thus, the equilibrium is gradually shifted completely to the side of the energetically favored 1Ter-H_2 adduct (Scheme 5).

Structure Elucidation. Crystals of 3OS and 3SS, which were obtained after recrystallization from benzene or toluene at ambient temperatures, crystallize isotypically in the monoclinic space group $P2_1/n$ with four formula units per cell. Interestingly, the cell volume increases only minimally when oxygen is replaced by sulfur in 3OS (5433 vs 5466 Å³). The selected structural data are given in Table 2. For crystals

Table 2. Selected Experimental Bond Lengths (Figure 1) along with 3Ac (Acetone Addition Product) for Comparison

	3SS	3OS	3Ac	3Fc ^b
$d(\text{C}-\text{X})/\text{\AA}$	1.838(2)	1.833(3)	1.466(16)	1.873(6)
$d(\text{C}-\text{P})/\text{\AA}$	1.975(2)	1.968(3)	1.918(10)	1.947(7)
$d(\text{S}-\text{P})/\text{\AA}$	2.1662(5)	2.173(1)	1.661(3)	2.161(8)
$d(\text{P}-\text{P})/\text{\AA}$	2.5575(5)	2.5510(12)	2.514(2)	2.559(4)
$d(\text{C}1-\text{C}2)/\text{\AA}$	1.532(2)	1.518(4)	1.507(15)	1.517(4)
$d(\text{C}2-\text{C}3)/\text{\AA}$	1.401(2)	1.391(4)	1.526(15)	1.557(5)
$d(\text{C}3-\text{X})/\text{\AA}$	1.756(2)	1.382(4)		
$\angle \text{X}-\text{C}1-\text{Y}/\text{deg}$	161.2(7)	148.7(1)		
$\angle \text{C}3-\text{X}-\text{C}4/\text{deg}$	99.03(8)	116.4(2)		
$\angle \Phi_{\text{max}}/\text{deg}^a$	-39.2	-27.0		

^aThe largest dihedral angle within the ring is listed. ^bBecause the crystals are very small, the data quality is rather poor, and the structure solution only serves as proof of connectivity.

of 3Fc, a data set in the triclinic space group $\bar{P}1$ could also be determined. Unfortunately, the data set is too poor to allow a detailed discussion. However, it clearly proves the connectivity, i.e., the presence of the ferrocenyl-substituted adduct compound 3Fc in the crystal. The molecular structures of all three crystallized thiocarbonyl species 3 are shown in Figure 1.

For all three molecular structures, the C–S bonds that lie between 1.83 and 1.87 Å (Figure 1 and Table 2) are clearly in the range of a slightly stretched C–S single bond [cf. $\Sigma r_{\text{cov}}(\text{C}-\text{S}) = 1.78$ and $\Sigma r_{\text{cov}}(\text{C}=\text{S}) = 1.61$ Å].⁴⁴ The C–P (1.95–1.98 Å) and S–P (2.16–2.17 Å) bond lengths are also clearly elongated compared to the sum of the covalent radii [cf. $\Sigma r_{\text{cov}}(\text{C}-\text{P}) = 1.86$ and $\Sigma r_{\text{cov}}(\text{S}-\text{P}) = 2.14$ Å].⁴⁴ From this finding, it can be concluded that in all of these adducts, in particular, the [2.1.1] cages (species 3) are strongly strained bicyclic systems. As a result of Pauli repulsion between the bulky terphenyl substituents of the biradical 1Ter and the heterocyclic backbone of the thioketones 2, there is a stretching of the cage-forming bonds (Table 2), in particular, of the P–C single bond. For example, in the experimentally known acetone adduct 3Ac, the P–C distance is 1.918 Å, while in 3OS (1.968 Å) and 3SS (1.975 Å), a significantly larger distance was found. Moreover, as expected, the widening of the bonds between the two fragment molecules that form 3 is even more obvious when looking at the P–O versus P–S bonds (cf. 1.661 Å in 3Ac vs 2.173 Å in 3OS).

The C–C bond lengths within the central six-membered ring of the heterocycle in 2OS and 2SS feature single-bond character for the C1–C2 and C1–C5 bonds [1.52–1.53 Å; cf. $\Sigma r_{\text{cov}}(\text{C}-\text{C}) = 1.50$ Å; Figure 1 and Table 1]⁴⁴ as well as double-bond character along the bonds C2–C3/C4–C5 [1.39–1.40 Å; cf. $\Sigma r_{\text{cov}}(\text{C}=\text{C}) = 1.34$ Å].⁴⁴ As expected, the C–S–C angle [99.03(8)°] in 3SS is significantly smaller than the C–O–C angle [116.4(2)°] in 3OS. Furthermore, a strong angling of the heterocyclic frame of 3OS and 3SS can be observed (Figure 1 and Table 1), similar to the wing folding of a butterfly. This angling between the two planes of the central six-membered ring is significantly more pronounced in 3SS than in 3OS, as indicated by the larger dihedral angle $\angle \Phi_{\text{max}}$ (–39.2 vs –27.0°).

COMPUTATIONS

To shed more light on the structural changes, thermodynamics of the adduct formation, and observed properties of 3, we carried out different types of computations (see the Supporting Information) at the DLPNO-CCSD(T)/def2-TZVP//PBE-D3/def2-TZVP level of theory.^{48–51}

Distortion Energies. Structure optimizations showed that the isolated thioketone 2SS is not planar compared to the homologue 2OS, as illustrated by the dihedral angles of $\phi = 168.3^\circ$ (2SS) and 180.0° (2OS), respectively (see the Supporting Information, section 5.2.3). The thioxanthenthione 2SS thus already has a more “suitable” conformation, similar to that in the adduct 3SS, which leads to a smaller distortion energy (158.1 kJ mol^{–1}) upon adduct formation with the biradical 1Ter. In contrast, for the planar 2OS and 2OO compounds, an unfavorable larger distortion energy (161.7 and 234.4 kJ mol^{–1}) arises from the distortion upon addition to 1Ter (Table 3). The very large distortion energy for the structural change from 2OO to 3OO is certainly one of the main reasons for the thermodynamic instability of 3OO (see below).

Table 3. Distortion Energies^b [DLPNO-CCSD(T)/def2-TZVP//PBE-D3/def2-TZVP] for the Reaction of 1Ter + 2XY → 3XY along with the Interaction Energy^c ΔE^{int}

	$\Delta E_{\text{B}}^{\text{dist}}$	$\Delta E_{\text{XY}}^{\text{dist}}$	$\Sigma \Delta E^{\text{dist}}$	ΔE^{int}
3SS	168.2	158.1	326.3	–482.2
3OS	165.7	161.7	327.4	–467.4
3OO	262.7	234.4	497.0	–590.3
3Ac	242.6	243.4	485.9	–605.0
3SAc	149.1	154.3	303.5	–473.5
3Fc	168.0	165.7	333.7	–502.9

^aThe acetone and thioacetone derivatives (3Ac and 3SAc) were added for comparison. ^b $\Delta E_{\text{B}}^{\text{dist}} = E^{\text{tot}}(3\text{XY})_{1\text{Ter fragment}} - E^{\text{tot}}(1\text{Ter})$, $\Delta E_{\text{XY}}^{\text{dist}} = E^{\text{tot}}(3\text{XY})_{2\text{XY fragment}} - E^{\text{tot}}(2\text{XY})$, $\Sigma \Delta E^{\text{dist}} = \Delta E_{\text{B}}^{\text{dist}} + \Delta E_{\text{XY}}^{\text{dist}}$. ^c $\Delta E^{\text{int}} = \Delta E^{\text{tot}} - \Sigma \Delta E^{\text{dist}}$.

For comparison, we also calculated the distortion energy for the experimentally known acetone derivative (3Ac) and found a high distortion energy similar to that for 3OO (243.4 vs 234.4 kJ mol^{–1}; Table 3). Furthermore, not only for the thioketone or ketone but also for the structural change of the biradical 1Ter should a distortion energy be considered during adduct formation. These are also significantly larger for 3OO (262.7) and 3Ac (242.6) compared to the thioketone derivatives (between 165 and 168 kJ mol^{–1}), so that the total distortion energy for 3OO and 3Ac is larger with over 160 kJ mol^{–1} (Table 3). Interestingly, the thioacetone derivative (3SAc) also displays much smaller distortion energies. Therefore, the significantly larger distortion energies in the ketone addition products (3OO and 3Ac) are the main reason for the significantly lower thermodynamic stability with

respect to dissociation, with 3Ac exhibiting a slightly lower distortion energy than 3OO, which agrees with our experimental data. In addition to the distortion energies of the individual fragments, the interaction energies are also listed in Table 3.

Thermodynamics. The computed reaction energies are summarized in Table 4. According to the calculated reaction

Table 4. Reaction Energies [DLPNO-CCSD(T)/def2-TZVP//PBE-D3/def2-TZVP, in kJ mol^{-1} ; $c^\circ = 1 \text{ mol L}^{-1}$; solvent = toluene] for the Reaction of 1Ter + 2XY \rightarrow 3XY^a

	ΔE^{int}	$\Delta_R H_{298}^\circ$	$\Delta_R G_{298}^\circ$	$\Delta_R G_{\text{soln}}^\circ$
3SS	-155.9	-149.1	-68.9	-41.0
3OS	-140.0	-133.9	-58.5	-30.0
3OO	-93.2	-87.5	-13.2	+14.2
3Ac	-119.1	-111.4	-42.6	-22.5
3SAc	-170.0	-162.2	-96.8	-76.3
3Fc	-169.2	-162.8	-84.2	-51.3

^aThe acetone and thioacetone derivatives (3Ac and 3SAc) were added for comparison.

enthalpies, all addition reactions of 2 with 1Ter are exothermic, and because the gas-phase Gibbs energies are negative for all four species, all four addition reactions should be thermodynamically allowed (at least for the gas phase). However, because this was not observed experimentally for 2OO (in solution), the Gibbs reaction energies were also calculated, taking solvent effects into account, for the solvent toluene (using the SMD model).^{52–57} Only these computed values correctly reflect the experimental facts because now the addition of 2OO is thermodynamically unfavorable with +14.2 kJ mol^{-1} , while all three of the other addition reactions that lead to 2OS (−30.1 kJ mol^{-1}), 2SS (−41.0 kJ mol^{-1}), and 2Fc (−51.3 kJ mol^{-1}) represent exergonic reactions, in accordance with our experimental observations. This is also reflected by the distortion energies, which are largest in 3OO > 3OS > 3SS (Table 3). The thermodynamic stability of the known acetone adduct 3Ac with respect to dissociation into 1Ter and acetone is also reproduced by computations ($\Delta_R G_{\text{soln}}^\circ = -22.6 \text{ kJ mol}^{-1}$). This is also best explained by a somewhat lower distortion energy compared to that of 3OO (Tables 3 and 4).

CONCLUSION

Thioketones derived from xanthone and thioxanthone skeletons (2) can be activated with the help of the open-shell singlet biradical 1Ter, forming stable bicyclic heterocycles of the type 3. These products are formed via thermodynamically favorable addition reactions of the thioketones 2FC, 2OS, and 2SS onto the cyclobutane-1,3-diyl 1Ter. In contrast, the reaction between the xanthone 2OO and 1Ter did not occur under tested conditions. All molecular structures were unambiguously determined by X-ray diffraction. Compounds 3OS, 3SS, and 3Fc showed strongly elongated P–C single bonds, which indicated a large cage tension within the formed [2.1.1]-cage compounds. Furthermore, dissociation of the adduct 3OS into the thioketone 2OS and biradical 1Ter upon thermal treatment was observed in temperature-variable NMR experiments. Because of the weakened, rather long P–C bond in the thioxanthone adducts 3, future experiments should be carried out that address their lability in follow-up chemistry. In this context, the reaction of molecular hydrogen with 3OS has already been investigated, which led to the elimination of free

2OS with simultaneous formation of the hydrogen addition product 1Ter-H₂. Quantum-chemically calculated solvent effects on the free reaction enthalpies of the addition reactions cause, for example, the adduct formation of 3OO to become thermodynamically unfavorable, while all other considered addition products 3 are thermodynamically stable with respect to dissociation.

EXPERIMENTAL SECTION

All manipulations were carried out under oxygen- and moisture-free conditions. Further information and a full set of analytical data for each compound as well as details on the computations can be found in the Supporting Information.

Synthesis of [2.1.1] Bicyclic P,S-Heterocycles 3. *Synthesis of [P(μ -Nter)]₂9H-xanthene-9-thione (3OS).* 9H-xanthene-9-thione (59 mg, 0.28 mmol) and [P(μ -Nter)]₂ (200 mg, 0.28 mmol) were combined and dissolved in benzene (15 mL). An immediate color change from red to greenish-yellow was observed. After stirring for 1 h, all volatile components were removed *in vacuo* (1×10^{-3} mbar), and the yellow residue was dried *in vacuo* (1×10^{-3} mbar) for 30 min at 40 °C (water bath). The product was crystallized from a minimal amount of fresh benzene at ambient temperature. The supernatant was removed by a syringe, and the crystals were dried *in vacuo* (1×10^{-3} mbar) for 30 min at 40 °C (in a water bath). Yield: 140 mg (0.660 mmol, 54%). Single crystals suitable for X-ray diffraction were grown from a saturated toluene solution at ambient temperature.

Chemical formula: C₆₁H₅₈N₂P₂OS (929.16 g mol⁻¹) Mp: 107 °C (dec). Elem anal. Calcd (found): C, 78.85 (78.58); H, 6.29 (6.33); N, 3.01 (2.68); S, 3.45 (2.83). ¹H NMR (25 °C, C₆D₆, 500.1 MHz): δ 1.06 (s, 6 H, *o*-CH₃), 2.28 (s, 6 H, *o*-CH₃), 2.33 (s, 6 H, *o*-CH₃), 2.35 (s, 12 H, *p*-CH₃), 2.56 (s, 6 H, *o*-CH₃), 6.44 (m, 4 H, arom. CH), 6.66 (m, 13 H, arom. CH), 6.84 (s, 2 H, arom. CH), 6.91 (d, 2 H, arom. CH), 7.41 (m, 2 H, arom. *p*-CH₃), 2.56 (s, 6 H, *p*-CH₃). ¹³C{¹H} NMR (25 °C, C₆D₆, 125.8 MHz): δ 19.9 (s, CH₃), 21.8 (s, CH₃), 22.0 (s, CH₃), 22.3 (s, CH₃), 22.6 (s, CH₃), 117.3 (s, arom. C), 121.2 (s, arom. C), 123.0 (s, arom. C), 125.8 (s, arom. C), 126.0 (s, arom. C), 128.9 (s, arom. C), 129.0 (s, arom. C), 129.2 (s, arom. C), 129.2 (s, arom. C), 129.7 (s, arom. C), 129.8 (s, arom. C), 130.3 (s, arom. C), 131.5 (s, arom. C), 132.9 (s, quart. C), 133.1 (s, quart. C), 133.5 (s, quart. C), 136.8 (s, quart. C), 137.9 (s, quart. C), 138.0 (s, quart. C), 140.2 (s, quart. C). ³¹P{¹H} NMR (25 °C, C₆D₆, 101.3 MHz): δ 215.0 (d, 1 P, ²J(³¹P,³¹P) = 33 Hz), 251.5 (d, 1 P, ²J(³¹P,³¹P) = 33 Hz). ¹⁵N HMBC NMR (25 °C, C₆D₆, 50.7 MHz): δ 173.1. ¹⁴N NMR (25 °C, C₆D₆, 18.1 MHz): no signals observed.

Synthesis of [P(μ -Nter)]₂9H-thioxanthene-9-thione (3SS). 9H-thioxanthene-9-thione (64 mg, 0.28 mmol) and [P(μ -Nter)]₂ (200 mg, 0.28 mmol) were combined and dissolved in benzene (15 mL). An immediate color change from red to green was observed. After stirring for 1 h, all volatile components were removed *in vacuo* (1×10^{-3} mbar), and the greenish residue was dried *in vacuo* (1×10^{-3} mbar) for 30 min at 40 °C (in a water bath). The product was crystallized from a minimal amount of fresh benzene at ambient temperature. The supernatant was removed by a syringe, and the crystals were dried *in vacuo* (1×10^{-3} mbar) for 30 min at 40 °C (in a water bath). Yield: 165 mg (0.170 mmol, 63%). Single crystals suitable for X-ray diffraction were grown from a saturated benzene solution at ambient temperature.

Chemical formula: C₆₁H₅₈N₂P₂S₂ (945.22 g mol⁻¹) Mp: 107 °C (dec). Elem anal. Calcd (found): C, 77.51 (77.73); H, 6.18 (6.09); N, 2.96 (2.65); S, 6.78 (5.81). ¹H NMR (25 °C, C₆D₆, 300.1 MHz): δ 1.02 (s, 6 H, CH₃), 2.30 (s, 6 H, CH₃), 2.31 (s, 6 H, CH₃), 2.39 (s, 6 H, CH₃), 2.40 (s, 6 H, CH₃), 2.51 (s, 6 H, CH₃), 6.39 (m, 2 H, arom. CH), 6.62 (m, 12 H, arom. CH), 6.83 (s, 2 H, arom. CH), 6.90 (s, 2 H, arom. CH), 7.23 (m, 2 H, arom. CH), 8.03 (m, 2 H, arom. CH). ¹³C{¹H} NMR (25 °C, C₆D₆, 75.5 MHz): δ 21.5 (s, CH₃), 21.9 (s, CH₃), 22.3 (s, CH₃), 22.6 (s, CH₃), 22.7 (s, CH₃), 22.8 (s, CH₃), 121.1 (s, arom. C), 125.8 (s, arom. C), 127.6 (s, arom. C), 128.9 (s, arom. C), 129.0 (s, arom. C), 129.3 (s, arom. C), 129.4 (s, arom. C), 129.8 (s, arom. C), 130.0 (s, arom. C), 131.3 (s, arom. C), 132.7 (s,

arom. C), 132.8 (s, arom. C), 133.2 (s, arom. C), 134.5 (s, arom. C), 136.8 (s, arom. C), 136.9 (s, arom. C), 137.7 (s, arom. C), 137.9 (s, arom. C), 138.0 (s, arom. C), 139.4 (s, arom. C), 139.5 (s, arom. C), 139.7 (s, arom. C), 140.6 (s, arom. C), 140.8 (s, arom. C). $^{31}\text{P}\{^1\text{H}\}$ NMR (25 °C, C_6D_6 , 121.5 MHz): δ 213.5 (d, 1 P, $^2J(^{31}\text{P},^{31}\text{P}) = 31$ Hz), 249.4 (d, 1 P, $^2J(^{31}\text{P},^{31}\text{P}) = 31$ Hz). ^{15}N HMBC NMR (25 °C, C_6D_6 , 50.7 MHz): δ 173.1. ^{14}N NMR (25 °C, C_6D_6 , 18.1 MHz): no signals observed.

Synthesis of $[\text{P}(\mu\text{-Nter})]_2\text{Fc-}\beta\text{-naphthyl Thioketone (3Fc)}$. Fc- β -naphthyl thioketone (50 mg, 0.14 mmol) and $[\text{P}(\mu\text{-Nter})]_2$ (100 mg, 0.14 mmol) were combined and dissolved in benzene (15 mL). An immediate color change from red to brown was observed. After stirring for 1 h, the solution turned purple. Afterward, all volatile components were removed *in vacuo* (1×10^{-3} mbar), and the purple residue was dried *in vacuo* (1×10^{-3} mbar) for 30 min at 40 °C (in a water bath). The residue was redissolved in toluene (4 mL). The product was crystallized from a minimal amount of toluene at ambient temperature. Crystals coated with an oily purple layer could be isolated. Dark-yellow crystals of low quality could be grown from a saturated toluene solution at ambient temperature. The adhering violet oily impurities were removed under a microscope. Separation of the oily violet residue from the crude product was not possible even after washing several times with different solvents. The following analytical data were obtained from the dried crude product. Only the $^{31}\text{P}\{^1\text{H}\}$ NMR resonances could be assigned because of a comparison with the isolated substances 3OS and 3SS. The Raman spectrum was recorded from a crystal cleaned under a microscope.

Chemical formula: $\text{C}_{69}\text{H}_{66}\text{N}_2\text{P}_2\text{SFe}$ ($1073.15 \text{ g mol}^{-1}$). Mp: 206–208 °C (dec). Elem anal. Calcd (found): C, 77.22 (74.65); H, 6.20 (5.94); N, 2.61 (2.46); S, 2.99 (2.71) (deviation due to adhering oily impurities). ^1H NMR (25 °C, C_6D_6 , 500.1 MHz): δ 0.84, 1.50, 1.64, 2.20, 2.23, 2.32, 2.35, 2.36, 2.43, 2.45, 2.91, 3.85, 6.41, 6.47, 6.57, 6.63, 6.68, 6.73, 6.87, 6.94, 7.02, 7.30, 7.35, 7.70, 7.79, 7.97, 8.27. $^{13}\text{C}\{^1\text{H}\}$ NMR (25 °C, C_6D_6 , 125.8 MHz): δ 21.0, 21.1, 21.2, 21.3, 21.6, 21.8, 21.9, 22.1, 22.5, 22.6, 22.7, 23.4, 67.5, 69.8, 70.1, 72.7, 73.2, 73.6, 121.3, 121.5, 126.0, 126.5, 127.6, 128.9, 129.6, 129.7, 130.5, 130.6, 131.5, 131.8, 133.1, 133.3, 133.4, 133.5, 133.6, 135.9, 136.0, 136.7, 136.8, 137.2, 137.4, 137.5, 138.2, 138.5, 138.8, 139.4, 141.4, 141.5. $^{31}\text{P}\{^1\text{H}\}$ NMR (25 °C, C_6D_6 , 202.5 MHz): δ -19.0, -21.1, 95.6, 199.5, 213.5 (d, 1 P, $^2J(^{31}\text{P},^{31}\text{P}) = 25$ Hz), 227.6, 249.1 (d, 1 P, $^2J(^{31}\text{P},^{31}\text{P}) = 25$ Hz). ^{15}N HMBC NMR (25 °C, C_6D_6 , 50.7 MHz): δ -11.2. ^{14}N NMR (25 °C, C_6D_6 , 18.1 MHz): no signals observed.

■ ASSOCIATED CONTENT

Supporting Information

The Supporting Information is available free of charge at <https://pubs.acs.org/doi/10.1021/acs.inorgchem.1c03207>.

Experimental section, preparation of the starting materials and compounds, structure elucidation, and additional spectroscopic and computational details (PDF)

Accession Codes

CCDC 2114484 and 2114485 contain the supplementary crystallographic data for this paper. These data can be obtained free of charge via www.ccdc.cam.ac.uk/data_request/cif, or by emailing data_request@ccdc.cam.ac.uk, or by contacting The Cambridge Crystallographic Data Centre, 12 Union Road, Cambridge CB2 1EZ, UK; fax: +44 1223 336033.

■ AUTHOR INFORMATION

Corresponding Authors

Axel Schulz – *Institut für Chemie, Universität Rostock, D-18059 Rostock, Germany; Leibniz-Institut für Katalyse eV, Universität Rostock, D-18059 Rostock, Germany;*

orcid.org/0000-0001-9060-7065; Email: axel.schulz@uni-rostock.de

Grzegorz Mlostoń – *Department of Organic and Applied Chemistry, University of Łódź, Tamka 12 PL-91-403 Łódź, Poland; Email: grzegorz.mloston@chemia.uni.lodz.pl*

Authors

Henrik Beer – *Institut für Chemie, Universität Rostock, D-18059 Rostock, Germany*

Alexander Linke – *Institut für Chemie, Universität Rostock, D-18059 Rostock, Germany; Leibniz-Institut für Katalyse eV, Universität Rostock, D-18059 Rostock, Germany*

Jonas Bresien – *Institut für Chemie, Universität Rostock, D-18059 Rostock, Germany; orcid.org/0000-0001-9450-3407*

Małgorzata Celeda – *Department of Organic and Applied Chemistry, University of Łódź, Tamka 12 PL-91-403 Łódź, Poland*

Alexander Villinger – *Institut für Chemie, Universität Rostock, D-18059 Rostock, Germany; Leibniz-Institut für Katalyse eV, Universität Rostock, D-18059 Rostock, Germany; orcid.org/0000-0002-0868-9987*

Complete contact information is available at:

<https://pubs.acs.org/10.1021/acs.inorgchem.1c03207>

Notes

The authors declare no competing financial interest.

■ ACKNOWLEDGMENTS

We gratefully acknowledge financial support by the Deutsche Forschungsgemeinschaft (Grant SCHU 1170/12-2). Moreover, we thank the ITMZ at the University of Rostock for access to the cluster computer and especially Malte Willert for his assistance with the queuing system and software installations. G.M. thanks the National Science Centre (Cracow, Poland) for financial support within the Project Beethoven-2 (Grant 2016/23/G/ST/5/04115).

■ DEDICATION

This work is dedicated to Professor Stefan Lis (Poznań) on the occasion of his 70th birthday.

■ REFERENCES

- (1) Sharma, M. K.; Rottschäfer, D.; Glodde, T.; Neumann, B.; Stämmler, H.; Ghadwal, R. S. Ein offenschaliges Singulett-Sn I -Diradikal und H 2 -Spaltung. *Angew. Chem., Int. Ed.* 2021, 133 (12), 6485–6489.
- (2) Intorp, S. N.; Hodecker, M.; Müller, M.; Tverskoy, O.; Rosenkranz, M.; Dmitrieva, E.; Popov, A. A.; Rominger, F.; Freudenberg, J.; Dreuw, A.; Bunz, U. H. F. Quinoidal Azaacenes: 99% Diradical Character. *Angew. Chem., Int. Ed.* 2020, 59 (30), 12396–12401.
- (3) Bauzá, A.; Escudero, D.; Frontera, A.; Streubel, R. Electronic Structure of N 2 P 2 Four-Membered Rings and the Effect of Their Ligand Coordination to M(CO) S (Cr, Mo, and W). *Organometallics* 2015, 34 (1), 355–360.
- (4) González-Gallardo, S.; Breher, F. Main Group Biradicaloids. *Comprehensive Inorganic Chemistry II*; Elsevier, 2013, pp 413–455.
- (5) Abe, M.; Borden, W. T.; Abe, M. Diradicals. *Chem. Rev.* 2013, 113 (9), 7011–7088.
- (6) Miliordos, E.; Ruedenberg, K.; Xantheas, S. S. Unusual Inorganic Biradicals: A Theoretical Analysis. *Angew. Chem., Int. Ed.* 2013, 125 (22), 5848–5851.

- (7) Yoshifuji, M.; Hirano, Y.; Schnakenburg, G.; Streubel, R.; Niecke, E.; Ito, S. New Aspects of 1, 3-Diphosphacyclobutane-2, 4-diyls. *Helv. Chim. Acta* 2012, 95, 1723–1729.
- (8) Beer, H.; Bresien, J.; Michalik, D.; Rölke, A.-K.; Schulz, A.; Villinger, A.; Wustrack, R. Heterocyclopentenediyls vs Heterocyclopentadienes: A Question of Silyl Group Migration. *J. Org. Chem.* 2020, 85 (22), 14435–14445.
- (9) Gerbig, D.; Bernhardt, B.; Wende, R. C.; Schreiner, P. R. Capture and Reactivity of an Elusive Carbon–Sulfur Centered Biradical. *J. Phys. Chem. A* 2020, 124 (10), 2014–2018.
- (10) Beer, H.; Bresien, J.; Michalik, D.; Schulz, A.; Villinger, A. Reversible switching between housane and cyclopentenediyl isomers: an isonitrile-catalysed thermal reverse reaction. *Dalton Trans.* 2020, 49 (40), 13986–13992.
- (11) Saalfrank, C.; Fantuzzi, F.; Kupfer, T.; Ritschel, B.; Hammond, K.; Krummenacher, L.; Bertermann, R.; Wirthensohn, R.; Finze, M.; Schmid, P.; Engel, V.; Engels, B.; Braunschweig, H. cAAC-Stabilized 9,10-diboraaanthracenes—Acenes with Open-Shell Singlet Biradical Ground States. *Angew. Chem., Int. Ed.* 2020, 59 (43), 19338.
- (12) Stuyver, T.; Chen, B.; Zeng, T.; Geerlings, P.; De Proft, F.; Hoffmann, R. Do Diradicals Behave Like Radicals? *Chem. Rev.* 2019, 119 (21), 11291–11351.
- (13) Schoeller, W. W. The Niecke Biradicals and Their Congeners - The Journey from Stable Biradicaloids to Their Utilization for the Design of Nonlinear Optical Properties. *Eur. J. Inorg. Chem.* 2019, 2019 (11–12), 1495–1506.
- (14) Bresien, J.; Kröger-Badge, T.; Lochbrunner, S.; Michalik, D.; Müller, H.; Schulz, A.; Zander, E. A chemical reaction controlled by light-activated molecular switches based on hetero-cyclopentenediyls. *Chem. Sci.* 2019, 10, 3486–3493.
- (15) Penotti, F. E.; Cooper, D. L.; Karadakov, P. B. Is the S_2N_2 ring a singlet diradical? Critical analysis of alternative valence bond descriptions. *Int. J. Quantum Chem.* 2018, e25845.
- (16) Hinz, A.; Schulz, A.; Villinger, A. Stable Heterocyclopentane-1,3-diyls. *Angew. Chem., Int. Ed.* 2015, 54 (9), 2776–2779.
- (17) Bresien, J.; Schulz, A.; Szych, L. S.; Villinger, A.; Wustrack, R. $[E(\mu\text{-NBbp})]_2$ ($E = P, As$) – group 15 biradicals synthesized from acyclic precursors. *Dalton Trans.* 2019, 48 (29), 11103–11111.
- (18) Hinz, A.; Kuzora, R.; Rosenthal, U.; Schulz, A.; Villinger, A. Activation of Small Molecules by Phosphorus Biradicaloids. *Chem. Eur. J.* 2014, 20 (45), 14659–14673.
- (19) Beveries, T.; Kuzora, R.; Rosenthal, U.; Schulz, A.; Villinger, A. $[P(\mu\text{-NTer})]_2$: A Biradicaloid That Is Stable at High Temperature. *Angew. Chem., Int. Ed.* 2011, 50 (38), 8974–8978.
- (20) Schulz, A. Group 15 biradicals: synthesis and reactivity of cyclobutane-1,3-diyl and cyclopentane-1,3-diyl analogues. *Dalton Trans.* 2018, 47 (37), 12827–12837.
- (21) Bresien, J.; Faust, K.; Schulz, A. Bicyclic and tricyclic phosphanes with p-block substituents. *Rev. Inorg. Chem.* 2021. DOI: 10.1515/revic-2020-0028.
- (22) Rivard, E.; Power, P. P. Multiple bonding in heavier element compounds stabilized by bulky terphenyl ligands. *Inorg. Chem.* 2007, 46 (24), 10047–10064.
- (23) He, G.; Shynkaruk, O.; Lui, M. W.; Rivard, E. Small Inorganic Rings in the 21st Century: From Fleeting Intermediates to Novel Soluble Entities. *Chem. Rev.* 2014, 114 (16), 7815–7880.
- (24) Chivers, T.; Manners, I. *Inorganic Rings and Polymers of the p-Block Elements*; Royal Society of Chemistry, 2009.
- (25) McGregor, W. M.; Sherrington, D. C. Some recent synthetic routes to thioketones and thioaldehydes. *Chem. Soc. Rev.* 1993, 22 (3), 199.
- (26) Murai, T. The Construction and Application of C = S Bonds. *Top. Curr. Chem.* 2018, 376 (4), 31.
- (27) Viola, H.; Hartenhauer, H.; Mayer, R. Thiophile Reaktionen an Thio-carbonylverbindungen und deren Redoxverhalten. *Zeitschrift für Chemie* 1988, 28 (8), 269–277.
- (28) Mayer, R.; Morgenstern, J.; Fabian, J. Aliphatische Thioketone. *Angew. Chem., Int. Ed.* 1964, 76 (4), 157–167.
- (29) Huisgen, R.; Fisera, L.; Giera, H.; Sustmann, R. Thiones as Superdipolarophiles. Rates and Equilibria of Nitrono Cycloadditions to Thioketones. *J. Am. Chem. Soc.* 1995, 117 (38), 9671–9678.
- (30) Rohr, U.; Schatz, J.; Sauer, J. Thio- and Selenocarbonyl Compounds as “Superdienophiles” in $[4 + 2]$ Cycloadditions. *Eur. J. Org. Chem.* 1998, 1998 (12), 2875–2883.
- (31) Elam, E. U.; Davis, H. E. Chemistry of dimethylketene dimer. VII. Dimers of dimethylthioacetone. *J. Org. Chem.* 1967, 32 (5), 1562–1565.
- (32) Tokitoh, N.; Kishikawa, K.; Okazaki, R. Synthesis and structure of the first germaketenedithioacetone. *J. Chem. Soc. Chem. Comm.* 1995, 14, 1425.
- (33) Okazaki, R.; Ishii, A.; Fukuda, N.; Oyama, H.; Inamoto, N. Synthesis of 2,4,6-tri-*t*-butylthiobenzaldehyde, the first stable thiobenzaldehyde. *J. Chem. Soc. Chem. Comm.* 1982, 20, 1187.
- (34) Ricci, A.; Degl’Innocenti, A.; Fiorenza, M.; Dembeck, P.; Ramadan, N.; Seconi, G.; Walton, D. R. M. Bis (trimethylsilyl) thioketone. *Tetrahedron Lett.* 1985, 26 (8), 1091–1092.
- (35) Greidanus, J. W. Chemistry of 2-substituted adamantanes. I. Adamantanethione, its dimer and trimer. *Can. J. Chem.* 1970, 48 (22), 3530–3536.
- (36) Mlostoń, G.; Hamera, R.; Heimgartner, H. Synthesis of Ferrocenyl Thioketones and their Reactions with Diphenyldiazomethane. *Phosphorus. Sulfur. Silicon Relat. Elem.* 2015, 190 (12), 2125–2133.
- (37) Mlostoń, G.; Hamera-Faldyga, R.; Celeda, M.; Heimgartner, H. Efficient synthesis of ferrocenyl and other ferrocenyl-substituted ethylenes via a ‘sulfur approach’. *Org. Biomol. Chem.* 2018, 16 (23), 4350–4356.
- (38) Cava, M. P.; Levinson, M. I. Thionation reactions of lawesson’s reagents. *Tetrahedron* 1985, 41 (22), 5061–5087.
- (39) Davy, H. A direct conversion of carboxylic acids into dithioesters. *J. Chem. Soc. Chem. Comm.* 1982, 8, 457.
- (40) Mlostoń, G.; Urbaniak, K.; Sobiecka, M.; Heimgartner, H.; Würthwein, E.-U.; Zimmer, R.; Lentz, D.; Reissig, H.-U. Hetero-Diels-Alder Reactions of In Situ-Generated Azoalkenes with Thioketones; Experimental and Theoretical Studies. *Molecules* 2021, 26 (9), 2544.
- (41) Reiss, F.; Schulz, A.; Villinger, A.; Weding, N. Synthesis of sterically encumbered 2,4-bis-*m*-terphenyl-1,3-dichloro-2,4-cyclo-dipnictadiazanes $[m\text{-TerNpNCl}]_2$, ($Pn = P, As$). *Dalton Trans.* 2010, 39 (41), 9962–9972.
- (42) Scheibye, S.; Shabana, R.; Lawesson, S.-O.; Romming, C. Studies on organophosphorus compounds—XL. *Tetrahedron* 1982, 38 (7), 993–1001.
- (43) Mlostoń, G.; Kowalczyk, M.; Augustin, A. U.; Jones, P. G.; Werz, D. B. Ferrocenyl-substituted tetrahydrothiophenes via formal $[3 + 2]$ -cycloaddition reactions of ferrocenyl thioketones with donor-acceptor cyclopropanes. *Beilstein J. Org. Chem.* 2020, 16, 1288–1295.
- (44) Pyykkö, P.; Atsumi, M. Molecular double-bond covalent radii for elements Li–E112. *Chem. Eur. J.* 2009, 15 (46), 12770–12779.
- (45) Hinz, A.; Kuzora, R.; Rosenthal, U.; Schulz, A.; Villinger, A. Activation of Small Molecules by Phosphorus Biradicaloids. *Chem. Eur. J.* 2014, 20 (45), 14659–14673.
- (46) Hinz, A.; Schulz, A.; Villinger, A. Metal-Free Activation of Hydrogen, Carbon Dioxide, and Ammonia by the Open-Shell Singlet Biradicaloid $[P(\mu\text{-NTer})]_2$. *Angew. Chem., Int. Ed.* 2016, 55 (40), 12214–12218.
- (47) Zhivonitko, V. V.; Beer, H.; Zakharov, D. O.; Bresien, J.; Schulz, A. Hyperpolarization Effects in Parahydrogen Activation with Pnictogen Biradicaloids: Metal-free PHIP and SABRE. *ChemPhysChem* 2021, 22 (9), 813–817.
- (48) Marenich, A. V.; Cramer, C. J.; Truhlar, D. G. Universal Solvation Model Based on Solute Electron Density and on a Continuum Model of the Solvent Defined by the Bulk Dielectric Constant and Atomic Surface Tensions. *J. Phys. Chem. B* 2009, 113 (18), 6378–6396.

(49) McLean, A. D.; Chandler, G. S. Contracted Gaussian basis sets for molecular calculations. I. Second row atoms, $Z = 11-18$. *J. Chem. Phys.* 1980, 72 (10), 5639–5648.

(50) Neese, F. The ORCA program system. *Wiley Interdiscip. Rev. Comput. Mol. Sci.* 2012, 2 (1), 73–78.

(51) Neese, F.; Wiley, J. Software Focus The ORCA program system PROGRAM DESIGN. *WIREs Comput. Mol. Sci.* 2012, 2, 73–78.

(52) Marenich, A. V.; Cramer, C. J.; Truhlar, D. G. Universal Solvation Model Based on Solute Electron Density and on a Continuum Model of the Solvent Defined by the Bulk Dielectric Constant and Atomic Surface Tensions. *J. Phys. Chem. B* 2009, 113 (18), 6378–6396.

(53) Glendening, E. D.; Badenhop, J. K.; Reed, A. E.; Carpenter, J. E.; Bohmann, J. A.; Morales, C. M.; Landis, C. R.; Weinhold, F. *NBO 6.0*; Theoretical Chemistry Institute, University of Wisconsin: Madison, WI, 2013.

(54) Sustmann, R.; Sicking, W.; Huisgen, R. A Computational Study of the Cycloaddition of Thiobenzophenone S-Methylide to Thiobenzophenone. *J. Am. Chem. Soc.* 2003, 125 (47), 14425–14434.

(55) Młostoń, G.; Hamera-Faldyga, R.; Linden, A.; Heimgartner, H. Synthesis of ferrocenyl-substituted 1,3-dithiolanes via [3 + 2]-cycloadditions of ferrocenyl hetaryl thioketones with thiocarbonyl S-methanides. *Beilstein J. Org. Chem.* 2016, 12, 1421–1427.

(56) Młostoń, G.; Pipiak, P.; Linden, A.; Heimgartner, H. Studies on the Reactions of Thiocarbonyl S-Methanides with Hetaryl Thioketones. *Helv. Chim. Acta* 2015, 98 (4), 462–473.

(57) Buday, P.; Seeber, P.; Zens, C.; Abul-Futouh, H.; Görls, H.; Gräfe, S.; Matczak, P.; Kupfer, S.; Weigand, W.; Młoston, G. Iron(0)-Mediated Stereoselective (3 + 2)-Cycloaddition of Thiohalcones via a Diradical Intermediate. *Chem. Eur. J.* 2020, 26 (50), 11412–11416.

6.6 Trapping of Brønsted acids with a phosphorus centered biradicaloid – synthesis of hydrogen pseudohalide addition products

Henrik Beer, Kevin Bläsing, Jonas Bresien, Lukas Chojetzki, Axel Schulz, Philip Stoer, Alexander Villinger

Dalton Trans. **2020**, *49*, 13655–13662.

DOI: 10.1039/d0dt03251d

No permission needed for authors reprinting full articles in a thesis/dissertation according to the Royal Society of Chemistry. © Copyright 2020 Royal Society of Chemistry.

Onlinelink: <https://doi.org/10.1039/D0DT03251D>

Cite this: *Dalton Trans.*, 2020, **49**, 13655

Trapping of Brønsted acids with a phosphorus-centered biradicaloid – synthesis of hydrogen pseudohalide addition products†

Henrik Beer,^a Kevin Bläsing,^a Jonas Bresien,^a Lukas Chojetzki,^a Axel Schulz,^{a,*} Philip Stoer^{a,b} and Alexander Villingner^a

The trapping of classical hydrogen pseudohalides (HX, X = pseudohalogen = CN, N₃, NCO, NCS, and PCO) utilizing a phosphorus-centered cyclic biradicaloid, [P(μ-NTer)]₂, is reported. These formal Brønsted acids were generated *in situ* as gases and passed over the trapping reagent, the biradicaloid [P(μ-NTer)]₂, leading to the formation of the addition product [HP(μ-NTer)₂PX] (successful for X = CN, N₃, and NCO). In addition to this direct addition reaction, a two-step procedure was also applied because we failed in isolating HPCO and HNCS addition products. This two-step process comprises the generation and isolation of the highly reactive [HP(μ-NTer)₂PX]⁺ cation as a [B(C₆F₅)₄]⁻ salt, followed by salt metathesis with salts such as [cat]X (cat = PPh₄, *n*-Bu₃NMe), which also gives the desired [HP(μ-NTer)₂PX] product with the exception of the reaction with the PCO⁻ salt. In this case, proton migration was observed, finally affording the formation of a [3.1.1]-hetero-propellane-type cage compound, an OC(H)P isomer of a HPCO adduct. All discussed species were fully characterized.

Received 19th August 2020,
Accepted 17th September 2020

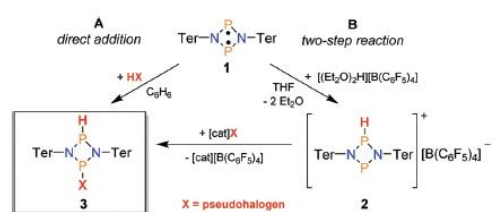
DOI: 10.1039/d0dt03251d

rsc.li/dalton

Introduction

Hydrogen halides such as HCl are classical Brønsted acids¹ when dissolved in water. They are stable at ambient temperatures in the gas phase as HX molecules or other aggregates depending on the pressure. In contrast, hydrogen pseudohalides^{2–4} such as HCN,^{5–8} HN₃,^{9–12} HNCO,^{13–22} HNCS^{23–29} or even HPCO,^{30–39} which could formally also form Brønsted acids in water, are highly labile species as molecules in the gas phase. For example, HCN or HNCO/HNCS are prone to oligomerize,⁸ while (highly dangerous) pure HN₃ can explode upon slightest manipulation or even without any external influence.¹¹ HPCO, a phosphorus-containing analogue of isocyanic acid, HNCO, was also found to be highly labile with respect to oligomerization but could be identified as elusive reactive intermediate.³⁹ Recently, we could demonstrate that some of these labile HX species can be stabilized and isolated when added to a strong Lewis acid such as B(C₆F₅)₃.^{40,41} A hydrogen azide adduct⁴⁰ and a dimer of hydrogen cyanide⁴¹ could be isolated by this procedure.

In a new approach to trap or even stabilize hydrogen pseudohalides, we studied the application of phosphorus-centered biradicaloids, [P(μ-NTer)]₂ (**1**, Scheme 1),⁴² as trapping reagents. Biradicaloid **1** (which can also be named a biradicaloid,^{43–47} since the biradical character amounts only to 25%)⁴⁸ belongs to the class of so-called “disjoint” biradicaloids,⁴³ which are open-shell singlet species in the localized orbital picture (but a two-configuration, closed-shell singlet molecule based on delocalized canonical orbitals).⁴³ Open-shell singlet biradicaloid **1** therefore includes both the reactivity of a closed-shell and an open-shell species.^{43,45} For example, biradicaloids such as **1** are known to add molecules bearing single bonds (H₂, NH₃, and chalcogens), multiple



Scheme 1 Synthesis of [HP(μ-NTer)₂PX] (**3**) utilizing (i) direct addition of HX onto biradicaloid **1** (A) and (ii) a two-step procedure (B) via the protonated biradicaloid, cation **2**⁺.

^aInstitut für Chemie, Universität Rostock, Albert-Einstein-Straße 3a, 18059 Rostock, Germany. E-mail: axel.schulz@uni-rostock.de

^bLeibniz-Institut für Katalyse an der Universität Rostock, Albert-Einstein-Straße 29a, 18059 Rostock, Germany

† Electronic supplementary information (ESI) available. CCDC 1976818–1976822, 2014417. For ESI and crystallographic data in CIF or other electronic format see DOI: 10.1039/d0dt03251d

bonds (alkynes, alkenes) or quench highly labile fragments of compounds.^{45,48}

Here we want to demonstrate that biradicaloid **1** can also be used to trap a series of labile, classical hydrogen pseudohalides (as addition products $[\text{HP}(\mu\text{-Nter})_2\text{PX}]$; HX , $\text{X} = \text{CN}$, N_3 , NCO , Scheme 1), while a two-step approach, utilizing the hitherto unknown protonated cationic species $[\text{HP}(\mu\text{-Nter})_2\text{P}]^+$ (2^+), can be applied to prepare the analogous NCS and PCO compounds. Biradicaloids of the type $[\text{RB}(\mu\text{-PR}'_2)]_2$ ($\text{R} = t\text{-Bu}$, $\text{R}' = i\text{-Pr}$)⁴⁹ and $[\text{RSi}(\mu\text{-NR}')_2]$ ($\text{R} = \text{Si}(i\text{-Pr})[\text{CH}(\text{SiMe}_3)_2]$, $\text{R}' = 3,5\text{-Me}_2\text{C}_6\text{H}_3$)⁵⁰ have been used to add acidic species such as HCl or MeOH . Only recently, the groups of Liu and Li used a N -heterocyclic carbene stabilized 6π -electron aromatic dicarbonylphosphide to activate E-H bonds ($\text{E} = \text{C}$, N , O)⁵¹ but, to the best of our knowledge, so far no pure hydrogen pseudohalide has been tested in the reaction with biradicaloids.

Results and discussion

Synthesis

As illustrated in Scheme 1, both synthetic methods were designed to prepare differently substituted 1,3-cyclo-diphosphadiazanes of the type $[\text{R}^1\text{-P}(\mu\text{-Nter})_2\text{P-R}^2]$.

Route A – direct HX addition. We started this project by studying the reaction of a benzene solution of $[\text{P}(\mu\text{-Nter})_2]$ (**1**) with a diethyl ether solution of HCl at ambient temperature (Scheme 1). This formal 1,3 addition reaction was used to find a proper setup for the reaction of **1** with other hydrogen pseudohalides. Upon addition of HCl , the initially orange reaction mixture turned colorless, and after all volatile components were removed, single crystals suitable for X-ray structure elucidation were grown from benzene overnight by cooling from 50°C to ambient temperature. X-ray structure elucidation unequivocally revealed the formation of the desired product *cis*- $[\text{H-P}(\mu\text{-Nter})_2\text{P-Cl}]$ (**3HCl**, Fig. 1). For the direct reaction of biradicaloid **1** with the hydrogen pseudohalides (HX), we first had to find a good procedure to generate pure, moisture free HX , since **1** is extremely sensitive to H_2O . For this reason, we treated the according sodium pseudohalide, NaX , with stearic acid (m.p. 69°C) at $80\text{--}100^\circ\text{C}$ under vacuum and passed the evolved gas into a second flask that was cooled with liquid nitrogen (Scheme 2).^{41,52,53} With the pure HX in hand, biradicaloid **1** was now treated with HX : gaseous HX was generated by gentle warming of the frozen HX and then passed over a benzene solution of the biradicaloid. The end of the reaction could again be recognized by the color change from orange (biradicaloid **1**) to colorless (addition product **3**). ^{31}P NMR spectroscopy was also suitable for observing the course of the reaction, since the singlet signal of the biradicaloid at 276.4 ppm disappeared, while two doublets for the addition products (**3**) appeared simultaneously (see below). All reactions led to yields between $50\text{--}80\%$ (Table 1). Unfortunately, this method could not be used for the synthesis of gaseous HNCS or HPCO , since both HPCO and HNCS are not stable in the gas phase and oligomerize at once. Moreover, it is interesting to

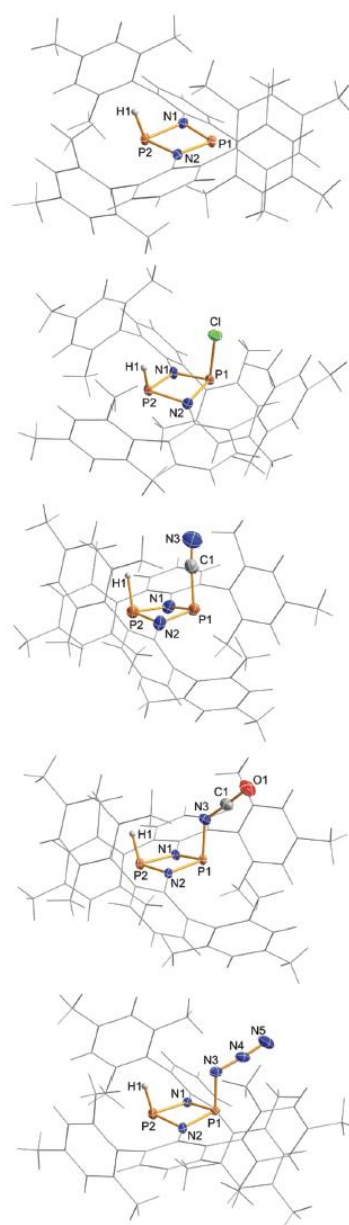
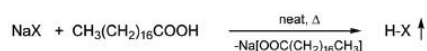


Fig. 1 Molecular structure of 2^+ (top, anion omitted for clarity) and **3HX** (CN , NCO , N_3) in the crystal. Thermal ellipsoids are drawn at 50% probability (123 K). Selected structural parameters are listed in Table 2.

Scheme 2 Synthesis of water free, gaseous HX (X = CN, NCO, and N₃).Table 1 Selected experimental data (T_{dec}^a in °C, yield in %, NMR^b data in ppm and Hz) of 3HX (X = Cl, CN, NCO, N₃, NCS, and PCO) and 2⁺

	T_{dec}	Yield	$\delta^{31}\text{P}^c$	$\delta^{31}\text{P}^d$	$\delta^1\text{H}$	$^1J_{\text{HP}}$	$^2J_{\text{PP}}$
3HCl	145	55	169.7	246.2	6.8	174	49
3HCN	45	70	185.0	163.9	6.8	152	33
3HNCO	118	72	170.7	195.7	6.6	160	30
3HN ₃	85	46	173.3	225.4	6.5	168	31
3NCS	^h	^h	176	200	6.5	162	36
3PC(H)O	170	21	216 ^f	226 ^g	7.71	3/3 ^e	41
2 ⁺	223	44	168.9	339.6	5.97	195	51

^a Always decomposition – no melting points found. ^b In C₆D₆ at RT. ^c P–H as doublet. ^d P–X. ^e Due to different connectivity, there is no $^1J_{\text{HP}}$ coupling (see Fig. 2) but two $^2J_{\text{HP}}$, $^2J_{\text{NPP}}$ unit, $^1J(^{31}\text{P},^{31}\text{P}) = 203$ Hz, $^2J(^{31}\text{P},^{31}\text{P}) = 17$ Hz, *cf.* 158 ppm as dd for PPC unit, $^1J(^{31}\text{P},^{31}\text{P}) = 203$ Hz, $^2J(^1\text{H},^{31}\text{P}) = 42$ Hz. ^f NPO, $^2J(^{31}\text{P},^{31}\text{P}) = 17$ Hz. ^g Could not be isolated as pure substance.

note that in case of 3HN₃ no Staudinger-type reaction was observed, even at elevated temperatures (two days at 60 °C). Decomposition, which leads to unidentified products, was observed at 85 °C according to DSC studies.

Route B – two step synthesis. Since the direct addition synthesis route did not work for some systems (X = NCS, PCO), we developed a second, two-step method (Scheme 1, method B). This approach is also based on biradicaloid **1**, but a protonation is first carried out, using Jutzi's acid, [(Et₂O)H][B(C₆F₅)₄],⁵⁴ followed by salt metathesis reaction with a pseudohalide salt. The reaction sequence was carried out in such a way that the protonated biradicaloid salt **2** was isolated first. To this end, biradicaloid **1** and Jutzi's acid were placed in a flask and dissolved in benzene, leading to a clear solution, which separated in two phases: an upper yellow phase and a lower deep red viscous phase. After concentration and cooling to 5 °C, red crystals could be isolated from the lower phase (44% yield). X-ray structure elucidation unequivocally revealed the presence of the desired salt [HP(μ-Nter)₂P][B(C₆F₅)₄] (**2**, Fig. 1). This reaction could also be easily monitored by ³¹P or ¹H NMR experiments (see below). With the protonated species in hand, the salt metathesis reaction was carried out by adding [*n*-Bu₃NMe]X (X = NCS, PCO; see Scheme 1 route B). [*n*-Bu₃NMe]X were utilized as these salts can be prepared moisture free and pure by treating [*n*-Bu₃NMe][CO₃Me] with Me₃Si-NCS or P(SiMe₃)₃, respectively.^{55,56} Here, upon liberating CO₂ and generating the silyl ethers Me₃Si-O-Me/Me₃Si-O-SiMe₃, pure [*n*-Bu₃NMe]X salts are formed (see ESI†). To prove the principle, we also produced 3HCN using this method, but using [Ph₄P]CN instead of HCN (see ESI†). While it was impossible to isolate 3NCS due to decomposition in the crystallization process and separation problems (though it was observed in NMR experiments, Table 1), we were able to isolate a HPCO addition product 3PC(H)O (Fig. 2) by extraction with

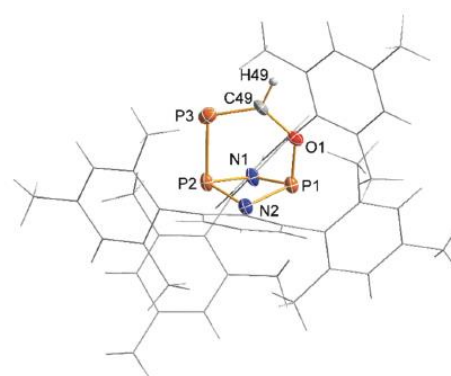


Fig. 2 Molecular structure of 3PC(H)O in the crystal. Thermal ellipsoids are drawn at 50% probability (123 K). Selected bond lengths [Å] and angles [°]: P1–O1 1.612(4), P2–P3 2.192(2), P3–C49 1.678(7), C49–O1 1.426(8), P1–P2 2.597(1), P1–N1 1.714(2), P1–N2 1.762(2), P2–N1 1.732(2), P2–N2 1.750(2); O1–C49–P3 126.4(5), P1–O1–C49 125.9(3), P2–P3–C49 102.7(3).

n-pentane followed by re-crystallization from toluene (21% yield). Already ³¹P and ¹H NMR experiments (see below) indicated that the connectivity of 3PC(H)O was different to all other 3HX compounds. Indeed, as proven by X-ray studies, 3HPCO (analogous to all other 3HX species, Fig. 1) was not formed but 3PC(H)O (Fig. 2), displaying the unexpected formation of a [3.1.1]-hetero-propellane-type cage compound, an OC(H)P isomer of a HPCO adduct. As seen in Fig. 2, the proton in the formal adduct 3HPCO must have migrated to the central carbon atom of the PCO moiety, while a three-atomic PCO bridge is formed across the four-membered P₂N₂ heterocycle, linking both P atoms of the four-membered ring (see computations). With the exception of 3NCS, all other species **3** could be isolated and were fully characterized including X-ray structure determination (Fig. 1).

NMR considerations. Interestingly, a strongly downfield shifted signal at 5.97 ppm is found in the ¹H NMR spectrum for the P–H proton of 2⁺, which is slightly less downfield shifted compared to the resonances in 3HX (between 6.5–6.8 ppm, Tables 1 and S3,† *cf.* 7.7 ppm for the acidic proton ¹H–C in 3PC(H)O). Moreover, two phosphorus resonances at 168.9 (PH) and 339.6 ppm (PNPH) were detected for 2⁺. While the first resonance for the tri-coordinated P atom (168.9 ppm) is in the range also found for the 3HX species, the second resonance of the di-coordinated P atom appears significantly low-field shifted (339.6 ppm, *cf.* 366 [P(μ-Nter)₂P–Cl]⁺ or 349 ppm in [P(μ-Nter)₂P–N₃]⁺).⁵⁷ The experimental $^1J(^1\text{H},^{31}\text{P}) = 195$ Hz and $^2J(^{31}\text{P},^{31}\text{P}) = 51$ Hz coupling constants are also in the range that was observed for all 3HX (Table 1).

In contrast to the ¹H NMR method, where all ¹H–P resonances of 3X (X = Cl, CN, NCO, N₃, and NCS) can be observed in the strongly downfield shifted range (see above), ³¹P NMR

spectroscopy is particularly well suited for the characterization of addition products 3. Except for 3HCN, the ^{31}P NMR signal for the X-bonded phosphorus atom is usually found at a lower field (doublet of doublets (dd) between 163–246 ppm) than the hydrogen-bonded phosphorus atom (dd 169–185 ppm). The geminal $^1J(^1\text{H}, ^{31}\text{P})$ coupling constants are in the expected range (152–174 Hz), as are the $^2J(^{31}\text{P}, ^{31}\text{P})$ coupling constants (30–49 Hz, cf. 51 Hz in 2^+). Due to the triple bond in 3HCN (and the associated anisotropic cone),⁵⁸ the ^{31}P resonance of the P-CN was found high-field shifted compared to that of the P-H atom. Since there is a different connectivity in 3PC(H)O compared to all other 3HX species, the ^{31}P as well as ^1H NMR resonances of 3PC(H)O cannot really be compared with those of the other 3HX compounds. For 3PC(H)O, three signals were found in the ^{31}P NMR spectrum at 158 (PCO), 216 ($N_{\text{ring}}\text{-PC}$ (H)O) and 226 ($N_{\text{ring}}\text{-O}$) ppm, assigned on the basis of their coupling pattern (see ESI†), in accord with structural data and computed NMR shifts (Table S11†). The proton resonance at 7.7 ppm for 3PC(^1H)O describes an acidic proton in agreement with NBO data (NBO = natural bond orbital theory, see below).^{59,60}

Structure elucidation

Colorless crystals of all 3HX compounds as well as red crystals of 2 were obtained from saturated benzene solutions. Single crystals of 3PC(H)O were grown from a toluene solution over two days by cooling from 50 °C to –40 °C.

Interestingly, all species 3 crystallized isotypically in the monoclinic space group $P2_1/n$ with four formula units per cell, while 2 crystallized in the triclinic space group $P\bar{1}$ with two formula units per cell. The molecular structures of all species are depicted in Fig. 1 and 2 and selected structural parameters are listed in Tables 2, S4–S6 and S12–S15† (computed data for comparison). There are no significant cation–anion interactions in 2 and intermolecular interactions in all species 3, respectively.

The most prominent structural feature of all considered species is the four-membered P_2N_2 ring and in addition, in the case of the 3HX species, the *cis*-arrangement of both substituents with the pseudohalide always pointing away from the ring (Fig. 1). As indicated by the P1–N1–P2–N1 dihedral angle, all four-membered rings in 3HX and 2^+ are slightly puckered (deviation from planarity <12.4°), in contrast to the planar P_2N_2 ring in the biradicaloid 1. The pseudohalide moiety X as

well as the hydrogen atom in 3HX are attached to the ring phosphorus atom with P–P–X/H angles significantly smaller than 100°, while the P–P–H angle in 2^+ is larger with 103(2)°. As expected for covalently bound pseudohalides, the pseudohalide moieties are slightly bent ($\angle(\text{N–N–N}) = 175.9(2)$, $\angle(\text{N–C–O}) = 175.7(2)^\circ$) and the P–X–Y angles strongly differ along the series 3HN₃ ($\angle(\text{P–N–N}) = 115.2(1)$) < 3HNCO ($\angle(\text{P–N–C}) = 130.8(1)$) < 3HCN ($\angle(\text{P–C–N}) = 175.0(6)^\circ$).

The smallest transannular P...P distance was found in 2^+ with 2.607 Å, and is slightly longer in 3HX ranging between 2.610–2.626 Å ($\sum r_{\text{dvw}}(\text{P}\cdots\text{P}) = 3.6$ Å).⁶¹ Obviously, the missing X group in 2^+ leads to less Pauli repulsion and the positive charge to orbital contraction and a better overlap. Therefore, the smallest P–N bond lengths are found in 2^+ with 1.663(2)/1.667(2) Å along the N1–P1–N2 unit, indicating partial double bond character ($\sum r_{\text{cov}}(\text{P}=\text{N}) = 1.62$ Å),⁶² while slightly longer distances were observed for the N1–P2(H)–N2 unit (1.774(3)/1.773(3) Å, cf. $\sum r_{\text{cov}}(\text{P–N}) = 1.82$ Å), in accord with polarized P–N single bonds.⁶² The latter two P–N distances compare well with those found for the tri-coordinated P atoms in 3HX (Table 2).

3PC(H)O, which is an isomer of 3HPCO (Fig. 2, see ESI† for computed structure), features a P–C–O bridge linking both phosphorus atoms of the four-membered P_2N_2 ring by a P–P and P–O single bond (P2–P3 2.192(2), P1–O1 1.612(4) Å) in a rather asymmetric way. Along the three-atomic bridge, the P–C bond can be described as a double bond (P3–C49 1.678(7), cf. $\sum r_{\text{cov}}(\text{P–C}) = 1.86$ Å, $\sum r_{\text{cov}}(\text{P}=\text{C}) = 1.69$ Å)⁶² and the C–O bond (1.426(8) Å) is in the range of a polarized C–O single bond with a small amount of double bond character (see section on bonding below). The P–C–O angle with 126.4(5)° is slightly widened for a formally sp^2 hybridized C atom.

Theoretical aspects

Energetics. To shed light onto the thermodynamics and kinetics of the formation of species 3, combined density functional and coupled cluster computations at the DLPNO-CCSD (T)/def2-TZVP//PBE-D3/def2-SVP level of theory were performed (see ESI† for details).

From a mechanistic point of view, the addition of HX to the biradicaloid may be understood in terms of frontier orbitals as a HOMO_(biradicaloid) (formal transannular π^* orbital)–LUMO_(HX) ($\sigma^*(\text{H–X})$) interaction in the initial approach as depicted in Fig. 3 for HCN, resulting for X = CN in the formation of 3HCN. It should be noted that the σ^* is not necessarily the LUMO of HX. For example, two degenerate $\pi^*(\text{CN})$ orbitals are the LUMOs in HCN (Fig. 3, bottom). If these orbitals were involved, the [2 + 2] addition product would be observed as found for R–CN (Fig. 3, bottom, e.g. R = Me).⁴⁵ However, in accord with computation, the 3HCN addition product is favored over the [2 + 2] product 4HCN by –7.81 kcal mol^{–1} (Table S10† and Fig. 3). Moreover, the HX addition does not represent a radical type reactivity, as always only the *cis*-isomer was experimentally observed. Neither the *trans*-isomer nor any X–X recombination product, which would be expected with a radical mechanism, were observed. For all 3HX species, apart

Table 2 Selected experimental bond lengths in 3HX (X = Cl, CN, NCO, and N₃) and 2^+

X	P1–X	P2–H	P1–N1	P1–N2	P2–N1	P2–N2
^a	—	1.38	1.774(3)	1.773(3)	1.663(2)	1.667(2)
Cl	2.174(1)	1.35	1.695(2)	1.680(2)	1.724(2)	1.803(2)
CN	1.863(5)	1.56	1.700(2)	1.717(2)	1.788(2)	1.717(2)
N ₃	1.810(2)	1.36	1.696(2)	1.714(2)	1.723(2)	1.780(2)
NCO	1.773(2)	1.32	1.697(2)	1.717(2)	1.730(2)	1.774(2)

^a For comparison structural parameters of 2^+ .

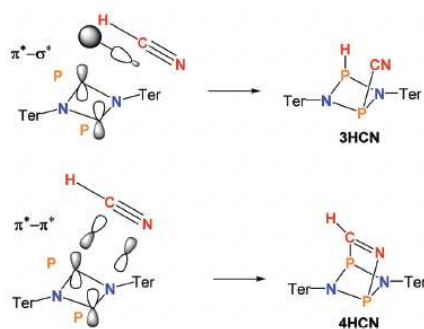


Fig. 3 Possible frontier orbital interactions for the reaction of biradicaloid 1 with HCN leading to the formation of either 3HCN or 4HCN.

from 3HPCO (see below), the *cis*-isomer represents both the thermodynamically and kinetically favored product. However, the difference for $\Delta_{298}G^\circ(\text{trans-cis})$ is rather small and lies between 2.7–4.3 kcal mol⁻¹ (Tables 3 and S9†). The overall addition reaction (biradicaloid 1 + HX → 3HX) for all considered species was computed to be exergonic ranging between -6.0 (3HCN) and -13.9 (3HNCS) kcal mol⁻¹ (Table S10†).

As mentioned above, the formation of a 1.3-bridged cage compound (notation: P¹C²O³ = 1.3-bridged) was observed only for 3PC(H)O in accordance with calculations. While for all X = Cl, CN, NCO, N₃, and (NCS) the *cis*-isomer 3HX is the thermodynamically preferred species and the 1.3-bridged cage (X¹Y²Z³) compound is always slightly less preferred (Table 3), the 3HPC(H)O cage species is preferred by -5.98 kcal mol⁻¹ over the *cis*-isomer in accordance with our experimental observation. We would like to note that we have calculated over 21 different isomers for the model compound 3HPCO_Ph (phenyl group instead of terphenyl, see Fig. S23 and Tables S17/18†). While the P–O(CP)-bound isomers were always at least 20 kcal mol⁻¹ energetically higher than the *cis-exo* isomer (Fig. 4 and S23, Table S17†), the 1.2-CO- or 1.2-CP-bridged isomers are somewhat thermodynamically less favourable than the 1.3-bridged isomer 3PC(H)O_Ph.

Table 3 Relative Gibbs enthalpies of all considered isomers of 3HX in kcal mol⁻¹ at the DLPNO-CCSD(T)//def2-TZVP level of theory

HX	<i>cis</i> ^a	<i>trans</i> ^a	Cage ^b
HCl	0.0	2.99	—
HCN	0.0	4.27	7.81
HN ₃	0.0	3.03	12.18
HNCO	0.0	2.69	1.04
HNCS	0.0	2.86	2.23
HPCO ^c	0.0	3.28	-5.98

^a X points away from the P₂N₂ ring, notation *cis-exo* (see Fig. 4). ^b 1.3-Bridged tri-atomic X¹-Y²(H)-Z³ species, for HCN only a 1.2-(C-N) bridge is possible. ^c More isomers can be found in the ESI†

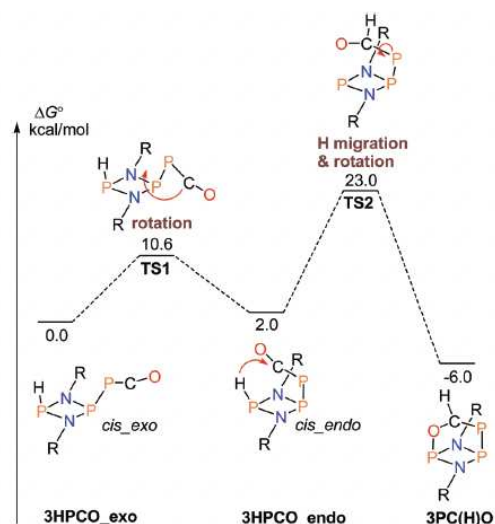


Fig. 4 Potential energy surface for the formation of 3PC(H)O starting from 3HPCO (R = terphenyl, DLPNO-CCSD(T)//def2-TZVP level of theory).

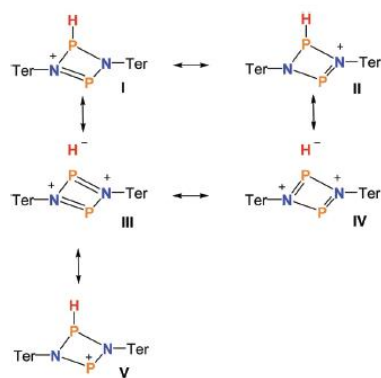
Since 3PC(H)O cannot have been formed directly in the reaction of 2⁺ with PCO⁻, we took a closer look at the formation of 3PC(H)O using quantum chemical calculations (Fig. 4). In the first reaction step, the approach of PCO⁻ to 2⁺, both *cis*- and *trans*-isomers can be formed in a barrier-free process. However, as shown in Fig. 4, only the *cis-endo* isomer can react to the observed thermodynamic product 3PC(H)O. For this reason, both *trans*-isomers and the *cis-exo* isomer must first be converted into the *cis-endo* isomer by rotation or inversion, respectively. The corresponding activation barriers are in the range 10 kcal mol⁻¹ for rotations and 33.0 kcal mol⁻¹ for inversion, which is rather large. However, it is known that proton tunnelling can significantly increase the rate of inversion.^{63,64}

The above-mentioned isomerization process, starting from the *cis-endo* isomer, includes an H-migration of the proton, which is attached to the ring phosphorus atom, to the C-atom of the PCO-unit, followed by rotation around the P–C axis (Fig. 4). Finally, this rotation around the P–C bond simultaneously forms the P–O bond, which is now spatially possible. The barrier to overcome is 21.0 kcal mol⁻¹ starting from the *cis-endo* isomer and leads in an exergonic process directly to the experimentally observed product 3PC(H)O. Also, the overall reaction along the isomerization path, starting from the *cis-exo* isomer, is exergonic with -6.0 kcal mol⁻¹ (Fig. 4). Note: For R = Ph, we found an intermediate for the H-migration process with a very small barrier to rotation (Fig. S25†), which disappeared for the bulky terphenyl substituent.

Bonding. According to NBO analyses carried out for all species 3, the P–N bonds of the P_2N_2 ring are strongly polarized (N: approx. 75%, P: 25%) and the P_2N_2 ring is electron-deficient ($Q = 0.09-0.27$ e, Table S16†). Interestingly, all covalent P–H bonds are nearly non-polar (P: 51%, H: 49%), while the C–H bond in 3PC(H)O is significantly polarized (C: 62%, H: 38%) and indicates an acidic proton, which agrees with the 1H NMR data (see above). This can also be seen from the NBO partial charges for the protons, which are all near zero for the P–H protons (0.00–0.01e), but +0.22e for the H–C proton in 3PC(H)O.

The best Lewis formula found by NBO analysis for 3PC(H)O has a $-P=C(H)-O-$ unit, *i.e.* a P=C double bond and P–P, C–O and O–P single bonds, in accord with the X-ray data. Inspection of delocalization effects (hyperconjugation) within the NBO scheme indicate also partial double bond character along the CO unit. For example, the donor–acceptor interaction between a p-atomic-orbital-type lone pair of the oxygen with the $\pi^*(C-P)$ bond affords 34 kcal mol $^{-1}$ and accounts for the resonance $-P=C(H)-O- \leftrightarrow P(-)-C(H)=O(+)-$. This delocalization is also visible in the MO representations (Fig. S26†).

Finally, a short comment on the electronic situation of the protonated species 2^+ . Upon addition of the proton, a tri-coordinated phosphorus atom and a di-coordinated phosphorus atom form the now non-planar P_2N_2 four-membered heterocycle. According to NBO analysis, the best Lewis description is a heteroallylic system with the positive charge delocalized along the N=P–N moiety (Lewis formulae I–II), while hyperconjugative effects, as depicted in Lewis formulae III–IV, display also partly π bonding along the tri-coordinated P atom (Scheme 3). Lewis formula V represents a classical phosphonium ion. The entire resonance illustrates a closed shell system, and indeed, CASSCF(6,4) calculations indicate a diminished biradicaloid character (3%) compared to biradicaloid 1 with a biradicaloid character of 25%.



Scheme 3 Lewis representations of 2^+ according to NBO analysis.

Conclusion

Two different synthesis strategies, each starting from the phosphorus biradicaloid 1, $[P(\mu-N\text{Ter})]_2$, were introduced to generate and isolate *cis*-3HX, $[HP(\mu-N\text{Ter})_2PX]$ ($X = \text{CN}, \text{NCO}, \text{N}_3$, and NCS), representing the kinetically and thermodynamically most favored isomer. So it was demonstrated that biradicaloid 1 can be utilized to trap highly labile, pure hydrogen pseudo-halides such as HCN, HNCO, or even explosive HN_3 , affording *cis*-3HX, except for 3HNCS and 3HPCO. Addition of *in situ* generated HPCO and HNCS failed due to oligomerization yielding an unidentified mixture of products. Because it was impossible to trap HPCO and HNCS with biradicaloid 1, a two-step-method, utilizing the protonated cationic species, $[HP(\mu-N\text{Ter})_2P]^+$ (2^+), was used to prepare 3HNCS and 3HPCO. The latter species, however, was found to isomerize affording the formation of a novel [3.1.1]-hetero-propellane-type cage compound, an OC(H)P isomer (3PC(H)O) of the formal *cis*-HPCO adduct (3HPCO). Theoretical studies of the 3PC(H)O formation mechanism revealed an isomerization process starting from *cis*-3HPCO with a proton migration followed by a rotation enabling P–O bond formation in an overall exergonic reaction.

3HX species are the first four-membered P_2N_2 heterocycles with two differently substituted phosphorus(III) atoms of which one is carrying a (pseudo)halide and the other one a proton.

Protonated biradicaloid 2^+ represents a rare example of a fully characterized salt bearing a phosphonium cation.^{65–68} Structural data of the cation in 2 (2^+) agree well with those of azido- and chlorido-substituted heterocyclic phosphonium cations of the type $[X-P(\mu-N\text{Ter})_2P]^+$ ($X = \text{Cl}, \text{N}_3$).^{69–76}

Conflicts of interest

There are no conflicts to declare.

Acknowledgements

We thank the University of Rostock for access to the high-performance computing facilities, and especially Malte Willert for his assistance with the queueing system and software installations. Furthermore, we wish to thank the DFG (SCHU 1170/12-2) for financial support.

Notes and references

- 1 J. N. Brønsted, *Recl. Trav. Chim. Pays-Bas*, 1923, 42, 718–728.
- 2 H. Brand, A. Schulz and A. Villinger, *Z. Anorg. Allg. Chem.*, 2007, 633, 22–35.
- 3 L. Birckenbach and K. Kellermann, *Ber. Dtsch. Chem. Ges.*, 1925, 58, 786–794.
- 4 L. Birckenbach and K. Kellermann, *Ber. Dtsch. Chem. Ges.*, 1925, 58, 2377–2386.

- 5 E. Pfeil and P. Hoffmann, *Ber. Bunsen-Ges. Phys. Chem.*, 1963, 67, 229–235.
- 6 D. Hasenberg and L. D. Schmidt, *J. Catal.*, 1985, 91, 116–131.
- 7 J. Sauer, M. Bewersdorf, M. Koestner, M. Rinner and D. Wolf, in *Handbook of Heterogeneous Catalysis*, Wiley-VCH Verlag GmbH & Co. KGaA, Weinheim, Germany, 2008.
- 8 F. Cataldo, G. Patanè and G. Compagnini, *J. Macromol. Sci., Part A: Pure Appl. Chem.*, 2009, 46, 1039–1048.
- 9 T. Curtius, *Ber. Dtsch. Chem. Ges.*, 1890, 23, 3023–3033.
- 10 E. F. V. Scriven and K. Turnbull, *Chem. Rev.*, 1988, 88, 297–368.
- 11 I. C. Tornieporth-Oetting and T. M. Klapötke, *Angew. Chem., Int. Ed.*, 1995, 34, 511–520.
- 12 *Organic Azides: Syntheses and Applications*, ed. S. Bräse and K. Banert, John Wiley & Sons, Ltd, Chichester, UK, 2009.
- 13 R. Porret, *J. Chem. Phys.*, 1908, 258–307.
- 14 N. L. Vauquelin, *J. Chem. Phys.*, 1819, 50–87.
- 15 J. Liebig and F. Wöhler, *Ann. Chem. Pharm.*, 1830, 96, 369–400.
- 16 F. Wöhler and J. Liebig, *Ann. Pharm.*, 1838, 26, 241–336.
- 17 C. Weltzien, *Ann. Chem. Pharm.*, 1858, 107, 219–223.
- 18 F. Klages and G. Lukaszcyk, *Chem. Ber.*, 1963, 96, 2066–2069.
- 19 D. Beierl and A. Schmidt, *Chem. Ber.*, 1973, 106, 1637–1642.
- 20 A.-H. Ismail, A. Hamed, M. G. Hitzler, C. Troll and J. C. Jochims, *Synthesis*, 1995, 820–826.
- 21 S. Padmaja, V. Au and S. A. Madison, *J. Chem. Soc., Dalton Trans.*, 1999, 2933–2938.
- 22 G. Fischer, J. Geith, T. M. Klapötke and B. Krumm, *Z. Naturforsch.*, 2002, 57, 19–24.
- 23 W. Clasen, *J. Prakt. Chem.*, 1818, 96, 349.
- 24 S. A. Krupoder, G. G. Furin, G. G. Yakobson, G. N. Dolenko, L. N. Mazalov, A. S. Sultanov and I. I. Furley, *J. Fluorine Chem.*, 1983, 22, 305–344.
- 25 S. E. Bradforth, E. H. Kim, D. W. Arnold and D. M. Neumark, *J. Chem. Phys.*, 1993, 98, 800–810.
- 26 J. Nelson, R. Spratt and S. M. Nelson, *Inorg. Phys. Theor.*, 1970, 583.
- 27 *The Chemistry of Organophosphorus Compounds: Primary, Secondary and Tertiary Phosphines, Polyphosphines and Heterocyclic Organophosphorus (III) Compounds*, ed. F. R. Hartley and S. Patai, John Wiley & Sons, Inc., Hoboken, NJ, USA, 1990, vol. 1.
- 28 S. Arlt, J. Harloff, A. Schulz, A. Stoffers and A. Villinger, *Inorg. Chem.*, 2019, 58, 5305–5313.
- 29 S. Nuzzo, B. Twamley, J. A. Platts and R. J. Baker, *Chem. Commun.*, 2016, 52, 13296–13298.
- 30 I. S. Matveev, *J. Struct. Chem.*, 1974, 15, 131–134.
- 31 I. S. Matveev, *J. Struct. Chem.*, 1975, 16, 926–929.
- 32 G. Becker, W. Schwarz, N. Seidler and M. Westerhausen, *Z. Anorg. Allg. Chem.*, 1992, 612, 72–82.
- 33 K. Hübler and P. Schwerdtfeger, *Inorg. Chem.*, 1999, 38, 157–164.
- 34 C. Dimur, F. Pauzat, Y. Ellinger and G. Berthier, *Spectrochim. Acta, Part A*, 2001, 57, 859–873.
- 35 S. Thorwirth, V. Lattanzi and M. C. McCarthy, *J. Mol. Spectrosc.*, 2015, 310, 119–125.
- 36 A. R. Jupp and J. M. Goicoechea, *J. Am. Chem. Soc.*, 2013, 135, 19131–19134.
- 37 A. R. Jupp, G. Trott, É. Payen de la Garanderie, J. D. G. Holl, D. Carmichael and J. M. Goicoechea, *Chem. – Eur. J.*, 2015, 21, 8015–8018.
- 38 A. M. Tondreau, Z. Benkő, J. R. Harmer and H. Grützmacher, *Chem. Sci.*, 2014, 5, 1545.
- 39 A. Hinz, R. Labbow, C. Rennick, A. Schulz and J. M. Goicoechea, *Angew. Chem., Int. Ed.*, 2017, 56, 3911–3915.
- 40 K. Bläsing, J. Bresien, R. Labbow, D. Michalik, A. Schulz, M. Thomas and A. Villinger, *Angew. Chem., Int. Ed.*, 2019, 58, 6540–6544.
- 41 K. Bläsing, J. Bresien, R. Labbow, A. Schulz and A. Villinger, *Angew. Chem., Int. Ed.*, 2018, 57, 9170–9175.
- 42 T. Beweries, R. Kuzora, U. Rosenthal, A. Schulz and A. Villinger, *Angew. Chem., Int. Ed.*, 2011, 50, 8974–8978.
- 43 T. Stuyver, B. Chen, T. Zeng, P. Geerlings, F. De Proft and R. Hoffmann, *Chem. Rev.*, 2019, 119, 11291–11351.
- 44 W. W. Schoeller, *Eur. J. Inorg. Chem.*, 2019, 2019, 1495–1506.
- 45 A. Schulz, *Dalton Trans.*, 2018, 47, 12827–12837.
- 46 M. Abe, *Chem. Rev.*, 2013, 113, 7011–7088.
- 47 L. Salem and C. Rowland, *Angew. Chem., Int. Ed.*, 1972, 84, 86–106.
- 48 A. Hinz, R. Kuzora, U. Rosenthal, A. Schulz and A. Villinger, *Chem. – Eur. J.*, 2014, 20, 14659–14673.
- 49 G. Fuks, N. Saffon, L. Maron, G. Bertrand and D. Bourissou, *J. Am. Chem. Soc.*, 2009, 131, 13681–13689.
- 50 K. Takeuchi, M. Ichinohe and A. Sekiguchi, *J. Am. Chem. Soc.*, 2011, 133, 12478–12481.
- 51 X. Zhang, X. Chen, H. Zhai, S. Liu, C. Hu, L. L. Liu, S. Wang and Z. Li, *Dalton Trans.*, 2020, 49, 6384–6390.
- 52 P. Günther, R. Meyer and F. Müller-Skjöld, *Z. Physiol. Chem.*, 1935, 175, 154–169.
- 53 R. Labbow, D. Michalik, F. Reiß, A. Schulz and A. Villinger, *Angew. Chem., Int. Ed.*, 2016, 55, 7680–7684.
- 54 P. Jutzi, C. Müller, A. Stammer and H.-G. Stammer, *Organometallics*, 2000, 19, 1442–1444.
- 55 J. Harloff, A. Schulz, P. Stoer and A. Villinger, *Z. Anorg. Allg. Chem.*, 2019, 645, 835–839.
- 56 M. Jost, L. H. Finger, J. Sundermeyer and C. von Hänisch, *Chem. Commun.*, 2016, 52, 11646–11648.
- 57 D. Michalik, A. Schulz, A. Villinger and N. Weding, *Angew. Chem., Int. Ed.*, 2008, 47, 6465–6468.
- 58 B. W. Tattershall, *Polyhedron*, 1990, 9, 553–555.
- 59 F. Weinhold, C. R. Landis and E. D. Glendening, *Int. Rev. Phys. Chem.*, 2016, 35, 399–440.
- 60 E. D. Glendening, C. R. Landis and F. Weinhold, *J. Comput. Chem.*, 2013, 34, 1429–1437.
- 61 M. Mantina, A. C. Chamberlin, R. Valero, C. J. Cramer and D. G. Truhlar, *J. Phys. Chem.*, 2009, 113, 5806–5812.
- 62 P. Pyykkö and M. Atsumi, *Chem. – Eur. J.*, 2009, 15, 12770–12779.

- 63 P. Schwerdtfeger, L. J. Laakkonen and P. Pyykkö, *J. Chem. Phys.*, 1992, 96, 6807–6819.
- 64 C. Sousa-Silva, J. Tennyson and S. N. Yurchenko, *J. Chem. Phys.*, 2016, 145, 1–5.
- 65 T. Chivers and I. Manners, *Inorganic Rings and Polymers of the p-Block Elements*, Royal Society of Chemistry, 2009.
- 66 T. A. Engesser, M. R. Lichtenthaler, M. Schleep and I. Krossing, *Chem. Soc. Rev.*, 2016, 45, 789–899.
- 67 P. P. Power, *Chem. Rev.*, 2003, 103, 789–810.
- 68 G. He, O. Shynkaruk, M. W. Lui and E. Rivard, *Chem. Rev.*, 2014, 114, 7815–7880.
- 69 A. Schulz, A. Villinger and A. Westenkirchner, *Inorg. Chem.*, 2014, 53, 3183–3193.
- 70 A. Hinz, A. Schulz and A. Villinger, *Chem. Commun.*, 2016, 52, 6328–6331.
- 71 J. Bresien, L. Eickhoff, A. Schulz, T. Suhrbier and A. Villinger, *Chem. – Eur. J.*, 2019, 25, 16311–16319.
- 72 C. Hering-Junghans, M. Thomas, A. Villinger and A. Schulz, *Chem. – Eur. J.*, 2015, 21, 6713–6717.
- 73 C. Hering, A. Schulz and A. Villinger, *Angew. Chem.*, 2012, 124, 6345–6349.
- 74 J. Bresien, K. Faust, A. Schulz and A. Villinger, *Angew. Chem., Int. Ed.*, 2015, 54, 6926–6930.
- 75 F. Reiß, A. Schulz and A. Villinger, *Eur. J. Inorg. Chem.*, 2012, 2012, 261–271.
- 76 C. Hering, M. Hertrich, A. Schulz and A. Villinger, *Inorg. Chem.*, 2014, 53, 3880–3892.

7 Anhang

7.1 Weitere Publikationen

7.1.1 Heterocyclopentandiyls vs Heterocyclopenta-dienes: A Question of Silyl Group Migration

Henrik Beer, Jonas Bresien, Dirk Michalik, Anne-Kristin Rölke, Axel Schulz, Alexander Villinger, Ronald Wustrack

J. Org. Chem. **2020**, *85*, 14435–14445.

DOI: 10.1021/acs.joc.0c00460

Reprinted with permission from *J. Org. Chem.* 2020, 85, 22, 14435–14445. Copyright 2020 American Chemical Society.

Onlinelink: <https://doi.org/10.1021/acs.joc.0c00460>

Heterocyclopentenediyls vs Heterocyclopentadienes: A Question of Silyl Group Migration

Henrik Beer, Jonas Bresink,* Dirk Michalik, Anne-Kristin Rölke, Axel Schulz,* Alexander Villinger, and Ronald Wustrack

Cite This: *J. Org. Chem.* 2020, 85, 14435–14445

Read Online

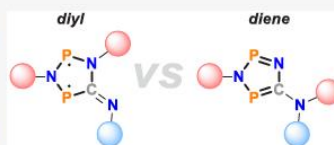
ACCESS |

Metrics & More

Article Recommendations

Supporting Information

ABSTRACT: The reaction of the singlet biradical $[P(\mu\text{-NHyp})]_2$ (Hyp = hypersilyl, $(\text{Me}_3\text{Si})_3\text{Si}$) with different isonitriles afforded a series of five-membered $\text{N}_2\text{P}_2\text{C}$ heterocycles. Depending on the steric bulk of the substituent at the isonitrile, migration of a Hyp group was observed, resulting in two structurally similar but electronically very different isomers. As evidenced by comprehensive spectroscopic and theoretical studies, the heterocyclopentadiene isomer may be regarded as a rather unreactive closed-shell singlet species with one localized $\text{N}=\text{P}$ and one $\text{C}=\text{P}$ double bond, whereas the heterocyclopentenediyl isomer represents an open-shell singlet biradical with interesting photochemical properties, such as photoisomerization under irradiation with red light to a [2.1.0]-housane-type species.



INTRODUCTION

Biradicals (sometimes also called “biradicaloids” if the interaction between the two radical sites is significant) are an interesting research topic for both theoretical and synthetic chemists, as they exhibit unusual electronic structures, intriguing properties, and high reactivity.^{1–11} They are therefore worthwhile targets for the study of structure–property relationships, but their isolation is a challenge due to their intrinsic instability.

The high reactivity of biradicals arises from their characteristic electronic structure, which comprises two electrons in two (nearly) degenerate orbitals.¹ Thus, the electrons are strongly correlated (i.e., nondynamically or “statically” correlated),¹² and multireference methods are needed to correctly describe the wave function of these systems.¹³ Depending on the magnitude and sign of the phenomenological Heisenberg exchange coupling constant $J = 1/2 \Delta E_{\text{ST}}$ (ΔE_{ST} = singlet–triplet energy gap),^{14,15} the two electrons can either be ferromagnetically ($J > 0$) or antiferromagnetically ($J < 0$) coupled,³ resulting in a triplet or singlet ground state, respectively. Solely in the borderline case $J \approx 0$, a “perfect” biradical is formed, that is, a molecule with two independent radical centers (a so-called “two-doublet species”),¹⁵ which for all intents and purposes behaves like a radical species.³ In all other cases, one should note that the terms “biradical” or “biradicaloid” can sometimes be misleading, since the reactivity especially of singlet species may differ fundamentally from the reactivity of radicals (doublet species).

Here, we shall be only concerned with singlet biradicals ($J < 0$). It is vital to understand that in singlet biradicals, the spin density is exactly zero at every point in space. Thus, the reactivity of a singlet biradical may be very different from that

of a doublet radical or triplet biradical. Due to the near degeneracy of their frontier orbitals, singlet biradicals can easily undergo (cyclo)addition reactions (vide infra),³ which typically involve the interaction between HOMO and LUMO of the reaction partners.

The presence of heteroatoms such as N and P in cyclic biradicals tends to stabilize the singlet ground state by increasing the antiferromagnetic coupling (and thus decreasing the biradical character), resulting in improved stability. Sterically demanding substituents further provide kinetic protection, rendering the isolation of such species possible (Scheme 1).^{16–31} In particular, our own group could demonstrate the versatile reactivity of the stable four-membered cyclic biradical $[P(\mu\text{-NR})]_2$ (1, R = Ter [2,6-dimesitylphenyl] or Hyp [tris(trimethylsilyl)silyl]), which is based solely on group 15 elements (Scheme 2).^{32–40}

Previously, we reported on the insertion of CO or isonitriles into one of the N–P bonds, leading to the formation of intensely colored, five-membered cyclic biradicals (e.g., heterocyclopentenediyls 2Ter; Scheme 3).^{34,35} Only recently we could demonstrate that these five-membered ring systems are light-sensitive molecular switches^{41–45} that can be utilized to control a chemical equilibrium by turning the biradical character on and off (Scheme 3, right).⁴⁶

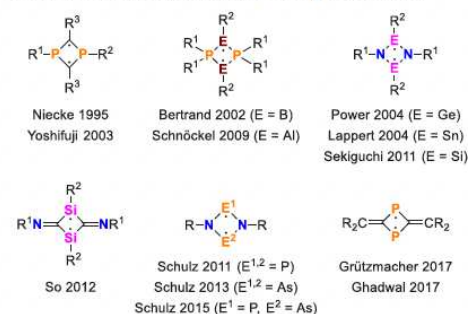
Special Issue: The New Golden Age of Organophosphorus Chemistry

Received: March 10, 2020

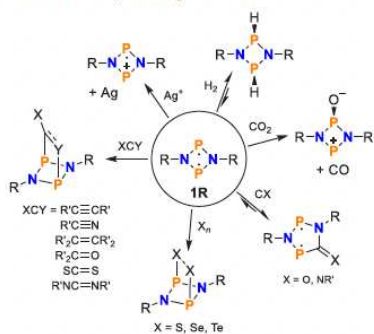
Published: May 12, 2020



Scheme 1. Some Examples of Open-Shell Singlet Biradicals Based on Four-Membered Main-Group Heterocycles

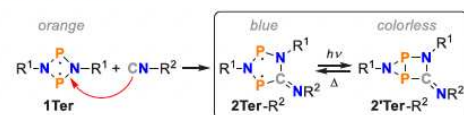


Scheme 2. Reactivity of Singlet Biradicals 1R[•]



^aThe reactions with S, Se, and multiple-bond systems (XCY) were reported for both R = Ter (1Ter) and R = Hyp (1Hyp). All other reactions were only investigated for the Ter system.

Scheme 3. Blue Heterocyclopentadienyls (2Ter-R²) Are Formed by Insertion of Isonitriles into an NP Bond of Biradical 1Ter[•]



^aUnder irradiation, they isomerize to the closed-shell housane-type species 2'Ter-R² (R¹ = Ter; R² = tBu, Dmp, Mes).

To explore the influence of the substituent R¹ at the N₂P₂ ring system on the reactivity, we started to investigate the analogous biradical system stabilized by Hyp groups (Hyp = (Me₃Si)₃Si, 1Hyp).³⁹ Substitution of Ter by Hyp resulted in a larger charge transfer of electron density from the substituent R into the P₂N₂ ring (Ter 0.4 vs Hyp 1.2 e) and hence to a higher reactivity in case of 1Hyp.³⁹ Of course, we were also interested in the possible utilization of this system as a molecular switch, so it was obvious to investigate its reactivity toward different isonitriles. However, contrary to aryl-based groups such as Ter, silyl groups such as Hyp can easily undergo

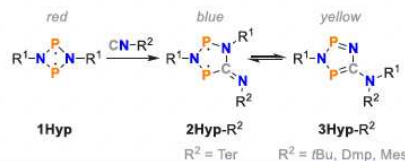
rearrangement reactions,^{47,48} which turned out to play an important role in the outcome of the reactions in case of 1Hyp.

RESULTS AND DISCUSSION

Reactions with Isonitriles. We started our investigation by treating the four-membered cyclic biradical [P(μ-NHyp)]₂ (1Hyp) with the isonitriles tBuNC, DmpNC (Dmp = 2,6-dimethylphenyl), MesNC (Mes = mesityl), and TerNC. To this end, a red solution of 1Hyp in *n*-hexane was reacted with the respective isonitrile at ambient temperature (25 °C), resulting in an immediate color change to yellow (tBu, Dmp, Mes) or dark blue (Ter). These different colors were somewhat unexpected, seeing that all reactions of the analogous biradical 1Ter with isonitriles had resulted in blue heterocyclopentadienyls (2Ter-R², Scheme 3).

Crystallization of the products and subsequent single-crystal X-ray diffraction (SC-XRD) analysis revealed that in case of tBuNC, DmpNC, and MesNC, one Hyp group had 1,3-migrated from one of the nitrogen atoms in the five-membered ring system to the exocyclic nitrogen atom of the former isonitrile group (3Hyp-R², Scheme 4), resulting in the

Scheme 4. Reaction of 1Hyp (R¹ = Hyp) with Isonitriles (CN-R²) Led to the Formation of Heterocyclopentadienyl 2Hyp-Ter or Heterocyclopentadienes 3Hyp-R², Depending on the Steric Bulk of the Substituent R²



formation of a heterocyclopentadiene rather than a heterocyclopentadienyl. Only in the case of TerNC, the expected product 2Hyp-Ter was formed, as evidenced by ³¹P NMR and UV-vis spectroscopy (vide infra).

Molecular and Electronic Structures. Due to their similar structures, the dienes 3Hyp-Dmp and 3Hyp-Mes formed isomorphous crystals (space group: C2/c). Their congener 3Hyp-tBu crystallized in the space group P2₁2₁2₁ with a distinctly different unit cell (cf. Supporting Information (SI)). Still, the molecular structures of all three derivatives are similar with respect to the nearly planar five-membered N₂P₂C ring system and exocyclic N atom, with one Hyp substituent being connected directly to the ring system and the other being linked to the exocyclic N atom which also bears the tBu, Dmp, or Mes group (Figure 1).

The structural parameters of the five-membered ring systems are nearly identical in all three cases (Table 1). All N–P, P–C, and C–N bond lengths range between typical single and double bonds (cf. Σ_{r_{av}}: N–P 1.82, N=P 1.62, P–C 1.86, P=C 1.69, C–N 1.46, C=N 1.27 Å),⁴⁹ indicating a delocalized π-bonding system.

Several attempts at crystallizing the blue Ter derivative 2Hyp-Ter remained unsuccessful, due to its instability. Nonetheless, it could be unequivocally identified by NMR and UV-vis spectroscopy (vide infra). In the following, we will thus compare the calculated structures (PBE-D3/def2-SVP)^{50–52} of the isomers 3Hyp-R² and 2Hyp-R² (R² = Dmp, Mes, tBu, Ter) to point out differences (Figure 2). First,

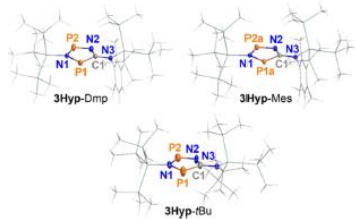


Figure 1. Molecular structures of 3Hyp-Dmp, 3Hyp-Mes, and 3Hyp-tBu in the crystal. Thermal ellipsoids set at 50% probability (123 K). Selected distances and angles can be found in Table 1.

Table 1. Selected Bond Lengths (Å) and Dihedral Angles (°) of 3Hyp-Dmp, 3Hyp-Mes, and 3Hyp-tBu in the Crystal

	3Hyp-Dmp	3Hyp-Mes	3Hyp-tBu
N1–P1	1.728(2)	1.726(1)	1.727(4)
N1–P2	1.663(2)	1.671(1)	1.670(4)
P1–C1	1.773(2)	1.777(2)	1.782(4)
P2–N2	1.617(2)	1.620(1)	1.612(4)
C1–N2	1.344(2)	1.345(2)	1.363(5)
C1–N3	1.376(2)	1.377(2)	1.371(5)
N1–P1–P2–N2	−179.8(1)	−179.6(1)	−179.0(3)
N1–P1–C1–N3	−179.0(1)	−178.1(1)	−179.2(4)

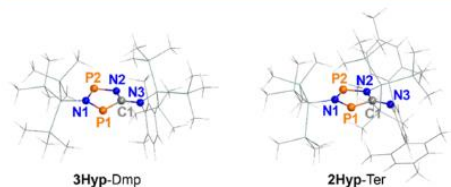


Figure 2. Calculated molecular structures of the experimentally observed species 3Hyp-Dmp and 2Hyp-Ter (PBE-D3/def2-SVP; cf. Tables S13 and S14).

it is worth noting that the calculated and experimental structures of 3Hyp-R² (R² = Dmp, Mes, tBu) are in reasonable agreement (mean difference in N–P/N–C/P–C bond lengths: 0.021 Å). When comparing the two sets of computed structures of 3Hyp-R² and 2Hyp-R², it becomes evident that in the case of 2Hyp-R², both Hyp groups are attached to the ring system (N1, N2), as opposed to 3Hyp-R², where one Hyp substituent is connected to the exocyclic N3 atom. Furthermore, the P1–C1 (av. 1.84 Å), P2–N2 (av. 1.71 Å), and C1–N2 (av. 1.41 Å) bond lengths are significantly longer in 2Hyp-R², now more in the range of polarized single bonds, whereas the C1–N3 bonds are shortened to an average of 1.30 Å, which corresponds to nearly isolated C=N double bonds. Thus, the bond lengths of both 2Hyp-R² and 3Hyp-R² are in nice agreement with the Lewis depictions in Scheme 4, indicating a rather different bonding situation in both species.

To compare the bonding situation in the cyclopentenediyl (2Hyp-R²) and cyclopentadiene derivatives (3Hyp-R²), calculations with the model systems 2SiH₃-Me and 3SiH₃-Me were performed. The calculated structural parameters of these models compare well with those of 2Hyp-R² and 3Hyp-R² (SI). CASSCF(8,6)^{53–61} computations correlating all π

electrons were performed to investigate the biradical character of both isomers (Figure 3). The calculations indicate that the

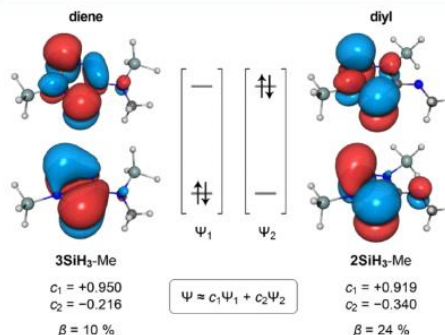


Figure 3. Frontier orbitals of the cyclopentadiene 3SiH₃-Me and cyclopentenediyl 2SiH₃-Me (CAS(8,6)/def2-TZVP//PBE-D3/def2-SVP, isovalue = 0.03). Only the largest contributions to the wave function are shown. For a depiction of all active orbitals, please see SI, p. S45f.

wave functions of both isomers have significant contributions from at least two determinants, the first one being the hypothetical closed-shell configuration, and the second one being the double substitution of two electrons from the HOMO into the LUMO, meaning that the two frontier orbitals are strongly correlated. However, the coefficient of the second determinant is significantly higher in the case of the cyclopentenediyl 2SiH₃-Me, resulting in a larger biradical character. The quantity $\beta = 2c_2^2/(c_1^2 + c_2^2)$ was proposed to estimate the biradical character⁶² and amounts to 24% for 2SiH₃-Me, which compares nicely with similar singlet biradicals such as 2Ter-R² (27%),⁴⁶ 1Ter (27%),⁶³ or 1Hyp (21%).³⁹ The biradical character of the cyclopentadiene 3SiH₃-Me ($\beta = 10\%$) is significantly smaller and at the edge of what might still be regarded as a singlet biradical.^{62,64} (For example, benzene has been attributed 5–10% biradical character,^{65,66} in accordance with our own computations, cf. SI.)

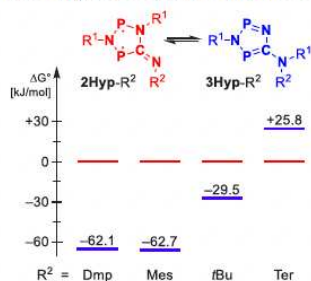
Moreover, the CAS orbitals indicate that the HOMO of 3SiH₃-Me contributes to the P1–C1 and P2–N2 double-bond character (the LUMO being the corresponding antibonding orbital), whereas the HOMO of 2SiH₃-Me is mainly localized at the P atoms, forming a π -type antibond between the two P atoms (and thus describing the “radical sites” at P in conjunction with the partly occupied, transannularly bonding LUMO, cf. Figure 3). In line with these considerations, NRT⁶⁷ analyses of the DFT as well as CAS densities identified the diyl and diene Lewis resonance formulas as the most important contributions to 2SiH₃-Me and 3SiH₃-Me, respectively (Scheme 5). Note that in the NRT formalism, the “biradical” structures do not represent the multireference character of the wave function, though, but merely imply that the electrons in the HOMO are rather localized in a π -type antibond between the two P atoms. As such, it gives qualitative information about the localization of the radical sites but does not provide a measure of the biradical character!

Why, now, do we observe the formation of the biradical 2Hyp-R² only in case of the Ter substituent, but formation of

Scheme 5. NRT Analyses of 2SiH₃-Me and 3SiH₃-Me^a

^aR¹ = SiH₃, R² = Me; PBE-D3/def2-SVP, delocalization threshold: 50 kcal/mol; please refer to the SI for the results using the CAS densities. Note that the “biradical” structures merely give information about the localization of the radical sites but not about the biradical character of the system!

the diene 3Hyp-R² in all other cases? To investigate this matter, comprehensive computations covering all derivatives of 2Hyp-R² and 3Hyp-R² (R² = *t*Bu, Dmp, Mes, Ter) were performed (see SI for a complete set of structures). At the DLPNO-CCSD(T)^{68–70}/def2-TZVP//PBE-D3/def2-SVP level of theory, it is apparent that the diene 3Hyp-R² is the thermodynamically favored isomer for all substituents R² except Ter (Scheme 6). This is easily understood in terms of

Scheme 6. Relative Gibbs Free Energies of Isomerization of 2Hyp-R² to 3Hyp-R² for Different Substituents R² (DLPNO-CCSD(T)/def2-TZVP//PBE-D3/def2-SVP)

large Pauli repulsion between the sterically demanding Hyp and Ter groups in the diene 3Hyp-R², where these two substituents are connected to the same N atom. In agreement with this consideration, the diene 3Hyp-*t*Bu is also less stabilized than the derivatives 3Hyp-Dmp and 3Hyp-Mes, whose aromatic substituents have the smallest steric demand due to their rather flat structure (see the SI for buried volumes⁷¹ of all four substituents). Thus, the equilibrium between the diyl 2Hyp-R² and diene 3Hyp-R² formally depends on the steric demand of the substituent R².

Spectroscopic Properties. The different electronic structures of the derivatives of 2Hyp-R² and 3Hyp-R² could most easily be proven experimentally by UV–vis spectroscopy (cf. SI, p S30). While the biradical 2Hyp-Ter showed broad absorption bands in the range of 500–680 nm (cf. 2Ter-Dmp: $\lambda_{\text{max}} = 643$ nm), the dienes 3Hyp-Dmp, 3Hyp-Mes, and 3Hyp-*t*Bu could be characterized by a single absorption maximum at 399–433 nm. This is in agreement with the calculated

biradical character (which depends, inter alia, on the HOMO–LUMO gap) and also corresponds to calculated values (TD-DFT PBE-D3/def2-TZVP, 2Hyp-Ter 635 and 562, 3Hyp-Dmp 494, 3Hyp-Mes 494, 3Hyp-*t*Bu 516 nm).

In the ³¹P NMR spectrum, diyl (2Hyp-R²) and diene (3Hyp-R²) are most readily distinguished by the *J*_{PP} coupling constant. Calculations for all isomers of 2Hyp-R² and 3Hyp-R² (R² = Dmp, Mes, *t*Bu, Ter; cf. SI) predicted rather small coupling constants (10–17 Hz) for the dienes 3Hyp-R², whereas the diyls 2Hyp-R² were predicted to have substantially larger coupling constants (76–93 Hz). This could be verified experimentally: Only 2Hyp-Ter displayed a large coupling constant of 118 Hz (calcd 93 Hz), while the other three species had small coupling constants of 10–15 Hz (calcd 10–13 Hz), in accordance with their diene character. While theory and experiment also agreed very nicely in case of the ³¹P NMR shifts, these were not suited to distinguish between diyl and diene, as they were quite similar for all species (Table 2).

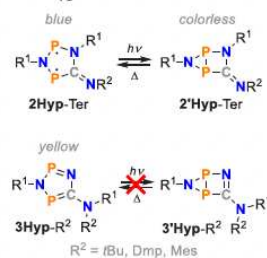
Table 2. Experimental ³¹P NMR Data of 2Hyp-R² and 3Hyp-R^{2a}

	$\delta(\text{P}_A)$ [ppm]	$\delta(\text{P}_B)$ [ppm]	<i>J</i> _{PP} [Hz]	
diyl	2Hyp-Dmp	– (211.8)	– (257.8)	– (79)
	2Hyp-Mes	– (213.6)	– (256.4)	– (79)
	2Hyp- <i>t</i> Bu	– (176.5)	– (245.5)	– (76)
	2Hyp-Ter	211.7 (222.7)	275.1 (249.5)	118 (93)
diene	3Hyp-Dmp	209.0 (203.7)	297.3 (277.1)	15 (10)
	3Hyp-Mes	209.1 (204.4)	297.5 (278.0)	10 (10)
	3Hyp- <i>t</i> Bu	230.7 (191.6)	281.9 (248.9)	15 (13)
	3Hyp-Ter	– (226.3)	– (253.6)	– (17)

^aCalculated data given in brackets (GIAO method,^{72–76} PBE-D3/def2-SVP).

Behavior under Irradiation. When a solution of the biradical 2Hyp-Ter was irradiated with red light (638 nm), it photoisomerized to the corresponding housane-type species 2'Hyp-Ter (Scheme 7). In the ³¹P NMR spectrum, the

Scheme 7. While the Diyl 2Hyp-Ter (R¹ = Hyp) Could Be Photoisomerized to the Housane-Type Species 2'Hyp-Ter in Solution, the Same Is Not True of the Dienes 3Hyp-Dmp, 3Hyp-Mes, and 3Hyp-*t*Bu



quantitative isomerization was evidenced by a large upfield shift of the two resonances to –128.1 and –69.2 ppm, respectively. In contrast, the dienes 3Hyp-Dmp, 3Hyp-Mes, and 3Hyp-*t*Bu could not be isomerized under irradiation, irrespective of the wavelength of the light (638, 520, and 445 nm). Even at –150 °C, we did not observe a change in the crystal structure when the samples were irradiated with white

light (in contrast to the previously published molecular switch 2Ter-Dmp, whose crystals disintegrated under light due to isomerization to the housane 2'Ter-Dmp).⁴⁶ Only in case of 3Hyp-Mes, a B layer containing approximately 2% of the housane 3'Hyp-Mes could be refined in the structural model, indicating either a very low quantum yield of the photoisomerization or a very fast thermal reverse reaction even at very low temperatures.

The photoproduct 2'Hyp-Ter isomerized back to the biradical 2Hyp-Ter under thermal regime. The reaction could be traced by in situ ³¹P NMR spectroscopy at different temperatures (Figure 4). The kinetic data allowed us to

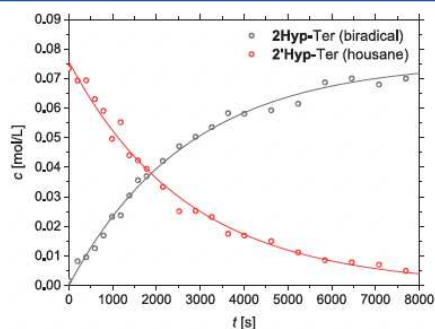
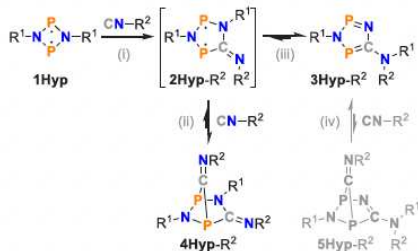


Figure 4. Thermal equilibration of the housane 2'Hyp-Ter at 25 °C. For a full set of data at different temperatures, please refer to the SI, p. S36ff.

estimate the activation barrier of the reaction, which amounts to $\Delta G^\ddagger = 93 \pm 2$ kJ/mol at 25 °C (cf. S1). This compares to the activation barriers of thermal equilibration of the housanes 2'Ter-Dmp (88 ± 4 kJ/mol) and 2'Ter-tBu (ca. 94 kJ/mol).⁴⁶

Adduct Formation with a Second Equivalent of Isonitrile. The tBu derivative 3Hyp-tBu proved to be most difficult to isolate. While 3Hyp-Dmp and 3Hyp-Mes could be isolated in 70–90% yield, only a few crystals of 3Hyp-tBu could be obtained. This was due to the formation of an adduct with a second equivalent of tBuNC (cf. Scheme 8), as evidenced by variable-temperature NMR spectroscopy. When 1Hyp was treated with 1 equiv of tBuNC at low temperatures,

Scheme 8. Trapping of the Biradical 2Hyp-R² (R¹ = Hyp) with a Second Equivalent of Isonitrile^a



^aThe adduct 4Hyp-tBu could be detected spectroscopically. The hypothetical adduct 5Hyp-R² is in gray.

exclusive formation of a new AX spin system (4Hyp-tBu) in a 1:1 ratio with the starting material was observed in the ³¹P NMR spectrum (Figure 5). Upon warming, the intensity of the

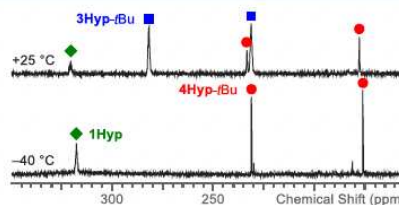


Figure 5. In situ ³¹P NMR spectra of the reaction of 1Hyp with tBuNC at -40 and 25 °C. For spectra at additional temperatures, please see Figure S15.

new AX spin system decreased, while formation of yet another AX spin system was observed, which could be attributed to the diene 3Hyp-tBu. At ambient temperature, the diene 3Hyp-tBu was the main product, although traces of the starting material 1Hyp as well as the intermediate 4Hyp-tBu were still present (10:1:3 ratio).

DFT and ab initio calculations indicated that the intermediate 4Hyp-tBu was in fact the tBuNC adduct of the transient biradical 2Hyp-tBu; that is, the unstable diyl 2Hyp-tBu could be trapped by adduct formation with tBuNC (Scheme 8; for calcd NMR data, please see Table S6). Upon warming, the adduct 4Hyp-tBu redissociated owing to the gain in entropy, and the transient biradical 2Hyp-tBu isomerized to the more stable diene 3Hyp-tBu. The hypothetical adduct 5Hyp-tBu was not observed (vide infra).

In case of the dienes 3Hyp-Dmp and 3Hyp-Mes, no adduct formation was observed. The same holds true for the stable diyl 2Hyp-Ter. All these observations nicely agree with calculated thermodynamic data (DLPNO-CCSD(T)/def2-TZVP//PBE-D3/def2-SVP) for the reactions shown in Scheme 8. While reaction (i) is exergonic for all derivatives, reaction (ii), that is, the adduct formation step, is strongly exergonic solely in case of the tBu derivative ($\Delta G^\circ = -40.5$ kJ/mol; cf. Table 3). As mentioned above, reaction (iii) is exergonic for R² = Dmp, Mes, and tBu. The lowest energy gain is predicted for the tBu derivative ($\Delta G^\circ = -29.5$ kJ/mol), in line with the observed equilibrium between the adduct 4Hyp-tBu and the diene 3Hyp-tBu at ambient temperature. Reaction (iv), that is, the formation of the hypothetical isonitrile adduct

Table 3. Gibbs Free Energies ΔG° ($c^\circ = 1$ mol/L, 298 K) for Reactions (i)–(iv) in kJ/mol (DLPNO-CCSD(T)/def2-TZVP//PBE-D3/def2-SVP, see also SI)^a

R ²	reaction			
	(i)	(ii)	(iii)	(iv)
Dmp	-63.5	-8.6	-62.1	+59.8
Mes	-58.8	-2.3	-62.7	+71.0
tBu	-15.2	-40.5	-29.5	+52.2
Ter	-47.4	+168.4 ^b	+25.8	+137.6 ^b

^aExperimentally observed reaction pathways are printed in italics, and values printed in bold refer to those reactions whose products were detected experimentally. ^b ΔG° based on DLPNO-CCSD energy (the triples correction was not computed due to the size of the system).

5Hyp-R², is strongly endergonic for all derivatives, and it was not observed. This is yet another indication for the low biradical character of the dienes 3Hyp-R².

CONCLUSION

In conclusion, we could demonstrate that the Hyp substituent introduced a new aspect into the chemistry of diphosphadiazanediyls (IR), namely the migration of a Hyp group depending on the stabilization and steric encumbrance of the product species. Accordingly, treatment of 1Hyp with different isonitriles either led to the formation of a five-membered biradical 2Hyp-Ter (in analogy to known 2Ter-R² derivatives) or afforded heterocyclopentadienes (3Hyp-R²), which to the best of our knowledge represent the first isolated derivatives of 3H-1,3-diaza-2,4-diphosphole.

In our study, the diyl 2Hyp-Ter displayed typical biradical reactivity, such as activation of small molecules or photoisomerization upon irradiation with visible light. In contrast, despite its similar molecular structure, the diene 3Hyp-R² was rather unreactive, as it represented the thermodynamically favored isomer for smaller substituents at the isonitrile. Comprehensive computations were carried out to understand the differences in structure, bonding, and reactivity between both isomers, revealing that the biradical character of the diyl 2Hyp-Ter is comparable to related compounds ($\beta = 24\%$), whereas the diene 3Hyp-R² does not possess a significant biradical character ($\beta = 10\%$). Experimental techniques could be applied to verify the conclusions drawn from the theoretical models.

The isomerization of the diyl 2Hyp-R² to the diene 3Hyp-R² demonstrates that steric bulk alone is not necessarily sufficient to stabilize biradicals and that apparently small structural changes can lead to quite a different electronic situation. Consequently, these results will help us to devise new, stable singlet biradicals and molecular switches in the future.

EXPERIMENTAL SECTION

General Information. If not stated otherwise, all manipulations were carried out under oxygen- and moisture-free conditions under an inert atmosphere of argon using standard Schlenk or Drybox techniques.

Solvents were obtained from commercial sources. CH₂Cl₂ was purified according to a literature procedure,⁷⁷ dried over P₄O₁₀, and stored over CaH₂ and was freshly distilled and degassed (by at least three freeze–pump–thaw cycles) prior to use. *n*-Hexane was dried over Na/benzophenone/tetraglyme. CD₂Cl₂ was dried over P₄O₁₀ and stored over CaH₂. C₆D₆ was dried over Na. THF-*d*₈ was dried over Na and stored over molecular sieves (4 Å) after distillation. All solvents were freshly distilled prior to use.

Reactants and starting materials were either purchased or synthesized according to literature procedures. NEt₃ (Sigma-Aldrich, 99%) was dried over Na and distilled. Mg turnings (abcr, 99.8%, for Grignards) were activated by stirring for several days under argon atmosphere using a glass-coated magnetic stir bar. POCl₃ (old stock) was dried over P₄O₁₀, distilled and degassed. DmpNH₂ (Acros, 99%) was distilled. [NEt₃]Br (Fluka, 98%), [PhNEt₃]Br (Sigma-Aldrich, 98%), and NaOH (Grüssing, 99%) were used as received. TerNH₂^{78,79} and [CIP(μ-NHyp)]₂⁸⁰ were synthesized according to literature procedures.

NMR Spectra. Spectra were obtained on Bruker spectrometers AVANCE 250, 300, or 500 and were referenced internally to the signals of deuterated solvents (¹³C: CD₂Cl₂ δ_{ref} = 54.0 ppm, C₆D₆ δ_{ref} = 128.4 ppm, THF-*d*₈ δ_{ref1} = 25.4 ppm, δ_{ref2} = 67.6 ppm), to the signals of protic species in the deuterated solvents (¹H: CHDCl₂ δ_{ref} = 5.32 ppm, C₆HD₅ δ_{ref} = 7.16 ppm, THF-*d*₇ δ_{ref1} = 1.73 ppm, δ_{ref2} =

3.58 ppm), or externally (³¹P: 85% H₃PO₄ δ_{ref} = 0 ppm). All measurements were carried out at ambient temperature (25 °C) unless denoted otherwise. NMR signals were assigned using experimental data (e.g., chemical shifts, coupling constants, integrals where applicable) in conjunction with computed NMR data (GIAO method, cf. Computational Details).

NMR Spectra under Irradiation. Spectra were recorded by means of an adopted setup previously published by the Gschwind group,⁸¹ who used a fiber-coupled light emitting diode (LED) to direct light into the NMR spectrometer. Instead of LEDs, a laser diode (Oclaro HL63193MG, 638 nm, 700 mW) was used. To ensure inert conditions, all samples were prepared in a glovebox, and the tubes were sealed with custom-made PTFE caps as well as 2–3 layers of PTFE tape.⁴⁶

IR Spectra. Spectra of crystalline samples were recorded on a Nicolet 380 FT-IR spectrometer equipped with a Smart Orbit ATR unit or a Bruker Alpha II FT-IR spectrometer with an ATR unit at ambient temperature (25 °C).

Raman Spectra. Spectra of crystalline samples were recorded using a LabRAM HR 800 Horiba Jobin YVON Raman spectrometer equipped with an Olympus BX41 microscope with variable lenses. The samples were excited by a red laser (633 nm, 17 mW, air-cooled HeNe laser) or blue laser (473 nm, 20 mW, air-cooled solid-state laser). All measurements were carried out at ambient temperature (25 °C) unless stated otherwise.

Elemental Analyses. Results were obtained using an Elementar vario Micro cube CHNS analyzer or a LECO TruSpec Micro CHNS analyzer.

Melting Points. Results (uncorrected) were determined using a Stanford Research Systems EZ Melt at a heating rate of 20 °C/min.

Mass Spectra. Spectra were recorded on a Thermo Electron MAT 95-XP sector field mass spectrometer using crystalline samples.

UV–vis Spectra. Spectra were acquired on a PerkinElmer Lambda 19 UV–vis spectrometer.

X-ray Structure Determination. Single crystals of 3Hyp-Dmp, 3Hyp-Mes, and 3Hyp-tBu were obtained by crystallization from *n*-hexane at –40 °C. X-ray quality crystals were selected in Fomblin YR-1800 perfluoro-ether (Alfa Aesar) at ambient temperature (25 °C). The samples were cooled to 123(2) K or 298(2) K during measurements. The data were collected on a Bruker D8 Quest diffractometer or a Bruker Kappa Apex II diffractometer using Mo K α radiation ($\lambda = 0.71073$ Å). The structures were solved by iterative methods (SHELXT)⁸² and refined by full matrix least-squares procedures (SHELXL).⁸³ Semiempirical absorption corrections were applied (SADABS).⁸⁴ All non-hydrogen atoms were refined anisotropically, and hydrogen atoms were included in the refinement at calculated positions using a riding model.

Computational Details. Computations were carried out using Gaussian 09⁸⁵ or ORCA 4.1.1⁸⁶ and the standalone version of NBO 6.0.^{87–92} Structure optimizations were performed using the pure DFT functional PBE^{93,94} in conjunction with Grimme's dispersion correction D3(B)^{93,94} and the def2-SVP basis set⁹⁵ (notation PBE-D3/def2-SVP). All structures were fully optimized and confirmed as minima by frequency analyses. The validity of the single-determinantal Kohn–Sham DFT approach was verified by stability analyses of the KS wave functions. Chemical shifts and coupling constants were derived by the GIAO method.^{72–76} The calculated absolute shifts ($\sigma_{calc,X}$) were referenced to the experimental absolute shift of 85% H₃PO₄ in the gas phase ($\sigma_{ref1} = 328.35$ ppm),⁹⁵ using PH₃ ($\sigma_{ref2} = 594.45$ ppm) as a secondary standard.⁹⁶

$$\begin{aligned}\delta_{calc,X} &= (\sigma_{ref,1} - \sigma_{ref,2}) - (\sigma_{calc,X} - \sigma_{calc,PH_3}) \\ &= \sigma_{calc,PH_3} - \sigma_{calc,X} - 266.1 \text{ ppm}\end{aligned}$$

At the PBE-D3/def2-SVP level of theory, σ_{calc,PH_3} amounts to +617.15 ppm. Thermal corrections to the total energy were computed at the PBE-D3/def2-SVP level of theory. More accurate estimates of the electronic energy were obtained by single-point DLPNO-CCSD(T)/def2-TZVP or DLPNO-CCSD/def2-TZVP^{68–70} computations (nota-

tion DLPNO-CCSD(T)/def2-TZVP//PBE-D3/def2-SVP or DLPNO-CCSD/def2-TZVP//PBE-D3/def2-SVP. The T_1 diagnostic was evaluated in each case to ensure reliable results. (Empirically, CCSD(T) results with T_1 values smaller than 0.02 are considered reliable.)¹³ To investigate the electronic structures of the diyls **2Hyp** and dienes **3Hyp** in more detail, the model systems **2SiH₃-Me** and **3SiH₃-Me** were used. CASSCF(8,6)/def2-TZVP^{53–61} computations including all π -type electrons in the active space were performed to investigate the biradical character. NRT analyses⁶⁷ of the DFT and CAS densities were computed to localize the electrons and obtain Lewis-type descriptions of the bonding patterns. It should be emphasized that all computations were carried out for single, isolated gas phase molecules. There may be significant differences between gas phase, solution, and solid state.

Syntheses. DmpNC. DmpNC was synthesized according to a modified literature procedure.³⁴ The synthesis was carried out under non-inert conditions. In a three-necked flask equipped with a reflux condenser and a dropping funnel, DmpNH₂ (3.36 g, 29.7 mmol), chloroform (3.55 g, 29.7 mmol), and [NEt₄]Br (90 mg, 0.43 mmol) are dissolved in CH₂Cl₂ (30 mL). Under vigorous stirring, a solution of NaOH (30 g, 0.75 mol) in water (30 mL) is added slowly over a period of 15 min. The mixture is stirred for 18 h without an external heat source, but with the reflux condenser turned on as to prevent evaporation of the organic solvents due to the exothermic reaction. Afterward, the reaction mixture is diluted with water (200 mL). The aqueous phase is extracted three times with CH₂Cl₂ (50 mL). The solvents of the combined organic phases are evaporated, and the solid residue is sublimed three times (1×10^{-3} mbar, 70 °C, oil bath). A final sublimation at ambient temperature (1×10^{-3} mbar, 25 °C) yields colorless crystals of the product (yield: 2.05 g, 15.6 mmol, 53%). C₈H₈N (131.18 g/mol). Mp. 77 °C. Anal. calcd for C₈H₈N: C, 82.41; H, 6.92; N, 10.68. Found: C, 82.75; H, 6.44; N, 10.90. ¹H NMR (CD₂Cl₂, 300.1 MHz): δ 2.41 (s, 6H), 7.12 (d, 1H, $J = 8$ Hz), 7.19 (t, 2H, $J = 7$ Hz). ¹³C{¹H} NMR (CD₂Cl₂, 75.5 MHz): δ 19.1, 128.1, 129.0, 135.3, 168.7. IR (ATR, 32 scans, cm⁻¹): $\tilde{\nu} = 3233$ (w), 3184 (w), 2984 (w), 2947 (w), 2920 (w), 2881 (w), 2739 (w), 2120 (m), 2085 (w), 1949 (w), 1879 (w), 1811 (w), 1655 (m), 1591 (w), 1525 (w), 1490 (w), 1471 (m), 1440 (m), 1379 (m), 1302 (w), 1282 (w), 1228 (w), 1170 (m), 1084 (m), 1036 (m), 991 (w), 977 (w), 923 (w), 800 (w), 775 (vs), 721 (m), 637 (w), 548 (w). Raman (633 nm, 20 s, 20 scans, cm⁻¹): $\tilde{\nu} = 3071$ (3), 3043 (3), 2985 (3), 2947 (4), 2919 (10), 2911 (9), 2885 (3), 2882 (3), 2873 (3), 2863 (4), 2740 (3), 2735 (3), 2119 (7), 1600 (1), 1590 (2), 1471 (1), 1464 (1), 1437 (1), 1423 (1), 1408 (1), 1383 (1), 1373 (1), 1264 (1), 1254 (2), 1171 (2), 1092 (1), 1078 (2), 990 (1), 796 (1), 779 (1), 727 (1), 719 (1), 636 (8), 565 (1), 542 (1), 518 (1), 505 (1), 491 (1), 458 (1), 361 (4), 284 (1), 240 (2). MS (GC-MS) m/z (%): 103 (30) [C₈H₈N]⁺, 116 (62) [C₈H₈N]⁺, 130 (100) [C₈H₈N]⁺, 131 (68) [M]⁺.

MesNC. MesNC was synthesized according to a modified literature procedure.³⁴ The synthesis was carried out under non-inert conditions. In a three-necked flask equipped with a reflux condenser and a dropping funnel, MesNH₂ (4.39 g, 32.4 mmol), chloroform (3.85 g, 33.0 mmol), and [PhNEt₃]Cl (0.18 mg, 0.8 mmol) are dissolved in CH₂Cl₂ (50 mL). Under vigorous stirring, a solution of NaOH (30 g, 0.75 mol) in water (30 mL) is added slowly over a period of 15 min. The mixture is stirred for 22 h without external heat source, but with the reflux condenser turned on as to prevent evaporation of the organic solvents due to the exothermic reaction. Afterward, the reaction mixture is diluted with water (200 mL). The aqueous phase is extracted three times with CH₂Cl₂ (50 mL). The solvents of the combined organic phases are evaporated, and the solid residue is sublimed (1×10^{-3} mbar, 60–70 °C, oil bath). The product was then crystallized from dry CH₂Cl₂ (yield: 2.50 g, 17.22 mmol, 53%). C₁₀H₁₁N (145.20 g/mol). Mp. 42 °C. Anal. calcd for C₁₀H₁₁N: C, 82.72; H, 7.64; N, 9.65. Found: C, 82.47; H, 7.51; N, 9.77. ¹H NMR (CD₂Cl₂, 250.1 MHz): δ 2.29 (s, 6H), 2.36 (s, 3H), 6.92 (s, 2H). ¹³C{¹H} NMR (CD₂Cl₂, 250.1 MHz): δ 18.9, 21.2, 128.7, 129.0, 134.9, 139.3, 168.0. IR (ATR, 25 °C, 32 scans, cm⁻¹): $\tilde{\nu} = 3031$ (w), 2976 (w), 2947 (w), 2916 (w), 2854 (w), 2739 (w), 2256 (w),

2116 (vs), 2083 (w), 1935 (w), 1902 (w), 1789 (w), 1754 (w), 1605 (m), 1556 (w), 1477 (m), 1445 (m), 1434 (m), 1377 (m), 1311 (w), 1284 (w), 1255 (w), 1199 (m), 1146 (w), 1127 (w), 1039 (m), 1020 (w), 956 (w), 944 (w), 931 (w), 896 (w), 859 (s), 816 (w), 719 (m), 707 (w), 666 (w), 598 (w), 573 (m), 503 (w), 422 (w). Raman (473 nm, 4 s, 20 scans, cm⁻¹): $\tilde{\nu} = 3033$ (1), 3021 (1), 2976 (1), 2922 (2), 2861 (1), 2737 (1), 2114 (10), 2080 (1), 1606 (3), 1476 (1), 1438 (1), 1418 (1), 1386 (1), 1307 (2), 1196 (1), 1143 (1), 1124 (1), 953 (1), 703 (1), 595 (1), 576 (2), 499 (1), 422 (1), 283 (1). MS (GC-MS) m/z (%): 103 (17) [C₈H₈N]⁺, 115 (12) [C₈H₈N]⁺, 130 (100) [C₈H₈N]⁺, 145 (50) [M]⁺.

TerN(H)CHO. Terphenyl formamide was synthesized according to a modified literature procedure.³⁷ The synthesis was carried out under non-inert conditions. TerNH₂ (1.698 g, 5.150 mmol), ZnCl₂ (0.627 g, 4.601 mmol), and formic acid (4.063 g, 88.27) are stored for 86 h at 60 °C (drying oven). The crystals are washed two times with water, and the aqueous phase is discarded. The product is dissolved in CH₂Cl₂ (20 mL) and separated from impurities and water residues in a separating funnel. The organic solvent is evaporated, and the solid is dried in vacuo (1×10^{-3} mbar). Yield: 1.320 g, 4.001 mmol, 80%. C₂₃H₂₂NO (357.50 g/mol). Mp. 305 °C. Anal. calcd for C₂₃H₂₂NO: C, 83.69; H, 7.61; N, 3.92. Found: C, 83.40; H, 7.66; N, 3.82. ¹H NMR (CD₂Cl₂, 250.1 MHz): δ 2.01 (s, 12H), 2.32 (s, 6H), 6.47 (br s, 1H), 6.98 (s, 4H), 7.13 (d, 2H, $J = 7.4$ Hz), 7.35 (t, 1H, $J = 7.4$ Hz), 7.58 (d, 1H, $J = 10$ Hz). ¹³C{¹H} NMR (CD₂Cl₂, 62.9 MHz): δ 20.7, 21.4, 126.6, 128.5, 128.9, 129.2, 130.8, 132.9, 134.4, 135.3, 136.4, 138.3, 162.6. IR (ATR, 25 °C, 32 scans, cm⁻¹): $\tilde{\nu} = 3358$ (w), 2972 (w), 2937 (w), 2912 (m), 2855 (w), 2733 (w), 1678 (s), 1612 (m), 1455 (m), 1408 (m), 1377 (m), 1272 (s), 1239 (s), 1206 (m), 1177 (m), 1101 (m), 1070 (m), 1033 (m), 1012 (m), 983 (m), 888 (m), 857 (s), 812 (s), 765 (m), 742 (m), 688 (m), 629 (m), 585 (m), 575 (m), 552 (m), 507 (m), 453 (m). Raman (633 nm, 10 s, 20 scans, cm⁻¹): $\tilde{\nu} = 3360$ (1), 3056 (1), 3023 (2), 2973 (2), 2915 (6), 2855 (2), 2735 (1), 1685 (2), 1613 (5), 1588 (2), 1575 (2), 1486 (2), 1458 (2), 1384 (4), 1308 (9), 1208 (1), 1168 (2), 1072 (2), 1009 (3), 947 (2), 889 (2), 743 (1), 690 (1), 577 (10), 563 (5), 522 (5), 456 (2), 374 (2), 327 (2), 269 (3), 244 (3).

TerNC. Terphenyl isonitrile was synthesized according to a modified literature procedure.³⁷ To a solution of terphenyl formamide (0.603 g, 1.687 mmol) in CH₂Cl₂ (13 mL), NEt₃ (1.697 g, 16.77 mmol) is added at 0 °C. Under stirring and cooling, POCl₃ (0.680 g, 4.44 mmol) is added slowly. The orange solution is stirred for 16 h at ambient temperature (25 °C). Afterward, the reaction mixture is quenched with water at 0 °C. The organic phase is extracted two times with water (20 mL) and three times with saturated aqueous NaHCO₃ (20 mL). The pale yellow organic layer is separated, dried over MgSO₄ and filtered. The organic solvent is removed under reduced pressure (1×10^{-3} mbar). The raw product is washed three times with *n*-hexane, and the colorless crystals are dried in vacuo (1×10^{-3} mbar). Yield: 0.231 g, 0.680 mmol, 40%. C₂₃H₂₃N (339.48 g/mol). Mp. 266 °C. Anal. calcd for C₂₃H₂₃N: C, 88.45; H, 7.42; N, 4.13. Found: C, 88.64; H, 7.48; N, 3.90. ¹H NMR (CD₂Cl₂, 300.1 MHz): δ 2.02 (s, 12H), 2.34 (s, 6H), 7.00 (s, 4H), 7.22 (d, 2H, $J = 7.7$ Hz), 7.54 (t, 1H, $J = 7.7$ Hz). ¹³C{¹H} NMR (CD₂Cl₂, 75.5 MHz): δ 20.4, 21.4, 128.8, 130.0, 130.1, 134.9, 136.2, 138.4, 139.8, 185.4. IR (ATR, 25 °C, 32 scans, cm⁻¹): $\tilde{\nu} = 2999$ (w), 2974 (w), 2943 (w), 2914 (m), 2853 (w), 2733 (w), 2624 (w), 2605 (w), 2496 (w), 2119 (m), 1614 (m), 1573 (w), 1455 (m), 1416 (m), 1377 (m), 1274 (w), 1183 (w), 1068 (w), 1035 (m), 1014 (m), 981 (w), 919 (w), 862 (m), 851 (m), 806 (s), 787 (m), 759 (s), 738 (m), 608 (m), 575 (m), 565 (m), 519 (m), 497 (m). Raman (633 nm, 10 s, 10 scans, cm⁻¹): $\tilde{\nu} = 3069$ (1), 3058 (1), 3012 (1), 2918 (1), 2857 (1), 2734 (1), 2121 (10), 2087 (1), 1614 (1), 1584 (1), 1490 (1), 1416 (1), 1381 (1), 1308 (4), 1288 (1), 1273 (1), 1188 (2), 1184 (2), 1161 (1), 1067 (3), 1000 (1), 947 (1), 612 (2), 579 (4), 564 (1), 524 (1), 499 (1), 406 (1), 380 (1), 336 (1), 255 (1), 233 (1).

[P(μ -NHyp)]₂ (1Hyp). [P(μ -NHyp)]₂ was synthesized according to a modified literature procedure.³⁹ [CIP(μ -NHyp)]₂ (1.912 g, 2.913 mmol) and Mg turnings (0.725 g, 26.8 mmol) are combined in a Schlenk flask. It is paramount to ensure that no grease finds its way into

the reaction vessel, as this may deactivate the Mg turnings. DME is added (50 mL), and the reaction mixture is stirred at ambient temperature (25 °C). The colorless mixture gradually turns dark red. The progress of the reaction must be monitored by ^{31}P NMR spectroscopy, as over-reduction and dimerization of the product occur very quickly. When the reaction is completed, the solvent is removed in vacuo (1×10^{-3} mbar), and the solids are dried at 50 °C (oil bath) for 30 min. *n*-Hexane (15 mL) is added, and the insoluble material is separated by filtration. If necessary, the cloudy suspension is filtered a second time over a Celite-padded frit. The product is crystallized from a minimal amount of *n*-hexane at -40 °C. After crystallization overnight, red crystals of the product are obtained. The supernatant is removed by syringe, concentrated, and stored at -40 °C, yielding a second crop of product. The isolated crystals are dried in vacuo (1×10^{-3} mbar). Yield: 1.338 g 2.286 mmol, 70%. $\text{C}_{18}\text{H}_{24}\text{N}_2\text{P}_2\text{Si}_6$ (585.27 g/mol). Mp. 205 °C. Anal. calcd for $\text{C}_{18}\text{H}_{24}\text{N}_2\text{P}_2\text{Si}_6$: C, 36.94; H, 9.30; N, 4.79. Found: C, 36.59; H, 9.34; N, 4.72. ^1H NMR (C_6D_6 , 300.1 MHz): δ 0.21 (s, 54H). $^{13}\text{C}\{^1\text{H}\}$ NMR (C_6D_6 , 125.5 MHz): δ 1.13. ^{14}N NMR: No signals observed. ^{29}Si -INEPT NMR (C_6D_6 , 59.6 MHz): δ -13.02 (m, 6Si), -35.02 (m, 2Si). $^{31}\text{P}\{^1\text{H}\}$ NMR (C_6D_6 , 121.5 MHz): δ 320.4 (quin, 2P, $J = 44$ Hz). IR (ATR, 32 scans, cm^{-1}): $\tilde{\nu} = 2949$ (w), 2893 (w), 2818 (w), 2794 (w), 2652 (w), 2368 (w), 2326 (w), 2085 (w), 2050 (w), 1984 (w), 1927 (w), 1863 (w), 1595 (w), 1495 (w), 1439 (w), 1396 (w), 1240 (m), 1053 (w), 982 (w), 947 (w), 816 (vs), 789 (s), 760 (s), 750 (s), 681 (s), 623 (s), 559 (m). Raman (633 nm, 10 s, 10 scans, cm^{-1}): $\tilde{\nu} = 2949$ (s), 2927 (3), 2890 (10), 1396 (1), 1259 (1), 1240 (1), 1138 (1), 1116 (1), 1070 (2), 865 (1), 834 (1), 802 (1), 744 (1), 686 (3), 625 (7), 587 (1), 464 (1), 431 (1), 370 (1), 304 (2), 263 (1), 215 (2), 178 (8), 173 (8), 164 (9), 161 (9). MS (CI pos., isobutane), m/z (%): 247 (1) $[\text{Si}(\text{Si}(\text{CH}_3)_2)_2]^+$, 264 (2) $[\text{Si}(\text{Si}(\text{CH}_3)_2)_3\text{NH}_3]^+$, 292 (2) $[\text{Si}(\text{Si}(\text{CH}_3)_2)_3\text{NP}]^+$, 555 (2) $[\text{Si}_2(\text{Si}(\text{CH}_3)_2)_6\text{NP}]^+$, 584 (100) $[\text{M}]^+$, 585 (67) $[\text{M} + \text{H}]^+$.

3Hyp-Dmp. To a solution of $[\text{P}(\mu\text{-NHyp})_2]$ (**1Hyp**; 274 mg, 0.470 mmol) in hexane (5 mL), DmpNC (60 mg, 0.47 mmol) is added. An immediate color change from orange to green to yellow is observed. After 2 h, the solvent is removed, and the yellow residue is dried in vacuo (1×10^{-3} mbar). The product is crystallized from a minimal amount of fresh *n*-hexane at -40 °C. The supernatant is removed by syringe, and the crystals are dried in vacuo (1×10^{-3} mbar). Yield: 230 mg, 0.32 mmol, 68%. $\text{C}_{27}\text{H}_{63}\text{N}_3\text{P}_2\text{Si}_6$ (715.45 g/mol). Mp. 205 °C. Anal. calcd for $\text{C}_{27}\text{H}_{63}\text{N}_3\text{P}_2\text{Si}_6$: C, 45.26; H, 8.86; N, 5.87. Found: C, 45.36; H, 9.04; N, 5.70. ^1H NMR (C_6D_6 , 300.1 MHz): δ 0.21 (s, 27H), 0.33 (s, 27H), 2.39 (s, 6H), 6.94 (s, 3H). $^{13}\text{C}\{^1\text{H}\}$ NMR (C_6D_6 , 75.5 MHz): δ 0.0, 1.9, 18.6 (d, $J = 3$ Hz), 127.2, 129.3, 136.0 (d, $J = 3$ Hz), 144.7 (d, $J = 4$ Hz). ^{14}N NMR: No signals observed. ^{29}Si -INEPT NMR (C_6D_6 , 59.6 MHz): δ -13.2 (m, 3Si), -14.3 (m, 3Si), -30.8 (m, 1Si), -33.8 (m, 1Si). $^{31}\text{P}\{^1\text{H}\}$ NMR (C_6D_6 , 121.5 MHz): δ = 209.0 (d, 1P, $J = 15$ Hz, CPN), 297.3 (d, 1P, $J = 15$ Hz, NPN). IR (ATR, 32 scans, cm^{-1}): $\tilde{\nu} = 2949$ (w), 2893 (w), 1599 (w), 1589 (w), 1539 (m), 1470 (w), 144 (w), 1398 (w), 1325 (w), 1242 (m), 1203 (m), 1194 (m), 1097 (w), 99 (m), 937 (m), 910 (m), 825 (vs), 791 (s), 744 (m), 685 (s), 621 (m), 553 (m), 540 (m). Raman (633 nm, 20 s, 20 scans, cm^{-1}): $\tilde{\nu} = 3068$ (1), 3036 (1), 3017 (1), 2952 (3), 2895 (7), 1594 (1), 1467 (1), 1441 (1), 1406 (1), 1380 (1), 1335 (2), 1332 (2), 1263 (2), 1241 (2), 1222 (1), 1197 (10), 1164 (1), 1101 (1), 1032 (1), 1017 (4), 913 (3), 894 (1), 890 (1), 862 (1), 828 (2), 794 (4), 780 (1), 748 (2), 738 (1), 726 (1), 713 (3), 690 (3), 632 (9), 623 (5), 556 (5), 544 (3), 530 (2), 490 (1), 472 (1), 455 (1), 440 (2), 415 (4), 397 (1), 375 (1), 348 (1), 320 (3), 295 (2), 272 (2), 253 (2), 241 (2), 221 (3), 176 (7), 127 (3), 81 (6). MS (CI pos., isobutane), m/z (%): 424 (18) $[\text{DmpNHypCNP}]^+$, 497 (2.6) $[\text{DmpNHypCNP}_2\text{Si}_2]^+$, 645 (4) $[\text{DmpNHypCNP}_2\text{Si}_2(\text{CH}_3)_2]^+$, 700 (21) $[\text{C}_7\text{H}_{14}\text{N}_2\text{P}_2\text{CHyp}_2]^+$, 701 (14) $[\text{C}_7\text{H}_{14}\text{N}_2\text{P}_2\text{CHyp}_2]^+$, 702 (10) $[\text{C}_7\text{H}_{14}\text{N}_2\text{P}_2\text{CHyp}_2]^+$, 715 (100) $[\text{M}]^+$, 716 (86) $[\text{M} + \text{H}]^+$. Single crystals suitable for X-ray structure determination can be obtained by recrystallization from fresh *n*-hexane at -40 °C.

3Hyp-Mes. To a solution of $[\text{P}(\mu\text{-NHyp})_2]$ (**1Hyp**; 271 mg, 0.464 mmol) in hexane (8 mL), MesNC (66 mg, 0.46 mmol) is added. An

immediate color change from orange to green to yellow is observed. After 2 h, the solvent is removed, and the yellow residue is dried in vacuo (1×10^{-3} mbar). The product is crystallized from a minimal amount of fresh *n*-hexane at -40 °C. The supernatant is removed by syringe, and the crystals are dried in vacuo (1×10^{-3} mbar). Yield: 315 mg, 0.43 mmol, 93%. $\text{C}_{28}\text{H}_{65}\text{N}_3\text{P}_2\text{Si}_6$ (730.48 g/mol). Mp. 207 °C. Anal. calcd for $\text{C}_{28}\text{H}_{65}\text{N}_3\text{P}_2\text{Si}_6$: C, 46.04; H, 8.97; N, 5.75. Found: C, 46.01; H, 9.09; N, 5.50. ^1H NMR (CD_2Cl_2 , 300.1 MHz): δ 0.13 (s, 27H), 0.21 (s, 27H), 2.18 (s, 6H), 2.29 (s, 3H), 6.91 (s, 2H). $^{13}\text{C}\{^1\text{H}\}$ NMR (C_6D_6 , 75.5 MHz): δ 0.0, 1.9, 18.5 (d, $J = 3$ Hz), 20.2, 127.2, 130.1, 135.5 (d, $J = 4$ Hz), 136.5. ^{14}N NMR: No signals observed. ^{29}Si -INEPT NMR (C_6D_6 , 59.6 MHz): δ -13.2 (m, 3Si), -14.4 (m, 3Si), -31.0 (m, 1Si), -33.6 (m, 1Si). $^{31}\text{P}\{^1\text{H}\}$ NMR (C_6D_6 , 121.5 MHz): δ = 209.1 (d, 1P, CPN), $^2J(^{31}\text{P},^{31}\text{P}) = 10$ Hz), 297.5 (d, 1P, NPN), $^2J(^{31}\text{P},^{31}\text{P}) = 10$ Hz). IR (ATR, 32 scans, cm^{-1}): $\tilde{\nu} = 2949$ (w), 2891 (w), 1529 (w), 1477 (w), 1439 (w), 1396 (w), 1333 (m), 1304 (w), 1259 (m), 1240 (m), 1200 (m), 1188 (w), 1157 (w), 1034 (w), 1012 (w), 984 (w), 957 (w), 930 (w), 908 (w), 825 (vs), 771 (m), 744 (m), 710 (m), 683 (m), 621 (m), 567 (m), 528 (m). Raman (633 nm, 10 s, 20 scans, cm^{-1}): $\tilde{\nu} = 3010$ (1), 2974 (2), 2952 (3), 2930 (2), 2894 (8), 2824 (1), 2779 (1), 2734 (0), 1610 (1), 1573 (0), 1484 (0), 1443 (0), 1407 (0), 1382 (1), 1374 (1), 1332 (1), 1304 (1), 1263 (1), 1244 (1), 1200 (4), 1188 (4), 1158 (0), 1015 (2), 957 (0), 908 (2), 859 (1), 823 (1), 774 (2), 747 (1), 736 (0), 712 (1), 690 (2), 633 (10), 579 (2), 570 (1), 568 (1), 549 (4), 530 (2), 504 (0), 454 (1), 445 (1), 425 (2), 401 (1), 366 (2), 327 (1), 301 (1), 240 (1), 220 (1), 177 (6), 133 (2), 102 (2). MS (CI pos., isobutane), m/z (%): 350 (1) $[\text{HypN}_2\text{P}_2\text{C}]^+$, 482 (1) $[\text{HypN}_2\text{P}_2\text{CMes}]^+$, 583 (1) $[\text{HypN}_2\text{P}_2\text{CSi}(\text{CH}_3)_2]^+$, 656 (28) $[\text{HypN}_2\text{P}_2\text{CSi}(\text{CH}_3)_3]^+$, 714 (28) $[\text{Hyp}_2\text{N}_2\text{P}_2\text{CC}_6\text{H}_5]^+$, 715 (19) $[\text{Hyp}_2\text{N}_2\text{P}_2\text{CC}_6\text{H}_5]^+$, 716 (13) $[\text{Hyp}_2\text{N}_2\text{P}_2\text{CC}_6\text{H}_5]^+$, 729 (100) $[\text{M}]^+$, 730 (83) $[\text{M} + \text{H}]^+$. Single crystals suitable for X-ray structure determination can be obtained by recrystallization from fresh *n*-hexane at -40 °C.

3Hyp-tBu. To a solution of $[\text{P}(\mu\text{-NHyp})_2]$ (**1Hyp**; 305 mg, 0.521 mmol) in hexane (5 mL), $^t\text{BuNC}$ (58 μL , 43 mg, 0.521 mmol) is added via microliter syringe. An immediate color change from orange to blue to green to yellow is observed. After 2 h, all volatiles are removed, and the yellow residue is dried in vacuo (1×10^{-3} mbar). The product is crystallized from a minimal amount of fresh *n*-hexane at -40 °C. Only a few crystals can be obtained due to the equilibrium chemistry described above. $\text{C}_{23}\text{H}_{63}\text{N}_3\text{P}_2\text{Si}_6$ (668.40 g/mol). ^1H NMR (CD_2Cl_2 , 300.1 MHz): δ 0.24 (s, 27H), 0.27 (s, 27H), 1.48 (s, 9H). $^{31}\text{P}\{^1\text{H}\}$ NMR (C_6D_6 , 121.5 MHz): δ 230.7 (d, 1P, $J = 15$ Hz, CPN), 281.9 (d, 1P, $J = 15$ Hz, NPN). Single crystals suitable for X-ray structure determination can be obtained by recrystallization from fresh *n*-hexane at -40 °C. Due to the dynamic equilibrium chemistry, no further analysis of the pure species was possible.

4Hyp-tBu. To a solution of $[\text{P}(\mu\text{-NHyp})_2]$ (**1Hyp**; 301 mg, 0.520 mmol) in hexane (5 mL), $^t\text{BuNC}$ (0.58 mL, 43 mg, 0.521 mmol) is added via microliter syringe. An immediate color change from orange to blue to green to yellow is observed. After 2 h, the solvent and excess $^t\text{BuNC}$ are removed, and the yellow residue is dried in vacuo (1×10^{-3} mbar). A mixture of several species is obtained, with the main components being **3Hyp-tBu** and **4Hyp-tBu** in a 2.5 ratio. $\text{C}_{28}\text{H}_{72}\text{N}_3\text{P}_2\text{Si}_6$ (751.58 g/mol). ^1H NMR (C_6D_6 , 300.1 MHz): diene **3Hyp-tBu**: δ 0.29 (s, 27H), 0.30 (s, 27H), 1.45 (s, 9H); adduct **4Hyp-tBu**: δ 0.31 (s, 27H), 0.39 (s, 27H), 1.48 (s, 9H). $^{31}\text{P}\{^1\text{H}\}$ NMR (C_6D_6 , 121.5 MHz): diene **3Hyp-tBu**: δ 230.7 (d, 1P, $J = 15$ Hz, CPN), 281.9 (d, 1P, $J = 15$ Hz, NPN); adduct **4Hyp-tBu**: δ 177.7 (d, 1P, $J = 22$ Hz, NPN), 233.1 (d, 1P, $J = 22$ Hz, NPN). Separation of the products and further analysis of the pure species was not possible.

2Hyp-Ter. To a solution of $[\text{P}(\mu\text{-NHyp})_2]$ (**1Hyp**; 139 mg, 0.236 mmol) in hexane (6 mL), TerNC (80 mg, 0.24 mmol) is added. An immediate color change from orange to blue is observed. After 2 h, the solvent is removed, and the blue residue is dried in vacuo (1×10^{-3} mbar). Due to the product's high sensitivity, some byproducts are obtained that prevented recrystallization, and the sample was used for further experiments. $\text{C}_{41}\text{H}_{79}\text{N}_3\text{P}_2\text{Si}_6$ (925.75 g/mol). ^1H NMR

(C_6D_6 , 500.1 MHz): δ 0.15 (s, 27H), 0.26 (s, 27H), 2.22 (s, 6H), 2.29 (s, 6H), 2.52 (s, 6H), 6.82 (m, 4H), 7.04 (s, 3H). $^{13}C\{^1H\}$ NMR (C_6D_6 , 125.8 MHz): δ 1.1, 1.9 (d, $J = 3$ Hz), 21.3, 23.2, 27.4, 123.4, 129.1, 129.4, 130.9, 132.5, 135.5, 136.3, 137.3, 137.6, 139.8, 155.6. ^{14}N NMR: No signals observed. ^{29}Si -INEPT NMR (C_6D_6 , 99.4 MHz): δ -11.9 (m, 3Si), -12.8 (m, 3Si), -26.2 (m, 1Si), -42.4 (m, 1Si). $^{31}P\{^1H\}$ NMR (C_6D_6 , 202.5 MHz): δ 211.7 (br d, 1P, $J = 118$ Hz, CPN), 275.1 (br d, 1P, $J = 118$ Hz, NPN). The product was highly labile. Therefore, isolation and further analysis of the pure species were not possible.

Irradiation of 2Hyp-Ter. 1Hyp (25.8 mg, 0.043 mmol) and TerNC (17.8 mg, 0.043 mmol) are dissolved in THF- d_6 (0.45 mL). The blue solution was irradiated in the NMR spectrometer with red light (638 nm). After full conversion to the housane 2'Hyp-Ter, the light source was shut off, and the thermal reverse reaction was traced by ^{31}P NMR spectroscopy. $^{31}P\{^1H\}$ NMR of 2'Hyp-Ter (THF- d_6 , 101 MHz): δ -128.0 (d, 1P, $J = 91$ Hz, NPC), -69.0 (d, 1P, $J = 91$ Hz, NPN).

■ ASSOCIATED CONTENT

Supporting Information

The Supporting Information is available free of charge at <https://pubs.acs.org/doi/10.1021/acs.joc.0c00460>.

Crystal structure of 3Hyp-Dmp (CIF)

Crystal structure of 3Hyp-Mes (CIF)

Crystal structure of 3Hyp-tBu (CIF)

Experimental and computational details, spectroscopic data including copies of experimental spectra, further information on irradiation experiments and kinetic studies. CCDC 1983541–1983543 contain the supplementary crystallographic data for this paper (PDF)

■ AUTHOR INFORMATION

Corresponding Authors

Jonas Bresien – Institute of Chemistry, University of Rostock, 18059 Rostock, Germany; orcid.org/0000-0001-9450-3407; Email: jonas.bresien@uni-rostock.de

Axel Schulz – Institute of Chemistry and Department Life, Light, and Matter, University of Rostock, 18059 Rostock, Germany; Leibniz Institute for Catalysis, 18059 Rostock, Germany; orcid.org/0000-0001-9060-7065; Email: axel.schulz@uni-rostock.de

Authors

Henrik Beer – Institute of Chemistry, University of Rostock, 18059 Rostock, Germany

Dirk Michalik – Institute of Chemistry, University of Rostock, 18059 Rostock, Germany; Leibniz Institute for Catalysis, 18059 Rostock, Germany

Anne-Kristin Rölke – Institute of Chemistry, University of Rostock, 18059 Rostock, Germany

Alexander Villinger – Institute of Chemistry, University of Rostock, 18059 Rostock, Germany; orcid.org/0000-0002-0868-9987

Ronald Wustrack – Institute of Chemistry, University of Rostock, 18059 Rostock, Germany

Complete contact information is available at:

<https://pubs.acs.org/doi/10.1021/acs.joc.0c00460>

Notes

The authors declare no competing financial interest.

■ ACKNOWLEDGMENTS

We are indebted to the ITMZ of the University of Rostock for access to the high-performance computing facilities. Especially, we wish to thank Malte Willert for his continuous support with all software-related issues. Furthermore, we wish to thank the DFG (SCHU/1170/12-2) for financial support.

■ REFERENCES

- (1) Salem, L.; Rowland, C. The Electronic Properties of Diradicals. *Angew. Chem., Int. Ed. Engl.* **1972**, *11* (2), 92–111.
- (2) *Diradicals*; Borden, W. T., Ed.; Wiley-Interscience: New York, 1982.
- (3) Stuyver, T.; Chen, B.; Zeng, T.; Geerlings, P.; De Proft, F.; Hoffmann, R. Do Diradicals Behave Like Radicals? *Chem. Rev.* **2019**, *119* (21), 11291–11351.
- (4) Grützmacher, H.; Breher, F. Odd-Electron Bonds and Biradicals in Main Group Element Chemistry. *Angew. Chem., Int. Ed.* **2002**, *41* (21), 4006–4011.
- (5) Breher, F. Stretching Bonds in Main Group Element Compounds — Borderlines between Biradicals and Closed-Shell Species. *Coord. Chem. Rev.* **2007**, *251*, 1007–1043.
- (6) Abe, M.; Ye, J.; Mishima, M. The Chemistry of Localized Singlet 1,3-Diradicals (Biradicals): From Putative Intermediates to Persistent Species and Unusual Molecules with a π -Single Bonded Character. *Chem. Soc. Rev.* **2012**, *41* (10), 3808–3820.
- (7) González-Gallardo, S.; Breher, F. Main Group Biradicaloids. In *Comprehensive Inorganic Chemistry II*; Elsevier: Amsterdam, 2013; Vol. 1, pp 413–455.
- (8) Abe, M. Diradicals. *Chem. Rev.* **2013**, *113* (9), 7011–7088.
- (9) Gryn'ova, G.; Coote, M. L.; Corminboeuf, C. Theory and Practice of Uncommon Molecular Electronic Configurations. *WIREs Comput. Mol. Sci.* **2015**, *5* (6), 440–459.
- (10) Schulz, A. Group 15 Biradicals: Synthesis and Reactivity of Cyclobutane-1,3-Diyl and Cyclopentane-1,3-Diyl Analogues. *Dalton Trans.* **2018**, *47* (37), 12827–12837.
- (11) Gopalakrishna, T. Y.; Zeng, W.; Lu, X.; Wu, J. From Open-Shell Singlet Diradicaloids to Polyradicaloids. *Chem. Commun.* **2018**, *54* (18), 2186–2199.
- (12) Hollett, J. W.; Gill, P. M. W. The Two Faces of Static Correlation. *J. Chem. Phys.* **2011**, *134* (11), 114111.
- (13) Cramer, C. J. *Essentials of Computational Chemistry: Theories and Models*; John Wiley & Sons, Ltd: Chichester, UK, 2004.
- (14) Noodleman, L. Valence Bond Description of Antiferromagnetic Coupling in Transition Metal Dimers. *J. Chem. Phys.* **1981**, *74* (10), 5737–5743.
- (15) Michl, J.; Bonačić-Koutecký, V. Biradicals and Biradicaloids: A Unified View. *Tetrahedron* **1988**, *44* (24), 7559–7585.
- (16) Niecke, E.; Fuchs, A.; Baumeister, F.; Nieger, M.; Schoeller, W. W. A P_2C_2 Four-Membered Ring with Unusual Bonding—Synthesis, Structure, and Ring Opening of a 1,3-Diphosphacyclobutane-2,4-Diyl. *Angew. Chem., Int. Ed. Engl.* **1995**, *34* (5), 555–557.
- (17) Schoeller, W. W.; Begemann, C.; Niecke, E.; Gudat, D. Electronic Structure of the 2,4-Diphosphacyclobutane-Diyl-1,3 and Substituted Derivatives. *J. Phys. Chem. A* **2001**, *105* (47), 10731–10738.
- (18) Zhang, S.-H.; Xi, H.-W.; Lim, K. H.; Meng, Q.; Huang, M.-B.; So, C.-W. Synthesis and Characterization of a Singlet Delocalized 2,4-Diimino-1,3-Disilacyclobutanediyl and a Silylenylsilamine. *Chem. - Eur. J.* **2012**, *18* (14), 4258–4263.
- (19) Demeshko, S.; Godemann, C.; Kuzora, R.; Schulz, A.; Villinger, A. An Arsenic-Nitrogen Biradicaloid: Synthesis, Properties, and Reactivity. *Angew. Chem., Int. Ed.* **2013**, *52* (7), 2105–2108.
- (20) Hinz, A.; Schulz, A.; Villinger, A. A Mixed Arsenic-Phosphorus Centered Biradicaloid. *Angew. Chem., Int. Ed.* **2015**, *54* (2), 668–672.
- (21) Rottschäfer, D.; Neumann, B.; Stammier, H.-G.; Ghadwal, R. S. N-Heterocyclic Vinylidene-Stabilized Phosphorus Biradicaloid. *Chem. - Eur. J.* **2017**, *23* (38), 9044–9047.

- (22) Li, Z.; Chen, X.; Andrada, D. M.; Frenking, G.; Benkő, Z.; Li, Y.; Harmer, J. R.; Su, C.-Y.; Grützmacher, H. $(\text{L})_2\text{C}_2\text{P}_2$: Dicarbondiphosphide Stabilized by N-Heterocyclic Carbenes or Cyclic Diamido Carbenes. *Angew. Chem., Int. Ed.* **2017**, *56* (21), 5744–5749.
- (23) Rottschäfer, D.; Neumann, B.; Stammer, H.; Kishi, R.; Nakano, M.; Ghadwal, R. S. A Phosphorus Analogue of p-Quinodimethane with a Planar P_4 Ring: A Metal-Free Diphosphorus Source. *Chem. - Eur. J.* **2019**, *25* (13), 3244–3247.
- (24) Scheschke, D.; Amii, H.; Gornitzka, H.; Schoeller, W. W.; Bourissou, D.; Bertrand, G. Singlet Diradicals: From Transition States to Crystalline Compounds. *Science* **2002**, *295* (5561), 1880–1881.
- (25) Sugiyama, H.; Ito, S.; Yoshifuji, M. Synthesis of a 1,3-Diphosphacyclobutane-2,4-Diyl from Mes*CP. *Angew. Chem., Int. Ed.* **2003**, *42* (32), 3802–3804.
- (26) Cox, H.; Hitchcock, P. B.; Lappert, M. F.; Piessens, L. J. M. A 1,3-Diaza-2,4-Distannacyclobutane: Synthesis, Structure, and Bonding. *Angew. Chem., Int. Ed.* **2004**, *43* (34), 4500–4504.
- (27) Cui, C.; Brynda, M.; Olmstead, M. M.; Power, P. P. Synthesis and Characterization of the Non-Kekulé, Singlet Biradicaloid $\text{Ar}'\text{Ge}(\mu\text{-NSiMe}_3)_2\text{GeAr}'$ ($\text{Ar}' = 2,6\text{-Dipp}_2\text{C}_6\text{H}_3$, $\text{Dipp} = 2,6\text{-i-Pr}_2\text{C}_6\text{H}_3$). *J. Am. Chem. Soc.* **2004**, *126* (21), 6510–6511.
- (28) Wang, X.; Peng, Y.; Olmstead, M. M.; Fetting, J. C.; Power, P. P. An Unsymmetric Oxo/Imido-Bridged Germanium-Centered Singlet Diradicaloid. *J. Am. Chem. Soc.* **2009**, *131* (40), 14164–14165.
- (29) Henke, P.; Pankewitz, T.; Klopper, W.; Breher, F.; Schnöckel, H. Snapshots of the Al-Al σ -Bond Formation Starting from $\{\text{AlR}_2\}$ Units: Experimental and Computational Observations. *Angew. Chem., Int. Ed.* **2009**, *48* (43), 8141–8145.
- (30) Takeuchi, K.; Ichinohe, M.; Sekiguchi, A. Access to a Stable Si_2N_2 Four-Membered Ring with Non-Kekulé Singlet Biradical Character from a Disilyne. *J. Am. Chem. Soc.* **2011**, *133* (32), 12478–12481.
- (31) Beweries, T.; Kuzora, R.; Rosenthal, U.; Schulz, A.; Villinger, A. $[\text{P}(\mu\text{-N}^-\text{Ter})]_2$: A Biradicaloid That Is Stable at High Temperature. *Angew. Chem., Int. Ed.* **2011**, *50* (38), 8974–8978.
- (32) Hinz, A.; Kuzora, R.; Rosenthal, U.; Schulz, A.; Villinger, A. Activation of Small Molecules by Phosphorus Biradicaloids. *Chem. - Eur. J.* **2014**, *20* (45), 14659–14673.
- (33) Hinz, A.; Schulz, A.; Seidel, W. W.; Villinger, A. A New Class of Azadipnictridines Generated by an Unusual Rearrangement Reaction. *Inorg. Chem.* **2014**, *53* (21), 11682–11690.
- (34) Hinz, A.; Schulz, A.; Villinger, A. Tunable Cyclopentane-1,3-Diyls Generated by Insertion of Isonitriles into Diphosphadiazane-diyls. *J. Am. Chem. Soc.* **2015**, *137* (31), 9953–9962.
- (35) Hinz, A.; Schulz, A.; Villinger, A. Stable Heterocyclopentane-1,3-Diyls. *Angew. Chem., Int. Ed.* **2015**, *54* (9), 2776–2779.
- (36) Brückner, A.; Hinz, A.; Priebe, J. B.; Schulz, A.; Villinger, A. Cyclic Group 15 Radical Cations. *Angew. Chem., Int. Ed.* **2015**, *54* (25), 7426–7430.
- (37) Hinz, A.; Schulz, A.; Villinger, A. Metal-Free Activation of Hydrogen, Carbon Dioxide, and Ammonia by the Open-Shell Singlet Biradicaloid $[\text{P}(\mu\text{-N}^-\text{Ter})]_2$. *Angew. Chem., Int. Ed.* **2016**, *55* (40), 12214–12218.
- (38) Hinz, A.; Schulz, A.; Villinger, A. On the Behaviour of Biradicaloid $[\text{P}(\mu\text{-N}^-\text{Ter})]_2$ towards Lewis Acids and Bases. *Chem. Commun.* **2016**, *52* (37), 6328–6331.
- (39) Hinz, A.; Kuzora, R.; Rölke, A.-K.; Schulz, A.; Villinger, A.; Wustrack, R. Synthesis of a Silylated Phosphorus Biradicaloid and Its Utilization in the Activation of Small Molecules. *Eur. J. Inorg. Chem.* **2016**, *2016* (22), 3611–3619.
- (40) Bresien, J.; Hinz, A.; Schulz, A.; Villinger, A. As-N and As-N-P Cage Compounds Generated by $[2 + 2]$ Addition of Diazenes and Diphosphenes to Diarsadiazanediyls. *Eur. J. Inorg. Chem.* **2018**, *2018* (15), 1679–1682.
- (41) Feringa, B. L.; van Delden, R. A.; Koumura, N.; Geertsema, E. M. Chiroptical Molecular Switches. *Chem. Rev.* **2000**, *100* (5), 1789–1816.
- (42) Russev, M.-M.; Hecht, S. Photoswitches: From Molecules to Materials. *Adv. Mater.* **2010**, *22* (31), 3348–3360.
- (43) Göstl, R.; Senf, A.; Hecht, S. Remote-Controlling Chemical Reactions by Light: Towards Chemistry with High Spatio-Temporal Resolution. *Chem. Soc. Rev.* **2014**, *43* (6), 1982–1996.
- (44) Bléger, D.; Hecht, S. Visible-Light-Activated Molecular Switches. *Angew. Chem., Int. Ed.* **2015**, *54* (39), 11338–11349.
- (45) Zhang, J. L.; Zhong, J. Q.; Lin, J. D.; Hu, W. P.; Wu, K.; Xu, G. Q.; Wee, A. T. S.; Chen, W. Towards Single Molecule Switches. *Chem. Soc. Rev.* **2015**, *44* (10), 2998–3022.
- (46) Bresien, J.; Kröger-Badge, T.; Lochbrunner, S.; Michalik, D.; Müller, H.; Schulz, A.; Zander, E. A Chemical Reaction Controlled by Light-Activated Molecular Switches Based on Hetero-Cyclopentane-diyls. *Chem. Sci.* **2019**, *10* (12), 3486–3493.
- (47) Krumlacher, W.; Siegl, H.; Hassler, K. Hypersilyl Compounds of Elements of Group 15. In *Organosilicon Chemistry IV: From Molecules to Materials*; Auner, N., Weis, J., Eds.; Wiley-VCH Verlag GmbH: Weinheim, Germany, 2000; pp 367–371.
- (48) Kira, M.; Iwamoto, T. Silyl Migrations. In *The Chemistry of Organic Silicon Compounds*; Rappoport, Z., Apeloig, Y., Eds.; John Wiley & Sons, Ltd: Chichester, UK, 2001; Vol. 3, pp 853–948.
- (49) Pyykkö, P.; Atsumi, M. Molecular Double-Bond Covalent Radii for Elements Li-E112. *Chem. - Eur. J.* **2009**, *15* (46), 12770–12779.
- (50) Perdew, J. P.; Burke, K.; Ernzerhof, M. Generalized Gradient Approximation Made Simple. *Phys. Rev. Lett.* **1996**, *77* (18), 3865–3868.
- (51) Perdew, J. P.; Burke, K.; Ernzerhof, M. Generalized Gradient Approximation Made Simple. *Phys. Rev. Lett.* **1997**, *78* (7), 1396–1396.
- (52) Weigend, F.; Ahlrichs, R. Balanced Basis Sets of Split Valence, Triple Zeta Valence and Quadruple Zeta Valence Quality for H to Rn: Design and Assessment of Accuracy. *Phys. Chem. Chem. Phys.* **2005**, *7* (18), 3297–3305.
- (53) Hegarty, D.; Robb, M. A. Application of Unitary Group Methods to Configuration Interaction Calculations. *Mol. Phys.* **1979**, *38* (6), 1795–1812.
- (54) Eade, R. H. A.; Robb, M. A. Direct Minimization in MC SCF Theory. The Quasi-Newton Method. *Chem. Phys. Lett.* **1981**, *83* (2), 362–368.
- (55) Schlegel, H. B.; Robb, M. A. MC SCF Gradient Optimization of the $\text{H}_2\text{CO} \rightarrow \text{H}_2 + \text{CO}$ Transition Structure. *Chem. Phys. Lett.* **1982**, *93* (1), 43–46.
- (56) Bernardi, F.; Bottoni, A.; McDouall, J. J. W.; Robb, M. A.; Schlegel, H. B. MCSCF Gradient Calculation of Transition Structures in Organic Reactions. *Faraday Symp. Chem. Soc.* **1984**, *19* (4), 137.
- (57) Siegbahn, P. E. M. A New Direct CI Method for Large CI Expansions in a Small Orbital Space. *Chem. Phys. Lett.* **1984**, *109* (5), 417–423.
- (58) Robb, M. A.; Niaz, U. The Unitary Group Approach to Electronic Structure Computation. In *Reports in Molecular Theory*; Weinstein, H., Náray-Szabó, G., Eds.; CRC Press: Boca Raton, FL, 1990; Vol. 1, pp 23–55.
- (59) Frisch, M. J.; Ragazos, I. N.; Robb, M. A.; Schlegel, H. B. An Evaluation of Three Direct MC-SCF Procedures. *Chem. Phys. Lett.* **1992**, *189* (6), 524–528.
- (60) Yamamoto, N.; Vreven, T.; Robb, M. A.; Frisch, M. J.; Schlegel, H. B. A Direct Derivative MC-SCF Procedure. *Chem. Phys. Lett.* **1996**, *250* (3–4), 373–378.
- (61) Klene, M.; Robb, M. A.; Frisch, M. J.; Celani, P. Parallel Implementation of the CI-Vector Evaluation in Full CI/CAS-SCF. *J. Chem. Phys.* **2000**, *113* (14), 5653–5665.
- (62) Miliordos, E.; Ruedenberg, K.; Xantheas, S. S. Unusual Inorganic Biradicals: A Theoretical Analysis. *Angew. Chem., Int. Ed.* **2013**, *52* (22), 5736–5739.
- (63) Bresien, J.; Hinz, A.; Schulz, A.; Villinger, A. Trapping of Transient, Heavy Pnictogen-Centred Biradicals. *Dalton Trans.* **2018**, *47* (13), 4433–4436.

- (64) Su, Y.-T.; Huang, Y.-H.; Witek, H. A.; Lee, Y.-P. Infrared Absorption Spectrum of the Simplest Criegee Intermediate CH₂OO. *Science* **2013**, *340* (6129), 174–176.
- (65) Doehner, D.; Koutecky, J. Occupation Numbers of Natural Orbitals as a Criterion for Biradical Character. Different Kinds of Biradicals. *J. Am. Chem. Soc.* **1980**, *102* (6), 1789–1796.
- (66) Stuyver, T.; Zeng, T.; Tsuji, Y.; Geerlings, P.; De Proft, F. Diradical Character as a Guiding Principle for the Insightful Design of Molecular Nanowires with an Increasing Conductance with Length. *Nano Lett.* **2018**, *18* (11), 7298–7304.
- (67) Glendening, E. D.; Weinhold, F. Natural Resonance Theory: I. General Formalism. *J. Comput. Chem.* **1998**, *19* (6), 593–609.
- (68) Riplinger, C.; Neese, F. An Efficient and near Linear Scaling Pair Natural Orbital Based Local Coupled Cluster Method. *J. Chem. Phys.* **2013**, *138* (3), 034106.
- (69) Liakos, D. G.; Sparta, M.; Kesharwani, M. K.; Martin, J. M. L.; Neese, F. Exploring the Accuracy Limits of Local Pair Natural Orbital Coupled-Cluster Theory. *J. Chem. Theory Comput.* **2015**, *11* (4), 1525–1539.
- (70) Riplinger, C.; Pinski, P.; Becker, U.; Valeev, E. F.; Neese, F. Sparse Maps—A Systematic Infrastructure for Reduced-Scaling Electronic Structure Methods. II. Linear Scaling Domain Based Pair Natural Orbital Coupled Cluster Theory. *J. Chem. Phys.* **2016**, *144* (2), 024109.
- (71) Falivene, L.; Cao, Z.; Petta, A.; Serra, L.; Poater, A.; Oliva, R.; Scarno, V.; Cavallo, L. Towards the Online Computer-Aided Design of Catalytic Pockets. *Nat. Chem.* **2019**, *11* (10), 872–879.
- (72) London, F. Théorie Quantique Des Courants Interatomiques Dans Les Combinaisons Aromatiques. *J. Phys. Radium* **1937**, *8* (10), 397–409.
- (73) McWeeny, R. Perturbation Theory for the Fock-Dirac Density Matrix. *Phys. Rev.* **1962**, *126* (3), 1028–1034.
- (74) Ditchfield, R. Self-Consistent Perturbation Theory of Diamagnetism. *Mol. Phys.* **1974**, *27* (4), 789–807.
- (75) Wolinski, K.; Hinton, J. F.; Pulay, P. Efficient Implementation of the Gauge-Independent Atomic Orbital Method for NMR Chemical Shift Calculations. *J. Am. Chem. Soc.* **1990**, *112* (23), 8251–8260.
- (76) Cheeseman, J. R.; Trucks, G. W.; Keith, T. A.; Frisch, M. J. A Comparison of Models for Calculating Nuclear Magnetic Resonance Shielding Tensors. *J. Chem. Phys.* **1996**, *104* (14), 5497–5509.
- (77) Fischer, C. B.; Xu, S.; Zipse, H. Steric Effects in the Uncatalyzed and DMAP-Catalyzed Acylation of Alcohols—Quantifying the Window of Opportunity in Kinetic Resolution Experiments. *Chem. - Eur. J.* **2006**, *12* (22), 5779–5784.
- (78) Reiß, F.; Schulz, A.; Völlinger, A.; Weding, N. Synthesis of Sterically Encumbered 2,4-Bis-*m*-Terphenyl-1,3-Dichloro-2,4-Cyclo-Dipnictadiazanes [m-TerNPnCl]₂ (Pn = P, As). *Dalton Trans.* **2010**, *39* (41), 9962–9972.
- (79) Bresien, J.; Hering-Junghans, C.; Schulz, A.; Thomas, M.; Völlinger, A. Reactivity of TerN(SiMe₃)BiCl₂—Synthesis of an Aminobismuthenium Cation and TerN(SiMe₃)Bi(N₃)₂. *Organometallics* **2018**, *37* (15), 2571–2580.
- (80) Kuzora, R.; Schulz, A.; Völlinger, A.; Wustrack, R. Hyper-silylated Cyclophosphadiazanes and Cyclophosphadiazanium Salts. *Dalton Trans.* **2009**, No. 42, 9304–9311.
- (81) Feldmeier, C.; Bartling, H.; Riedle, E.; Gschwind, R. M. LED Based NMR Illumination Device for Mechanistic Studies on Photochemical Reactions – Versatile and Simple, yet Surprisingly Powerful. *J. Magn. Reson.* **2013**, *232*, 39–44.
- (82) Sheldrick, G. M. SHELXT – Integrated Space-Group and Crystal-Structure Determination. *Acta Crystallogr., Sect. A: Found. Adv.* **2015**, *71* (1), 3–8.
- (83) Sheldrick, G. M. Crystal Structure Refinement with SHELXL. *Acta Crystallogr., Sect. C: Struct. Chem.* **2015**, *71* (1), 3–8.
- (84) Sheldrick, G. M. SADABS; University of Göttingen: Germany, 2004.
- (85) Frisch, M. J.; Trucks, G. W.; Schlegel, H. B.; Scuseria, G. E.; Robb, M. A.; Cheeseman, J. R.; Scalmani, G.; Barone, V.; Mennucci, B.; Peterson, G. A.; Nakatsuji, H.; Caricato, M.; Li, X.; Hratchian, H. P.; Izmaylov, A. F.; Bloino, J.; Zheng, G.; Sonnenberg, J. L.; Hada, M.; Ehara, M.; Toyota, K.; Fukuda, R.; Hasegawa, J.; Ishida, M.; Nakajima, T.; Honda, Y.; Kitao, O.; Nakai, H.; Vreven, T.; Montgomery, J. A., Jr.; Peralta, J. E.; Ogliaro, F.; Bearpark, M.; Heyd, J. J.; Brothers, E.; Kudin, K. N.; Staroverov, V. N.; Keith, T.; Kobayashi, R.; Normand, J.; Raghavachari, K.; Rendell, A.; Burant, J. C.; Iyengar, S. S.; Tomasi, J.; Cossi, M.; Rega, N.; Millam, J. M.; Klene, M.; Knox, J. E.; Cross, J. B.; Bakken, V.; Adamo, C.; Jaramillo, J.; Gomperts, R.; Stratmann, R. E.; Yazyev, O.; Austin, A. J.; Cammi, R.; Pomelli, C.; Ochterski, J. W.; Martin, R. L.; Morokuma, K.; Zakrzewski, V. G.; Voth, G. A.; Salvador, P.; Dannenberg, J. J.; Dapprich, S.; Daniels, A. D.; Farkas, O.; Foresman, J. B.; Ortiz, J. V.; Cioslowski, J.; Fox, D. J. *Gaussian 09*, Revision E.01; Gaussian Inc.: Wallingford, CT, 2013.
- (86) Neese, F. Software Update: The ORCA Program System, Version 4.0. *Wiley Interdiscip. Rev.: Comput. Mol. Sci.* **2018**, *8* (1), e1327.
- (87) Glendening, E. D.; Badenhop, J. K.; Reed, A. E.; Carpenter, J. E.; Bohmann, J. A.; Morales, C. M.; Landis, C. R.; Weinhold, F. *NBO 6.0. Theoretical Chemistry Institute*; University of Wisconsin: Madison, WI, 2013.
- (88) Carpenter, J. E.; Weinhold, F. Analysis of the Geometry of the Hydroxymethyl Radical by the “Different Hybrids for Different Spins” Natural Bond Orbital Procedure. *J. Mol. Struct.: THEOCHEM* **1988**, *169*, 41–62.
- (89) Weinhold, F.; Carpenter, J. E. The Natural Bond Orbital Lewis Structure Concept for Molecules, Radicals, and Radical Ions. In *The Structure of Small Molecules and Ions*; Naaman, R., Vager, Z., Eds.; Springer: Boston, MA, 1988; pp 227–236.
- (90) Weinhold, F.; Landis, C. R. *Valency and Bonding. A Natural Bond Orbital Donor-Acceptor Perspective*; Cambridge University Press: Cambridge, UK, 2005.
- (91) Weinhold, F.; Landis, C. R. *Discovering Chemistry with Natural Bond Orbitals*; John Wiley & Sons, Inc.: Hoboken, NJ, 2012.
- (92) Weinhold, F.; Landis, C. R.; Glendening, E. D. What Is NBO Analysis and How Is It Useful? *Int. Rev. Phys. Chem.* **2016**, *35* (3), 399–440.
- (93) Grimme, S.; Antony, J.; Ehrlich, S.; Krieg, H. A Consistent and Accurate Ab Initio Parametrization of Density Functional Dispersion Correction (DFT-D) for the 94 Elements H-Pu. *J. Chem. Phys.* **2010**, *132* (15), 154104.
- (94) Grimme, S.; Ehrlich, S.; Goerigk, L. Effect of the Damping Function in Dispersion Corrected Density Functional Theory. *J. Comput. Chem.* **2011**, *32* (7), 1456–1465.
- (95) Jameson, C. J.; De Dios, A.; Keith Jameson, A. Absolute Shielding Scale for ³¹P from Gas-Phase NMR Studies. *Chem. Phys. Lett.* **1990**, *167* (6), 575–582.
- (96) van Wüllen, C. A Comparison of Density Functional Methods for the Calculation of Phosphorus-31 NMR Chemical Shifts. *Phys. Chem. Chem. Phys.* **2000**, *2* (10), 2137–2144.
- (97) Wu, S.; Huang, J.; Gazzarrini, S.; He, S.; Chen, L.; Li, J.; Xing, L.; Li, C.; Chen, L.; Neochoritis, C. G.; et al. Isocyanides as Influenza A Virus Subtype H5N1 Wild-Type M2 Channel Inhibitors. *ChemMedChem* **2015**, *10* (11), 1837–1845.

7.1.2 Hyperpolarization Effects in Parahydrogen Activation with Pnictogen Biradicaloids: Metal-free PHIP and SABRE

Vladimir V. Zhivonitko, Henrik Beer, Danila O. Zakharov, Jonas Bresien, Axel Schulz

ChemPhysChem **2021**, *22*, 813–817.

DOI: 10.1002/cphc.202100141

This Open Access article is licensed under a Creative Commons Attribution 4.0 International Unported Licence.

Onlinelink: <https://doi.org/10.1002/cphc.202100141>

VIP Very Important Paper

Special
Collection

Hyperpolarization Effects in Parahydrogen Activation with Pnictogen Biradicaloids: Metal-free PHIP and SABRE

Vladimir V. Zhivonitko,^{*[a]} Henrik Beer,^[b] Danila O. Zakharov,^[a] Jonas Bresien,^[b] and Axel Schulz^[b, c]

Biradicaloids attract attention as a novel class of reagents that can activate small molecules such as H₂, ethylene and CO₂. Herein, we study activation of parahydrogen (nuclear spin-0 isomer of H₂) by a number of 4- and 5-membered pnictogen biradicaloids based on hetero-cyclobutanediyl [X(μ-Nter)₂Z] and hetero-cyclopentanediyyl [X(μ-Nter)₂ZC(NDmp)] moieties (X, Z = P, As; Ter = 2,6-Mes₂-C₆H₃, Dmp = 2,6-Me₂-C₆H₃). The concerted mechanism of this reaction allowed observing strong nuclear spin hyperpolarization effects in ¹H and ³¹P NMR experiments. Signal enhancements from two to four orders of magnitude were detected at 9.4 T depending on the structure. It is demonstrated that 4-membered biradicaloids activate H₂ reversibly, leading to SABRE (signal amplification by reversible exchange) hyperpolarization of biradicaloids themselves and their H₂ adducts. In contrast, the 5-membered counterparts demonstrate rather irreversible parahydrogen activation resulting in hyperpolarized H₂ adducts only. Kinetic measurements provided parameters to support experimental observations.

Biradicaloids receive considerable attention due to the unique reactivity that can be used to create new functional materials. For instance, recent applications include photoswitching,^[1] non-linear optics,^[2] molecular magnets^[3] and activation of small molecules such as CO₂, NH₃ and also H₂.^[4] Among other matters, activation of molecular hydrogen is interesting for parahydrogen-based nuclear spin hyperpolarization methods such as PASADENA (parahydrogen and synthesis allows dramatically

enhanced nuclear alignment),^[5] ALTADENA (adiabatic longitudinal transport after dissociation engenders net alignment)^[6] and SABRE.^[7] The hyperpolarization requires a chemical activation of parahydrogen, the spin-0 nuclear spin isomer of H₂.^[8] If the activation is pairwise, i.e., the two H atoms do not lose each other, a strong nuclear spin hyperpolarization and orders of magnitude NMR signal enhancements are observed due to the parahydrogen-induced polarization (PHIP).^[8a,9] Typically, metal-based catalysts such as various Rh, Ir or other metal complexes are used for this purpose.^[10] In principle, metal-free catalysts/activators made of light biogenic elements can provide a new useful alternative to the traditional catalytic systems.

So far, a few metal-free systems were demonstrated to produce nuclear spin hyperpolarization effects with parahydrogen (Scheme 1, 1–8). These are mainly N–B intramolecular frustrated Lewis pairs (FLP) (1–7) such as ansa-amino boranes,^[11] and there is also an example of FLP based C–P pair of aromatic triphosphenzene 7.^[12] Quite recently, a P–P biradicaloid 8 was demonstrated to show hyperpolarization effects both in ¹H and ³¹P NMR spectra while activating parahydrogen molecules.^[13] The symmetry of 8-H₂ adduct led to observation of unusual ¹H and ³¹P signal multiplets with enhancements exceeding at least one order of magnitude at 7 Tesla.

Herein, we study promising novel pnictogen (P, As) biradicaloids 9–12, addressing the nuclear spin hyperpolarization effects observed upon activation of parahydrogen molecules. We show that all these biradicaloids can activate H₂, which leads to strong hyperpolarization of biradicaloid-parahydrogen

[a] Prof. Dr. V. V. Zhivonitko, D. O. Zakharov
NMR Research Unit
University of Oulu
P.O. Box 3000, 90014 Oulu (Finland)
E-mail: vladimir.zhivonitko@oulu.fi

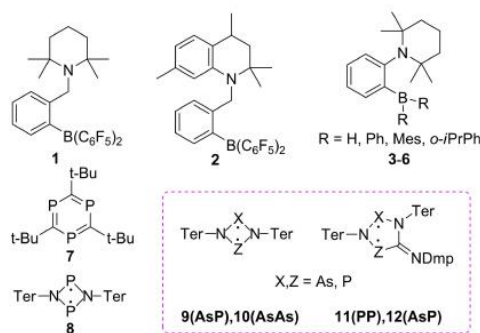
[b] H. Beer, Dr. J. Bresien, Prof. Dr. A. Schulz
Institute of Chemistry
University of Rostock
Albert-Einstein-Strasse 3a, 18059 Rostock (Germany)

[c] Prof. Dr. A. Schulz
Leibniz-Institut für Katalyse e.V.
Universität Rostock
Albert-Einstein-Strasse 29a, 18059 Rostock (Germany)

Supporting information for this article is available on the WWW under <https://doi.org/10.1002/cphc.202100141>

An invited contribution to a Special Collection on Parahydrogen Enhanced Resonance

© 2021 The Authors. ChemPhysChem published by Wiley-VCH GmbH. This is an open access article under the terms of the Creative Commons Attribution License, which permits use, distribution and reproduction in any medium, provided the original work is properly cited.



Scheme 1. Metal-free compounds known to activate parahydrogen and demonstrate nuclear spin hyperpolarization effects.

adduct molecules. We demonstrate that H₂ activation properties of four- and five-membered biradicaloids are different since the former ones show facile reversible activation that leads to metal-free SABRE of the biradicaloids themselves and incorporation of As atoms promotes the reversibility. Unusual hyperpolarization effects related to the biradicaloid structures were detected.

First, we studied nuclear spin hyperpolarization effects for the four-membered biradicaloids **8**–**10** at room temperature. The experiments were performed by bubbling parahydrogen gas through biradicaloid solutions in a 9.4 T magnet, which was followed by a $\pi/4$ -pulse and NMR signal detection (see Supporting Information). The corresponding ¹H NMR spectra are shown in Figure 1.

The asymmetrical As–P biradicaloid **9** demonstrated the most prominent hyperpolarization effect, leading to a substantial enhancement of P–H^a and As–H^b ¹H NMR signals of 9–H₂ adduct. As the parahydrogen activation takes place at the high magnetic field, the antiphase signals are observed in this case, as it should be for a weakly coupled spin system according to PASADENA experiment in theory.^[8a,9] Due to the *J*-coupled ³¹P, the enhanced antiphase resonances are split for the both H^a and H^b protons (H^a: *dd* δ = 6.91 ppm, ⁴*J*_{HH} = 5.2 Hz, ¹*J*_{HP} = 135.0 Hz; H^b: *dd* δ = 8.36 ppm, ⁴*J*_{HH} = 5.2 Hz, ³*J*_{HP} = 5.8 Hz). The measured enhancement factor ϵ is ca. 250 at 9.4 T and 298 K.

Hyperpolarization effects for the symmetrical As–As (**10**) and P–P (**8**) counterparts cannot be interpreted in a straightforward way as compared to **9** (Figure 1b and 1c). The activation

products 10–H₂ and 8–H₂ form AA'XX' spin systems (A = ¹H, X = ⁷⁵As or ³¹P), and this feature complicates corresponding NMR signal shapes significantly. Since the spin pairs of the same kind are strongly coupled, the resulting NMR spectra are expected to have complex signal structures due to the second-order effects.^[14] The observed resonances correspond to superposition states of the spin pairs rather than to the individual spins.

Our measurements show that As–As derivative **10** has a clear central transition in the thermal ¹H NMR spectrum, while the strongest hyperpolarization effects are observed at the side bands (Figure 1b). Since the side band transitions were invisible in the thermal spectrum due to their weak intensities, the precise measurement of signal enhancement is not possible. However, comparing the enhanced signals to the scaled noise level in the thermal spectrum with extensive scan accumulations, we estimated that the enhancement factor must be at least $> 10^4$ (Figure S1, see Supporting Information). Our attempts to simulate thermal and hyperpolarized spectra based on computed *J*-couplings (see Supporting Information, Table S8) didn't provide good matching of the experiment and theory, most likely due to the quadrupolar nature of ⁷⁵As. Indeed, among possible reasons for the discrepancy are errors in the computed parameters, presence of relatively fast chemical exchange that modulates *J*-coupling constants and strong quadrupolar relaxation of ⁷⁵As (spin-3/2). The latter two sources should lead to shifts of spectral lines and to the scalar relaxation of the first and the second kinds, respectively.^[15] The detailed consideration of these mechanisms, however, is beyond the scope of this study and will be addressed in the future.

¹H signal enhancements for **8** are more than one order of magnitude, as was also shown elsewhere.^[13] In principle, the signal enhancements in the symmetrical systems cannot be interpreted very easily in terms of conventional PASADENA theory in the weak coupling limit.^[8a] The signal enhancements are observed for "forbidden" transitions, which are not considered in that theory. At the same time, it is possible to use SLIC (Spin-Lock Induced Crossing)^[16] to convert antiphase polarization to in-phase, which was shown for **8** earlier.^[13]

In the case of mixed As–P biradicaloid **9**, the substantial ¹H polarization can be efficiently transferred to ³¹P nuclei. For instance, we utilized recently introduced ESOTERIC (Efficient Spin Order Transfer via Relayed Inept Chains)^[17] to perform the polarization transfer (see Supporting Information). Figure 2a shows ³¹P NMR spectra at 308 K after the polarization transfer and after the relaxation to thermal equilibrium. The comparison reveals a ³¹P signal enhancement factor (ϵ) of 2000 at 9.4 T for 9–H₂ adduct, demonstrating the high efficiency of this process. We should note that this is an unusually high signal enhancement for metal-free parahydrogen activations, highlighting the high efficiency of this biradicaloid system. Moreover, the reversibility of H₂ activation/addition by **9** opens a way for hyperpolarizing this molecule simply by waiting for 9–H₂ to dissociate. Indeed, setting a 300 ms delay between polarization transfer pulse-sequence and acquisition leads to the ³¹P NMR spectrum depicted in Figure 2b. It is clearly seen

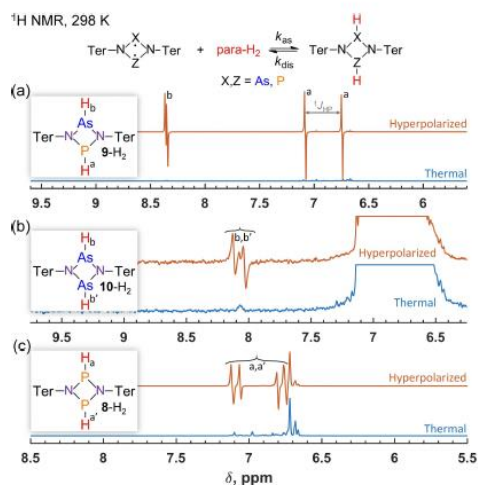


Figure 1. ¹H NMR spectra showing nuclear spin hyperpolarization effects observed at room temperature in the reversible interaction of parahydrogen with four-membered biradicaloids **9** (a), **10** (b) and **8** (c). The red traces are acquired in first moments after introduction of parahydrogen to 0.04 M solutions of the biradicaloids in toluene-d₈. The blue traces show the thermal polarization level. The high-intensity signals corresponding to thermal protons are off-scale and clipped in (b) for a better visibility of other signals.

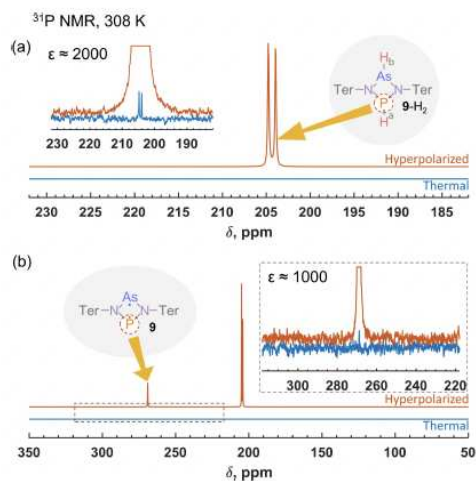


Figure 2. ^{31}P NMR spectra acquired immediately after the hyperpolarization transfer from ^1H to ^{31}P (a) and with a 300 ms mixing time delay (b). The insets show comparisons of the thermal (blue trace) and hyperpolarized (red trace) signals of 9-H_2 (a) and **9** (b). In the insets, the strong hyperpolarization signals are off-scale and clipped in.

that in addition to 9-H_2 , the initial resonance of **9** becomes strongly enhanced with the factor of ca. 1000-fold. The hyperpolarization of molecules without the actual chemical modification is the feature of SABRE technique. There is a natural difference between our observations and the original SABRE experiment,^[7] since we don't use metal complexes. However, the hyperpolarization of the initial biradicaloid molecule is facilitated by the reversible exchange and the polarization transfer is mediated through the J-couplings. Therefore, we call this effect metal-free SABRE. This is another example of metal-free SABRE, complementing one reported for spontaneous ^{15}N hyperpolarization with FLPs based on ansa-aminoboranes.^[11c] However, the SABRE efficiency in the current work was better by at least two orders of magnitude.

In contrast to **9**, heteronuclear hyperpolarization with the symmetrical four membered biradicaloids **8** (^{31}P) and **10** (^{75}As) may not require the use of any polarization transfer pulse sequences. In both cases, the symmetry properties of the resulting AA'XX', wherein A and A' nuclei come from parahydrogen, allows inherent hyperpolarization of X nuclei. This feature was demonstrated for ^{31}P in 8-H_2 adduct,^[13] providing up to ca. 300-fold signal enhancement. In this work, we attempted to observe the inherent hyperpolarization of ^{75}As in 10-H_2 , but no visible enhancement was detected. Most likely, this is due to the destructive effect of the fast ^{75}As relaxation leading to extremely broad ^{75}As signals and collapsing partially the multiplet structure.

An important feature of the four-membered biradicaloids **8**–**10** is the reversibility of H_2 addition under ambient temperatures, which leads to the dynamic exchange between bound

and free H_2 pools. This feature allows one to hyperpolarize the corresponding adducts constantly, provided that the continuous supply of parahydrogen is present. It should be noted that the reverse reaction rate increases with replacement of P atoms with As. For instance, at room temperature the dissociation of biradicaloid- H_2 adducts is characterized by the experimentally measured rate constants (k_{dis}) 1×10^{-4} , 0.15, 24 s^{-1} for **8**, **9** and **10**, correspondingly. The replacement of P with As leads to a clear gradual decrease of the activation energy (Table 1) which qualitatively correlates with computational data shown in Table S5 in Supporting Information. This is reasonable since bonds between hydrogen and atoms of the same main group weaken as we go down the group due to the decreased overlap integral between valence orbitals of the bonded atoms (cf. bond dissociation energies (BDE): $\text{BDE}(\text{As-H}) = 319.2(0.8)$ vs. $\text{BDE}(\text{P-H}) = 351.0(-2.1) \text{ kJ/mol}$).^[18]

In contrast to the four-membered biradicaloids, the five-membered ones, **11** and **12**, bind H_2 rather irreversibly. Moreover, strong ^1H NMR hyperpolarization effects with parahydrogen were observed only for P–P derivative **11**. The corresponding ^1H NMR spectrum is shown in Figure 3. As a result of the weak spin-spin coupling between nuclei of two $^{31}\text{P}^1\text{H}$ pairs in 11-H_2 , the spectrum reveals a signal pattern that includes the system of eight antiphase doublets corresponding to protons "a" and "b" originating from parahydrogen (H^{a} : $m \delta = 4.20 \text{ ppm}$, $^4J_{\text{HH}} = 2.5 \text{ Hz}$, $^1J_{\text{HP}} = 169.7 \text{ Hz}$, $^3J_{\text{HP}} = 4.1 \text{ Hz}$; H^{b} : $m \delta = 5.08 \text{ ppm}$, $^4J_{\text{HH}} = 2.5 \text{ Hz}$, $^1J_{\text{HP}} = 202.2 \text{ Hz}$, $^3J_{\text{HP}} = 9.6 \text{ Hz}$).

Due to the reaction irreversibility, the hyperpolarization effects were observed only at the first moments after para-

Compound	ΔH^\ddagger , [kcal/mol]	ΔS^\ddagger , [kcal/mol·K]
8 - H_2 ^[a]	21 ± 2	-8 ± 5
9 - H_2	16 ± 1	-8 ± 3
10 - H_2	13 ± 2	-9 ± 7

[a] Published in Ref. [13]

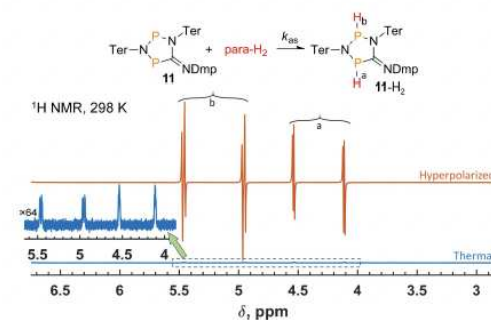


Figure 3. ^1H NMR spectra acquired at the first moment after bubbling parahydrogen (red trace, top) through 0.04 M solution of **11** and after the relaxation to thermal equilibrium (blue trace, bottom) at room temperature. The inset shows the level of thermal signals multiplied by a factor of 64.

hydrogen bubbling for adduct 11-H₂. The direct comparison of the resulting signal amplitudes with those in thermal spectra shows ca. 120-fold signal enhancement. We should note, however, that the H–H spin coupling in the adduct is only about 2.5 Hz whereas the linewidth is ca. 2 Hz, which led to a significant mutual cancellation of the signal components of the antiphase doublets. The lineshape fitting predicted at least 250-fold enhancement. Moreover, the determination of the exact enhancement factor through comparison to the thermal spectra is not a straightforward procedure under such experimental conditions because of the continuous accumulation of the adduct 11-H₂. Therefore, 250 is the lowest possible estimate. The ¹H hyperpolarization was easy to transfer to ³¹P nuclei via coherent polarization transfer with ESOTERIC, providing 130-fold signal enhancements for both phosphorus centers in 11-H₂ (see Supporting Information, Figure S3).

The reaction of 12 with parahydrogen at room temperature resulted in observation of thermally polarized signals of 12-H₂ in ¹H NMR spectra (see Supporting Information, Figure S6), meaning that this process does not lead to the observable polarization effects. The mechanism of parahydrogen activation with this biradicaloid most likely is still pairwise, but H atoms originating from parahydrogen are not coupled strongly enough by J-coupling. In this circumstance, the parahydrogen nascent nuclear spin order cannot be efficiently converted into the observable magnetization, thus effectively producing no hyperpolarization effects. The corresponding J-coupling constant of ≤ 1 Hz estimated by analysis of experimental thermal spectra supports this conclusion.

Interestingly, weak hyperpolarization effects in ¹H and ³¹P NMR spectra of 12-H₂ were nevertheless observed by heating its equilibrium solution in the presence of parahydrogen. For instance, in-phase doublet of 12-H₂ in ³¹P NMR spectrum was converted into antiphase doublet at 334 K, indicating the weak but still detectable reversibility of the H₂ activation by 12 (see Figure S7 and corresponding discussion in Supporting Information). Similar effect was observed also by heating 11-H₂ but at a higher temperature (373 K) (Figure S5 in Supporting Information), implying that activation H₂ by 11 also shows signs of reversibility. Attempts to synthesize the five-membered As–As analogue of 11 and 12 were not successful, since the initial four membered biradicaloid did not react with 2,6-dimethylphenylisocyanide to give the desired product.

Herein, we considerably expanded the range of metal-free biradicaloids that demonstrate hyperpolarization effects upon interaction with parahydrogen. The strongest hyperpolarization effects are observed for As–P four-membered compound 9 in both ¹H and ³¹P NMR spectra. The experimentally measured signal enhancements exceed three orders of magnitude at 9.4 T, i. e., correspond to at least 3% spin polarization for both nuclei. To date, this is a record high signal enhancement that was observed using metal-free parahydrogen activation. Comparing to much more widely explored metal-free activation with ansa-aminoboranes,^[11] it provides an order of magnitude improvement of the observed hyperpolarization. The reversibility of activation was used to hyperpolarize biradicaloids themselves via a high-field SABRE effect, providing another

example of SABRE in metal-free systems in addition to ansa-aminoboranes.^[11c] Symmetrical P–P and As–As four-membered biradicaloid adducts (8-H₂ and 10-H₂) form symmetrical AA'XX' spin systems (A=¹H, X=P,As) resulting in complex NMR multiplets having features of second-order spectra.^[14] This can be viewed as a consequence of chemical equivalence of ¹H and pnictogen spin pairs at the simultaneous magnetic inequivalence of spins in these pairs. This allows one to observe unusual effects such as hyperpolarization of ³¹P without a need for polarization transfer radio-frequency pulses for 8-H₂, or strongly enhanced ¹H side band resonances in the case of 10-H₂. Among five-membered biradicaloids, P–P based 11 provided strong signal enhancements of at least 250-fold, and all studied members of this class are shown to activate H₂ rather irreversibly, as compared to four-membered biradicaloids. However, the experiments with 11-H₂ and 12-H₂ performed at high temperatures (334 and 373 K) under parahydrogen pressure showed slight hyperpolarization of these adducts, indicating a weak reversibility of H₂ activation that was practically impossible to detect without the hyperpolarization. Altogether, we demonstrated versatile possibilities of hyperpolarization using metal-free pnictogen biradicaloids. Immediately, these biradicaloids cannot be used for NMR sensitivity enhancement *in vivo* because of air-sensitivity and toxicity of As. So far, they were not shown to mediate hydrogenation reactions, either. However, we would expect that a rational design of biradicaloids for parahydrogen activation may lead to applications in these areas in the future.

Experimental Section

Biradicaloids 8–12 were synthesized using modifications of synthetic approaches described elsewhere,^[1,19] and detailed in Supporting information. The experiments with parahydrogen were performed by using 5 mm gas-tight NMR tubes containing ca. 0.04 M solutions of biradicaloids in toluene-d₈ under elevated pressure of parahydrogen (92% enrichment). Dissociation constants were measured using saturation transfer method similarly as described in Ref. [11b, 13] Other essential details are presented in Supporting Information.

Acknowledgements

This work was supported by the Academy of Finland (grant no. 323480), the University of Oulu (Kvantum Institute) and the European Research Council (ERC) under Horizon 2020 (H2020/2018-2022/ERC Grant Agreement No. 772110). We gratefully acknowledge funding by the DFG (SCHU 1170/12-2).

Conflict of Interest

The authors declare no conflict of interest.

Keywords: biradicaloid · parahydrogen · NMR · hyperpolarization · metal-free activation

- [1] J. Bresien, T. Kröger-Badge, S. Lochbrunner, D. Michalik, H. Müller, A. Schulz, E. Zander, *Chem. Sci.* **2019**, *10*, 3486–3493.
- [2] a) K. Okuno, Y. Shigeta, R. Kishi, M. Nakano, *J. Phys. Chem. Lett.* **2013**, *4*, 2418–2422; b) J. J. Wang, Z. J. Zhou, H. M. He, D. Wu, Y. Li, Z. R. Li, H. X. Zhang, *J. Phys. Chem. C* **2016**, *120*, 13656–13666.
- [3] a) D. Cho, K. C. Ko, J. Y. Lee, *J. Phys. Chem. A* **2014**, *118*, 5112–5121; b) N. Orms, A. I. Krylov, *Phys. Chem. Chem. Phys.* **2018**, *20*, 13127–13144.
- [4] a) A. Hinz, A. Schulz, A. Villinger, *Angew. Chem. Int. Ed.* **2016**, *55*, 12214–12218; *Angew. Chem.* **2016**, *128*, 12402–12406; b) A. Hinz, R. Kuzora, U. Rosenthal, A. Schulz, A. Villinger, *Chem. Eur. J.* **2014**, *20*, 14659–14673.
- [5] C. R. Bowers, D. P. Weitekamp, *J. Am. Chem. Soc.* **1987**, *109*, 5541–5542.
- [6] M. G. Pravica, D. P. Weitekamp, *Chem. Phys. Lett.* **1988**, *145*, 255–258.
- [7] R. W. Adams, J. A. Aguilar, K. D. Atkinson, M. J. Cowley, P. I. Elliott, S. B. Duckett, G. G. Green, I. G. Khazal, J. Lopez-Serrano, D. C. Williamson, *Science* **2009**, *323*, 1708–1711.
- [8] a) C. R. Bowers, in *Encyclopedia of Nuclear Magnetic Resonance*, Vol. 9 (Eds.: D. M. Grant, R. K. Harris), Wiley, Chichester, **2002**, pp. 750–769; b) D. P. Weitekamp, in *eMagRes*, John Wiley & Sons, Ltd, **2007**, DOI: 10.1002/9780470034590.emrhp9780470030195; c) C. R. Bowers, D. P. Weitekamp, *Phys. Rev. Lett.* **1986**, *57*, 2645–2648.
- [9] J. Natterer, J. Bargon, *Prog. Nucl. Magn. Reson. Spectrosc.* **1997**, *31*, 293–315.
- [10] a) S. B. Duckett, N. J. Wood, *Coord. Chem. Rev.* **2008**, *252*, 2278–2291; b) S. B. Duckett, in *Encyclopedia of Spectroscopy and Spectrometry (Third Edition)* (Eds.: J. C. Lindon, G. E. Tranter, D. W. Koppenaal), Elsevier, Academic Press, **2016**, pp. 527–534.
- [11] a) V. V. Zhivonitko, V.-V. Telkki, K. Chernichenko, T. Repo, M. Leskelä, V. Sumerin, I. V. Koptiyug, *J. Am. Chem. Soc.* **2014**, *136*, 598–601; b) V. V. Zhivonitko, K. Sorochkina, K. Chernichenko, B. Kotai, T. Foldes, I. Papal, V.-V. Telkki, T. Repo, I. Koptiyug, *Phys. Chem. Chem. Phys.* **2016**, *18*, 27784–27795; c) K. Sorochkina, V. V. Zhivonitko, K. Chernichenko, V. V. Telkki, T. Repo, I. V. Koptiyug, *J. Phys. Chem. Lett.* **2018**, *9*, 903–907.
- [12] L. E. Longobardi, C. A. Russell, M. Green, N. S. Townsend, K. Wang, A. J. Holmes, S. B. Duckett, J. E. McGrady, D. W. Stephan, *J. Am. Chem. Soc.* **2014**, *136*, 13453–13457.
- [13] V. V. Zhivonitko, J. Bresien, A. Schulz, I. V. Koptiyug, *Phys. Chem. Chem. Phys.* **2019**, *21*, 5890–5893.
- [14] P. J. Stevenson, *Org. Biomol. Chem.* **2011**, *9*, 2078–2084.
- [15] J. Kowalewski, L. Mäler, *Nuclear Spin Relaxation in Liquids: Theory, Experiments, and Applications*, Taylor & Francis Group, New York, London, **2006**.
- [16] S. J. DeVience, R. L. Walsworth, M. S. Rosen, *Phys. Rev. Lett.* **2013**, *111*, 173002.
- [17] a) S. Korchak, S. J. Yang, S. Mamone, S. Glöggler, *ChemistryOpen* **2018**, *7*, 344–348; b) S. Korchak, S. Mamone, S. Glöggler, *ChemistryOpen* **2018**, *7*, 672–676.
- [18] Y.-R. Luo, *Comprehensive handbook of chemical bond energies*, CRC Press, Boca Raton, London, **2007**.
- [19] a) S. Demeshko, C. Godemann, R. Kuzora, A. Schulz, A. Villinger, *Angew. Chem. Int. Ed.* **2013**, *52*, 2105–2108; *Angew. Chem.* **2013**, *125*, 2159–2162; b) A. Hinz, A. Schulz, A. Villinger, *Angew. Chem. Int. Ed.* **2015**, *54*, 668–672; *Angew. Chem.* **2015**, *127*, 678–682; c) H. Beer, J. Bresien, D. Michalik, A. Schulz, A. Villinger, *Dalton Trans.* **2020**, *49*, 13986–13992; d) A. Hinz, A. Schulz, A. Villinger, *Chem. Sci.* **2016**, *7*, 745–751.

Manuscript received: February 21, 2021
Revised manuscript received: March 11, 2021
Accepted manuscript online: March 16, 2021
Version of record online: April 7, 2021

7.1.3 Insertion of Ruthenium into an inorganic, cyclic biradicaloid

Jan Oswald, Moritz T. Scharnhölz, Peter Coburger, Henrik Beer, Jonas Bresien, Axel Schulz, Hansjörg Grützmacher

Z. Anorg. Allg. Chem. **2022**, e202200093 (Early View).

DOI: 10.1002/zaac.202200093

This Open Access article is licensed under a Creative Commons Attribution 4.0 International Unported Licence.

Onlinelink: <https://onlinelibrary.wiley.com/doi/full/10.1002/zaac.202200093>

DOI: 10.1002/zaac.202200093

Insertion of Ruthenium into an inorganic, cyclic biradicaloid

Jan Oswald,^[a] Moritz T. Scharnhözl,^[a] Peter Coburger,^{*[a]} Henrik Beer,^[b] Jonas Bresien,^[b] Axel Schulz,^[b, c] and Hansjörg Grützmacher^{*[a]}

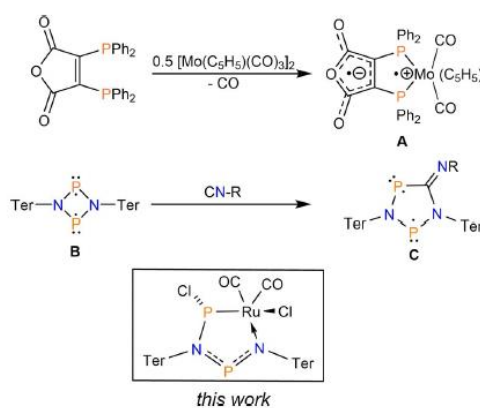
Dedicated to Professor Dieter Fenske on the occasion of his 80th birthday

The reaction between $[\text{Ru}_2\text{Cl}_2(\mu_2\text{-Cl})(\text{CO})_6]$ and the biradicaloid $[\text{P}(\mu\text{-NTer})_2]$ proceeds under insertion of a $\text{Ru}(\text{II})\text{Cl}(\text{CO})_2$ fragment into one P–N bond and addition of chloride to the adjacent phosphorus center. Thereby an unprecedented inorganic ruth-

enacycle is obtained that was investigated by single crystal X-ray analysis, NMR and IR spectroscopy and DFT calculations. The reactivity of the complex in a halide-pseudo-halide exchange reaction and a coordination reaction were investigated.

Metallacycles are always good for surprises and exhibit interesting photochemical^[1] and magnetic^[2] properties, as well as remarkable chemical reactivity.^[3] For example, almost 50 years ago, Fenske et al. reported the reaction between bis(diphenylphosphino)maleic anhydride derivatives and the dinuclear Mo(I) complex $[\text{Mo}_2(\text{Cp})_2(\text{CO})_6]$ ^[1,4-5] which, under loss of CO, led to a diphosphamolybdacycle **A** (Scheme 1) in which Mo became oxidized to Mo(II) and the ligand reduced to a radical anion, which was confirmed by EPR spectroscopy.^[6] Generally, radicals as ligands are intensively studied and their complexes are used in batteries, MOFs (metal-organic frameworks), and as catalysts.^[7]

The non-Kekulé molecule **B** with a central P_2N_2 heterocycle, which is best described as a biradicaloid, has been intensively investigated in the last decade.^[8-9] The addition to small molecules,^[9-10] radical reactivity,^[11] complexation of metal fragments,^[12-14] and ring expansion by insertion of an organic moiety has been reported.^[15] In the reaction with carbon monoxide or isonitriles, the expansion of the four-membered to a five-membered ring such as **C** is achieved by insertion of the



Scheme 1. Synthesis of a bis(diphenylphosphino)maleic anhydride complex (**A**) by Fenske.^[6] Insertion of an isonitrile into a stable biradicaloid (**B**) reported by Schulz (**C**).^[15] Ter = 2,6-bis(2,4,6-trimethylphenyl)phenyl.

[a] J. Oswald,^{*} M. T. Scharnhözl,^{*} P. Coburger, H. Grützmacher
Department of Chemistry and Applied Biosciences, ETH Zürich
Vladimir-Prelog-Weg 1, 8093 Zürich (Switzerland)
E-mail: hgruetzmacher@ethz.ch
pcoburger@inorg.chem.ethz.ch

[b] H. Beer, J. Bresien, A. Schulz
Institut für Chemie, Universität Rostock
Albert-Einstein-Str. 3a, 18059 Rostock (Germany)

[c] A. Schulz
Leibniz-Institut für Katalyse an der Universität Rostock e.V. (LIKAT)
Albert-Einstein-Str. 29a, 18059 Rostock (Germany)

[*] These authors contributed equally to this work.

Supporting information for this article is available on the WWW under <https://doi.org/10.1002/zaac.202200093>

© 2022 The Authors. Zeitschrift für anorganische und allgemeine Chemie published by Wiley-VCH GmbH. This is an open access article under the terms of the Creative Commons Attribution Non-Commercial NoDerivs License, which permits use and distribution in any medium, provided the original work is properly cited, the use is non-commercial and no modifications or adaptations are made.

carbon atom (Scheme 1).^[16] No insertion of a metal fragment into the P_2N_2 ring moiety has been reported so far.

Metallacycles are of general interest,^[17] and play a pivotal role in homogeneously catalyzed processes such as cyclo-trimerizations^[18] and metathesis reactions. For example, ruthenacyclobutanes play a key role in the metathesis of olefins^[19-20] and therefore ruthenacycles as such attract interest.^[21-23] A large number of ruthenacycles containing a carbon atom in the ring have been reported, while, to the best of our knowledge, purely “inorganic” ruthena-heterocycles (that is cycles without carbon) have not been described so far.

In order to further investigate the properties of biradicaloids as ligands in transition metal complexes, $[\text{P}(\mu\text{-NTer})_2]$ (**B**) was reacted with half an equivalent of the dinuclear ruthenium(II) complex $[\text{Ru}_2\text{Cl}_2(\mu_2\text{-Cl})(\text{CO})_6]$ in toluene at room temperature. In the course of 16 hours the orange mixture turned brown.

$^{31}\text{P}\{^1\text{H}\}$ NMR spectroscopy of an aliquot of the crude reaction mixture revealed that the starting material (singlet at $\delta = 276$ ppm) was fully consumed. Instead, three singlet resonances were observed in a ratio of 1:1:1. The products could be identified as the inorganic ruthenacycle **1** [$\delta(^{31}\text{P}\{^1\text{H}\}) = 319, 383$ ppm], [*trans*- $\text{P}(\mu\text{-N}(\text{Ter}))_2$ (**B^{Cl}**) [$\delta(^{31}\text{P}\{^1\text{H}\}) = 264$ ppm] and $\text{Ru}_3(\text{CO})_{12}$ (see Scheme 2). Surprisingly, a ruthenium atom is inserted into one P–N bond of the N_2P_2 ring leading to a ring expansion from four to five members. While in this reaction one chloride from the metal precursor complex is transferred to the α -P atom, the other is scavenged by another equivalent of the biradicaloid **B**. Interestingly, only the *trans*-isomer **B^{Cl}** is formed in the reaction, as confirmed by $^{31}\text{P}\{^1\text{H}\}$ NMR spectroscopy.^[24] As a result of this redox reaction, the formal oxidation state at Ru remains +2 while the oxidation state at each phosphorus center in **B^{Cl}** increases to +3 and the dodecacarbonyl triruthenium cluster $[\text{Ru}_3(\text{CO})_{12}]$ containing Ru(0) is formed as reduced species.

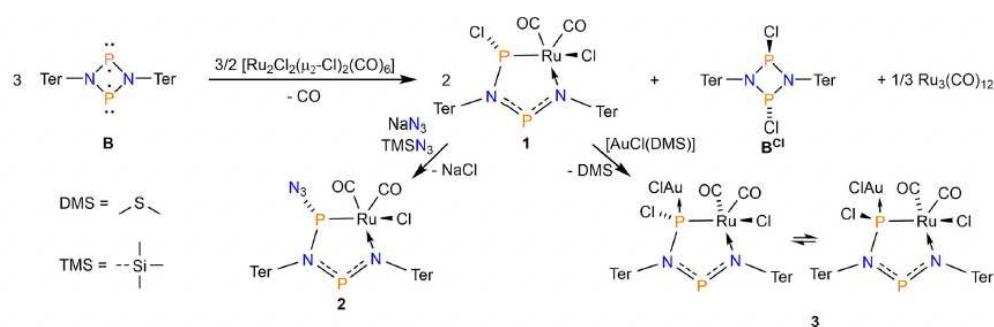
In an attempt to increase the yield, the reaction was carried out in the presence of activated magnesium turnings. This did not lead to re-reduction of **B^{Cl}**, but in fact completely prevented the formation of **1**.

The new metallacycle **1** possesses two reactive element chlorine bonds, P–Cl and Ru–Cl, and an exchange reaction was conceived to probe which one would be more reactive. Candidates for such substitution reactions are pseudo-halides such as the azide group, which is known to be a strong nucleophile.^[25] However, the reaction between **1** and NaN_3 in THF did not lead to full conversion. Therefore, TMS-N_3 ($\text{TMS} = \text{trimethylsilyl}$) as a more soluble azide source was utilized. But also this approach left some starting material unreacted, which indicates that an equilibrium between all reagents is established. To shift the reaction to full conversion, both NaN_3 and TMS-N_3 were applied in combination. Under these conditions, the by-product TMS-Cl reacts with NaN_3 under reformation of TMS-N_3 and precipitation of NaCl . The new product **2** turned out to be a rather delicate species. It decomposes slowly in solution at room temperature and rapidly in solid or solution at elevated temperature. Still, the compound could be character-

ized by single crystal X-ray analysis and poly-nuclear NMR spectroscopy. These analyses show that exclusively the P–Cl bond is affected in the reaction with azide.

In order to investigate whether and which phosphorus center in complex **1** can be engaged in a coordination reaction, one equivalent of $[\text{AuCl}(\text{DMS})]$ ($\text{DMS} = \text{dimethylsulfide}$), was added to a DCM ($\text{DCM} = \text{dichloromethane}$) solution of **1** at room temperature in the dark. $^{31}\text{P}\{^1\text{H}\}$ NMR spectroscopy of the reaction mixture revealed the formation of two products ($^{31}\text{P}\{^1\text{H}\}$ NMR shift [ppm]: $\delta = 206.4, 212.0, 315.5, 320.3$). These signals appear broad at 298 K but become narrow at 273 K (*vide infra*). Interestingly, these products could be identified as the *cis*- and *trans*-isomers of **3**. All other products (**1**, **2** and **B^{Cl}**) were formed in stereo-specific reactions. The coordination of gold chloride allows for the isomerization of the two chlorides in **3** though. Because the two mesitylene substituents in each isomer are magnetically inequivalent, the ^1H and $^{13}\text{C}\{^1\text{H}\}$ NMR spectra of solutions containing both isomers are complex. At elevated temperatures using toluene- D_8 as solvent, the NMR spectra indicate the decomposition of **3** by de-coordination of the AuCl fragment and formation of **1** (for details see the SI).

Single crystals of all new compounds **1**, **2**, and **3** were analyzed by X-ray diffraction methods. Compound **1** crystallizes with two molecules in the asymmetric unit. Averaged values are given. The individual values can be found in the SI and Figure 1. The central ring in **1** adopts an envelope conformation. Ru1, N1, P1 and N2 are virtually in one plane, while P2 is bent out of that plane by $30.0(1)^\circ$. The ruthenium(II) center resides in a square pyramidal coordination sphere. One carbonyl ligand is arranged in plane with the ring, while the other is bonded in an orthogonal position *trans* to Cl1. The 16-electron ruthenium center is further stabilized by a weak interaction with the *ipso*-carbon center of one mesityl group of the terphenyl substituent (C9) at a distance of $2.7457(1)$ Å. The Ru1–N1 bond has a length of $2.122(2)$ Å, which is in the range of reported ruthenium-nitrogen single bonds.^[26] The Ru1–P2 bond is $2.2706(5)$ Å long, which is shorter than a standard single bond between a Ru(II) center and a phosphane ligand,^[27] but longer compared to a Ru(II)–phosphanide-bond.^[28] The three P–N-bonds within the



Scheme 2. Reaction of **B** with $[\text{Ru}_2\text{Cl}_2(\mu_2\text{-Cl})_2(\text{CO})_6]$. Follow up reactions of **1** with azide sources lead to a selective exchange of the phosphorus-bound chloride. Reaction of **1** with $[\text{AuCl}(\text{DMS})]$ gives a mixture of products.

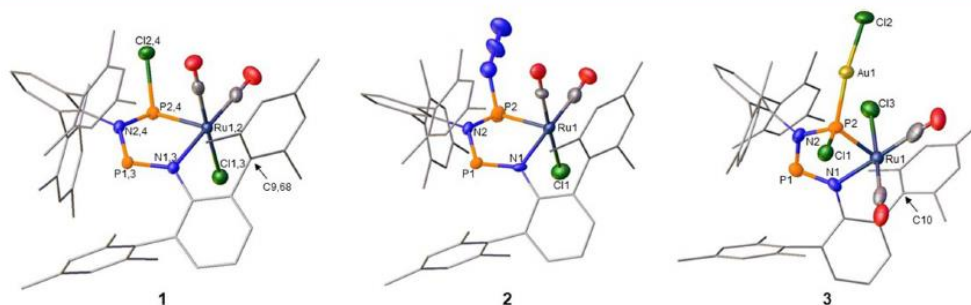


Figure 1. Structures of **1**, **2** and **3** in the solid state. **1** crystallizes with two independent molecules in the asymmetric unit. Therefore, two atom numbers and values are given here. In the main text averaged values are used. H atoms and co-crystallised solvent molecules are omitted for clarity. For details see the SI. Colour code: P (orange), N (blue), Ru (dark blue), O (red), Cl (green), C (grey), Au (gold). Selected bond lengths [Å]: **1**: Ru1–N1: 2.123(2), N1–P1: 1.612(2), P1–N2: 1.661(2), N2–P2: 1.799(2), Ru1–P2: 2.277(3), Ru1–Cl1: 2.3907(9), Ru1–C9: 2.794(2), P2–Cl2: 2.1190(7); **2**: Ru2–N3: 2.120(2), N3–P3: 1.610(2), P3–N4: 1.661(2), N4–P4: 1.812(2), Ru2–P4: 2.273(3), Ru2–Cl3: 2.4150(6), Ru2–C68: 2.697(2), P4–Cl4: 2.1085(1); **3**: Ru1–N1: 2.126(6), N1–P1: 1.617(7), P1–N2: 1.668(7), N2–P2: 1.791(6), Ru1–P2: 2.277(3), Ru1–Cl1: 2.418(2); **3**: Ru1–N1: 2.11(1), N1–P1: 1.59(1), P1–N2: 1.671(1), N2–P2: 1.75(1), Ru1–P2: 2.263(3), P2–Cl1: 2.064(4), P2–Au1: 2.220(3), Au1–Cl2: 2.268(4), Ru1–C10: 2.52(1).

RuPNPN cycle differ considerably in length. While P2–N2 is clearly a single-bond (1.806(2) Å), P1–N1 and P1–N2 are only 1.611(2) Å and 1.661(2) long which is even shorter than the P–N bonds in the starting material **B** (1.716(1) Å).^[6] The lengths of these two P–N bonds opposite to the Ru center in the ring are akin to other conjugated NPN-systems, with a higher weight of the P=N double bond character in P1–N2.^[29]

The solid state structure of the azide complex **2** shows features which are very similar to the structure of **1**.^[30] The azide group is in *trans* position to the RuCl unit and faces away from the central ring. Interestingly, the coordination of AuCl to P2 in **3** promotes isomerization of the chloride ligand bound to ruthenium. The *trans*-isomer is still dominant in the solid state structure at a probability of 82%. The gold chloride (Cl2) unit is pointing away from the ring, the Cl1–P2–Au1 angle amounts to 109.5(2)° and the N2–P2–Ru1 angle to 101.7(4)°. The structural parameter τ_4 ^[31] of 0.90 aligns well with a tetrahedral coordination environment, which indicates that P2 behaves as phosphane donor center forming a formal single bond.

This description is further bolstered by DFT calculations (for details see the SI, chapter 2). Bonding from P1 to Ru1 is covalent with a NLMO/NPA bond order of 0.88. The Ru1–N1 bond is best understood as a donor-acceptor interaction [(LP(N1)→σ*(Ru1–C2)] interaction: 76.2 kcal/mol). Note that the experimental (2.122(2) Å) and calculated Ru1–N1 distances (2.19 Å) differ somewhat; which is likely due to packing effects in the solid state leading to compression of this bond. The carbonyl substituents act as donor ligands to Ru1 with extensive backbonding from d-orbitals at Ru into the π*-CO orbitals which is worth approx. 50 kcal/mol for each CO ligand. Cl1 is best described as a chlorido ligand and the Ru1–Cl1 bond is largely of electrostatic nature. According to the reaction equation (Scheme 2) and considering the electronegativity of N and P, a formal oxidation state of +2 may be assigned to the

Ru center in **1**. However, an NBO analysis based on a DFT wavefunction reveals the high covalency of the Ru–P bond (see the SI), making an assignment of a physical oxidation state to Ru rather ambiguous. This is supported by a slight shift of the CO stretching frequencies in the IR spectrum to lower wavenumbers (**1**: $\nu_{\text{CO}} = 1982, 2045 \text{ cm}^{-1}$; $[\text{Ru}_2\text{Cl}_2(\mu_2\text{-Cl})_2(\text{CO})_6]$: $\nu_{\text{CO}} = 2003, 2073 \text{ cm}^{-1}$ ^[32]), indicating a slightly more electron rich Ru center in **1** than in the starting material.

Owing to the covalency of the Ru–P bond, **1** may be best described as a ruthenium phosphido complex in which the conjugated NPN unit binds via a nitrogen atom to the ruthenium center as indicated by the Lewis structure shown in Scheme 2. In summary the unprecedented ring expansion of a biradicaloid by a metal fragment is presented. Analysis of the obtained inorganic metallacycle revealed covalent character of the Ru–P bond and dative character of the Ru–N bond. It was possible to selectively replace the Cl atom at the phosphorus atom by an azide and to coordinate an [AuCl]-fragment to that very phosphorus atom.

Experimental Section

Experimental procedures for substances **1**, **2** and **3** are given here. Spectra and further analytic and synthetic details can be found in the supporting information.

Synthesis of $[\text{RuCl}(\text{CO})_2(\kappa\text{N}\{(\text{N}^-\text{Ter})\text{P}(\text{N}^-\text{Ter})-\kappa\text{P}(\text{PCl})\})]$ (**1**)

A Schlenk flask was equipped with a stirrer bar and charged with $[\text{P}(\mu\text{-N}^-\text{Ter})_2]$ (304 mg, 0.42 mmol) and $[\text{Ru}_2\text{Cl}_2(\mu_2\text{-Cl})_2(\text{CO})_6]$ (108 mg, 0.21 mmol, 0.5 Eq) and dissolved in 21 mL dry toluene. The mixture was stirred at room temperature overnight. Colour changed from orange to brown. After stirring the mixture at room temperature overnight, volatiles were removed *in vacuo* (1×10^{-3} mbar for 1 h at

25 °C). The crude product was extracted using acetonitrile and *n*-hexane, phases were separated and the acetonitrile phase was dried *in vacuo* (1×10^{-3} mbar for 1 h at 25 °C), dissolved in 4 mL of dry fluorobenzene and 24 mL dry *n*-hexane followed by celite filtration. The crude compound was subsequently washed with a small amount of *n*-pentane to remove grease. Product was dried *in vacuo* (1×10^{-3} mbar for 16 h at 25 °C) to yield a brownish-orange solid. Compound 1 is heat sensitive. Yield: 89 mg (44%).

Melting point: 151 °C (dec.). **CHN** for $C_{50}H_{50}RuN_2O_2P_2Cl_2$ (944.88 g·mol⁻¹) found (calc.): C 63.51 (63.56), H 5.23 (5.33), N 3.38 (2.96). **¹H NMR** (C_6D_6 , 500.1 MHz): δ [ppm] = 1.75 (s, 3 H, $-CH_3$), 1.83 (s, 3 H, $-CH_3$), 1.88 (s, 3 H, $-CH_3$), 1.98 (s, 3 H, $-CH_3$), 2.08 (s, 3 H, $-CH_3$), 2.13 (s, 3 H, $-CH_3$), 2.20 (s, 3 H, $-CH_3$), 2.24 (s, 3 H, $-CH_3$), 2.36 (s, 3 H, $-CH_3$), 2.48 (s, 3 H, $-CH_3$), 2.50 (s, 3 H, $-CH_3$), 2.51 (s, 3 H, $-CH_3$), 6.42 (dd, $^3J(H, ^3P) = 1.7$ Hz, $^3J(H, ^1H) = 7.6$ Hz, 1 H, *para*- $C^{\alpha}H$), 6.58 (dd, $^3J(H, ^3P) = 1.7$ Hz, $^3J(H, ^1H) = 7.5$ Hz, 1 H, *para*- $C^{\alpha}H$), 6.70–7.07 (m, 12 H, $C^{\alpha}H$). **¹³C{¹H} NMR** (C_6D_6 , 125.8 MHz): δ [ppm] = 20.85 (s, 1 C, CH_3), 20.92 (s, 1 C, CH_3), 21.15 (s, 1 C, CH_3), 21.22 (s, 1 C, CH_3), 21.27 (s, 1 C, CH_3), 21.99 (s, 2 C, CH_3), 22.38 (s, 1 C, CH_3), 22.55 (s, 1 C, CH_3), 22.91 (s, 1 C, CH_3), 23.01 (s, 1 C, CH_3), 23.15 (s, 1 C, CH_3), 125.3 (s, 1 C, $C^{\alpha}H$), 126.85 (s, 1 C, $C^{\alpha}H$), 127.53 (s, 1 C, $C^{\alpha}H$), 128.55 (s, 1 C, $C^{\alpha}H$), 128.82 (s, 1 C, $C^{\alpha}H$), 129.05 (s, 1 C, $C^{\alpha}H$), 129.44 (s, 1 C, $C^{\alpha}H$), 130.15 (s, 1 C, $C^{\alpha}H$), 130.66 (s, 1 C, $C^{\alpha}H$), 130.72 (s, 1 C, $C^{\alpha}H$), 130.95 (s, 2 C, $C^{\alpha}H$), 131.04 (s, 1 C, $C^{\alpha}H$), 131.19 (s, 1 C, $C^{\alpha}H$), 133.02 (s, 1 C, $C^{\alpha}H$), 135.16 (s, 1 C, C^{α}), 135.68 (s, 1 C, C^{α}), 135.74 (s, 1 C, C^{α}), 135.78 (s, 1 C, C^{α}), 136.10 (s, 1 C, C^{α}), 136.13 (s, 1 C, C^{α}), 137.55 (s, 1 C, C^{α}), 137.58 (s, 1 C, C^{α}), 137.68 (s, 1 C, C^{α}), 137.80 (s, 1 C, C^{α}), 137.99 (s, 1 C, C^{α}), 138.04 (s, 1 C, C^{α}), 138.13 (s, 1 C, C^{α}), 138.25 (s, 1 C, C^{α}), 138.52 (s, 1 C, C^{α}), 138.61 (s, 1 C, C^{α}), 140.07 (s, 1 C, C^{α}), 140.32 (s, 1 C, C^{α}), 140.72 (s, 1 C, C^{α}), 140.79 (s, 1 C, C^{α}), 143.39 (s, 1 C, C^{α}), 192.35 (s, CO, $\nu_{1/2} = 7.5$ Hz), 194.32 (s, CO, $\nu_{1/2} = 8$ Hz). **³¹P{¹H} NMR** (C_6D_6 , 202.5 MHz): δ [ppm] = 318.5 (s, 1 P, ClP(Ru)), 382.7 (s, 1 P, NPN). **IR** (ATR, 25 °C, 64 scans): ν [cm⁻¹] = 2960 (w), 2915 (w), 2854 (w), 2045 (s), 1982 (s), 1608 (w), 1585 (w), 1572 (w), 1480 (w), 1433 (m), 1398 (w), 1378 (w), 1335 (w), 1302 (w), 1260 (m), 1209 (w), 1174 (m), 1160 (m), 1100 (s), 1011 (s), 997 (m), 924 (m), 882 (m), 850 (s), 799 (s), 753 (m), 714 (m), 677 (m), 620 (m), 596 (m), 566 (m), 538 (m), 507 (m), 454 (m), 430 (m).

Synthesis of $[RuCl(CO)_2\{\kappa N-(NTer)P(NTer)-\kappa P-(PN_3)\}]$ (2)

A vial was equipped with a stirrer bar and charged with 1 (40 mg, 0.042 mmol) and NaN_3 (12.7 mg, 0.2 mmol, 5 Eq.) and dissolved in 5 mL dry DCM. $TMS-N_3$ (0.1 mL, 0.84 mmol, 20 Eq.) were added *via* syringe. The mixture was stirred at room temperature for 24 hours. After stirring the mixture at room temperature overnight, volatiles were removed *in vacuo* (1×10^{-3} mbar for 1 h at 25 °C). The crude product was extracted using *n*-hexane, followed by celite filtration. The crude solution was subsequently concentrated to obtain a super saturated solution which was stored in the freezer (–25 °C). Dark orange crystals were obtained. Product was dried *in vacuo* (1×10^{-3} mbar for 1 h at 25 °C) to yield an orange solid.

¹H NMR (CD_2Cl_2 , 500.1 MHz, 248 K): δ [ppm] = 1.47 (s, 3 H, $-CH_3$), 1.64 (s, 3 H, $-CH_3$), 1.72 (s, 3 H, $-CH_3$), 1.85 (s, 3 H, $-CH_3$), 1.98 (s, 3 H, $-CH_3$), 2.06 (s, 3 H, $-CH_3$), 2.15 (s, 3 H, $-CH_3$), 2.20 (s, 3 H, $-CH_3$), 2.26 (s, 3 H, $-CH_3$), 2.29 (s, 3 H, $-CH_3$), 2.31 (s, 3 H, $-CH_3$), 2.35 (s, 3 H, $-CH_3$), 6.67 (s, 1 H, *para*- $C^{\alpha}H$), 6.69 (s, 1 H, *para*- $C^{\alpha}H$), 6.80 (s, 1 H, $C^{\alpha}H$) 6.85–7.05 (m, 11 H, $C^{\alpha}H$). **¹³C{¹H} NMR** (CD_2Cl_2 , 125.8 MHz, 248 K): δ [ppm] = 20.37 (s, 1 C, CH_3), 20.44 (s, 1 C, CH_3), 21.05 (s, 1 C, CH_3), 21.11 (s, 1 C, CH_3), 21.15 (s, 1 C, CH_3), 21.33 (s, 1 C, CH_3), 21.94 (s, 1 C, CH_3), 22.01 (s, 1 C, CH_3), 22.20 (s, 1 C, CH_3), 22.23 (s, 1 C, CH_3), 22.50 (s, 1 C, CH_3), 22.60 (s, 1 C, CH_3), 125.00 (s, 1 C, $C^{\alpha}H$), 126.86 (s, 1 C, $C^{\alpha}H$), 127.26 (s, 1 C, C^{α}), 127.92 (s, 1 C, $C^{\alpha}H$), 128.18 (s, 1 C, $C^{\alpha}H$), 128.67 (s, 1 C, $C^{\alpha}H$), 128.81 (s, 1 C, $C^{\alpha}H$), 128.94 (s, 1 C, $C^{\alpha}H$), 129.10 (s, 1 C, $C^{\alpha}H$), 129.34 (s, 1 C, C^{α}), 130.05 (s, 1 C, $C^{\alpha}H$), 130.25 (s,

1 C, $C^{\alpha}H$), 130.54 (s, 1 C, C^{α}), 130.63 (s, 1 C, $C^{\alpha}H$), 130.72 (s, 1 C, $C^{\alpha}H$), 130.83 (s, 1 C, $C^{\alpha}H$), 132.70 (s, 1 C, $C^{\alpha}H$), 132.92 (s, 1 C, C^{α}), 134.70 (s, 1 C, C^{α}), 134.85 (s, 1 C, C^{α}), 136.36 (s, 1 C, C^{α}), 136.52 (s, 1 C, C^{α}), 136.80 (s, 1 C, C^{α}), 137.60 (s, 1 C, C^{α}), 137.82 (s, 1 C, C^{α}), 137.92 (s, 1 C, C^{α}), 138.04 (s, 1 C, C^{α}), 138.19 (s, 1 C, C^{α}), 138.43 (s, 1 C, C^{α}), 140.10 (s, 1 C, C^{α}), 141.10 (s, 1 C, C^{α}), 141.13 (s, 1 C, C^{α}), 143.31 (s, 1 C, C^{α}), 146.81 (s, 1 C, C^{α}), 146.87 (s, 1 C, C^{α}), 150.18 (s, 1 C, C^{α}), 191.14 (s, CO, $\nu_{1/2} = 6$ Hz), 193.88 (s, CO, $\nu_{1/2} = 5$ Hz). **³¹P{¹H} NMR** (CD_2Cl_2 , 202.5 MHz, 248 K): δ [ppm] = 313.4 (s, 1 P, NPN), 329.4 (s, 1 P, NPN). **IR** (ATR, 25 °C, 64 scans): ν [cm⁻¹] = 2962 (w), 2915 (w), 2855 (w), 2188 (w), 2140 (w), 2101 (s), 2049 (s), 2038 (s), 1978 (s), 1649 (w), 1608 (w), 1441 (w), 1398 (s), 1378 (w), 1300 (w), 1258 (w), 1211 (w), 1173 (m), 1161 (w), 1116 (w), 1081 (w), 1035 (w), 1011 (m), 928 (m), 848 (m), 805 (m), 755 (m), 731 (w), 689 (w), 676 (w), 654 (w), 622 (w), 597 (w), 577 (m), 557 (w), 538 (w), 518 (w), 501 (s), 483 (w), 458 (w), 438 (m).

Synthesis of $[(AuCl)\{RuCl(CO)_2\{\mu_2-(PCl)(NTer)P-2\kappa N-(NTer)\}]$ (3)

A vial was equipped with a stirrer bar and charged with 1 (20 mg, 0.021 mmol) and AuCl·DMS (7 mg, 0.021 mmol, 1 Eq.) and dissolved in 3 mL dry DCM. The mixture was stirred at room temperature for 24 hours under the exclusion of light. Afterwards, volatiles were removed *in vacuo* (1×10^{-3} mbar for 1 h at 25 °C). The crude product was extracted using acetonitrile/*n*-hexane biphasic system (as described for 1. Product is in the *n*-hexane phase). The crude product was crystallized by layering a difluorobenzene solution with *n*-hexane and storing it in the freezer at –25 °C. Yellow crystals were obtained and washed with small amount of pentane. The product was dried *in vacuo* to yield a yellow solid. A ¹H NMR spectrum of the product (Figure S11) can be found in the SI. As the signals cannot be matched to corresponding isomer we chose to not explicate the shifts here. The presence of two isomers furthermore lead to a bad signal/noise ratio. Yield: 15 mg (60%)

Melting point: 210 °C (dec.). **CHN** for $C_{50}H_{50}RuAuN_2O_2P_2Cl_2$ (1177.308 g·mol⁻¹) found (calc.): C 49.40 (51.01), H 4.09 (4.28), N 2.63 (2.38). **³¹P{¹H} NMR** (CD_2Cl_2 , 202.5 MHz, 273 K): δ [ppm] = 206.4 (s, 1 P, ClPAu(Ru)), $\nu_{1/2} = 213$ Hz), 212.0 (s, 1 P, ClPAu(Ru)), $\nu_{1/2} = 50$ Hz), 315.5 (s, 1 P, NPN), $\nu_{1/2} = 50$ Hz), 320.3 (s, 1 P, NPN), $\nu_{1/2} = 213$ Hz). **IR** (ATR, 25 °C, 64 scans): ν [cm⁻¹] = 3254 (w), 2914 (w), 2378 (w), 2323 (w), 2061 (s), 2004 (s), 1607 (w), 1442 (w), 1405 (w), 1374 (w), 1303 (m), 1236 (s), 1152 (s), 1082 (m), 1015 (w), 982 (m), 917 (s), 864 (m), 845 (m), 805 (m), 751 (w), 684 (w), 612 (m), 570 (m), 548 (w), 531 (w), 499 (w), 477 (m).

Acknowledgements

This work was supported by the Swiss National Science Foundation (SNF; grant 200020_181966) and the ETH Zürich (grant ETH-36 17-2). PC gratefully acknowledges funding by the Deutsche Forschungsgemeinschaft (DFG, grant 438203135). We thank Dr. M. Wörle for valuable help with the X-ray diffraction measurements and Dr. R. Vérel for valuable help with acquisition and interpretation of NMR data. We wish to thank the ITMZ at the University of Rostock for access to the cluster computer, and especially Malte Willert for his assistance with the queuing system and software installations. Background picture of TOC: www.freepik.com. Open access funding provided by Eidgenössische Technische Hochschule Zürich.

Conflict of Interest

The authors declare no conflict of interest.

Data Availability Statement

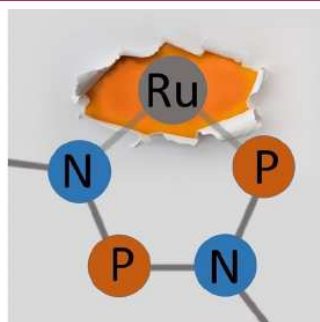
The data that support the findings of this study are available in the supplementary material of this article.

Keywords: Phosphorus heterocycles · Ruthenium · Metallacycles · Coordination chemistry · N,P ligands

- [1] D. Fenske, W. Bensmann, *Z. Naturforsch. B* 1985, 40, 1093–1096.
- [2] F. Mao, S. K. Sur, D. R. Tyler, *J. Am. Chem. Soc.* 1989, 111, 7627–7628.
- [3] H. J. Becher, W. Bensmann, D. Fenske, *Chem. Ber.* 1977, 110, 315–321.
- [4] D. Fenske, H. J. Becher, *Chem. Ber.* 1974, 107, 117–122.
- [5] D. Fenske, *Angew. Chem. Int. Ed.* 1976, 15, 381–382; *Angew. Chem.* 1976, 88, 415–415.
- [6] D. Fenske, A. Christidis, *Angew. Chem. Int. Ed.* 1981, 20, 129–131; *Angew. Chem.* 1981, 93, 113–115.
- [7] T. Storr, R. Mukherjee, *Inorg. Chem.* 2018, 57, 9577–9579.
- [8] T. Beweries, R. Kuzora, U. Rosenthal, A. Schulz, A. Villinger, *Angew. Chem. Int. Ed.* 2011, 50, 8974–8978; *Angew. Chem.* 2011, 123, 9136–9140.
- [9] Z. Li, X. Chen, D. M. Andrada, G. Frenking, Z. Benko, Y. Li, J. R. Harmer, C. Y. Su, H. Grützmacher, *Angew. Chem. Int. Ed.* 2017, 56, 5744–5749; *Angew. Chem.* 2017, 129, 5838–5843.
- [10] A. Hinz, R. Kuzora, U. Rosenthal, A. Schulz, A. Villinger, *Chem. Eur. J.* 2014, 20, 14659–14673.
- [11] Z. Li, X. Chen, L. L. Liu, S. Liu, H. Grützmacher, *Angew. Chem. Int. Ed.* 2020.
- [12] A. Hinz, A. Schulz, A. Villinger, *Chem. Commun.* 2016, 52, 6328–6331.
- [13] Z. Li, X. Chen, L. L. Liu, M. T. Scharnhölz, H. Grützmacher, *Angew. Chem. Int. Ed.* 2020, 59, 4288–4293; *Angew. Chem.* 2020, 132, 4318–4323.
- [14] Z. Li, Y. Hou, Y. Li, A. Hinz, X. Chen, *Chem. Eur. J.* 2018, 24, 4849–4855.
- [15] A. Hinz, A. Schulz, A. Villinger, *J. Am. Chem. Soc.* 2015, 137, 9953–9962.
- [16] A. Hinz, A. Schulz, A. Villinger, *Angew. Chem. Int. Ed.* 2015, 54, 2776–2779; *Angew. Chem.* 2015, 127, 2815–2819.
- [17] T. R. Cook, P. J. Stang, *Chem. Rev.* 2015, 115, 7001–7045.
- [18] M. R. Shaaban, R. El-Sayed, A. H. M. Elwahy, *Tetrahedron* 2011, 67, 6095–6130.
- [19] M. S. Sanford, J. A. Love, R. H. Grubbs, *J. Am. Chem. Soc.* 2001, 123, 6543–6554.
- [20] A. G. Wenzel, R. H. Grubbs, *J. Am. Chem. Soc.* 2006, 128, 16048–16049.
- [21] M. Albrecht, *Chem. Rev.* 2010, 110, 576–623.
- [22] B. Schmidt, *Angew. Chem. Int. Ed.* 2003, 42, 4996–4999; *Angew. Chem.* 2003, 115, 5146–5149.
- [23] D. Chen, Y. Hua, H. Xia, *Chem. Rev.* 2020.
- [24] By-product $\text{Ru}_3(\text{CO})_{12}$ was identified by subliming an aliquot out of the crude reaction mixture and analyzing it by IR-spectroscopy in *n*-hexane-solution (see the SI).
- [25] H. Brand, A. Schulz, A. Villinger, *Z. Anorg. Allg. Chem.* 2007, 633, 22–35.
- [26] I. S. Sinopalnikova, T. A. Peganova, V. V. Novikov, I. V. Fedyanin, O. A. Filippov, N. V. Belkova, E. S. Shubina, R. Poli, A. M. Kalsin, *Chem. Eur. J.* 2017, 23, 15424–15435.
- [27] J. M. Goicoechea, M. F. Mahon, M. K. Whittlesey, P. G. Kumar, P. S. Pregosin, *Dalton Trans.* 2005, 588–597.
- [28] E. J. Derrah, D. A. Pantazis, R. McDonald, L. Rosenberg, *Organometallics* 2007, 26, 1473–1482.
- [29] G. A. Seisenbaeva, V. G. Kessler, R. Pazik, W. Strek, *Dalton Trans.* 2008, 3412–3421.
- [30] Crystals of 2 of suitable quality for single crystal X-ray diffraction were only obtained from reaction mixtures that still contained 1. The crystal analyzed here contained 25% of 1 cocrystallized with 75% 2.
- [31] L. Yang, D. R. Powell, R. P. Houser, *Dalton Trans.* 2007, 955–964.
- [32] J. T. King, M. R. Ross, K. J. Kubarych, *J. Phys. Chem. B* 2012, 116, 3754–3759.

Manuscript received: March 1, 2022
 Revised manuscript received: March 25, 2022
 Accepted manuscript online: March 26, 2022

RESEARCH ARTICLE



J. Oswald, M. T. Scharnhölz, P. Coburger, H. Beer, J. Bresien, A. Schulz, H. Grützmacher**

1 – 6

Insertion of Ruthenium into an inorganic, cyclic biradicaloid



Henrik Beer

Praxiserfahrung

10/2018 – 09/2022

**Wissenschaftlicher Mitarbeiter Anorganische Chemie
(Promotionsstudent)**

Universität Rostock (Rostock, DE)

- Anorganische Chemie, Arbeitskreis Prof. Schulz

03/2018 – 09/2018

wissenschaftliche Hilfskraft Betriebsstofflabor

Universität Rostock (Rostock, DE)

- Fakultät für Maschinenbau und Schiffstechnik

Bildungsweg

10/2011 – 08/2016

Studium der Chemie (M.Sc.)

Universität Rostock (Rostock, DE)

- Abschlussarbeit: "Hetero-Cyclopentan-1,3-diyle: Modifikation von molekularen Schaltern"

▪

10/2011 – 08/2016

Studium der Chemie (B.Sc.)

Universität Rostock (Rostock, DE)

- Abschlussarbeit: "Aktivierung von weißem Phosphor in ionischen Flüssigkeiten"

▪

10/2011 – 08/2016

Abitur

- Goethe Gymnasium Schwerin (Schwerin, DE)

Weitere Kenntnisse

Sprachen:

Deutsch – Muttersprache

Englisch – gut in Wort und Schrift (Sprachniveau C1)

Software:

MS Powerpoint, MS Word – sehr gut

MS Excel – sehr gut

TopSpin – gut

ACD/Labs – sehr gut

Sonstige:

Führerscheinklasse B

Konferenzbeiträge

- 04/2019 **16th European Workshop in Phosphorus Chemistry (EWPC)**
Bristol (England)
 - Posterpräsentation
 - "Different Hetero – Cyclopentane – 1.3 diyls
Modification of molecular switches"
- 06/2018 – 07/2018 **The 15th International Symposium on Inorganic Ring Systems (IRIS)**
Kyoto (Japan)
 - Posterpräsentation
 - "Different Hetero – Cyclopentane – 1.3 diyls
Modification of molecular switches with different sterically
demanding groups"
- 03/2018 **15th European Workshop in Phosphorus Chemistry (EWPC)**
Upsalla (Schweden)
 - Posterpräsentation
 - "Different Hetero – Cyclopentane – 1.3 diyls
Modification of molecular switches with different sterically
demanding groups"

Publikationen

- 02/2019 **A Chemical reaction controlled by light-activated molecular
switches based on heterocyclopentenediyls**
J. Bresien, T. Kröger-Badge, S. Lochbrunner, D. Michalik, H.
Müller, A. Schulz, E. Zander, *Chem. Sci.* **2019**, *10*, 3486-
3493
 - DOI: 10.1039/c8sc04893b
- 05/2020 **Heterocyclopentenediyls vs. Heterocyclopentane-dienes: A
Question of Silyl Group Migration**
H. Beer, J. Bresien, D. Michalik, A.-K. Rölke, A. Schulz, A.
Villinger, R. Wustrack *J. Org. Chem.* **2020**, *85*, 14435-14445
 - DOI: 10.1021/acs.joc.0c00460
 -
- 08/2020 **Reversible switching between housane and cyclopentenediyl
isomers: an isonitrile-catalysed thermal reverse reaction**
H. Beer, J. Bresien, D. Michalik, A. Schulz, A. Villinger,
Dalton Trans. **2020**, *49*, 13986-13992
 - DOI: 10.1039/d0dt02688c
 -
- 09/2020 **Trapping of Brønsted acids with a phosphorus centered
biradicaloid – synthesis of hydrogen pseudohalide addition products**
H. Beer, K. Bläsing, J. Bresien, I. Chojetzki, A. Schulz, P.
Stoer, A. Villinger, *Dalton Trans.* **2020**, *49*, 13655-13662
 - DOI: 10.1039/d0dt03251d

- 03/2021 **Photoisomerization of a phosphorus-based biradicaloid: ultrafast dynamics through a conical intersection**
T. Völzer, H. Beer, A. Schulz, S. Lochbrunner, J. Bresien, *Phys. Chem. Chem. Phys.* **2021**, 23, 7434-7441
▪ DOI: 10.1039/d1cp00428j
- 03/2021 **Hyperpolarization Effects in Parahydrogen Activation with Pnictogen Biradicaloids: Metall-free PHIP and SABRE**
V. V. Zhivonitko, H. Beer, D. O. Zakharov, J. Bresien, A. Schulz, *ChemPhysChem*. **2021**, 22, 813-817
DOI: 10.1002/cphc.202100141
- 01/2022 **Synthesis of Bicyclic P,S-Heterocycles via the Addition of Thioketones to a Phosphorus-Centered Open-Shell Singlet Biradical**
H. Beer, A. Linke, J. Bresien, G. Mloston, M. Celeda, A. Villinger, A. Schulz, *Inorg. Chem.*. **2022**, 61, 2031-2038
▪ DOI: 10.1021/acs.inorgchem.1c03207
▪
- 03/2022 **Insertion of Ruthenium into an inorganic, cyclic biradicaloid**
J. Oswald, M. T. Scharnhözl, P. Coburger, H. Beer, J. Bresien, A. Schulz, H. Grützmacher, *Z. Anorg. Allg. Chem.* **2022**, e202200093 (early view)
▪ DOI: 10.1002/zaac.202200093
▪
- 04/2022 **A Cyclic Thioketone as Biradical Heterocyclopentane-1,3-diy: Synthesis, Structure and Activation Chemistry**
H. Beer, A. Linke, J. Bresien, A. Villinger, A. Schulz, *Inorg. Chem. Front.* **2022**, 9, 2659-2667
▪ DOI: 10.1039/D2QI00482H

Rostock, 11.07.2022

Henrik Beer